

ANGLIA RUSKIN UNIVERSITY

EFFECT OF MALALIGNMENT ON KNEE JOINT  
CONTACT MECHANICS

by

FRANZISKA REISSE

A thesis in partial fulfilment of the requirements of Anglia Ruskin  
University for the degree of Doctor of Philosophy

This research was sponsored by the Medical and Educational Research  
Trust and was conducted in collaboration with the Hospital for Special  
Surgery in New York, US.

Submitted: June 2014

## Acknowledgements

This research has been gratefully funded by the Chelmsford Medical Education and Research Trust.

I would like to dedicate this work to various people who provided support, guidance and encouragement throughout each stage of this study and without whose support this thesis would not have been possible.

My special thanks go to my supervisory team, Dr Rajshree Mootanah, Dr Howard Hillstrom and Dr Robert Walker, who kept their patience with me throughout the years and provided support whenever needed. Their leadership has been greatly appreciated and has helped me finish this project.

I am also thankful to Professor John Dowell and Professor Kevin Cheah for inviting me to theatre to gain an understanding of the actual surgery. Thanks are also due to Professor Paul Ingle for proof reading my thesis and Diagarajen Carpanen for helping with the process of creating and validating the model.

I would like to thank the scientists at the Hospital for Special Surgery Mark Lenhoff, Chief Engineer of the Motion Analysis Lab, for writing the MatLab programme and providing great support with the transformation matrices, Dr Matthew Koff, Assistant Scientist in the Department of Radiology and Imaging – MRI Division, for providing excellent quality MRI images that made the process of creating the knee model substantially easier and Dr Carl Imhauser, Assistant Scientist in the Biomechanics Department, for carrying out all the cadaveric work necessary to validate the model.

On a personal note I warmly thank my family, especially my mother Eva Maria Reisse, my grandparents Dr Werner and Inge Reisse and my grandmother Petronilla Kaufmann for supporting me with my decision to study in England and Katharina, Stephanie and Benjamin Reisse for being the best siblings someone could ask for. My family has endlessly shown me the right path and has always supported me in all my interests.

I am grateful to Conny, Uwe, Jan and Kai Stetzer and Constantin Lack for helping me with my studies in Germany and for always treating me as part of their family.

I also thank all my friends in Germany, especially Andrea, Fritzi and Werner Schaefer, Yvonne and Isabelle Schneider and Dodi, Reiner, Alina and Nico von Hayn, for staying such a huge part of my life even though there is a big distance between us.

Last but not least I am very thankful to all my friends in England, particularly Amy Woods, Georgina van Dort, Alexandra Johnston, Danni Strange, Tim Fox and my MG's Clare Bond, Kerrie Moss, Nicola Lopez and Lorraine Mahana for always being there for me.

ANGLIA RUSKIN UNIVERSITY

ABSTRACT

FACULTY OF SCIENCE AND TECHNOLOGY

DOCTOR OF PHILOSOPHY

EFFECT OF MALALIGNMENT ON KNEE JOINT CONTACT MECHANICS

FRANZISKA REISSE

June 2014

Osteoarthritis (OA) is a debilitating joint disease that leads to significant pain, loss of mobility and quality of life. Knee malalignment results in increased joint pressure, which is a primary cause for OA progression. High Tibial Osteotomy (HTO) is a surgical procedure to correct malalignment and redistribute load in the knee joint, reduce peak pressure and delay OA progression. However, clinical outcomes have been unpredictable. Therefore, the aim of this study was to determine the relationship between malalignment and knee contact mechanics.

A 3D computational model was created from magnetic resonance images of a cadaveric knee joint. A ligament tuning process was conducted to determine material properties. Finite element analyses were conducted, simulating end of weight acceptance during walking. Different wedge geometries were virtually removed to simulate malalignments from 14° valgus to 16° varus.

Contact mechanics were sensitive to soft tissue material properties. *In-vitro* experiments were compared with computational modelling of the same specimen. Percent full-scale errors for contact force and pressure were less than 8%, demonstrating a unique subject-specific model validation. The native alignment of the cadaveric knee (1° varus) had medial and lateral compartment peak pressures of 4.28 MPa and 2.42 MPa, respectively. The medial:lateral force ratio was 70%:30%. Minimum contact stress did not occur at a Mechanical Axis Deviation (MAD) of zero millimetres nor at the Fujisawa Point, which are common targets for HTO correction. Results showed very strong correlations ( $r > 0.94$ ) between MAD and joint contact loading.

This study is the first to demonstrate the relationship between stress (normal, shear, contact pressure) and MAD in a subject-specific model. This is a prerequisite for the development of a tool that could help surgeons make informed decisions on the degree of realignment required to minimise peak joint loading, thereby delaying OA progression.

Keywords: Osteoarthritis, Knee Malalignment, Realignment, High Tibial Osteotomy, Finite Element Methods

# Preface

This thesis is part of a larger project. The initial concept for this project was formed by Dr Howard Hillstrom and Dr Rajshree Mootanah at the ISB meeting in 2007. A collaboration between the Hospital for Special Surgery (HSS), New York and Anglia Ruskin University (ARU), Chelmsford was established and two different doctoral theses were developed as part of this effort. Cadaveric studies were conducted at HSS for the purposes of model validation, as well as acquiring imaging data for the two theses at ARU (1: Effect of Malalignment on Knee Joint Contact Mechanics (F. Reisse)); 2: Effect of Meniscectomy upon Joint Contact Mechanics (D. Carpanen)). Both ARU theses are unique and different in content. All computational analyses were conducted at ARU by the two PhD students under the supervision of Dr Mootanah and Dr Walker from ARU and Dr Hillstrom from HSS.

The concept of conducting a validation study required different expertise from radiology, mechanical engineering, biomedical engineering, electrical engineering and anatomy, in order to be successfully accomplished. Through this collaboration the investigational team developed and validated a computational knee model that was within an error of less than 8%. This led to a publication, where each author had different task(s) and contributed substantially to the outcome (Table A). The computational part of the validation study forms a component of this doctoral thesis as the author (F. Reisse) had to participate in the study in order to develop a valid model, which is the first of its kind.

The author of this thesis (F. Reisse), segmented imaging data, developed the geometry of each part comprising the knee joint, participated in weekly meetings to discuss all results and problems, developed a working model in Abaqus including applying correct boundary conditions and meshing each anatomical structure, conducted sensitivity analyses, conducted the ligament tuning, and simulated different alignments in order to investigate the relationship between contact mechanics and knee alignment.

Abstracts documenting the author's process are listed in Appendix F-1. Results of this thesis provide a basic understanding of knee contact mechanics for different alignments and are the foundation for developing a tool that predicts subject-specific alignment prior to high tibial osteotomy surgery. Based on the outcome of this thesis,

and the lessons learned, an Arthritis Research United Kingdom (ARUK) grant was written and awarded to determine the difference in contact mechanics for 10 cadaveric specimens with completely different anatomical geometries.

**Table A: The contribution of each author to the validation study**

Author	Tasks									
	1	2	3	4	5	6	7	8	9	10
R. Mootanah	x		x	x		x	x	x	x	x
C.W. Imhauser	x			x				x	x	x
<b>F. Reisse</b>			<b>x</b>			<b>x</b>	<b>x</b>	<b>x</b>	<b>x</b>	<b>x</b>
D. Carpanen			x			x		x	x	x
R.W. Walker			x			x		x	x	x
M.F. Koff		x							x	x
M.W. Lenhoff				x	x		x	x	x	x
S.R. Rozbruch									x	x
A.T. Fragomen									x	x
Z. Dewan				x				x		x
Y.M. Kirane									x	x
K. Cheah									x	x
J.K. Dowell									x	x
H.J. Hillstrom	x		x	x	x	x	x	x	x	x

- 1: Feasibility Study
- 2: Radiology
- 3: Model Development
- 4: In Vitro Testing
- 5: Motion Analysis
- 6: Sensitivity Analysis
- 7: Ligament Tuning
- 8: Validation
- 9: Interpretation (Clinical & Biomechanical)
- 10: Writing up

# Table of Contents

1. Introduction.....	1
2. Literature Review .....	4
2.1. Anatomy of the Knee .....	4
2.1.1. Bones of the Knee Joint .....	4
2.1.2. The Cartilage.....	6
2.1.3. Meniscal Structure .....	8
2.1.4. Ligaments of the Knee Joint .....	9
2.1.5. Synovial fluid.....	10
2.1.6. Musculo-tendonous Structures.....	10
2.2. Kinematics .....	10
2.2.1. The Gait Cycle .....	12
2.3. Kinetics .....	13
2.3.1. Distribution of Load in the Knee Joint.....	15
2.4. Osteoarthritis.....	15
2.4.1. Classification of Osteoarthritis.....	16
2.4.2. Effects of Osteoarthritis .....	17
2.4.3. Causes of Osteoarthritis .....	18
2.4.4. Prevalence of Osteoarthritis .....	19
2.5. Malalignment of the Knee.....	20
2.5.1. Hip-Knee-Ankle Angle .....	20
2.5.2. Mechanical Axis Deviation.....	21
2.5.3. Anatomical Axes.....	22
2.5.4. Causes of Malalignment.....	23
2.5.5. Effects of Malalignment.....	23
2.5.6. Current Surgical Malalignment Corrections and their Outcomes .....	25
2.6. Mechanics of the Diseased Knee .....	28
2.7. High Tibial Osteotomy.....	29
2.7.1. Results of High Tibial Osteotomy.....	31
2.7.2. Pre- and Intraoperative Planning.....	34
2.7.3. Risk Factors of High Tibial Osteotomy .....	35
2.7.4. Alternatives to High Tibial Osteotomy .....	37

2.8.	Finite Element Analysis .....	39
2.8.1.	Application of FEA in Biomedical Problems .....	40
2.8.2.	High Tibial Osteotomy in Finite Element Analysis .....	50
2.8.3.	Model Validation .....	52
2.8.4.	Concluding Remarks .....	55
2.9.	Need for Improvement/ Gap in Knowledge .....	56
2.10.	Conceptual framework .....	59
2.11.	Specific Aims and Hypotheses .....	60
3.	Methods .....	62
3.1.	Flow chart of methods .....	63
3.2.	Collaboration .....	64
3.3.	MRI scanner .....	65
3.4.	Cadaveric specimen .....	66
3.5.	Six-Degree-of-Freedom Robot .....	67
3.6.	Development of an Accurate 3D FE Knee Model .....	67
3.6.1.	Creation of 3D Osseous and Soft Tissues from MRI .....	67
3.6.2.	Non-Manifold Assembly of Bone and Cartilage .....	72
3.7.	Mesh Quality .....	75
3.8.	Joint Coordinate System .....	80
3.9.	Material Properties .....	86
3.9.1.	Bone Properties .....	87
3.9.2.	Cartilage Properties .....	87
3.9.3.	Meniscus Properties .....	87
3.9.4.	Ligament Properties .....	88
3.10.	Ligament Tuning .....	89
3.10.1.	Transformation Matrices .....	90
3.11.	Contact Definitions .....	93
3.12.	Boundary and Loading conditions .....	96
3.13.	Validation .....	100
3.14.	Analysis .....	104
3.15.	Malaligned Knee Joint .....	108

3.16.	Static Equilibrium .....	121
4.	Results and Analysis .....	124
4.1.	Effect of Mesh Type on Knee Joint Contact Mechanics.....	124
4.2.	Effect of Mesh Size on Contact Pressure .....	132
4.3.	Effect of Material Properties on Knee Joint Contact Pressure.....	134
4.4.	Ligament Tuning.....	138
4.4.1.	Matching Kinematics to Tune the Ligament Properties.....	138
4.4.2.	Material Properties after Tuning .....	141
4.5.	Validation.....	143
4.5.1.	Peak Pressure in the Tibial Cartilage .....	147
4.5.2.	Compartmental Forces in the Tibial Cartilage .....	147
4.5.3.	Static Equilibrium .....	149
4.6.	Malaligned Knee Joint Simulations .....	151
4.6.1.	Forces in the Medial and Lateral Compartments .....	151
4.6.2.	Pressure and Stress in the Medial and Lateral Compartments .....	154
4.6.3.	Volumetric Stress Distribution.....	158
4.6.3.	Contact Area .....	163
4.7.	Correlation of Alignment with Joint Loading.....	164
4.8.	Static Equilibrium .....	165
5.	Discussion.....	167
5.1.	Discussion of Sensitivity Analyses .....	168
5.1.1.	Mesh.....	168
5.1.2.	Material Properties.....	168
5.1.3.	Concluding Remarks.....	172
5.2.	Discussion of Validation Study.....	172
5.2.1.	Forces and Pressure between FE Model and <i>In Vitro</i> Study.....	173
5.2.2.	Ligament Tuning.....	177
5.2.3.	Validation.....	178
5.2.4.	Concluding Remarks.....	179
5.3.	Discussion of Analysis of Intact Knee .....	180
5.3.1.	Pressure and Forces in the Intact Joint .....	182
5.4.	The Malaligned Knee.....	184



5.4.1.	Load Application.....	184
5.4.2.	Forces in the Malaligned Models.....	185
5.4.3.	Pressure in the Malaligned Models.....	189
5.5.	Static Equilibrium .....	194
5.6.	The broader field of OA research .....	194
5.7.	Limitations .....	196
6.	Case Study .....	202
7.	Conclusions.....	205
7.1.	Hypothesis 1.....	205
7.2.	Hypothesis 2.....	205
7.3.	Hypothesis 3.....	206
7.4.	Hypothesis 4.....	206
7.5.	Outcomes of the Study.....	207
8.	Future Investigations.....	209
	References .....	210

## List of Figures

Figure 1.1: Human knee joint structure: a) anterior view and b) posterior view .....	1
Figure 2.1: The shape of the tibiofemoral articular surfaces .....	5
Figure 2.2: Articular cartilage (a) chondrocyte and (b) collagen fibre organisation in articular cartilage From A.J. Steward, Y. Liu, and D.R. Wagner, “Engineering Cell Attachments to Scaffolds in Cartilage Tissue Engineering,” in JOM, Volume 63, Issue 4, April 2011, p. 75, Figure A. Copyright © 2011 by The Minerals, Metals & Materials Society. Reprinted with permission. ....	6
Figure 2.3: Cartilage structure from the anterior perspective .....	7
Figure 2.4: Meniscal structure from the axial perspective .....	8
Figure 2.5: Knee joint motions in six degrees of freedom .....	11
Figure 2.6: The human gait cycle.....	12
Figure 2.7: Knee joint flexion during level walking .....	13
Figure 2.8: Normative knee forces during level walking.....	14
Figure 2.9: Normative knee moments during level walking.....	14
Figure 2.10: Osteoarthritic knee.....	16
Figure 2.11: Joint space narrowing for a) healthy knee and b) osteoarthritic knee ...	18
Figure 2.12: Frontal plane alignment of the knee a) varus b) neutral c) valgus ; MA: mechanical axis of the lower limb; HKA: Hip-knee-ankle angle; FM: Femoral mechanical axis; TM: Tibial mechanical axis; L: Lateral; M: Medial.....	21
Figure 2.13: Mechanical axis deviation of the knee joint .....	22
Figure 2.14: Loading of the knee with a) normal frontal-plane alignment and b) varus, or bowlegged, malalignment; where $F_{lat}$ = Force in the lateral compartment (internal); $F_{med}$ = Force in the medial compartment (internal); $F_{lcl}$ = Force in the lateral collateral ligament (internal); $F_m$ = Net forces from muscles (internal); $F_{mcl}$ = Force in the medial collateral ligament (internal); $M_{add}$ = External knee adduction moment; $F_{knee}$ = External force acting on the knee. Note: Varus malalignment increases compressive load on the medial tibiofemoral compartment. ....	24
Figure 2.15: Opening wedge high tibial osteotomy with Taylor Spatial Frame .....	30
Figure 2.16: Survival rates of High Tibial Osteotomy reported in the literature .....	33

Figure 2.17: Different element mesh types .....	40
Figure 2.18: Axi-symmetric 2D model .....	41
Figure 2.19: Stress-Strain curve for ligaments 1 = toe region; 2 = intermediate region; .....	47
Figure 2.20: Conceptual Framework.....	59
Figure 3.1: Flow Chart of Methods.....	63
Figure 3.2: Collaboration flow chart. Boundary conditions from the Leon Root Motion Analysis Lab are to simulate the end of weight acceptance ( $F_{axial} = 811\text{ N}$ , $M_{bending} = 20\text{ Nm}$ ) for HTO assessment at the Medical Engineering Research Group; whereas boundary conditions for the Medical Engineering Research Group are to: (1) match those of the robot for model validation ( $F_{axial} = 374\text{ N}$ , $M_{bending} = 0\text{ to }15\text{ Nm}$ ) and (2) to simulate the end of weight acceptance to perform HTO assessments ( $F_{axial} = 811\text{ N}$ , $M_{bending} = 20\text{ Nm}$ ). .....	64
Figure 3.3: MRI images of the coronal view of the knee joint in (a) CUBE sequence for accurate representation of meniscus and ligament and (b) SPGR sequence for accurate representation of cartilage and bone .....	66
Figure 3.4: MR image of the knee joint (coronal view).....	68
Figure 3.5: Mimics workspace; a) coronal view; b) axial view; c) sagittal view and d) 3D view .....	69
Figure 3.6: The 3D Live Wire algorithm: a) to create geometries of the different tissues, b) 3D Live Wire with mask .....	69
Figure 3.7: Editing mask in 3D .....	70
Figure 3.8: Multiple slice editing .....	71
Figure 3.9: Creating the 3D model.....	71
Figure 3.10: The use of the ‘non-manifold algorithm’ to create common contact areas between adjacent tissue, such as the distal femur and femoral cartilage. a) The inner geometry of the cartilage (in pink) was overestimated to protrude into the femur (outlined in b in blue) and eliminate any gap at the femur-cartilage boundary. b) The non-manifold assembly technique superimposed the accurately-identified femur with the overestimated cartilage image to remove overlaps between the femur and cartilage, creating a common boundary between the adjacent femur and cartilage surfaces. c) 3D view of femur with cartilage before non-manifold algorithm. d) 3D view of femur with cartilage after non-manifold algorithm .....	73

Figure 3.11: Solid 3D geometry of the full knee assembly. a) anterior view; b) cross sectional view.....	74
Figure 3.12: Model preparation for hexagonal meshing a) A 3D spline was created near the edge of the cartilage surface. b) The 3D spline was used to truncate the very thin edge to produce a finite thickness that would accommodate hexahedral elements. ....	75
Figure 3.13: 3D model of the femur a) before and b) after virtual topology technique .....	75
Figure 3.14: Planes to generate even partitions and mesh distribution within soft tissues (e.g. tibial cartilage). Each grid represents a partition of the tissue. ....	76
Figure 3.15: Element validity check to obtain high-quality elements, using the “verify mesh” tool .....	77
Figure 3.16: Finite element mesh of the knee a) anterior view and b) posterior view .....	79
Figure 3.17: Hourglassing between the femoral and tibial cartilage contact.....	79
Figure 3.18: Femoral and tibial axes to represent the knee joint coordinate system. $e_1$ = a line connecting the femoral epicondyles, represented by points 8 and 9; $e_3$ = a line connecting the $e_1$ bisection and most distal posterior tibia (point 7); $e_2$ = cross product of $e_1$ and $e_3$ .....	81
Figure 3.19: Equations to calculate the femoral embedded frame.....	82
Figure 3.20: Equations to calculate the tibial embedded frame .....	83
Figure 3.21: Position of tibial and femoral embedded frames .....	84
Figure 3.22: Position of the knee joint coordinate system axes.....	85
Figure 3.23: Boundary conditions, showing contact pairs between (1.) femur – femoral cartilage, (2.) femoral cartilage – tibial cartilage, (3.) femur – LCL, (4.) femoral cartilage – meniscus, (5.) tibia – fibula.....	94
Figure 3.24: Meniscal attachment with the tibia and the MCL; a) posterior view and b) anterior view .....	95
Figure 3.25: Meniscus movement when the meniscus a) was not attached at peripheral borders and b) was attached at peripheral borders. Note the amount of exposed posterior medial tibial cartilage when the meniscus was not attached. ....	95
Figure 3.26: Steps sequence used in Abaqus for analysis.....	96

Figure 3.27: Setting up boundary conditions for the femur .....	97
Figure 3.28: Creating boundary conditions for tibia.....	98
Figure 3.29: Loading conditions on the FE knee joint model.....	100
Figure 3.30: Cadaveric knee a) with Taylor Spatial Frame for subsequent simulations of malalignment; b, c) mounted on a six degree-of-freedom robot for controlled loading (Courtesy of Hospital for Special Surgery, New York).....	101
Figure 3.31: Specification of the transducer .....	102
Figure 3.32: Tekscan IScan sensor equilibration .....	103
Figure 3.33: Sensors fixed <i>in vitro</i> between the tibial cartilage and the femur. Note: A different specimen from that used in this study is depicted to show the positioning of the Tekscan sensor.....	103
Figure 3.34: Rotation angles during the gait cycle of level walking. The dashed line represents the end of weight acceptance. ....	105
Figure 3.35: Knee joint forces during the gait cycle of level walking. The dashed line represents the end of weight acceptance. ....	106
Figure 3.36: Knee joint moments during the gait cycle of level walking. The dashed line represents the end of weight acceptance. ....	106
Figure 3.37: 2D scheme of the malaligned lower limb to determine the mechanical axis deviation (MAD) for various alignments; where $\alpha$ = angle of alignment; $l_f$ = length of femur (femoral mechanical axis FM); $l_t$ = length of tibia (tibial mechanical axis TM); and $\beta$ = angle between the mechanical axis and the femur. ....	109
Figure 3.38: Knee joint with virtually extended tibia .....	112
Figure 3.39: FE tibia (pink) shows similar alignment with CT scan (blue) for both the coronal (left) and sagittal (right) plane views. ....	113
Figure 3.40: Extended tibia with the knee joint CS and the projected distal CS. ....	114
Figure 3.41: Rotation of the tibial extension during the load application step. ....	119
Figure 3.42: Knee joint with a) 16° varus alignment and b) 14° valgus alignment. ....	120
Figure 3.43: Static equilibrium; Where $F_{MCL}$ = Force in the MCL; $F_{LCL}$ = Force in the LCL; $F_{ACL}$ = Force in the ACL; $F_{PCL}$ = Force in the PCL; $F_M$ = Force in the medial compartment of the knee joint; $F_L$ = Force in the lateral compartment of the knee joint; $F_{med/lat}$ = Medial/lateral force from gait analysis; $F_{axial}$ = Axial force from gait	

analysis; $M_{ext}$ = varus/valgus moment from gait analysis; $d_{MCL}$ = distance from the centre of the MCL to the centre of the knee; $d_{LCL}$ = distance from the centre of the LCL to the centre of the knee; $d_M$ = distance from the centre of the medial compartment to the centre of the knee; $d_L$ = distance from the centre of the lateral compartment to the centre of the knee .....	123
Figure 4.1: Force distribution for a model with linear mesh elements compared to a model with quadratic mesh elements .....	125
Figure 4.2: Peak contact pressure for a model with linear mesh elements compared to a model with quadratic mesh elements .....	126
Figure 4.3: Contact pressure area a) model with linear mesh elements b) model with quadratic mesh elements .....	127
Figure 4.4: Peak maximum compressive stress for a model with linear mesh elements compared to a model with quadratic mesh elements .....	128
Figure 4.5: Maximum compressive stress area for a) model with linear mesh elements compared to b) model with quadratic mesh elements.....	129
Figure 4.6: Peak maximum shear stress for a model with linear mesh elements compared to a model with quadratic mesh elements .....	130
Figure 4.7: Maximum shear stress area for a) model with linear mesh elements compared to b) model with quadratic mesh elements.....	131
Figure 4.8: Effect of bone material properties on medial peak joint pressure .....	134
Figure 4.9: Effect of bone material properties on medial tibial cartilage loading ...	135
Figure 4.10: Effect of cartilage material properties on medial peak joint pressure .	135
Figure 4.11: Effect of cartilage material properties on medial tibial cartilage loading .....	136
Figure 4.12: Effect of meniscus material properties on medial peak joint pressure	136
Figure 4.13: Effect of meniscus material properties on medial tibial cartilage loading .....	137
Figure 4.14: The ligament tuning process: the ligament properties were adjusted in an iterative process until the kinematics of the tibia relative to the femur in the model closely matched those <i>in vitro</i> in all six degrees of freedom for a) translational and b) rotational kinematics during a sagittal rotation from full extension to 65° flexion (Source: Mootanah et al., 2014).....	139

Figure 4.15: The ligament tuning process: the ligament properties were adjusted in an iterative process until the kinematics of the tibia relative to the femur in the model closely matched those <i>in vitro</i> in all six degrees of freedom for a) translational and b) rotational kinematics during 0–12 Nm valgus / varus bending moments.....	140
Figure 4.16: Material properties for the lateral collateral ligament (LCL), medial collateral ligament (MCL), anterior cruciate ligament (ACL) and posterior cruciate ligament (PCL) at every angle of flexion, following the ligament tuning process. (Source: Mootanah et al., 2014).....	142
Figure 4.17: Evaluation of finite element (FE) model. Pressure distributions in the tibiofemoral joint in response to a 374 N axial load and a 15 Nm varus / valgus bending moment for a) <i>in vitro</i> testing and b) FE model predictions; A=Anterior, P=Posterior, L=Lateral, M=Medial (Source: Mootanah et al., 2014).....	144
Figure 4.18: <i>In vitro</i> and FE predicted medial and lateral compartment loading in response to a 374 N axial load and 0 to 15 Nm varus and valgus bending moments for a) normalised peak pressure and b) normalised force .....	145
Figure 4.19: <i>In vitro</i> and FE predicted forces in the medial and lateral compartments as percentages of the total axial force during 0 to 15 Nm varus and valgus bending moments .....	148
Figure 4.20: Tibiofemoral compartment contact forces during the end of weight acceptance for different alignments. ....	151
Figure 4.21: Medial to lateral force ratio for each alignment with the corresponding MAD and HKA angle .....	152
Figure 4.22: Peak contact pressure in the tibial-femoral compartments during the end of weight acceptance for different alignments .....	155
Figure 4.23: Peak maximum compressive stress in the tibial-femoral compartments during the end of weight acceptance for different alignments .....	155
Figure 4.24: Peak maximum shear stress in the tibial-femoral compartments during the end of weight acceptance for different alignments .....	156
Figure 4.25: Percent of medial tibial cartilage volume below a threshold of maximum compressive stress.....	159
Figure 4.26: Percent of medial femoral cartilage volume below a threshold of maximum compressive stress.....	159
Figure 4.27: Percent of medial tibial cartilage volume below a threshold of maximum shear stress. ....	160

Figure 4.28: Percent of medial femoral cartilage volume below a threshold of maximum shear stress. ....	160
Figure 4.29: Percent of lateral tibial cartilage volume below a threshold of maximum compressive stress. ....	161
Figure 4.30: Percent of lateral femoral cartilage volume below a threshold of maximum compressive stress. ....	161
Figure 4.31: Percent of lateral tibial cartilage volume below a threshold of maximum shear stress. ....	162
Figure 4.32: Percent of lateral femoral cartilage volume below a threshold of maximum shear stress. ....	162
Figure 4.33: Contact area in the tibial-femoral compartments during the end of weight acceptance for different alignments .....	164
Figure 5.1: Illustration of the ground reaction vector (blue) and the mechanical axis of the lower limb (red) during the end of weight acceptance in walking .....	182
Figure 6.1: Simulated tri-planar osteotomy a) frontal plane view and b) sagittal plane view. Blue tibia= well aligned knee; Green tibia= knee with 5° malalignment in the sagittal and coronal planes .....	203



## List of Tables

Table 2.1: Function of the knee ligaments (Woo et al., 1999; Nordin and Frankel, 2001; Amis et al., 2003; Woo et al., 2006; Robinson et al., 2006) .....	9
Table 2.2: Kellgren and Lawrence classification of Osteoarthritis.....	17
Table 2.3: Recommended postsurgical knee alignment after HTO .....	27
Table 2.4: Summary of survival rates of HTO.....	32
Table 3.1: Aspect ratio of tibial and femoral cartilage and menisci .....	78
Table 3.2: Final mesh sizes for the knee assembly .....	78
Table 3.3: The root mean square and percent full scale error between FE models with and without hourglass control .....	80
Table 3.4: Coordinates of the five bony landmarks used to create the joint coordinate system.....	85
Table 3.5: Range of properties applied to the FE model for each tissue .....	87
Table 3.6: Loading conditions of the knee model at the end of weight acceptance during walking applied to knee coordinate system. ....	107
Table 3.7: MAD for different alignments for a person with a tibial length of 395 mm and a femoral length of 432 mm .....	111
Table 3.8: Forces and moments acting in the knee joint CS (left) at the end of weight acceptance during level walking acquired from inverse dynamics. Corresponding forces and moments after transformation to the distal tibial CS (right).....	117
Table 3.9: The root mean square and percent full scale error between cortical and cortical/cancellous bone material properties for the tibial shaft. ....	117
Table 3.10: Root means square and percent full scale error between the model with the short and longer tibias .....	118
Table 3.11: Knee adduction moments applied to the knee joint due to varus (positive) and valgus (negative) alignments.....	121
Table 4.1: Comparison of force between 4-noded (linear) and 10-noded (quadratic) meshed bones. Step interval 0 represents the initial loading of the knee joint and step interval 10 represents completion of the task.....	125

Table 4.2: Comparison of contact pressure between linear and quadratic meshed bones. Step interval 0 represents the initial loading of the knee joint and step interval 10 represents completion of the task. ....	126
Table 4.3: Comparison of maximum compressive stress between linear and quadratic meshed bones. Step interval 0 represents the initial loading of the knee joint and step interval 10 represents completion of the task. ....	128
Table 4.4: Comparison of maximum shear stress between linear and quadratic meshed bones. Step interval 0 represents the initial loading of the knee joint and step interval 10 represents completion of the task. ....	130
Table 4.5: Mesh sensitivity analysis for element sizes in osseous tissues .....	132
Table 4.6: Mesh sensitivity analysis for element sizes in soft tissues .....	133
Table 4.7: RMSE for each degree of freedom between finite element model predictions and <i>in vitro</i> results .....	141
Table 4.8: Young's modulus values of the medial collateral ligament (MCL), lateral collateral ligament (LCL), anterior cruciate ligament (ACL) and posterior cruciate ligament (PCL) before and after application of varus and valgus bending moments. Linear increments in ligament Young's moduli were applied in the model as bending moments increased from 0 Nm to 15 Nm varus and valgus. ....	142
Table 4.9: Root mean square error (RMSE) and percentage full scale error (FSE) in medial and lateral force and peak pressure values between <i>in vitro</i> and FE results for axial load of 374 N and varus/valgus bending moments ranging from 0 to 15 Nm. Percentage FSE was obtained by expressing the RMSE as a percentage of the maximum corresponding value. ....	146
Table 4.10: Static equilibrium for the validation of the subject-specific FE model	150
Table 4.11: Different load ratios with their corresponding mechanical axis deviation (MAD), hip-knee-ankle (HKA) angle and the point where the mechanical axis of the lower limb (MA) intersects with the tibial plateau. FM = mechanical axis of the femur; TM = mechanical axis of the tibia. ....	153
Table 4.12: Peak contact pressure and stress for the intact knee joint .....	154
Table 4.13: Peak pressure and stress values for different correction targets .....	157
Table 4.14: Pearson product-moment correlation coefficients between knee joint contact mechanics and joint geometry (MAD) .....	165
Table 4.15: Static equilibrium for the analysis of different alignment simulations.	166

Table 5.1: Summary of FE-model validations in the literature.....	176
Table 5.2: Movement data for posture (Courtesy of Dr Hillstrom, Leon Root MD, Motion Analysis Lab, Hospital for Special Surgery, New York) .....	181
Table 5.3: Summary of lowest and highest targets from literature with their equivalent mechanical axis deviation, hip-knee-ankle angle and the point where the mechanical axis of the lower limb intersects the tibial plateau.....	187
Table 5.4: Results of Reinbolt et al.'s (2008) study. The percent increase of peak knee adduction moment with the corresponding HKA angle. ....	190
Table 5.5: Summary of results obtained by Yang et al. (2010) .....	191
Table 5.6: Results of McKellop et al.'s (1991) study in comparison to the current investigation. Peak maximum pressure in the medial and lateral compartments for varus and valgus alignments of the knee.....	193
Table 5.7: Estimated errors during model developement .....	197
Table 6.1: Knee joint contact pressure and force values before and after a 5° varus-anterior tri-planar osteotomy .....	204

## List of Equations

### Equations 1 – 5

Set of equations to calculate the embedded femoral frame.....82

### Equations 6 – 10

Set of equations to calculate the embedded tibial frame.....83

### Equations 11 – 13

Set of equations to calculate the joint coordinate system.....86

### Equations 14 – 17

Set of equations to calculate material properties of the ligaments.....88

### Equation 18

Transformation to calculate the position of the global coordinates with respect to the abaqus coordinates .....91

### Equation 19

Transformation to calculate the origin of the tibia at full extension.....91

### Equation 20

Transformation to calculate the origin of the tibia during motion.....91

### Equation 21

Transformation to calculate the position of the tibia with respect to the femur.....92

### Equation 22

Identity Check.....92

### Equations 23 – 31

Set of equations to calculate the Mechanical Axis Deviation .....110

### Equations 32 – 37

Set of equations to transform forces and moment between coordinate systems.....115

### Equations 38 – 40

Equations for static equilibrium.....122

### Equation 41

Equations for static equilibrium.....164

## Appendices

### Appendix A

A-1	Donor Summary Report.....	242
A-2	Ethics approval from HSS to use cadaver.....	244

### Appendix B

B-1	Sensitivity analyses for model with and without hourglass control.....	245
B-2	Sensitivity analysis for model with a pure cortical tibia and a tibia with cortical and cancellous bone.....	249
B-3	Sensitivity analysis for model with a short and long tibia.....	253

### Appendix C

C-1	Transformation matrices.....	257
-----	------------------------------	-----

### Appendix D

D-1	Matlab file.....	261
-----	------------------	-----

### Appendix E

E-1	Numerical results of contact force.....	265
E-2	Numerical results of contact pressure.....	265
E-3	Numerical results of maximum compressive stress.....	266
E-4	Numerical results of shear stress.....	266
E-5	Numerical results of contact area.....	267

### Appendix F

F-1	List of publications.....	268
F-2	List of awards.....	269

## Copyright

“Attention is drawn to the fact that copyright of this thesis rests with

- (i) Anglia Ruskin University for one year and thereafter with
- (ii) Franziska Reisse (Candidates name)

This copy of the thesis has been supplied on condition that anyone who consults it is bound by copyright.”

## Abbreviations

%FSE	Percentage Full Scale Error
2D	Two-Dimensional
3D	Three-Dimensional
ACL	Anterior Cruciate Ligament
AP	Anterior-Posterior
BMI	Body Mass Index
BW	Body Weight
CAD	Computer Aided Design
CL	Coronary Ligaments
CS	Coordinate System
CT	Computer Tomography
CWO	Closing Wedge Osteotomy
DOF	Degree of Freedom
E	Modulus of Elasticity
FE	Finite Element
FEA	Finite Element Analysis
FM	Femoral Mechanical Axis
GPa	Giga Pascal
GR	Ground Reaction
HKA	Hip-Knee-Ankle
HSS	Hospital for Special Surgery
Ht	Height
HTO	High Tibial Osteotomy

KAM	Knee Adduction Moment
LCL	Lateral Collateral Ligament
MA	Mechanical Axis of the Lower Limb
MAD	Mechanical Axis Deviation
MCL	Medial Collateral Ligament
MPa	Mega Pascal
MRI	Magnetic Resonance Imaging
N	Newton
OA	Osteoarthritis
OWO	Opening Wedge Osteotomy
PA	Posterior-Anterior
PCL	Posterior Cruciate Ligament
RMSE	Root Mean Square Error
SPGR	Spoiled Gradient Recalled Echo
TKA	Total Knee Arthroplasty
TE	Echo Time of MRI
TM	Tibial Mechanical Axis
TR	Repetition Time of MRI
UKA	Unicompartmental Knee Arthroplasty
WHO	World Health Organisation



# 1. Introduction

The knee joint (Figure 1.1), located below the centre of gravity of the body, is one of the most heavily loaded joints within the human body. The large range of flexion can generate significant lever arms, which subject the knee to very high moments and contact stress, making it prone to injury.

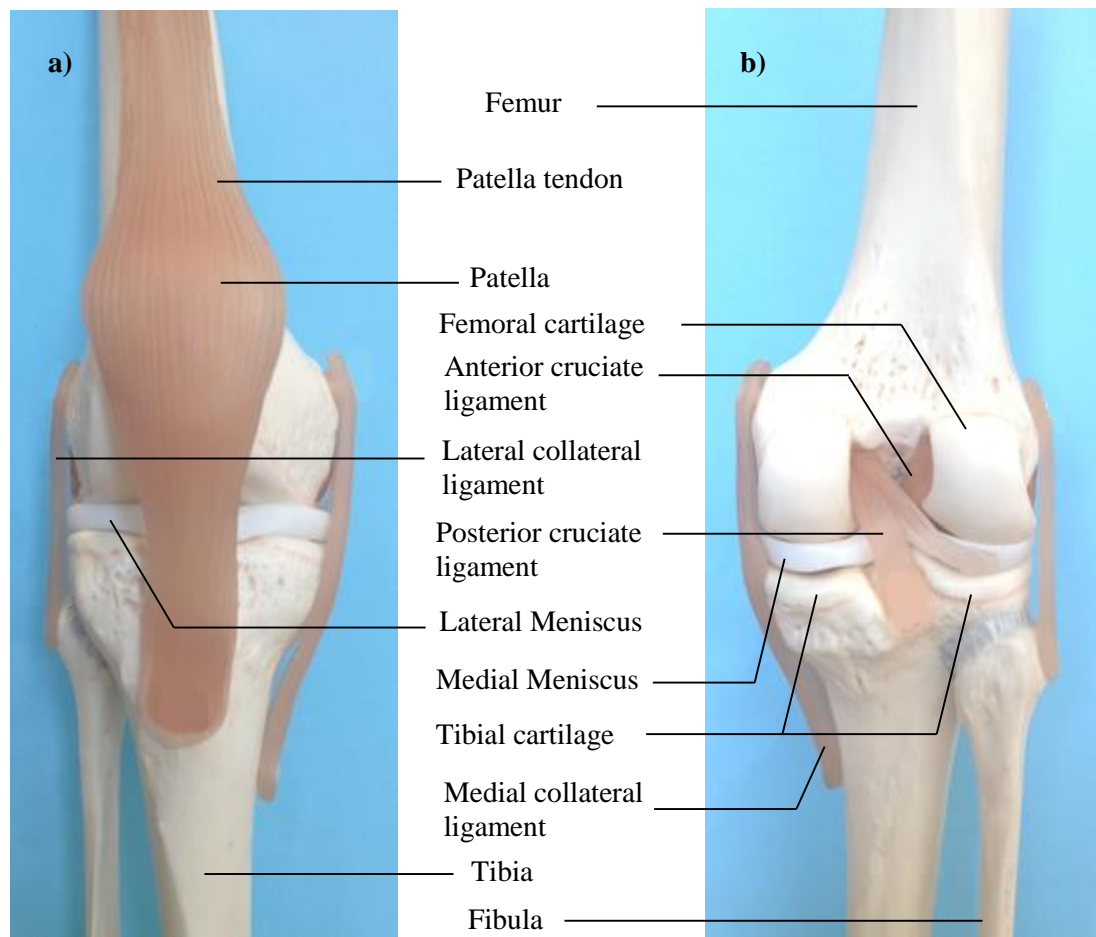


**Figure 1.1: Human knee joint structure: a) anterior view and b) posterior view**

Osteoarthritis (OA) is a debilitating degenerative disease which can affect all the tissues within the diarthrodial joint, often leading to significant pain, loss of joint function and diminished quality of life. It occurs when a combination of mechanical wear and biomechanical degradation erodes the articular cartilage. OA is the leading cause of physical disability in the elderly (Vos et al., 2013). The increased activity level of middle-aged and early retirees has increased the incidence of knee OA in younger age groups (Cushnaghan and Dieppe, 1991).

Joint malalignment (Sharma et al., 2001; Sharma et al., 2010), obesity (Messier, 2008) and tissue injury (Lo et al., 2009; Stein et al., 2011; Potter et al., 2012) are primary biomechanical factors associated with the onset and progression of OA (Englund, 2010). As little as 5° of varus malalignment ("bow-legged") increases the compressive loading in the medial compartment from 70% to 90% (Tetsworth and Paley, 1994). Coventry (1965) explained how such a slight malalignment initiates a 'vicious circle', in which the resulting excessive stress in the joint produces more laxity and joint deformity, thereby repeating the cyclic degradation process (Coventry, 1965). This intense increase in compressive loads can lead to a fourfold increase in the odds of medial tibiofemoral OA worsening over 18 months (Sharma et al., 2001).

It is well documented that shear stress is related to cartilage degeneration (Donahue et al., 2002; Andriacchi et al., 2006; Wilson et al., 2006; Peña et al., 2008). Friction in a healthy knee joint is reported to be almost negligible (Scholes et al., 2004). However, an increase in cartilage degeneration will increase the friction experienced within the knee joint. Neu et al. (2010) reported an  $r^2 = 0.99$  between OA severity and the coefficient of friction.

The World Health Organisation (WHO) reported that OA accounted for 1% of total deaths in 2002, and is projected to be one of the ten leading causes of disability adjusted life years (2.5%) in high-income countries in 2015 (Mathers and Loncar, 2005). The reported total cost of OA on the UK economy is estimated at 1% of annual gross national product and \$185.5 billion annually in the United States (Mathers and Loncar, 2005). There is no known cure for OA and current therapeutic approaches cannot arrest or reverse disease progression (Guccione et al., 1994). A lack of knowledge of the natural history of the disease contributes to the slow development of interventions that could effectively target the reduction of OA progression (Sharma et al., 2001).

A middle-aged osteoarthritic patient who is not age-appropriate for a Total Knee Arthroplasty (TKA) may be treated for malalignment with a High Tibial Osteotomy (HTO), which is a surgical realignment technique, used in mild to moderate knee OA patients. HTO is usually performed by surgically opening or closing a wedge shaped region in the medial (or lateral) proximal tibia to correct for the varus (or valgus) deformity associated with medial (or lateral) knee OA.

Surgical reconstruction of the knee joint is a widely accepted treatment for malalignment and pain associated with knee OA. By preserving the natural tissues, HTO is more successful at restoring a normal gait pattern and is more suitable for the younger and more active patient than TKA. However, surgical realignment outcomes by HTO have been unpredictable in comparison to arthroplasty for reasons not known at this time (Dorsey et al., 2006; Esenkaya et al., 2007; Bhatnagar and Jenkyn, 2010). The physical impact of shifting the mechanical axis of the lower limb (MA), which is a line connecting the centre of the hip with the centre of the ankle (Kirane, Zifchock and Hillstrom, 2010), has yet to be clearly validated (Hopkins et al., 2010).

Still, as a realignment surgery, HTO enables the preservation of all the natural tissues of the joint, including bone stock and intra-articular structures, and, hence, has the potential to alleviate the excessive stress that damage the cartilage matrix while delaying the need for TKA. Given that malalignment correction is a three-dimensional (3D) problem, pre-surgical planning should be improved by complementing two-dimensional (2D) radiographic measurements that reflect static postural loading with 3D dynamic loading information (gait), including important activities of daily living (Johnson, Leitzl and Waugh, 1980). While there have been many studies on osteotomy realignment (Zhim et al., 2005; Agneskirchner et al., 2006; Dorsey et al., 2006; Esenkaya et al., 2007), none has optimised the correction and assessed the effects on contact stress in a subject-specific manner.

Computer modelling (Chao, 2003; Reinbolt et al., 2008), cadaveric (Shaw, Dungy and Arsht, 2004) and gait (Wang et al., 1990) investigations have examined the effects of surgery on medial-lateral load distribution in the knee. The mechanical axis deviation (MAD) defines the horizontal distance between the centre of the knee and the MA. However, despite the importance of MAD in the clinical decision making process, none of these approaches has sought to elucidate the relationship between MAD, peak joint stress and compartment forces. Therefore, the overarching purpose of this study was to find the relationship between peak tibiofemoral joint stress, compartment forces and MAD.

## **2.Literature Review**

This chapter provides a detailed summary of previous research on HTO. The anatomy of the knee joint, including articulation and kinetics, is explained in detail to elucidate the importance of joint alignment. Different surgical procedures of treating OA are compared to help the reader appreciate the need for improvement in surgical procedures.

### **2.1. Anatomy of the Knee**

In order to understand the mechanical factors associated with OA and HTO, it is necessary to have a solid understanding of joint anatomy and contact mechanics (Papaioannou et al., 2008). The main task of the knee joint is to allow movement with minimum energy requirements from the muscles and to promote stability for posture and locomotion. Additionally, the knee transmits, absorbs and redistributes forces, stress and moments acting on the structure during activities of daily living (Masouros, Bull and Amis, 2010).

#### **2.1.1. Bones of the Knee Joint**

The knee consists of four bones (femur, tibia, fibula and patella), in addition to a complex network of ligaments and stabilising muscles. The patella is a flat bone embedded anterior to the distal femur (femoral condyles) and consists of uniformly dense trabecular bone (Standring, 2008). The femur is the longest and strongest bone in the human body. Its distal end presents two condyles (medial and lateral) that articulate with the tibia. The femoral shaft is a cylinder of cortical bone with a large medullary cavity. The wall is thick in its middle third, where the femur is narrowest and the medullary cavity most capacious. Proximally and distally, the compact wall becomes progressively thinner and the cavity gradually fills with trabecular bone. The extremities consist of trabecular bone within a thin shell of cortical bone (Standring, 2008).

The tibia is triangular in section and has a cortical bone wall filled with trabecular bone. Like the femur the tibia has a medial and a lateral condyle for articulation. The expanded proximal end of the tibia acts as a bearing surface for body weight, which is

transmitted through the femur. The bones serve as the primary support of the knee and provide a rigid structure (Standring, 2008).

According to Wolff's law, bone remodels in the direction of the maximum time-averaged stress. Its exterior shape and internal construction reorganises to best support stress acting upon it. Bone is a minimal-weight structure that is adapted to its applied stress (Frost, 1994). The mechanical properties of bone also vary according to age, weight, gender and nutrition habits (Lesso-Arroyo, et al., 2004).

The areas in a joint that are in contact are called the articulation patches. The medial patch of the knee joint is about a third bigger than the lateral patch because of the greater weight carried through the medial compartment (Walker and Hajek, 1972). Additionally, the medial compartment of the tibia is concave for direct contact with the femur, whereas the lateral compartment is convex (Figure 2.1). The reason for this outline is for medial stability with lateral mobility (De Peretti et al., 1983).

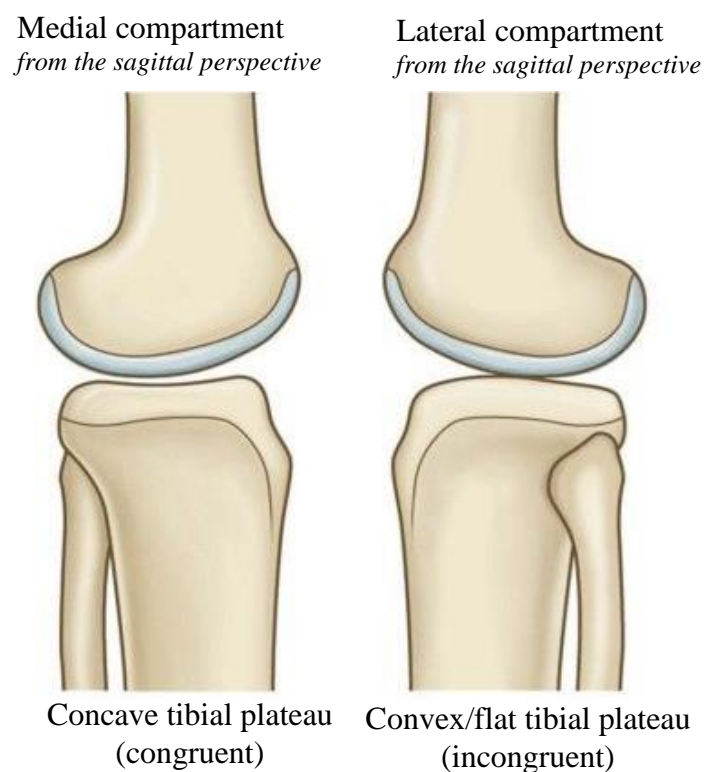


**Figure 2.1: The shape of the tibiofemoral articular surfaces**  
(Source: Standring, 2008; Reprinted with permission)

### 2.1.2. The Cartilage

The ends of articulating bones are covered by a thin cartilage layer, which is an extremely hard and even substance, providing a smooth sliding and uniform load transfer from the femur to the tibia. This structure reduces high stress concentrations in the articulating bones.

Articular cartilage is separated into four zones in which the content and structure of the collagen fibrils networks change (Figure 2.2). At the superficial zone, which is the top layer providing a gliding surface, fibrils are oriented horizontally, parallel to the articulating surface (Minns and Steven, 1977). In the transitional zone, collagen fibres are larger and randomly orientated (Broom and Marra, 1986). In the deep zone, the collagen fibres have the largest diameter and are perpendicular to the subchondral bone. Finally, in the calcified zone, which is the layer in contact with the subchondral bone, the fibrils turn perpendicular to the bone–cartilage interface, providing a firm anchor (Minns and Steven, 1977). The calcified zone is approximately 5% of the cartilage thickness (Fox, Bedi and Rodeo, 2009).

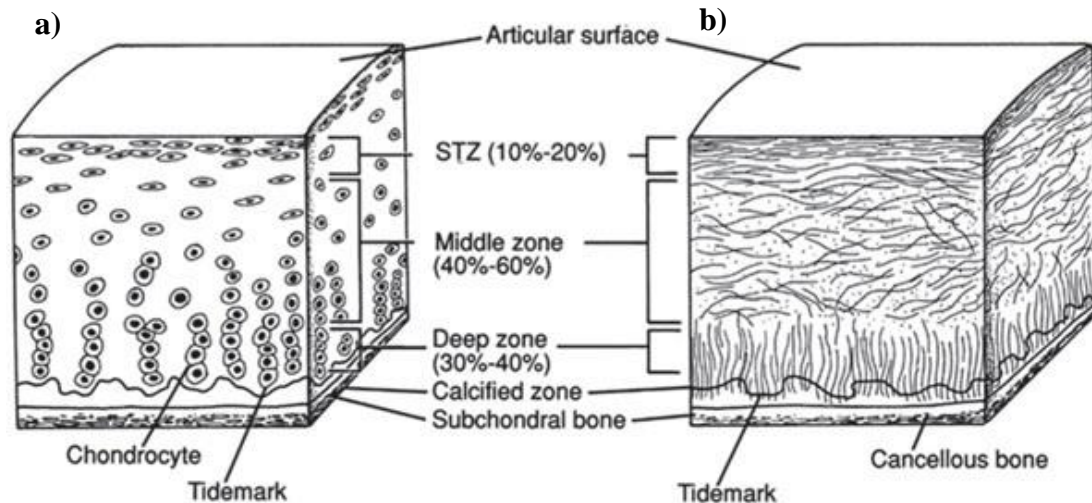


**Figure 2.2: Articular cartilage (a) chondrocyte and (b) collagen fibre organisation in articular cartilage** From A.J. Steward, Y. Liu, and D.R. Wagner, “Engineering Cell Attachments to Scaffolds in Cartilage Tissue Engineering,” in JOM, Volume 63, Issue 4, April 2011, p. 75, Figure A. Copyright © 2011 by The Minerals, Metals & Materials Society. Reprinted with permission.

Shirazi et al. (2008) concluded in their study that the vertical fibrils play a crucial role in stiffening and protecting articular cartilage from large tensile/shear strains, in particular at the subchondral junction where peak strains occur. Superficial horizontal fibrils, on the other hand, protect the tissue mainly from excessive strains at the superficial layers (Shirazi and Shirazi-Adl, 2008).

The medial and lateral plateaus of the tibia are covered by articulating cartilage. Cartilage is not found on the intercondylar area, where the cruciate ligaments and the horns of the menisci are attached. On the femur, the areas for articulation with the tibia and the meniscus are joined to form a large area of articular cartilage (Figure 2.3).

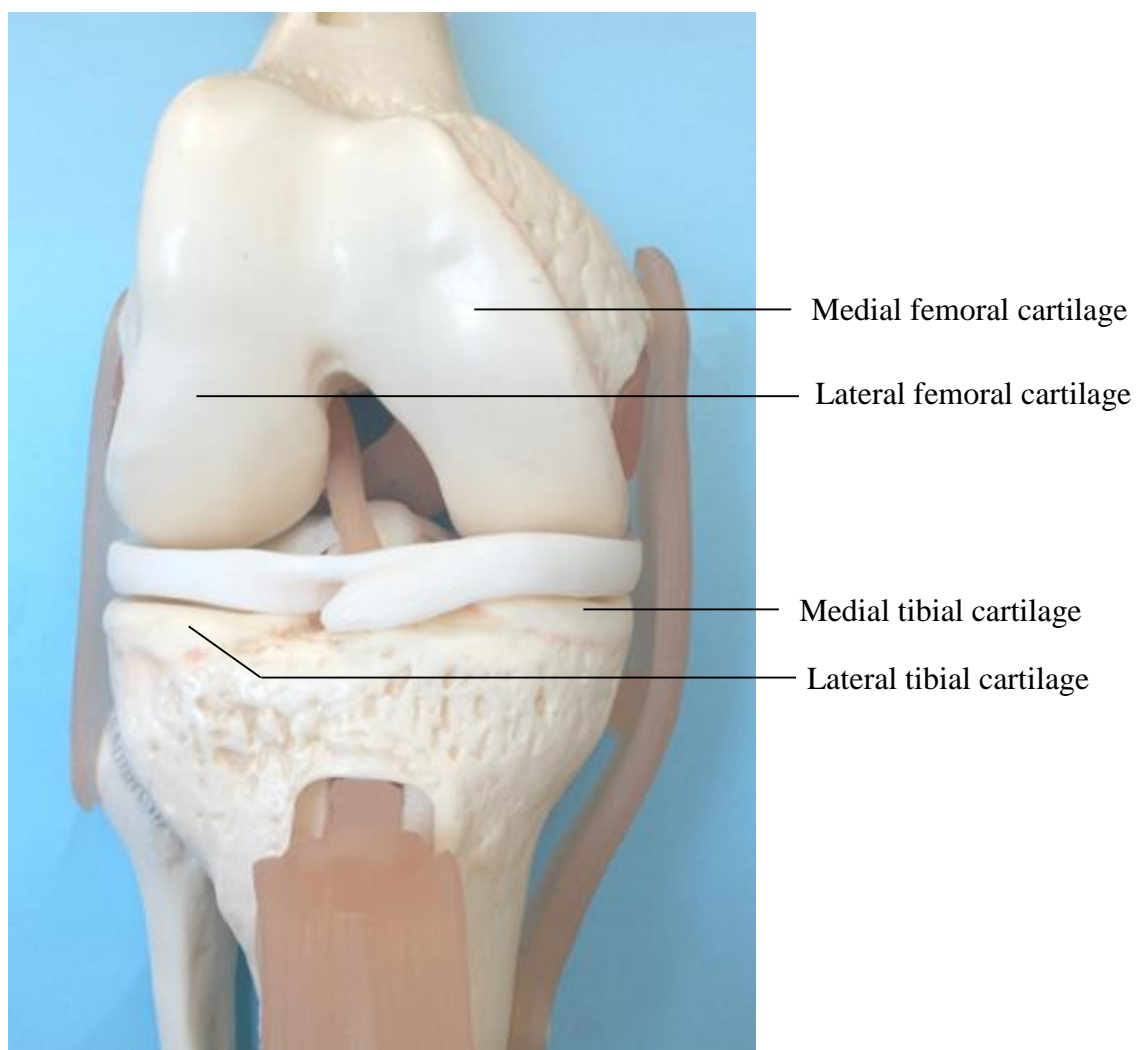


**Figure2.3: Cartilage structure from the anterior perspective**

### 2.1.3. Meniscal Structure

The meniscal structure (Figure 2.4) is another element within the knee that has important functions. It is divided into two dense fibrous semi-circular soft structures with a wedge-shaped cross section. The meniscal structures are attached to the tibia through the horn and coronary ligaments (Standring, 2008).

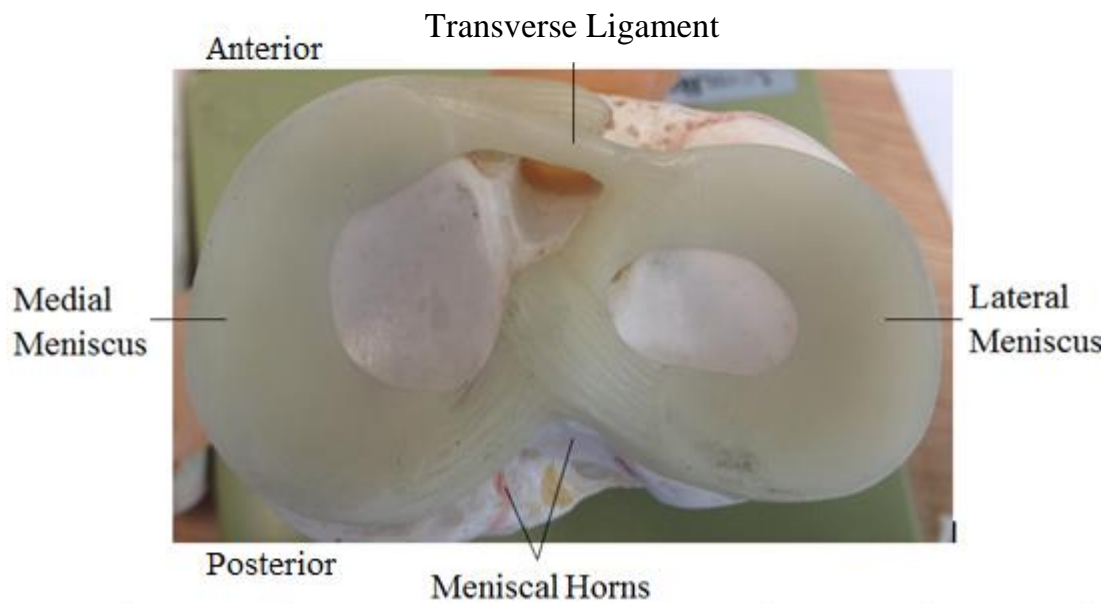


**Figure 2.4: Meniscal structure from the axial perspective**

The inner portion of the meniscus is suited to resisting compressive forces, while the periphery is capable of resisting tensional forces, thereby distributing the load across the tibiofemoral joint (Andrews, Shrive and Ronsky, 2011). However, with ageing and degeneration, compositional changes occur within the menisci, reducing their ability to resist the forces generated in motion.

Fukubayashi and Kurosawa (1980) conducted a pressure distribution study and concluded that the menisci carried a significant portion of the total load applied. Thus, after removal of the menisci, high loads act upon a small area of cartilage, increasing stress, leading to degeneration of the cartilage structure (Fukubayashi and Kurosawa, 1980).



#### 2.1.4. Ligaments of the Knee Joint

To maintain stability throughout the complex range of motion of the knee, there are four different primary ligaments, which are connective tissues that bind the bones in positions of extreme stress (Yang, Nayeb-Hashemi and Canavan, 2007). The anterior cruciate ligament (ACL) connects the anterior proximal end of the tibia to the posterior distal aspect of the femur. The posterior cruciate ligament (PCL) connects the posterior proximal surface of the tibia to the anterior distal surface of the femur. The medial collateral ligament (MCL) stabilises the inner surfaces of the distal femur to the proximal tibia. The lateral collateral ligament (LCL) stabilises the outer surface of the distal femur to the proximal fibula (Table 2.1). Both collateral ligaments are tight during extension and relatively loose during flexion (Standring, 2008). All four ligaments are capable of sustaining finite strains and rotations without causing damage to their structure.

**Table 2.1: Function of the knee ligaments (Woo et al., 1999; Nordin and Frankel, 2001; Amis et al., 2003; Woo et al., 2006; Robinson et al., 2006)**

Ligament	Function
MCL	Primary restraint to valgus at all angles and internal rotation during flexion
LCL	Primary restraint to varus rotation. Limits external rotation of the tibia.
ACL	Primary restraint to excessive anterior translation of the tibia or excessive posterior translation of the femur. Most fibres limit full knee extension, preventing hyperextension. Secondary restraint to varus/valgus and internal/external rotation. Controls the screw-home motion of the knee which is a coupled motion of internal rotation during the last 30° of extension.
PCL	Primary restraint to posterior tibial translation of the tibia or excessive anterior translation of the femur. Most fibres become taut at full flexion. Restraining maximal hyperextension and the extremes of varus/valgus and internal/external rotation.

### **2.1.5. Synovial fluid**

The load bearing structures of the knee move with minimal resistance due to the presence of synovial fluid. This lubricant has a low coefficient of friction which permits the gentle gliding and rotation of the tibial cartilage with respect to the femoral cartilage, especially when forces are high. During weight bearing when a portion of the joint is in contact, synovial fluid is exuded from the cartilage in that region. Once that cartilage is unloaded the synovial fluid is imbibed back into the cartilage. This squeeze film lubrication system in conjunction with the viscoelastic nature of cartilage forms a unique deformable bearing that protects the joint during weight bearing activities (Nordin and Frankel, 2001; Standring, 2008).

### **2.1.6. Musculo-tendonous Structures**

The quadriceps (rectus femoris, vastus lateralis, vastus medialis and vastus intermedius) act to extend the knee through the quadriceps-patellar tendon mechanism. The medial (semitendinosis and semiomembranosus) and lateral (biceps femoris) hamstrings act to flex the knee through their respective tendons with some assistance from the Sartorius, Gastrocnemius, and the Plantaris muscles (Standring, 2008). In addition, the iliotibial band crosses the lateral aspect of the hip and knee acting as a counterbalance to the knee adduction moment, providing lateral stabilisation (Inman, 1947).

In conclusion, the human knee joint structure, consisting of components including menisci, cartilage, ligaments, and muscle forces, as well as synovial fluid, enable the knee to carry out activities of daily living and allow complex mechanical responses to different types of physiological loads. Each structure has a particular function maintaining knee stability in more than one degree of freedom (DOF).

## **2.2. Kinematics**

Kinematics is the quantitative study of motion and is usually measured in linear (metres and feet) and angular (radians and degree) units. Although the knee joint possesses six DOF (Figure 2.5), the dominant motions are flexion-extension, internal-external rotation and anterior-posterior translation. Varus-valgus rotations, medial-lateral translations and compression-distraction are smaller motions typically

restrained by ligaments. Valgus rotation, also called abduction, is the motion of a segment away from the midline in the frontal plane. Varus rotation, also called adduction, is the movement back towards the midline. The knee is locked at full extension, allowing the leg to support the body weight like a simple strut when standing still, without requiring any muscular activity (Standring, 2008).

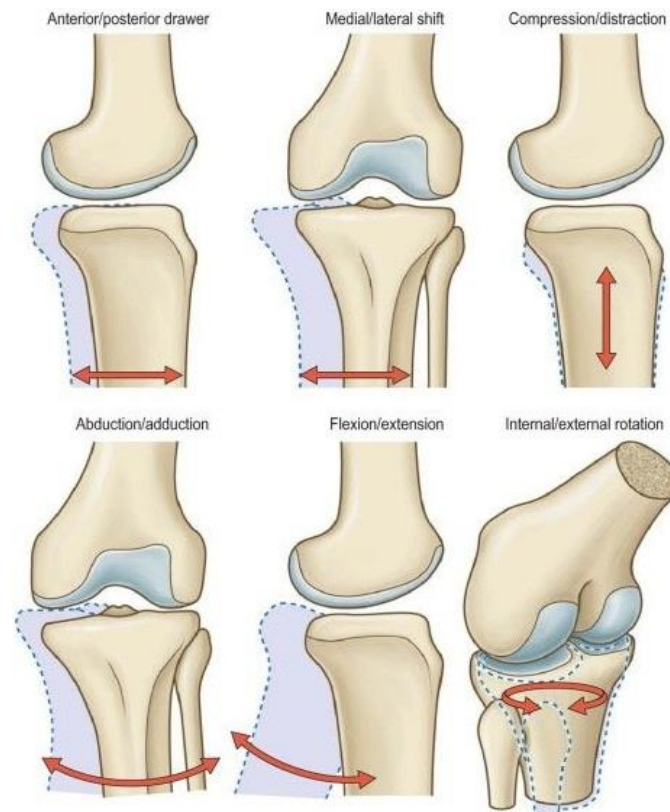


**Figure 2.5: Knee joint motions in six degrees of freedom**  
(Source: Standring, 2008; Reprinted with permission)

Active or physiological movements of the joint happen voluntarily such as flexion-extension and medial-lateral rotation. Coupled movements happen in combination with other movements due to the underlying anatomy and corresponding mechanics of the joint. As the knee extends, there is a gradual coupled lateral rotation of the tibia on the femur because the medial femoral epicondyle is typically 1.7 cm longer than the lateral (Standring, 2008). This coupled motion at the knee is called the screw-home mechanism (Nordin and Frankel, 2001). If the foot is fixed, as in the stance phase of walking, the femur rotates internally on the tibia.

### 2.2.1. The Gait Cycle

The gait cycle (Figure 2.6) is the most frequent human movement and is defined by the function achieved of one limb during gait (Perry and Davids, 1992). It is divided into stance and swing phase. The stance phase, where the foot is in contact with the ground, is subdivided into the following five events; heel strike, flat foot, midstance, heel off and toe off. Heel strike is typically the first contact of the foot with the ground and initiates double limb support. The load starts to transfer to the stance limb and is directed upward and posteriorly (Burstein and Wright, 2001). At heel strike the knee is flexed at approximately  $10^\circ$  (Figure 2.7), with all muscles that control the joint being active (co-contraction) for stability. Midstance, also called single limb support, starts with toe off of the opposite foot, where load is transferred to the stance limb (Burstein and Wright, 2001). When body weight transfers over the forefoot of the stance limb, the heel rises and toe off occurs.

As soon as the foot leaves contact with the ground, swing phase commences. Swing phase consists of three sub phases; initial swing, midswing and terminal swing. Initial swing starts with toe-off and lasts till maximum knee flexion when midswing occurs. During swing phase the knee is flexed between  $60^\circ$  and  $75^\circ$  to help prevent the toes from dragging (Standring, 2008; Masouros, Bull and Amis, 2010). As the tibia moves to the vertical position, terminal swing commences until the foot touches the ground and the cycle repeats.

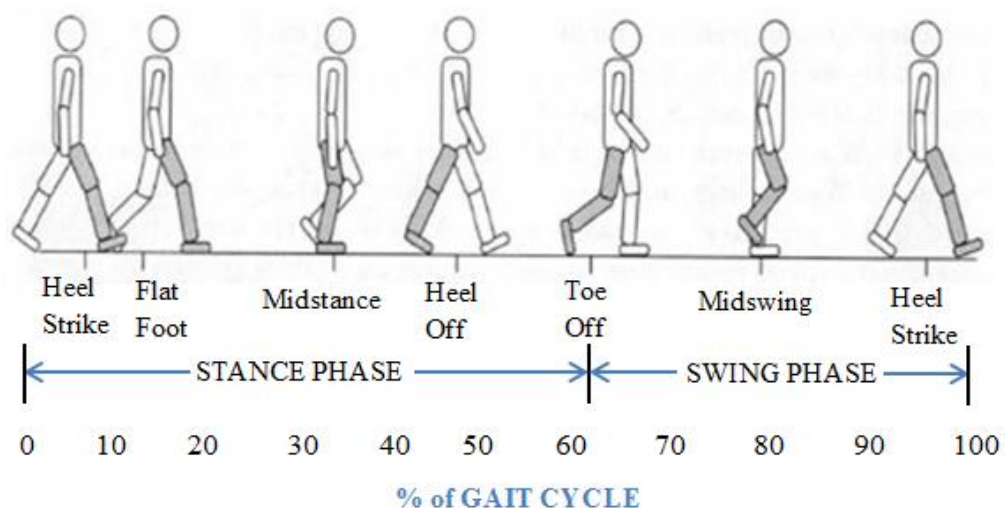
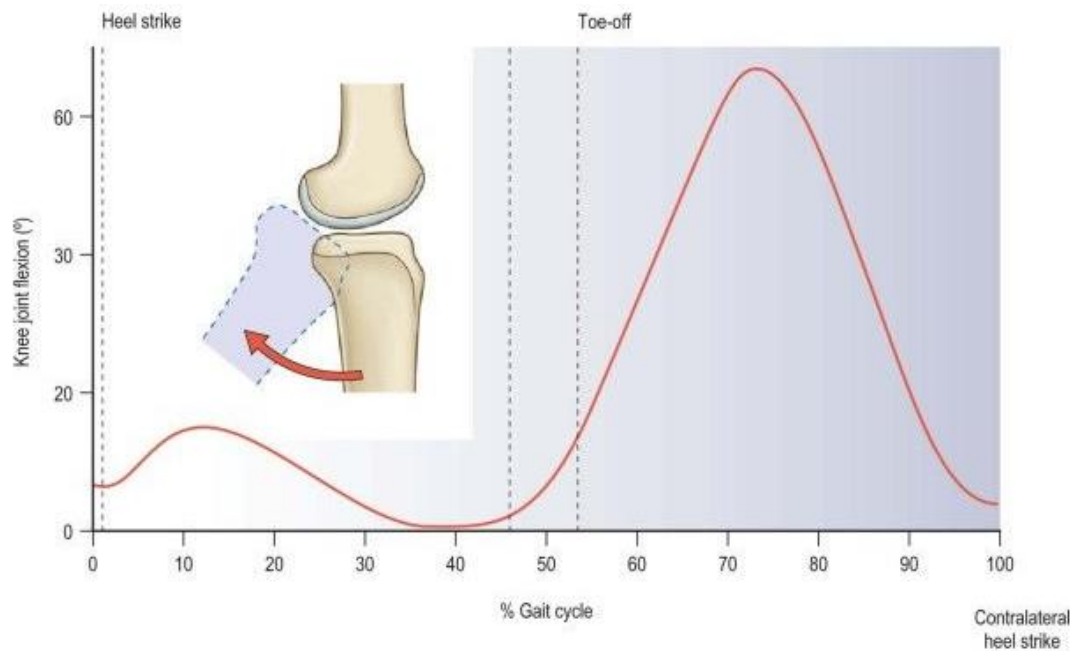


Figure 2.6: The human gait cycle



**Figure 2.7: Knee joint flexion during level walking**  
(Source: Standring, 2008; Reprinted with permission)

### 2.3. Kinetics

Kinetics is the quantitative study of the forces that cause motion (Knudson et al., 2003). The mechanical function of the skeletal joints is to allow motion of the bones while carrying various loads (Burstein and Wright, 2001). In the lower limb the external ground reaction (GR) vector is counteracted by the internal muscle forces around each limb segment. Whenever a force is applied at a distance from the joint centre, a moment occurs (Tanamas et al., 2009). Alternative load transmissions through the joint are generated through ligament forces, which are developed in response to joint motion or external loading. Figures 2.8 and 2.9 demonstrate the normative data of 46 adults between 41-60 years of age during level walking.

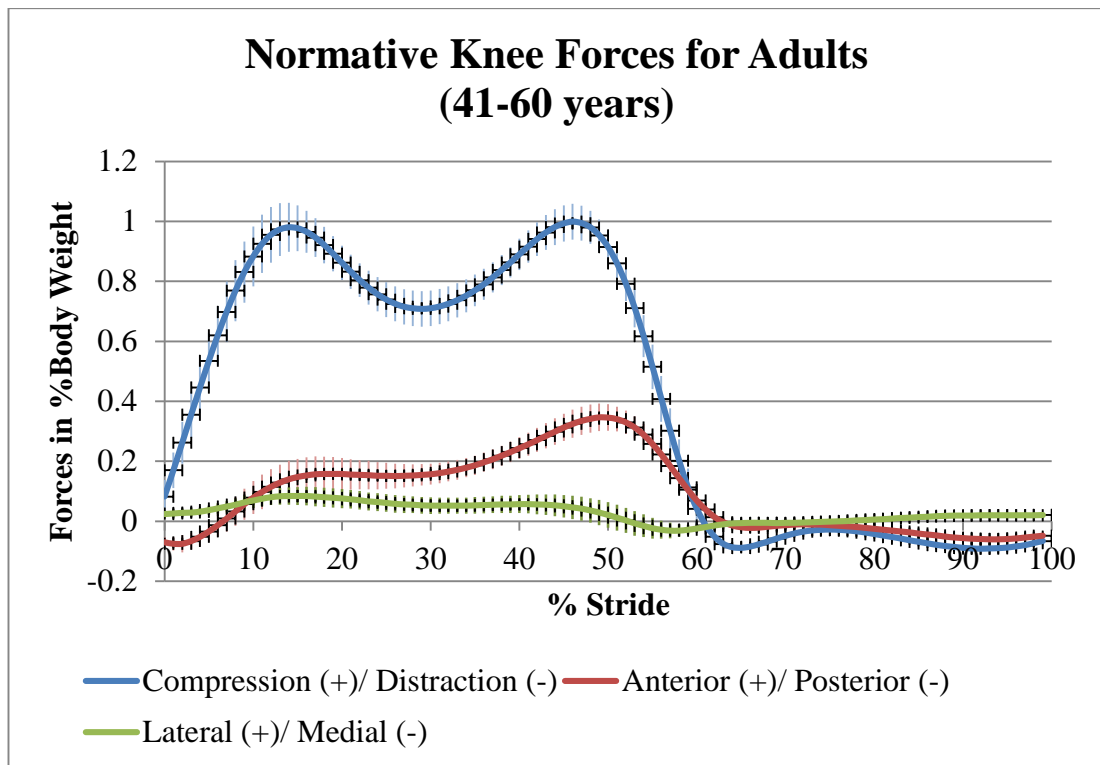


**Figure 2.8: Normative knee forces during level walking**  
 (Courtesy of Dr Hillstrom, Leon Root MD, Motion Analysis Lab, Hospital for Special Surgery, New York, USA)

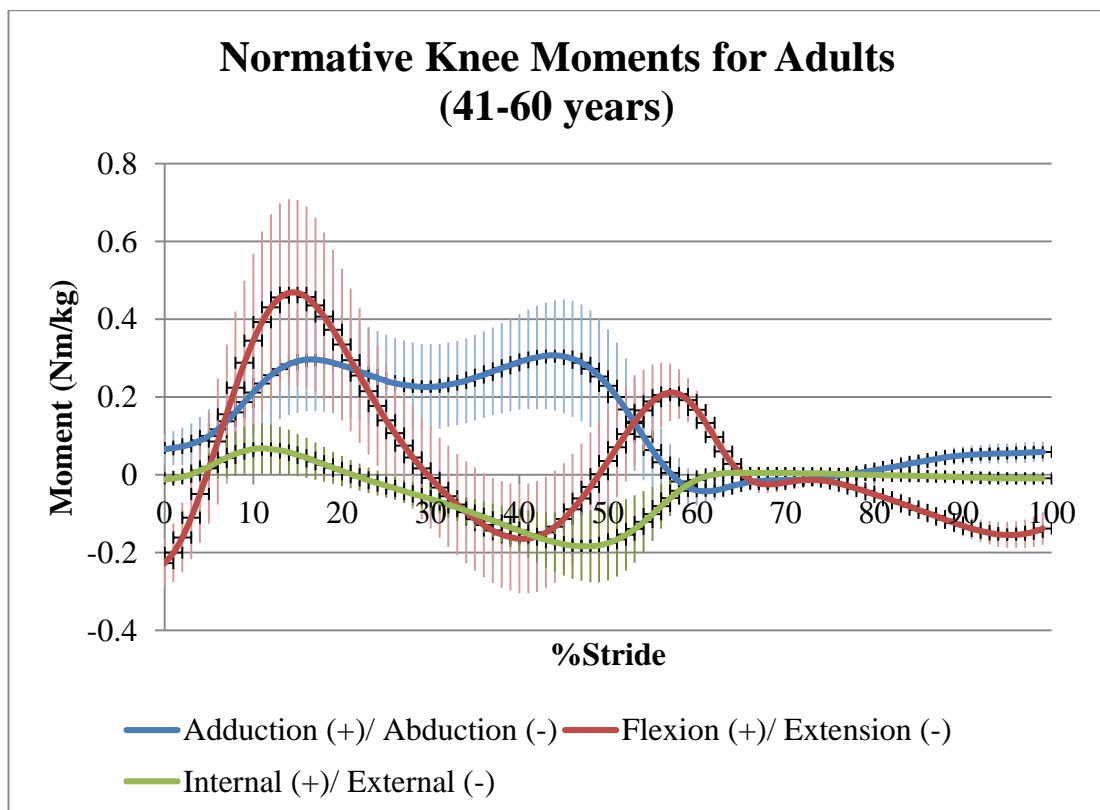


**Figure 2.9: Normative knee moments during level walking**  
 (Courtesy of Dr Hillstrom, Leon Root MD, Motion Analysis Lab, Hospital for Special Surgery, New York, USA)

During level walking, the knee is subjected to two peak loads. The first is due to the large quadriceps tension required when weight transfers from the leg that is pushing off, to the leg that is accepting load after heel strike. The second occurs when the knee and hip are extended, the heel is raised and the forefoot is pushing off (Amis, 2012). The magnitude of knee joint stress depends on, both, joint reaction forces and contact area. Recently, some patients have received instrumented knee prostheses, which were able to measure contact forces and moments acting in the knee joint. Average peak contact forces as a percentage of body weight (BW), were highest during stair descent (346% of BW), followed by stair ascent (316% of BW), level walking (261% of BW), one-legged stance (259% of BW), knee bending (253% of BW), standing up (246% of BW), sitting down (225% of BW) and two-legged stance (107% of BW) (Kutzner et al., 2010).

### **2.3.1. Distribution of Load in the Knee Joint**

Masouros et al. (2010) demonstrated that the adduction moment in the TF joint led to a greater force in the medial condyle than the lateral. This theory is supported by Andriacchi (1994) who found that, in neutral alignment, 60–80% of total compressive load transmitted through the knee was on the medial plateau. In the FE analysis by Perie and Hobatho (1998) the predicted medial pressure was about three times higher than the lateral.

To maintain equilibrium in the varus knee joint, stress on the articular cartilage must be redistributed to counterbalance the additional moment due to malalignment (Chantarapanich et al., 2009). Many studies showed that a shift from neutral alignment increased the load on either the lateral or medial compartment (Bruns, Volkmer and Luessenhop, 1993; Tetsworth and Paley, 1994; Yang, Nayeb-Hashemi and Canavan, 2007). Agneskirchner et al. (2007) studied the medial and lateral compartment pressures before and after HTO in cadavers and concluded that a strong relationship between the medial-to-lateral compartment load ratio and knee alignment existed.

## **2.4. Osteoarthritis**

Knee osteoarthritis is a degenerative disease that involves a gradual worsening of the articular cartilage of the joint which can lead to a total loss of this cartilage. ‘Osteo’ is derived from the Latin word for bone and ‘arthritis’ is derived from the “arthros”

(Greek) meaning joint and “-itis” (Greek) meaning damage and swelling (inflammation) (Arthritis Research UK, 2014). Alterations in the collagen network and a reduction in collagen content take place (Buckwalter and Mankin, 1998; Bi et al., 2006). In combination, these changes decrease the stiffness of the cartilage, thereby weakening its mechanical function. This can further accelerate OA progression (Buckwalter and Mankin, 1998).

Similar to bone, articular cartilage must be exposed to constant loading in order to operate in a healthy manner (Arokoski et al., 2000). However, large strain and stress and repetitive mechanical loading cause irreversible damage, which then lead to cartilage degeneration (Andriacchi et al., 2004). In the degeneration process, the bone beneath the cartilage thickens and grows outwards, forming an overgrowth of new bone over the edges of osteoarthritic joints, which are called osteophytes (Figure 2.10). Additionally, inflammation in the joint occurs and extra fluid is produced, causing it to swell. Gradual muscle weakening creates an unstable environment so that the knee cannot support full body weight and therefore “gives way” under loading.

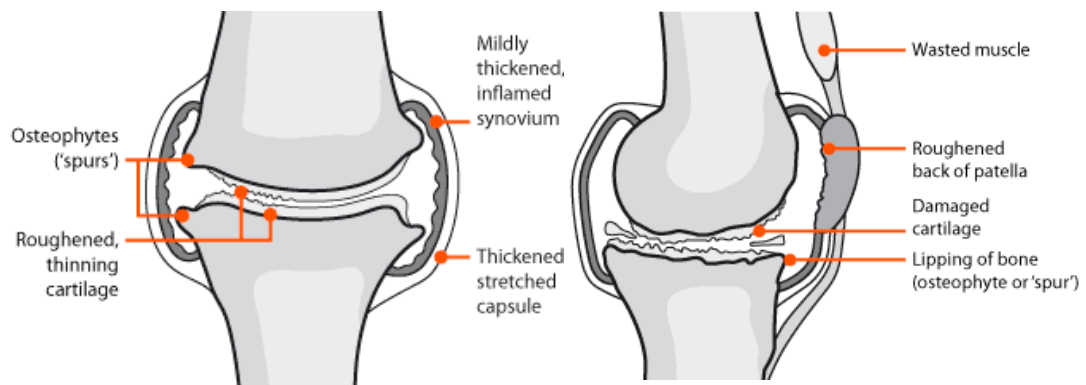


**Figure 2.10: Osteoarthritic knee**  
(Source: Arthritis Research UK, 2014; Reprinted with permission)

#### 2.4.1. Classification of Osteoarthritis

According to Kellgren and Lawrence (1957), there are 5 different stages of OA progression (Table 2.2). It can be concluded that for a grade IV lesion the use of a HTO is questionable because of the complete erosion of cartilage down to exposed subchondral bone (Kellgren and Lawrence, 1957).



**Table 2.2: Kellgren and Lawrence classification of Osteoarthritis**  
(Source: Kellgren and Lawrence, 1957)

<b>Grade</b>	<b>Classification system for OA of the knee</b>
<b>0</b>	Healthy cartilage
<b>I</b>	Softening and swelling of the cartilage
<b>II</b>	Fragmentation and fissuring in an area 0.5 inches (1.27 cm) or less in diameter
<b>III</b>	Fragmentation and fissuring in an area 0.5 inches (1.27 cm) or more in diameter
<b>IV</b>	Erosion of cartilage down to bone

#### **2.4.2. Effects of Osteoarthritis**

With complete cartilage erosion, bone-to-bone contact occurs; the friction of the bone-to-bone contact leads to bone wearing, which, in turn, may cause an alteration in shape. The bones are forced out of their normal alignment, causing deformity and malalignment (Figure 2.11). This abnormal axial alignment induces an eccentric redistribution of normal stress (Hsu et al., 1990), causing the previously-described vicious circle (Coventry, 1965). Greater pressure is exerted on the side of the knee that is clinically involved and the ligaments on the opposite side are stretched (Jackson, Waugh and Green, 1969).

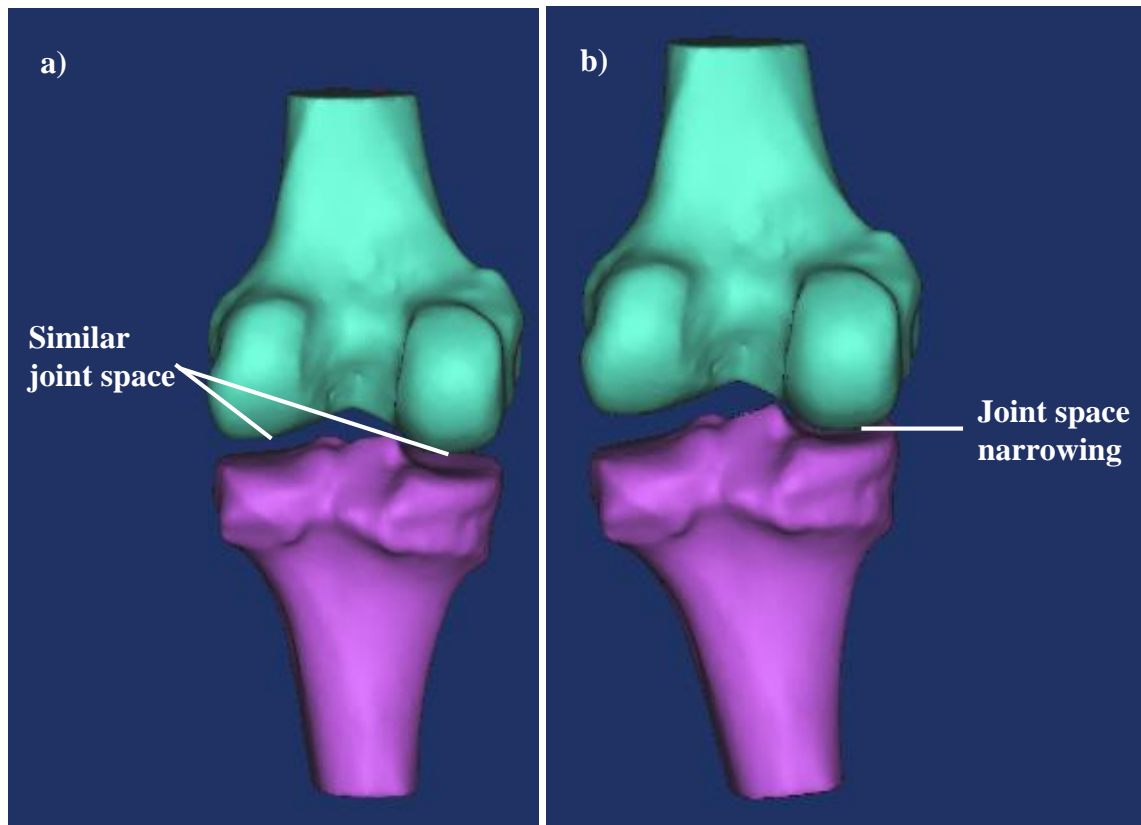


**Figure 2.11: Joint space narrowing for a) healthy knee and b) osteoarthritic knee**

### 2.4.3. Causes of Osteoarthritis

Chao and Sim (1995) stated that, because of its weight-bearing requirement and high mobility, the knee is the most affected peripheral joint in patients with symptomatic OA and is more commonly found on the articular cartilage in the medial compartment (Sharma, Kapoor and Issa, 2006). Other joints which are often affected are the hands, spine, hip joint and big toe joint (Arthritis Research UK, 2014). Various factors seem to increase the risk of OA (Coggon et al., 2000; Zhang et al., 2001; Qing-Yu et al., 2006).

#### *Age*

OA usually starts from the late 40s onwards and becomes most problematic from the late 50s onwards (Arthritis Research UK, 2014). The probability of developing knee OA by the age of 85 is nearly 50% (Murphy et al., 2008). Muscle weakening, bone aging and reduced body healing capacity lead to onset of OA, which then advances to progressive joint deterioration as the bones continue to change physiologically (Cooke, Scudamore and Greer, 2003).

## ***Obesity***

Obesity (BMI- Body Mass Index  $>30 \text{ kg/m}^2$ ) is another important factor influencing the development of knee OA. Prodromos et al. (1985) reported that patients with greater loads at the knee during walking had a higher rate of cartilage degeneration than patients with lower loads. Murphy et al. (2008), who conducted a study among 3068 participants, reported that the lifetime risk of OA is nearly 2 in 3 for obese people.

## ***Knee injury***

Injuries to the knee joint, such as a torn meniscus or ligament after a twisting injury, can also be a cause of OA later in life because in many cases the injured component is removed during surgery. In Murphy et. al.'s study (2008), it was reported that the lifetime risk of symptomatic knee OA is more than 1 in 2 among the patients that had a history of a knee injury.

## ***Limb malalignment***

People with lower limb malalignment are 4 times more likely to develop knee OA due to the higher load on one knee compartment compared to the other (Sharma et al., 2001).

## ***Other factors***

Other factors that cause OA are joint abnormalities such as Perthes' disease, genetic factors and other types of joint disease such as rheumatoid arthritis (Buckwalter, Saltzman and Brown, 2004; Arthritis Research UK, 2014). Patient gender also plays a role, as women are more likely to develop OA than men, especially in knees and hands.

### **2.4.4. Prevalence of Osteoarthritis**

OA is the most frequent joint disorder with a worldwide increase over the past few years. The incidence is still rising along with the advancing age of the general population and its soaring rates of obesity (Floerkemeier et al., 2013). In 1995, 15% of the US population had some degree of OA. By the year 2020, an estimated 18.2% will be affected (Lawrence et al., 1998). In the UK, it is estimated that more than six million people have painful OA of the knee (Arthritis Research UK, 2014). In 1994 it was reported that among adults over 55 years of age, the prevalence of symptomatic

knee OA was one in eight (12.5%) (Tetsworth and Paley, 1994). In 2001, there were an estimated 1.33 - 1.75 million OA patients in England and Wales (Department of Health, 2006). In 2005 radiographic studies of US and European populations showed that 14.1% of men and 22.8% of women over 45 years of age showed symptoms of knee OA (Mathers and Loncar, 2005).

Many experimental investigations have been conducted to examine what type of load and stress cartilage can be exposed to without becoming damaged (Repo and Finlay, 1977; Zhang, et al., 1999; Chen et al., 1999; Clements et al., 2001; Chen et al., 2003; Borrelli Jr et al., 2004). However, to date, it is unclear what type of loading and stress most appropriately describes mechanical failure of cartilage because it is difficult to measure cartilage mechanics *in vivo* (Griffin and Guilak, 2005).

## **2.5. Malalignment of the Knee**

Lower extremity malalignment and the corresponding overloading of specific regions within the joint have been associated with knee OA and are considered to be an important factor for disease onset and progression (Andriacchi et al., 2000; Fregly et al., 2007). Malalignment of the lower limb is defined in various ways and there is no universally-standardised measurement (Cooke, Sled and Scudamore, 2007).

### **2.5.1. Hip-Knee-Ankle Angle**

A common method of defining malalignment is the orientation of the femur to tibia, in terms of their mechanical axes, the femoral mechanical axis (FM) and the tibial mechanical axis (TM) (Figure 2.12). The FM is the axis from the femoral head centre to the centre of the femoral intercondylar notch. The TM runs from the centre of the tibial spine tips to the ankle talus centre (Hsu et al., 1990; Tetsworth and Paley, 1994; Chao et al., 1994). The angle of intersection of these two axes is the hip-knee-ankle (HKA) angle and determines the angular alignment of the knee. This can be varus (bowlegged), valgus (knock-kneed), or neutral (Figure 2.12).

In the neutrally-aligned limb, the HKA angle is 0° and the FM and TM pass through the knee centre (the bisection of the femoral epicondyles). When the lower limb is in varus, the femoral axis passes medially to the ankle and the knee centre is lateral to the MA. In a valgus malalignment, the femoral axis passes laterally to the ankle and the

knee centre is medial to the MA (Prodromos, Andriacchi and Galante, 1985; Cooke, Sled and Scudamore, 2007).

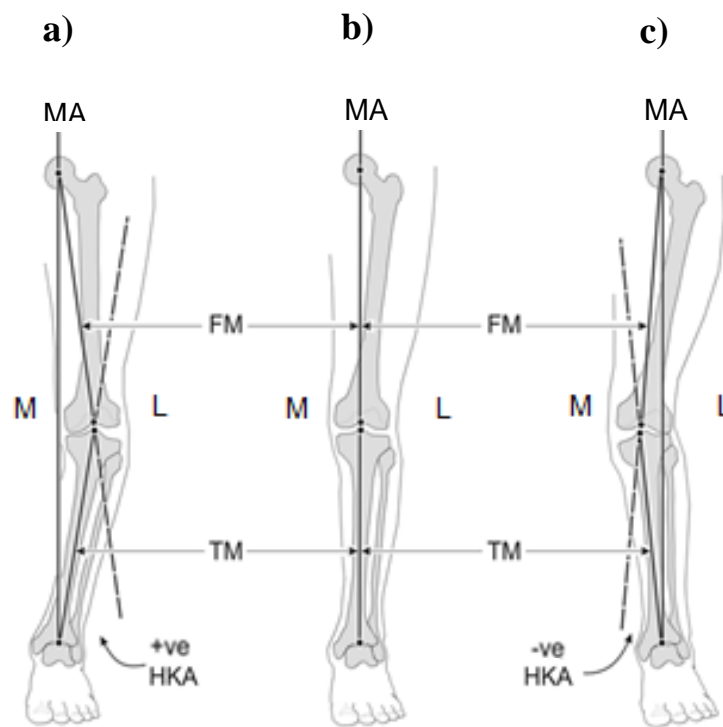


**Figure 2.12: Frontal plane alignment of the knee a) varus b) neutral c) valgus ; MA: mechanical axis of the lower limb; HKA: Hip-knee-ankle angle; FM: Femoral mechanical axis; TM: Tibial mechanical axis; L: Lateral; M: Medial (Source: Cooke, Sled & Scudamore 2007; Reprinted with permission.)**

Cooke et al (1994) employed a quantitative radiographic method to determine frontal plane malalignment in 167 individuals with knee OA. The mean plus one standard deviation ranged from  $12^{\circ}$  for varus to  $12.6^{\circ}$  for valgus in this population (Cooke, Li and Scudamore, 1994).

### 2.5.2. Mechanical Axis Deviation

The mechanical axis deviation (MAD), the horizontal distance between the mechanical axis and the centre of the knee (Figure 2.13), is also used to measure limb alignment. Medial and lateral MADs are referred to as varus or valgus malalignment, respectively.

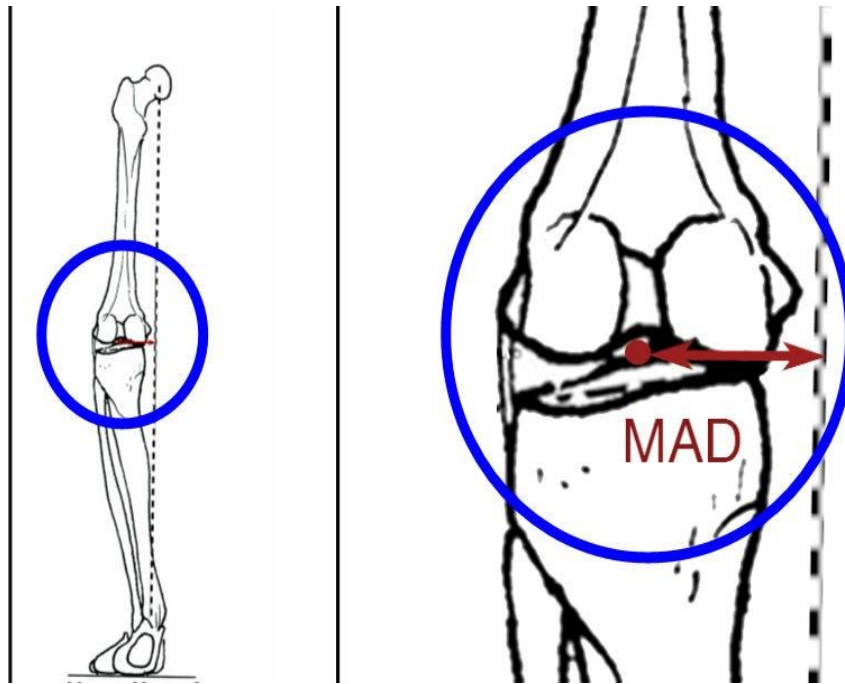


**Figure 2.13: Mechanical axis deviation of the knee joint**  
(Courtesy of the Hospital for Special Surgery, New York)

### 2.5.3. Anatomical Axes

Other authors refer to the angle between the anatomical axes of the femur and the tibia (Brown and Amendola, 2012). The anatomical axis of the femur runs from the piriformis fossa to the centre of the knee and therefore deviates from the mechanical axis (Tetsworth and Paley, 1994). The mechanical and anatomical axes of the tibia are essentially represented by the same line (Tetsworth and Paley, 1994).

Normal alignment is often referred to when the MA passes through the centre of the knee. However, many authors reported that the MA typically passes slightly medial to the knee centre and defined a normal alignment as  $1.2^{\circ} \pm 2.8^{\circ}$  varus for the HKA angle (Insall, Joseph and Msika, 1984; Moreland, Bassett and Hanker, 1987; Hsu et al., 1990; Chao et al., 1994) and about  $6^{\circ} \pm 2^{\circ}$  valgus for the intersection of the two anatomical axes (Insall, Joseph and Msika, 1984; Moreland, Bassett and Hanker, 1987; Chao et al., 1994). However, large standard deviations ( $\pm 2.8^{\circ}$ ) are reported, which suggests that there is substantial variability in knee alignments within the population. Brouwer et al. (2007) found that out of 2664 knees, 1012 (38%) were considered to have normal alignment, 693 (26%) had varus alignment, and 959 (36%) had valgus alignment using the anatomical axes as a reference.

#### 2.5.4. Causes of Malalignment

Some individuals suffer from malalignment indirectly due to OA caused by obesity or joint trauma, whilst others suffer from OA due to malalignment directly. In both cases cartilage damage can be considered a progressive failure which subsequently results in increased malalignment (Chantarapanich et al., 2009). The malalignment maintains a high stress concentration on the articular cartilage and, as a result, the damage continues to grow.

Constitutional varus is another form of malalignment where the patients suffered from a varus alignment since they reached skeletal maturity (Bellemans et al., 2012). In Bellemans et al.'s (2012) investigation, 32% of men and 17% of women had constitutional varus knees with a natural mechanical alignment of  $3^\circ$  varus or more. Constitutional varus has been associated with increased sports activity during growth, increased femoral varus bowing, an increased varus femoral neck-shaft angle and an increased femoral anatomic mechanical angle (Bellemans et al., 2012).

#### 2.5.5. Effects of Malalignment

Lower limb alignment is a fundamental factor for the static and the dynamic loading of the knee joint. Changes in the axial leg alignment can affect knee kinematics, contact forces and overall gait (Kendoff et al., 2008). Hsu et al. (1990) demonstrated that even small modifications of the MA caused significant changes of the load distribution in the knee joint. Individuals with varus alignment are exposed to higher stress in the medial compartment of the knee due to the increased adduction moment that occurs during single-leg support (Figure 2.14).

The external forces and moments ( $F_{\text{knee}}$  and  $M_{\text{add}}$ ) must be balanced by the internal forces ( $F_{\text{med}}$ ,  $F_{\text{lat}}$ ,  $F_{\text{lcl}}$ ,  $F_{\text{mcl}}$ , and  $F_{\text{m}}$ ) in the anatomical structures to maintain static equilibrium. As the knee goes into varus (Figure 2.14b), external adduction moment will increase, which imposes an increase in internal medial compartment force. In response to the varus angulation, force in the LCL will increase to maintain joint stability (Kettelkamp and Chao, 1972; Gross and Hillstrom, 2008; Foroughi, Smith and Vanwanseele, 2009). In the dynamic case, it is known that net forces from inverse dynamics, ligaments forces, and muscular forces act together to produce the total contact force within the joint. Several studies have shown that during walking, for

example, contact forces can be 100% higher than net forces from inverse dynamics (Kutzner et al., 2010; Hillstrom, et al., 2013).

Dowd et al. (2006) confirmed that malalignment as a result of unicompartmental OA increased stress upon the damaged articular cartilage, which in turn led to more joint degeneration or OA. Majima et al. (2000) established that the alignment following surgery directly related to the rate of progression of OA, meaning that a higher valgus correction led to a slower progression of medial compartment arthritis.

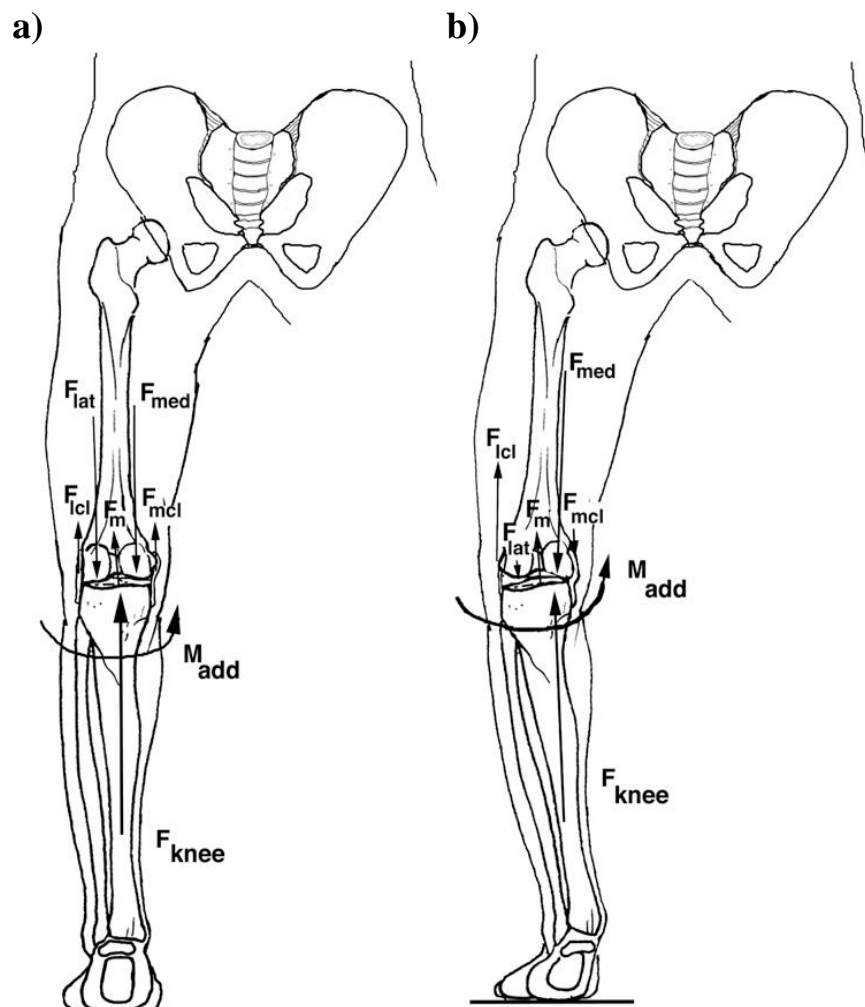


**Figure 2.14: Loading of the knee with a) normal frontal-plane alignment and b) varus, or bowlegged, malalignment; where  $F_{lat}$ = Force in the lateral compartment (internal);  $F_{med}$ = Force in the medial compartment (internal);  $F_{lcl}$ = Force in the lateral collateral ligament (internal);  $F_m$ = Net forces from muscles (internal);  $F_{mcl}$ = Force in the medial collateral ligament (internal);  $M_{add}$ = External knee adduction moment;  $F_{knee}$ = External force acting on the knee. Note: Varus malalignment increases compressive load on the medial tibiofemoral compartment.**

(Reprinted from Rheumatic Disease Clinics of North America, 34 /3, Gross, K.D. & Hillstrom, H.J., Noninvasive Devices Targeting the Mechanics of Osteoarthritis / pages 755-776, Copyright (2008), with permission from Elsevier)



### 2.5.6. Current Surgical Malalignment Corrections and their Outcomes

#### *Intersection of the mechanical axis of the lower limb with the tibial plateau*

The postsurgical knee alignment technique after HTO has been disputed and varies widely in the literature (Table 2.3). The correction target is commonly defined as the intersection between the MA and the tibial plateau at 62% from the medial to the lateral aspects of the knee joint (Fujisawa, Masuhara and Shiomi, 1979). Over- and under-correction may cause an incomplete weight transfer to the opposing compartment and the patient may still experience pain and OA progression (Koshino, Murase and Saito, 2003; Lee and Byun, 2012).

Dugdale et al. (1992) reported that a tolerable correction range was from 50% to 75% of the tibial plateau width, measured from the medial aspect of the joint. The specific amount of correction was also dependent on the tibia and femur lengths. The recommended target HKA angle was 3-5° valgus (Dugdale, Noyes and Styer, 1992). Other authors confirmed these findings. El-Azab et al. (2011), for example, evaluated the accuracy of alignment after HTO and its effect on clinical outcome. The planned correction was for the MA to pass through 62% of the tibial plateau width. The suggested zone for an acceptable correction was between 50% and 70% of the tibial plateau width, measured from the medial aspect of the joint (Miniaci et al., 1989; Niemeyer et al., 2010; El-Azab et al., 2011; Reising et al., 2013).

#### *Anatomical axis angle*

Sprenger et al. (2003) conducted a survival analysis over a period of 22 years. Survival at 10 years was 90% when the anatomical valgus angle at one year was between 8° and 16° (Sprenger and Doerzbacher, 2003). Aglietti et al. (2005) reported that limb alignment did not change after a 2-19 years follow up if the postoperative alignment was between 8° and 14° of valgus for the anatomical angle.

Insall et al. (1984) obtained the best results for knees positioned between 10° to 14° of anatomical valgus postoperatively. Kettelkamp et al. (1972) suggested at least 5° of valgus angulation, while Coventry (1973) recommended a valgus position between 10° and 13°. Later on, Coventry and colleagues defined an anatomic valgus of 8° to be

the optimal correction (Coventry, Ilstrup and Wallrichs, 1993). Koshino et al. (1989) also recommended 8-10° valgus.

### ***Hip-knee-ankle angle***

Hernigou et al. (1992) used the FM and TM as references and recommended 3° to 5° valgus as optimal. However, after 10-13 years' follow up, 21 out of 65 osteoarthritic knees developed recurrence of varus deformity. Five knees were slightly overcorrected to more than 6° valgus angulation of the MA and all of them had suffered progressive lateral compartment degeneration by the time of their review (Hernigou et al., 1987; Hernigou, Ovadia and Goutallier, 1992). Nevertheless, some of these studies are old and more advanced techniques to determine the optimal angle are now available.

### ***Other procedures***

Jakob and Murphy (1992) modified the position of the Fujisawa point, based on the degree of medial articular cartilage damage. The medial third of the lateral tibial plateau was divided into thirds. If the extent of degeneration of the medial compartment was minimal, the goal would be correction of the MA through the medial third (one-third of the distance to Fujisawa's point). If the medial compartment damage was more advanced, then the MA would pass through the middle third. With severe arthritis of the medial compartment, the MA was shifted to pass through the Fujisawa point (Jakob and Murphy, 1992). Müller and Strecker (2008) also proposed a modified procedure, depending on the extent of cartilage lesion.

**Table 2.3: Recommended postsurgical knee alignment after HTO**

<b>Authors</b>	<b>Recommended postoperative correction angle (°) (all in valgus)</b>	<b>Intersection of the mechanical axis with the tibial plateau measured from medial to lateral (%)</b>	<b>Number of patients studied</b>
Coventry et al. (1973)	10-13 (Anatomical tibiofemoral angle)		87
Kettelkamp et al. (1976)	>5 (Anatomical tibiofemoral angle)		48
Fujisawa et al. (1979)		62	54
Insall et al. (1984)	10-14 (Anatomical tibiofemoral angle)		83 (95 knees)
Hernigou et al. (1987)	3-5 (HKA angle)		93
Koshino et al. (1989)	8-10 (Anatomical tibiofemoral angle)		138 (176 knees)
Miniaci et al. (1989)		60-70	36 (41 knees)
Dugdale et al. (1992)	3-5 (HKA angle)	50-75	10
Sprenger et al. (2003)	8-16 (Anatomical tibiofemoral angle)		66 (67 knees)
Aglietti et al. (2003)	8-14 (Anatomical tibiofemoral angle)		102 (120 knees)
El-Azab et al. (2011)		50-70	56

Table 2.3 shows that there is a consensus among authors that a postsurgical overcorrection in valgus results in more satisfying results. However, there seems to be a large span of recommended postsurgical angles. This may be due to the differences in patient groups studied. In addition, at the date of these publications it was not clear how joint alignment was related to specific levels of compartment stress.

## 2.6. Mechanics of the Diseased Knee

Studies have demonstrated that, during the walking cycle, people with knee OA and varus alignment showed specific knee biomechanics and muscular function. Mundermann et al. (2005) and Barrios et al. (2009) both reported a 54% greater peak lateral GR in patients with medial OA in comparison to controls. Many different experimental studies have been carried out to prove that the rate of loss of articular cartilage, and, hence, the progression of OA, is directly linked with the peak knee adduction moment (KAM) during gait (Kumar, Manal and Rudolph, 2013). Schipplein and Andriacchi (1991) were the first to propose that KAM is the primary determinant of medial compartment load during gait. Foroughi et al. (2009) found that KAM increased with OA severity and was directly related to varus malalignment.

Prodromos et al. (1985) tested the gait of twenty-one HTO patients before HTO, one year after surgery, and at an average of 3.2 years follow-up. KAM was reduced in all patients directly after HTO. However, at an average of 3.2-year follow-up, patients with low preoperative KAM had significantly better outcomes than did patients with a high KAM (Prodromos, Andriacchi and Galante, 1985). Wang et al. (1990) and Andriacchi et al., (2000) carried out similar studies and came to the same conclusions. The results of these studies suggest that preoperative peak adduction moment during walking is a valid and reliable predictor for the medial to lateral load distribution across the knee and is a potential risk factor for OA progression. Stief et al. (2014) investigated the gait of eighteen subjects with varus knee alignment. Their results showed that changes in knee alignment led to substantially increased internal knee rotation (Stief et al., 2014).

Many studies have used 3D motion analysis to demonstrate that HTO not only restores a more normal static alignment, but can also reduce the high KAM present in an OA patient. Lind et al. (2012) investigated knee kinematics and kinetics before and after HTO and noted reduced loading of the medial compartment during stance. At the same time, there were improvements in sagittal plane kinematics and kinetics which may also have contributed to a reduction in pain (Lind et al., 2012).

Lind et al. (2013) expanded their study by investigating the effect of altering the lower limb alignment on eleven patients with medial OA two weeks before and 12 months

after medial opening HTO. It was concluded that, in addition to a decreased knee adduction moment, walking speed, maximum knee flexion and knee flexion moment increased significantly and were the same as controls. It was concluded that HTO restored several dynamic knee function parameters (Lind et al., 2013).

Agneskirchner et al. (2007) tested the direct effect of HTO upon peak knee contact pressure for different simulated loading alignments (varus, neutral and valgus) on six human cadavers. Higher peak contact pressure resulted medially compared to laterally when in the varus loading condition. When the loading axis was shifted neutrally or to the lateral side, the peak contact pressure increased laterally and decreased medially, indicating a significant correlation between contact pressure and the direction of the loading axis. It was concluded that favourable HTO results strongly depended on a precise correction of the loading axis (Agneskirchner et al., 2007).

Taken together, these studies provide convincing evidence that HTO should be considered an effective treatment for delaying knee OA because it can shift the loading axis medially or laterally, thereby reducing the external moments and commensurate compartmental contact stress. High external moments have been reported as strong indicators of knee OA.

## **2.7. High Tibial Osteotomy**

HTO surgery is usually performed as a treatment for knee OA resulting from lower limb malalignment. It aims to relieve pain and restore high level function in active patients by realigning the lower limb and relieving damaged tissues from excessive contact stress. Sharma et al. (2001) studied the relationship between malalignment of the lower extremity and knee OA. It was demonstrated that varus and valgus deformity can accelerate the development of OA in the medial and lateral compartments, respectively (Sharma et al., 2001). In the HTO, knee alignment is altered by creating a controlled fracture (horizontal osteotomy) of the tibia just below the knee joint. After either an opening or closing wedge osteotomy the knee joint reaction force is moved from the articulating surface of the affected compartment to the opposite healthy one to slow OA progression (Maquet, Van de Berg and Simonet, 1975).

In the closing wedge osteotomy, a bone wedge is removed laterally and fixed with staples, a plate, or a tension-band system (Coventry, 1979). In the opening wedge osteotomy (Figure 2.15), the proximal tibia is dissected medially and a wedge shaped bone substitute is slowly inserted in the gap (Lobenhoffer and Agneskirchner, 2003). In doing so, the MAD may be restored to, or close to, 0 mm. HTO is best performed relatively early in the course of OA, even though good results may be attained in knees that are in a late stage provided the correct alignment is achieved (Hernigou et al., 1987).



**Figure 2.15: Opening wedge high tibial osteotomy with Taylor Spatial Frame**  
(Courtesy of the Hospital for Special Surgery, New York)

Until the advent of widely available knee replacement prostheses in the early 1970s (Freeman, Swanson and Todd, 1973; Walker, 1973; Ranawat and Sculco, 1985), HTO remained the primary surgical treatment for knee arthritis. Even in the current era of proven and successful total and unicompartmental knee arthroplasty, many surgeons believe HTO is still indicated in some degenerative knee disorders, particularly for young and active patients, where preservation of the natural tissues are its major advantages (Fragomen et al., 2005). Hui et al. (2011) stated that many patients still perceived HTO as a useful and worthwhile procedure to alleviate pain and improve quality of life. The main advantage of HTO is that it will allow the native knee to survive longer. The

older the patient is at the time of TKA, the more likely the implant will outlive the patient. Therefore, the prevalence of physiologically young active patients presenting with medial compartment OA has renewed interest in HTO (Wright et al., 2005). Young patients have the opportunity of maintaining a high level function and a more active lifestyle, thereby buying time for a TKA (Tang and Henderson, 2005).

The following literature survey illustrates that suitable patient selection, careful surgical planning and the correct operative techniques can provide favourable outcomes for HTO.

### **2.7.1. Results of High Tibial Osteotomy**

HTO, undertaken for the treatment of medial OA, has been very successful. However, despite the large number of publications on HTO, comparison is challenging due to the large variation in HTO fixations, surgical techniques and study designs, such as sample size or different patient groups (Amendola et al., 2010; Floerkemeier et al., 2013). The classic radiographic system for grading knee OA is the Kellgren-Lawrence scale, which ranges from 1 (mild) to 4 (severe) grades. It is expected that the milder grades of knee OA are more likely to positively respond to HTO. Once substantial pain and a grade 4 is reached, the standard of care is a TKA. These individuals with end stage disease are not as likely to respond to a HTO realignment.

#### ***Kaplan-Meier probability***

Using the Kaplan-Meier probability, many studies reported good to excellent results on the survival of HTO. An important advantage of the Kaplan–Meier probability is that the method can take into account incomplete data sets such as the death of a patient. The endpoint of HTO survival studies was set to the patient needing a knee replacement. Hui et al. (2011) examined the survival of HTO in 413 patients, up to 19 years after surgery. The probability of survival at 5, 10 and 15 years was 95%, 79% and 56%, respectively (Hui et al., 2011). These results are consistent with the outcomes of Pinczewski et al.'s study (2012) on the probability in survival of over 400 patients up to 19 years after surgery. Other investigators also reported relatively good survivals of HTO, as summarised in Table 2.4 and Figure 2.16.

**Table 2.4: Summary of survival rates of HTO**

	Survival rates of HTO in percent					
	1-year	5-years	10-years	15-years	18-years	Sample Size
(Matthews et al., 1988)	86	50	28			<b>40</b>
(Naudie et al., 1999)		73	51		31	<b>85</b>
(Billings et al., 2000)	100	85	53			<b>56</b>
(Koshino, Murase and Saito, 2003)		97.3	95.1	86.9		<b>21</b>
(Sprenger and Doerzbacher, 2003)		86	65-74	56		<b>76</b>
(Tang and Henderson, 2005)		89.5	74.7	66.9	66.9	<b>67</b>
(Flecher et al., 2006)					85	<b>301</b>
(van Raaij et al., 2007)		98	92	71		<b>100</b>
(Akizuki et al., 2008)			97.6	90.4		<b>118</b>
(Gstöttner et al., 2008)		94	79.9	65.5	54.1	<b>134</b>
(Hui et al., 2011)		95	79	56		<b>413</b>
(Schallberger et al., 2011)			75			<b>54</b>
(Pinczewski et al., 2012)		95	79	56		<b>455</b>



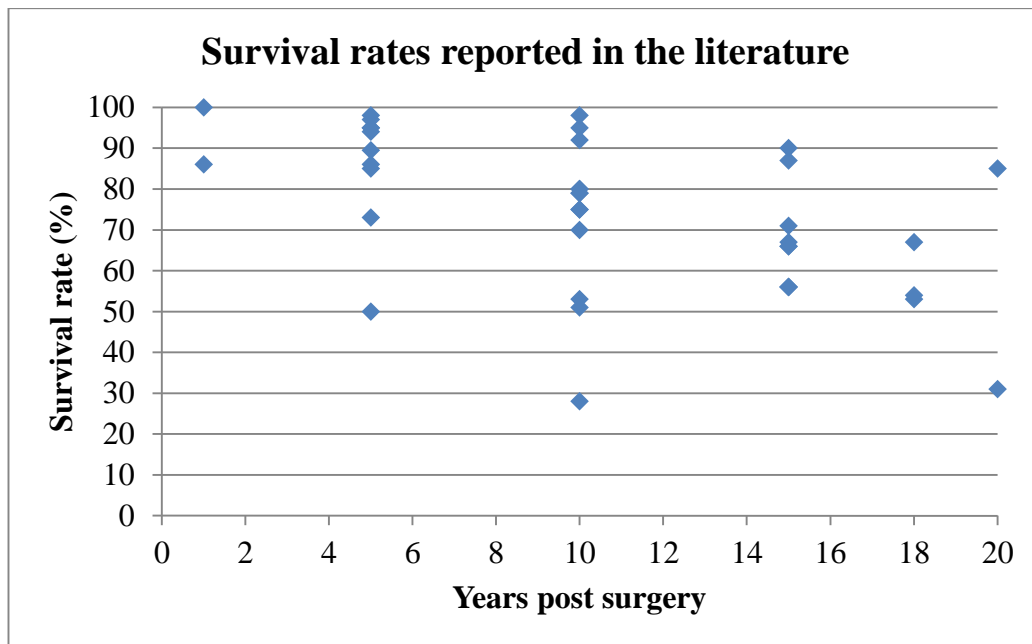


**Figure 2.16: Survival rates of High Tibial Osteotomy reported in the literature**

Despite the good results, it should be noted that a good survival rate does not address functional improvement or reduction of pain postoperatively (Floerkemeier et al., 2013). However, a ten year-survival may be considered a good outcome for HTO, because it delays the need for a knee replacement.

### ***HSS knee score***

Another method of evaluating the outcome of HTO is the 100-point HSS knee score which measures pain, deformity, stability and function of the knee joint. Rinonapoli et al. (1998) found excellent or good results in 55% of knees and fair to poor results in 45% of knees 15 years after HTO. Akizuki et al., (2008) reported excellent and good results in 87 out of 153 knees (73.7%), using the HSS score. The preoperative mean value of the HSS score in Giagounidis and Sell's study was 63.5 (range 40–95). This increased to a mean of 75.3 after an average follow-up of 9 years (Giagounidis and Sell, 1999).

### ***Other ratings***

Tang et al. (2005) evaluated the outcome of HTO taking into consideration pre- and postoperative activity. After HTO, 48% of patients were able to perform at a higher level of activity than before surgery, although no one was able to perform at the level prior to onset of knee pathology (Tang and Henderson, 2005). Nagel et al. (1996)

evaluated the functional results of patients following HTO according to the level of participation in work and sports activities. This was graded on a scale from 0 points (*complete disability*) to 10 points (*the ability to participate in competitive sports at the elite professional level*). The average functional score was 5.4 points preoperatively and 4.8 points postoperatively (Nagel, Insall and Scuderi, 1996). Salzmann et al. (2009) showed that HTO in the active patient demonstrated favourable clinical outcomes, while allowing patients to return to sports and recreational activities similar to the preoperative level.

The literature supports the theory that HTO is, not only successful in terms of patients' subjective pain relief, but also with respect to survivorship. Although the clinical success of TKA has resulted in fewer HTO surgeries, the procedure remains useful in appropriately selected patients (Wright et al., 2005).

### **2.7.2. Pre- and Intraoperative Planning**

A careful geometrical analysis of lower-limb malalignment is essential before surgical realignment since long-term outcomes after HTO are correction precision dependent (Dugdale, Noyes and Styer, 1992; Bae, Song and Yoon, 2009; Niemeyer et al., 2010; Hui et al., 2011).

#### ***Current preoperative planning***

Full-length standing radiographs are regarded to be the current gold standard (Tetsworth and Paley, 1994). However, full-length standing radiographs cannot determine rotational deformities (Wright, Treble and Feinstein, 1991). Measurements acquired from computer tomography (CT) have proven to be more precise and sensitive to tri-planar deformity than full-length standing radiographs. A drawback is that they are performed in a supine, non-load-bearing position, and, therefore, may not represent the anatomical and physiological positioning associated with daily activities (Lützner et al., 2010). Magnetic resonance imaging (MRI) may also be used to evaluate preoperative alignment, and has the advantage of using non-ionising radiation.

Hinterwimmer et al. (2008) investigated use of MRI on two phantoms and 30 patients, but found a significant underestimation of valgus angulation. Liodakis et al. (2011)

used upright MRI for measurement of MA, but concluded that MAD was underestimated.

### ***Intraoperative planning***

Various intraoperative methods have been developed to improve postoperative alignment. Krettek et al. (1998) described the ‘cable technique’ for the determination of malalignment measurements. A cautery cable is spanned between the femoral head and the tibial plafond centres. The position of the cable relative to the centre of the knee joint indicates frontal plane alignment. However, radiation in terms of x-ray is required for this image-based technique (Krettek et al., 1998).

Accuracy has improved with the introduction of computer-assisted limb geometry measurements. Schröter et al. (2013) found these measurements to be reliable, even if made by inexperienced users. Reising et al. (2013) compared patients, who were treated with HTO, using a navigation system to a retrospective control group. Despite similar mean values, a significantly higher number of corrections were outside the reference area in the control group. The use of a navigation device did not lead to improvement of overall outcomes, but over- and under-correction could be reliably prevented (Reising et al., 2013). Ribeiro et al. (2014) also compared the outcomes of a non-navigated HTO to a navigated system. It was concluded that outcomes using navigation were significantly better (Ribeiro, Severino and De Barros Fucs, 2014).

Bae et al. (2009) and Luetzner et al. (2010) carried out similar studies and drew the same conclusions. However, a drawback of computer-assisted limb geometry measurements is that they ignore the effect of ligamentous laxity on the MA and could therefore lead to severe under- or over-correction (El-Azab et al., 2011). Even though advanced pre- and intraoperative planning tools have been developed, none of these take into account the postoperative stress acting on the knee joint.

### **2.7.3. Risk Factors of High Tibial Osteotomy**

Successful HTO outcome has many associated risk factors including: age, activity, obesity (BMI >30 kg/m<sup>2</sup>), preoperative OA grade, abnormal biomechanics/ preoperative range of motion and correction angle (Coventry, 1973; Cuschnaghan and Dieppe, 1991; Berman et al., 1991). Appropriate patient selection, suitable osteotomy

types and precise planning are also important to a successful outcome. However, there are controversies about ideal indications for surgery.

Van Raaij et al. (2008) found a fivefold higher need of TKA in patients with more severe OA. No failure was found in 62% of patients at 10 year follow-up if the preoperative Ahlback OA grade (Ahlback, 1968) was higher than two. The survival rate of patients with an OA grade of  $\leq 1$  was found to be 90% (van Raaij et al., 2008). Odenbring et al. (1990) and Flecher et al. (2006) came to the same conclusions. Mathews et al. (1988) concluded that obesity, advanced age and over- or under-correction had the worst outcomes. Akizuki et al. (2008) also indicated early failure for patients with a pre-operative BMI  $> 27.5 \text{ kg/m}^2$ .

Contradicting relationships between patient age and HTO outcome are reported. While Saito et al. (2014), Hankemeier et al. (2010) and Odenbring et al. (1990) found that age at surgery had no significant influence on HTO outcome, other studies reported that the risk of revision is strongly related to patient age (Odenbring et al., 1990; Hankemeier et al., 2010; Saito et al., 2014). Trieb et al. (2006) concluded that patients of 65 years or more have a significantly higher risk of HTO failure than younger patients. Hui et al. (2010) analysed the long-term survival of HTO up to 19 years after surgery. Results showed that patients under 50 years of age and BMI less than 25 were associated with better odds of HTO survival (Hui et al., 2011).

Naudie et al. (1999) concluded that patients who were younger than 50 years and who had preoperative knee flexion greater than  $120^\circ$  had a higher chance of survival. Fragomen et al. (2005) identified the ideal candidate for HTO to be younger than 60 years with complaints of isolated medial joint line pain aggravated by weight-bearing activities.

Despite the controversial findings of HTO risk factors, the procedure is successful if patient selection is done carefully, taking into consideration preoperative conditions. Coventry et al. (1993) observed that, when osteotomy was performed correctly on carefully selected patients, excellent results were obtained for more than ten years post-operative. Knee osteotomy, if performed correctly, can stop and even reverse the “vicious circle”. Proper timing must be taken into consideration in order for surgery to be effective before the joint is irreversibly damaged (Chao and Sim, 1995).

#### 2.7.4. Alternatives to High Tibial Osteotomy

##### ***Total knee arthroplasty***

For many years, HTO was the main treatment for knee OA, but the devolvement of TKA and improvement of its long-term results have made HTO fall into slight disfavour (Virolainen and Aro, 2004). Reported outcomes of HTO subsequent to performing TKA are controversial. However, most investigators state no significant clinical differences between the outcomes of primary TKA and TKA after HTO. Staeheli et al. (1987) found comparable results whether patients had a previous HTO or not, and reported that the osteotomy could easily be converted to TKA when needed. Amendola et al. (1989) noted that an HTO revision to TKA might be more demanding and entailed a greater risk of complications than primary arthroplasty. Similar conclusions were drawn by Meding et al. (2011), who reported a Kaplan-Meier survival of 100% after 15 years for knees without previous HTO and 97% for knees with previous HTO. Gupta et al. (2013) and Efe et al. (2010) reported that, although TKA patients with prior HTO had more complications and showed a lower range of motion, no statistically significant differences were noted. It can be concluded that most studies did not find significant differences between primary TKA and TKA following HTO.

##### ***Unicompartmental knee arthroplasty***

Another alternative for HTO is the unicompartmental knee arthroplasty (UKA), which has gradually become more popular (Dowd, Somayaji and Uthukuri, 2006). UKA preserves the cruciate ligaments, gives a better range of motion and is therefore less invasive than TKA.

According to Dettoni et al. (2010), HTO and UKA share the same indications in selected cases of medial OA. However, HTO was more suitable for active patients with a malalignment of 5° varus or more (Dettoni et al., 2010). Most authors found no significant differences in HTO and UKA survival outcomes (Stukenborg-Colsman et al., 2001; Börjesson et al., 2005; Chang and Bennett, 2005; Yim et al., 2013; Fu et al., 2013).

Spahn et al. (2013) carried out a global meta-analysis and reported that HTO was more appropriate for younger patients who accepted a slight decrease in physical activity. UKA was more appropriate for older patients requiring sufficient pain relief but with highly reduced physical activity (Spahn et al., 2013). Bonnin et al. (2013) reported that patients could return to strenuous activities following HTO.

Nevertheless, HTO is capable of providing sufficient pain relief and should be considered first before other more aggressive and expensive joint replacement procedures are performed (Chao and Sim, 1995). As a realignment surgery, HTO enables preservation of all the natural tissues within the joint, bone stock and intra-articular structures. HTO has the potential to alleviate the excessive stress that damages the cartilage matrix, while delaying the need for TKA (Virolainen and Aro, 2004). Sambatakakis et al. (1993) stressed how significant the role of ligaments was in the overall success or failure of knee replacements. Recently, technology has been developed (VERASENSE, ORTHOSENSOR™, Florida, USA) to provide surgeons with intra-operative compartmental loads to objectively perform soft tissue re-balancing to provide a mechanically appropriate environment for long-term operation of the TKA.

For older patients, knee arthroplasty may be a better alternative than osteotomy (Insall, Joseph and Msika, 1984). However, if a patient is vigorous and in good general health, it is believed that osteotomy may be appropriate until the age of seventy-five (Hernigou et al., 1987).

### ***Knee Braces***

Similar to surgical realignment, knee braces also target correcting the MAD by inducing a valgus moment which shifts the load more laterally thereby unloading the affected medial compartment (Kutzner et al., 2010; Hillstrom, et al., 2013). Although, most brace studies are limited in sample size and often lack independent controls, visual analogue scale pain is generally substantially reduced. However braces, regardless of type, are known to lose their alignment with the joint centre by sliding or rotating, making them less effective (Kirane, Zifchock and Hillstrom, 2010).

There are a number of biomechanically-based therapies in addition to knee bracing, such as lateral or medial wedged insoles, flexible shoes (Dr. Comfort, DJO, CA, USA),

compliant medial outsole shoes (Abeo, NC, USA) and neuromuscular re-education shoes (APOS, NY, USA), which use different strategies to offload the medial compartment of the OA knee. Although some of these non-surgical approaches show promising results, further research is needed to understand the link between each treatment strategy, pain and the appropriate biomechanical ‘dosing’. A computational model that links alignment to compartmental loading in a subject-specific manner is needed.

## **2.8. Finite Element Analysis**

Finite Element Analysis (FEA) consists of decomposing a continuous mechanical problem into a set of simpler discrete problems by defining a finite number of variables (Hrennikoff, 1941). A structure is considered as a whole and divided into many small units, called finite elements, which are connected at nodes (Zhong et al., 2011). The method may be applied to static, dynamic, linear and non-linear type problems and, through the use of such simulations, greatly reduces the time required for experimentation and prototype testing.

Each finite element potentially consists of six DOF, which represent a possible movement (translation and rotation) of that element under loaded conditions. An infinite number of simultaneous equations are required to determine the movement of each element and the resulting stress and strain.

An FE model must be restrained in all six DOF, otherwise a solution cannot be found, however, the structure must not be over restrained, or else the analysis will give false results. To split a part into a finite number of elements, a process, known as meshing, must be performed. Meshing is analogous to the many bricks that make up a wall. Elements typically range from 2-noded (one-dimensional) for framework analysis up to 20-noded (3D) for complex solid parts (Figure 2.17). Each meshed element may have its own material properties.

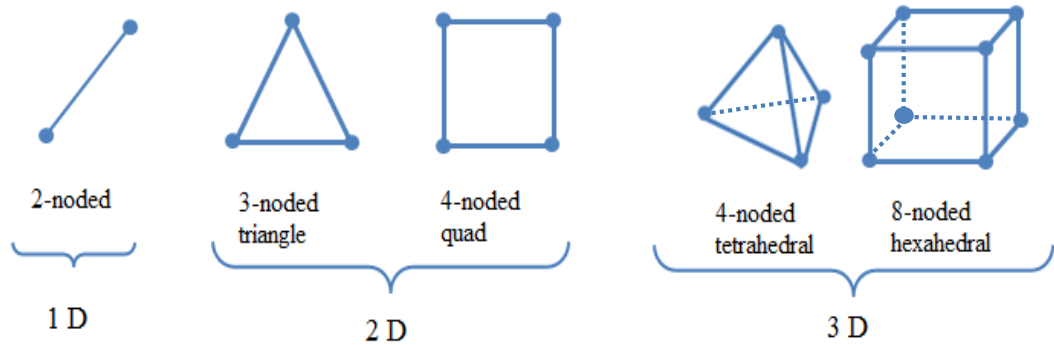


**Figure 2.17: Different element mesh types**

To increase FE model accuracy, its mesh must not only be fine enough, but must also have a satisfactory shape. Viceconti et al. (1998) considered five different mesh methods (mapped mesh, tetrahedral mesh, voxel mesh and hexagonal mesh) for the human femur. It was concluded that all meshes were correct, with no disconnection or degenerated elements and were able to predict the displacements with errors lower than 4%. The mapped mesh was the most accurate in reducing errors (<1%). The hexahedral and mapped mesh both took a few hours to generate but gave more accurate results compared to the tetrahedral and voxel mesh, which only took a few minutes to generate (Viceconti et al., 1998). Computational requirements and execution time have to be considered before choosing a mesh type. Although a model may be plausible in theory, direct (experimental) and indirect (theoretical) validation is required to obtain reliable results.

### **2.8.1. Application of FEA in Biomedical Problems**

Since 1972, FEA has been extensively used in orthopaedic biomechanics to investigate the performance of surgical techniques, design of total joint replacements, and provide an estimate of related mechanical and geometrical quantities (Viceconti et al., 1998). Biomechanical computational models are an economical way to predict the consequences of invasive surgical techniques, while avoiding time-consuming experiments. However, experiments are necessary to validate the models and provide kinematic and material data for computational inputs.

FEA has been widely used to provide insight into healthy and injured knees, for example, the simulation of internal fixation methods in the femur (Chen et al., 2004) and tibia (Blecha et al., 2005; Raja Izaham et al., 2012), simulation of total hip



replacement (Mootanah et al., 2007) and ankle arthrodesis (Vázquez et al., 2003; Alonso-Vázquez et al., 2004).

### *Axisymmetric model*

Because the human knee joint has a complex 3D structure, it is not easy to represent its geometry by a solid model. Therefore, Donzelli et al. (1999) created an axisymmetric representation of the knee (Figure 2.18), which has been adopted by numerous 2D studies (Donzelli et al., 1999; Dunbar et al., 2001; Wilson et al., 2003; Dar and Aspden, 2003; Federico et al., 2004; Wilson et al., 2005; Vadher, et al., 2006; Vaziri et al., 2008; Guo, Maher and Spilker, 2013).

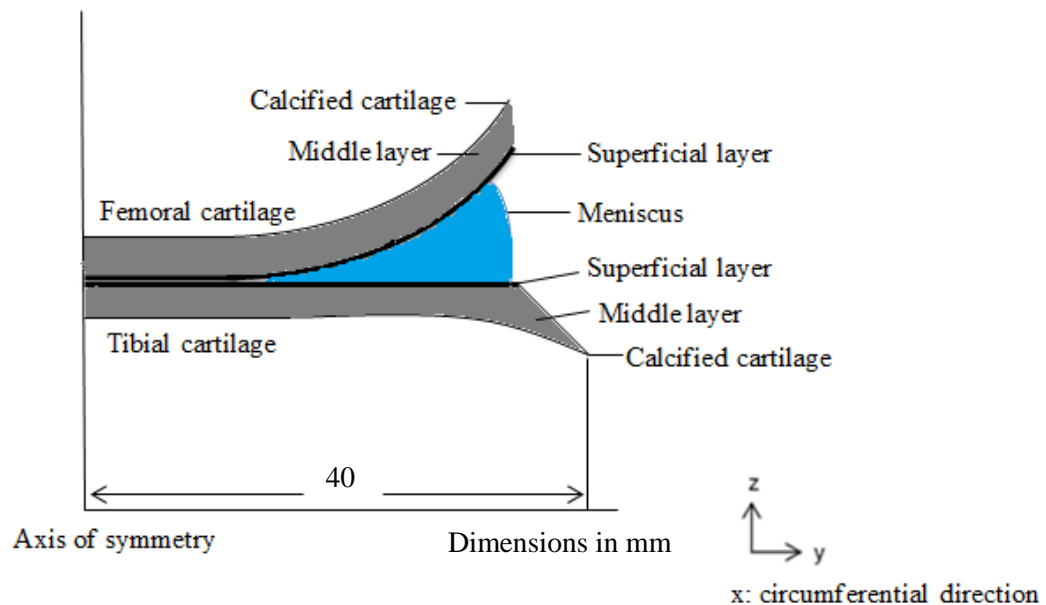


**Figure 2.18: Axi-symmetric 2D model**

This simplified geometry of 2D FE models makes it easier to represent complex and more realistic material property conditions. Vaziri et al. (2008), for example, modelled the cartilage as three layers consisting of an isotropic poroelastic superficial layer, a transversely isotropic poroelastic middle layer and an isotropic elastic calcified layer (Vaziri et al., 2008).

However, these models do not accurately represent the true 3D geometry of the tibiofemoral joint, which may have an impact on the actual stress distribution.

### ***3D model development***

3D knee joint models have been developed, using various techniques to obtain the true geometry. Early 3D models by Wismans et al. (1980) used geometric data points of the tibial and femoral articular surfaces to obtain surface polynomials using the least square method. Pandey et al. (1997) created the femur, tibia and patella geometry, based on cadaver data reported for an average-sized knee.

The geometries of the femur and the tibia in Lesso-Arroyo et al.'s study (2004) were obtained via a 3D laser scanner in Initial Graphics Exchange Specification (IGES) format. The menisci were drawn in a computer aided design (CAD) software package, taking into account the space between the tibia and femur. Although, not anatomically accurate, the menisci model provided an approximation of knee behaviour (Lesso-Arroyo, et al., 2004). Bratianu et al. (2004) constructed a simplified representation of the tibiofemoral compartments, using a CAD package, and prepared an FE model. Zielinska and Donahue (2006) studied the effect of partial meniscectomy to quantify changes in knee joint contact behaviour from a 3D laser coordinate digitising system that imaged the cartilage and menisci of human knee. A more efficient method of acquiring 3D geometries of knee anatomy was required.

Keyak et al. (1990) used digital computed tomographic (CT) scan to derive patient-specific FE models representing bone with accurate geometry and inhomogeneous material properties. Many other studies have since used CT to represent accurate geometry (Bendjaballah, Shirazi-Adl and Zukor, 1995; Donahue et al., 2002; Gardiner and Weiss, 2003; Guo et al., 2009; Hopkins et al., 2010; Pauchard, et al., 2013). However, soft tissues cannot be modelled from CT images.

Donahue et al. (2002) determined cartilage thickness, *in vitro*, by subtracting the image after cartilage removal from the scan with intact cartilage. Hopkins et al. (2010) constructed the soft tissues through selective expansion of the rigid-body elements in the bone. Hexahedral elements were used to generate a uniform 2-mm-thick layer for the cartilage and a 3-mm layer for the menisci (Hopkins et al., 2010). Losch et al. (1997) developed a computational method for generating maps of cartilage thickness using a 3D minimal distance algorithm that determined the minimal distance from the articular surface to the bone-cartilage interface at each point. A more systematic non-

invasive method of accurately determining soft tissue geometry for computational modelling was required.

Several investigators obtained knee joint geometrical data from MRI (Li and Lopez, 1999; Yang, Nayeb-Hashemi and Canavan, 2007; Yang, Nayeb-Hashemi and Canavan, 2009; Yang et al., 2010). Li and Lopez (1999) found FE models constructed from MRI to be reliable for cartilage stress analysis with the caveat that a 10% variation in results might be attributed to the manual digitisation. Other studies have used CT images to obtain geometrically-accurate representations of bone, and registered MRI for accurate soft tissue geometries (Peña et al., 2006; Mootanah, et al., 2009; Kiapour et al., 2013).

### ***Material properties of bones***

Although it is possible to model physiological bone material properties, most studies assume bone as rigid body, which is justified by the difference in stiffness between hard and soft tissues (Andriacchi et al., 1983; Blankevoort et al., 1991; Gardiner and Weiss, 2003; Bratianu, Rinderu and Gruionu, 2004; Peña et al., 2006; Zielinska and Donahue, 2006; Yang, Nayeb-Hashemi and Canavan, 2007; Peña et al., 2008; Kazemi et al., 2011; Mononen et al., 2012). Haut Donahue et al. (2002) verified this assumption by showing that the change in any contact variable was less than 2% while reducing computation time by 50% when bones were modelled as a rigid body (Donahue et al., 2002). Peña et al. (2006) came to the same conclusion.

Other investigators assumed linear elastic, isotropic, homogenous mechanical properties for bone and used an average Young's modulus ( $E$ ) for cortical and cancellous bone (Wilson et al., 2003; Guo et al., 2009). A third group of authors differentiated the bones into cancellous ( $E \approx 500\text{MPa}$ ) and cortical ( $E \approx 17\text{ GPa}$ ) components (Kubicek and Florian, 2009; Walker and Ingle, 2009; Chantarapanich et al., 2009; Mootanah, et al., 2009). Subchondral bone is reported to have a Young's modulus of  $1\text{GPa}$  (Choi et al., 1990). The Poisson's ratio used for bony structures within most knee models is between 0.3 and 0.4.

### ***Material properties of cartilage***

Cartilage has a major role in load distribution across the knee joint. It is therefore important to input realistic properties for these tissues in FE knee models to accurately predict loading across the articulating surfaces of the joint.

Early models represented the soft tissue structures by basic spring- and beam-type elements (Andriacchi et al., 1983; Hsu et al., 1990; Chao and Sim, 1995). Later on, cartilage was assumed to behave as a linearly elastic, homogenous, isotropic material. The Young's modulus of cartilage reported in the literature varies from 0.69 MPa (Wilson et al., 2003; Yang, Nayeb-Hashemi and Canavan, 2007), 5 MPa (Blankevoort et al., 1991; Perie and Hobatho, 1998; Peña et al., 2006; Guo et al., 2009), 12 MPa (Li and Lopez, 1999; Chantarapanich et al., 2009; Mootanah, et al., 2009; Hopkins et al., 2010), 13 MPa (Yao et al., 2008), 15 MPa (Haut Donahue et al., 2003; Bratianu, Rinderu and Gruionu, 2004; Zielinska and Donahue, 2006; Yang, Nayeb-Hashemi and Canavan, 2009; Pauchard, et al., 2013) and 50 MPa (Kubicek and Florian, 2009). The Poisson's ratio in all studies varied from 0.3 to 0.5. Assuming a linearly elastic and isotropic behaviour is considered sufficient because the loading time in most models corresponds to that of a single leg stance, which is less than one second. Cartilage has to be loaded for approximately 1500 s to display viscoelastic characteristics (Armstrong, Lai and Mow, 1984; Donahue et al., 2002).

Results of some *in-vitro* studies suggested that healthy cartilage can have a Young's modulus of 100 MPa. However, it is expected that this value will vary for different activities (Hart et al., 1999; Park, Hung and Ateshian, 2004; Vrana and Michalec, 2005).

Cartilage is able to retain and restrict the flow of water, which gives it its viscoelastic properties. However, it has been shown by many authors (Armstrong, Lai and Mow, 1984; Eberhardt et al., 1990; Donahue et al., 2002) that the synovial fluid within the tissue does not move significantly over short loading spans. Thus, the mechanical response of cartilage does not vary significantly over time. Yosibash et al. (2010) found that FE models with inhomogeneous orthotropic material properties produced similar results to those obtained with isotropic material properties for a short time frame. Depending on the application, cartilage models may require several

components and enhanced complexity to describe the overall mechanical behaviour in a realistic manner.

Shirazi and Shirazi-Adl (2005) developed a fibre-reinforced composite model for cartilage. The collagen fibrils were modelled as reinforcement in a nonlinear isotropic poroelastic configuration (Shirazi and Shirazi-Adl, 2005). This model was enhanced by implementing a detailed microstructure for femoral and tibial cartilage layers as well as menisci in 3D (Shirazi and Shirazi-Adl, 2008). The cartilage nonfibrillar matrix was modelled by an incompressible isotropic hyper elastic solid with depth-dependent properties. The modulus increased from 0.3 to 0.5, 0.8 and 1.2 MPa when moving from the articular surface to the subchondral bone, respectively (Shirazi and Shirazi-Adl, 2008). This approach has been adopted by several authors (Kazemi et al., 2011; Mononen, Jurvelin and Korhonen, 2013).

### ***Material properties of the menisci***

Similarly to cartilage, many studies have assumed the behaviour of the menisci to be linearly elastic. Material properties varied from 5 MPa to 112 MPa for Young's modulus and 0.4 to 0.49 for Poisson's ratio (Perie and Hobatho, 1998; Peña et al., 2006; Peña et al., 2008; Chantarapanich et al., 2009; Guo et al., 2009; Kubicek and Florian, 2009; Mootanah, et al., 2009; Hopkins et al., 2010; Pauchard, et al., 2013). An early study by Li and Lopez (1999) represented the menisci by equivalent-resistance springs. It was demonstrated that a representation of the meniscus was important for accurate calculation of knee kinematics (Li and Lopez, 1999). Donahue et al. (2003) included a more complete model of the meniscal attachment. With this model, it was shown that contact variables of the tibial plateau were most sensitive to the circumferential modulus, axial/radial modulus and the total horn stiffness (Haut Donahue et al., 2003).

Additionally, it was shown by Donahue et al. (2003) that the meniscal attachment was important in defining overall function. Many studies subsequently implemented realistic meniscal attachments and material properties. The menisci were typically modelled as linearly elastic, transversely isotropic with moduli of 20 MPa in the radial and axial directions and 140 MPa in the circumferential direction. Meniscal horns were attached to the tibial plateau by linear springs (Donahue et al., 2002; Haut Donahue et

al., 2003; Zielinska and Donahue, 2006; Yao et al., 2008; Yang, Nayeb-Hashemi and Canavan, 2009; Netravali et al., 2011; Mononen, Jurvelin and Korhonen, 2013; Kiapour et al., 2014).

In addition to the meniscal horns, there are coronary ligaments (CL) that attach the meniscus to the tibial plateau along the meniscal periphery. Results of Li et al.'s study (2012) showed that the presence and stiffness of the CL affected both the magnitude and location of maximum stress predicted in both menisci. Perie and Hobatho (1998) fixed the external nodes of the menisci periphery in the sagittal plane to prevent the meniscus from extruding from the femorotibial joint in order to compare theoretical and experimental contact area values.

Yao et al. (2006) modelled the peripheral attachments, using one dimensional spring elements connecting the inferior edge of the meniscus with the edge of the cartilage layer. The stiffness coefficients varied from 1-10 kN/mm (Yao et al., 2006). It was concluded that special attention had to be paid to the material properties of the peripheral attachments. Other studies adopted that method (Peña et al., 2006; Hopkins et al., 2010; Li, Evans and Holt, 2012).

### ***Material properties of ligaments***

Knee ligaments have a key role in maintaining stability of the lower limb joints. Because of the complex geometry and behaviour of the ligaments, many studies either ignored them entirely (Viceconti et al., 1998; Walker and Ingle, 2009; Strickland et al., 2011) or represented them by nonlinear spring elements (Blankevoort and Huiskes, 1996; Mommersteeg et al., 1996; Li and Lopez, 1999; Donahue et al., 2002; Haut Donahue et al., 2003; Beillas et al., 2004; Peña et al., 2006; Yang, Nayeb-Hashemi and Canavan, 2007; Shirazi and Shirazi-Adl, 2008; Netravali et al., 2011).

Uniaxial tensile tests are commonly used to characterise ligament material properties (Figure 2.19) (Butler, Kay and Stouffer, 1986; Quapp and Weiss, 1998). Ligament strain is the deformation per unit length and stress represents the load per unit cross-sectional area. The Young's modulus is the stress divided by strain. The toe region of the ligament stress-strain is characterised by an initial low modulus, which is attributed to straightening of the "crimped" collagen fibres within the relaxed tissue (Region 1 of Figure 2.19) (Rigby et al., 1959). Small forces are required to produce

large elongations in the toe region. The modulus of the intermediate region gradually increases as the fibrils start to resist tensile load. The load-elongation curve is non-linear and concave, requiring greater forces an elongation in the intermediate region (Region 2 of Figure 2.19). In the linear region the fibrils become taut and align with the loading direction, such that the tensile stress increases linearly with increasing strain (Region 3 of Figure 2.19). After the ultimate tensile strength is reached, the modulus decreases as groups of fibrils begin to fail, before complete tissue rupture occurs (Kwan and Woo, 1989).

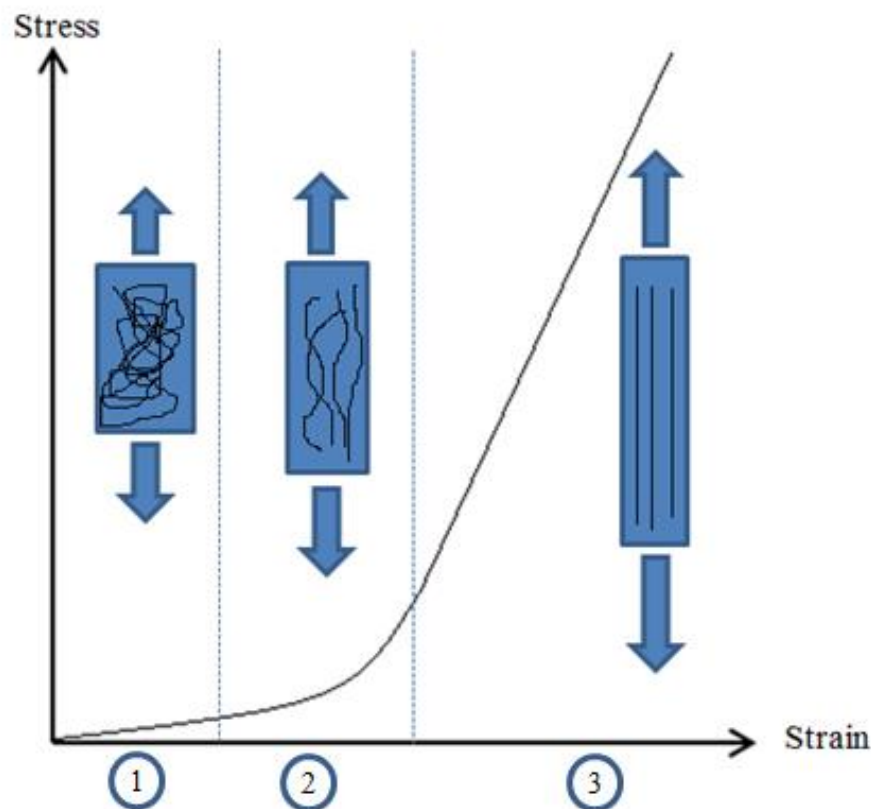


**Figure 2.19: Stress-Strain curve for ligaments 1 = toe region; 2 = intermediate region; 3 = linear region**

Due to the linear region of the stress-strain curve, many studies assumed ligaments to be linear elastic (Fung, 1967; Veronda and Westmann, 1970; Demiray, 1972; Kubicek and Florian, 2009; Chantarapanich et al., 2009; Pauchard, et al., 2013). However, a linear elastic model of the ligament overestimates the modulus of elasticity in the toe region. Isotropic models fail to capture anisotropic characteristics and lead to unrealistic results (Limbert and Taylor, 2001).

Peña et al. (2006) represented their ligaments as hyperelastic isotropic with a neo-Hookean model with values of 6.06, 6.43, 5.83 and 6.06 MPa for LCL, MCL, ACL and PCL, respectively. Weiss et al. (1996) developed an incompressible transversely isotropic hyperelastic model, representing material anisotropy, to characterise the mechanical behaviour of soft tissues. Some authors implemented this theory in their FE knee models (Peña et al., 2008; Guo et al., 2009).

Peña et al. (2008) presented a full 3D finite strain anisotropic visco-hyperelastic (Kelvin-Voigt) model for ligaments. A local multiplicative decomposition of the deformation gradient into volume-preserving and dilatational parts has been used to model the incompressible properties of soft biological tissues (Peña et al., 2008). Holzapfel and Gasser (2001) stated that the typical anisotropic behaviour was caused by several collagen fibre families (usually one or two fibres coincide at each point) that are arranged in a matrix of soft material referred to as ground substance (Holzapfel and Gasser, 2001). Recently, studies have represented ligaments by more realistic anisotropic material properties. Kiapour et al. (2013) used the Holzapfel-Gasser-Ogden material model (Gasser, Ogden and Holzapfel, 2006) to investigate the effect of ligament modelling technique on knee joint kinematics. An isotropic non-collagenous ground matrix was modelled by the incompressible neo-Hookean part of the strain energy density function, whereas transversely isotropic fibrous parts were modelled by a function developed by Gasser (Kiapour et al., 2013). Although ligaments have been described as nonlinear, anisotropic, viscoelastic structures, it is not clear that this level of complexity is required in a finite element model of joint stress. There are several practical aspects of describing ligament behaviour including the “slack length” that occurs as a function of joint angle, that must be addressed to incorporate the appropriate loading that each ligament is contributing.

### ***Mesh size***

Another factor that influences cartilage stress is the mesh size. Keyak et al. (1992) analysed three models of a human proximal femur, each with a different element size (3.1 mm, 3.8 mm and 4.8 mm). Results of their study indicated that use of larger elements decreased predicted stress and strain (Keyak and Skinner, 1992). Papaioannou et al.'s (2008) recorded the contact variables (peak pressure, total force and contact area) with two different mesh sizes. The convergence test indicated that



changing the mesh size from 1 mm  $\times$  1 mm to 4 mm  $\times$  4 mm increased all but one of the contact variables by up to 45% (Papaioannou et al., 2008). Most investigators represented their geometry with 8-noded hexahedral elements as it offered a good compromise between computational cost and accuracy (Perie and Hobatho, 1998; Limbert and Taylor, 2001; Donahue et al., 2002; Bratianu, Rinderu and Gruionu, 2004; Peña et al., 2006; Guo et al., 2009; Yang, Nayeb-Hashemi and Canavan, 2009; Kiapour et al., 2013; Kiapour et al., 2014). To reduce analysis time, some authors have used triangular elements for bones and hexahedral elements for soft tissues (Hopkins et al., 2010; Mattei et al., 2014). It is reported that a sensible compromise between minimum mesh size and computational time would be to select the largest mesh size that provided <5% change in contact mechanics compared to smaller mesh (Donahue et al., 2002; Anderson et al., 2005; Jones and Wilcox, 2008; Yang, Nayeb-Hashemi and Canavan, 2009; Kazemi et al., 2011; Bae et al., 2012; Kiapour et al., 2014).

### ***Boundary and loading conditions***

Load-displacement response of the knee is highly dependent on constraints to coupled degrees of freedom (Andriacchi et al., 1983). Therefore, it is important to define accurate boundary conditions. Donahue et al. (2002) reported that previous FE models had used unrealistic constraints on rotational DOF under compressive loading of the knee joint. In Bendjaballah et al.'s (1995) study varus-valgus rotation was constrained. In another study compressive translational displacements were applied which constrained all rotational DOF to zero (Zhang, et al., 1999). It was shown by Donahue et al. (2002) that differences in contact variables up to 19% occurred when rotations other than flexion/extension were constrained. In other studies flexion/extension was fixed to simulate specific knee positions (Donahue et al., 2002; Peña et al., 2006; Zielinska and Donahue, 2006; Shirazi and Shirazi-Adl, 2008; Yang, Nayeb-Hashemi and Canavan, 2009). A third group of studies adapted boundary conditions from knee simulators (e.g. the Stanmore simulator developed by Walker et al., 1997) (Godest et al., 2002; Halloran, Petrella and Rullkoetter, 2005; Hopkins et al., 2010; Baldwin et al., 2011).

Some FE models have received loading and boundary conditions from movement analysis. Yang et al. (2010) determined loading and boundary conditions from 3D kinematics and force platform data. Forces applied to FE models were a summation of

joint reaction forces and muscle forces (Yang, Nayeb-Hashemi et al., 2010). Saveh et al. (2011) measured knee joint kinematics, using gait and fluoroscopy for boundary conditions of FE models.

Contact surfaces between the parts are mostly modelled as frictionless (Bendjaballah, Shirazi-Adl and Zukor, 1995; Donahue et al., 2002; Haut Donahue et al., 2003; Peña et al., 2006; Zielinska and Donahue, 2006). A few studies specify a cartilage-cartilage coefficient of friction ranging from 0.002 to 0.01 to simulate fluid flow (Beillas et al., 2004; Yang, Nayeb-Hashemi and Canavan, 2009).

Many published FE models are static or quasi-static in nature. Kiapour et al. (2013) simulated quasi-static loading conditions in order to compare the predicted FE kinematics with experimental measurements from an *in vitro* study of 19 fresh frozen cadaveric legs. Currently, very few FE models are dynamic and hence cannot report knee joint stress and strain during functional tasks such as gait. Those studies that perform dynamic simulations have not included the ligaments as a 3D geometry (Yang et al., 2010; Netravali et al., 2011; Saveh, Katouzian and Chizari, 2011; Baldwin et al., 2011; Adouni, Shirazi-Adl and Shirazi, 2012; Nicolella, et al., 2012; Mononen, Jurvelin and Korhonen, 2013). Kiapour et al. (2013) demonstrated that an FE model with 3D ligaments closely reproduced experimentally measured knee kinematics. Higher variations from average experimental measurements were observed when non-linear elastic 1D representations of the ligaments were used in the same model (Kiapour et al., 2013).

Recently, musculoskeletal models with active and passive elements have been integrated with FEA (Adouni and Shirazi-Adl, 2014). However, these models are difficult to validate. The methodological aim of this study was to simulate knee joint contact mechanics in normal and malaligned knees during the weight acceptance phase of the gait cycle with a validated 3D FE model.

### **2.8.2. High Tibial Osteotomy in Finite Element Analysis**

Very few FE models have been developed that examine the effects of HTO on knee joint contact mechanics. Bendjaballah et al. (1997) applied varus and valgus moments of up to 15 Nm, simulating different alignments, and observed the load and stress in

the tibial plateau. Results showed compressive stress in the tibial plateau increased with the application of higher moments (Bendjaballah, Shirazi-Adl and Zukor, 1995).

Blecha et al. (2005) developed a numerical model of the medial opening wedge HTO and found that the supporting plate position influenced the biomechanical behaviour under maximal load during gait. They also concluded that, in order to avoid fibrous tissue formation at the bone-wedge interface, the osteotomy should be subjected to less than 18.8% of normal gait loading until union is achieved (Blecha et al., 2005).

Several plates have been designed to support and apply the intended angle of the opening wedge HTO during the healing process (Puddu, Athrex, Florida and Tomofix, Depuy Synthes, Switzerland). These plates are affixed to the proximal and distal aspects of the opening wedge with cortical screws. Izaham et al. (2011) compared the Puddu and Tomofix HTO plates using FEA and found that the Tomofix plate produced higher stability for bony fixation in HTO procedures. The displacement of the Puddu plate was 3.25 mm higher than that of the Tomofix plate. However, their model only included the tibia and the fibula and stress within the distal tibia were not reported (Raja Izaham et al., 2012).

Chantarapanich et al. (2009) created 3D models of three normal and three varus knee joints and applied a vertical concentrated force to the femoral head, simulating a single limb stance. Results indicated that, on average, the varus knee joint experienced a 1.45 MPa higher maximum normal stress in the medial compartment compared to well-aligned knees (Chantarapanich et al., 2009).

Mootanah et al. (2009) developed a model to assess how HTO geometry related to joint stress. A load of 2.1 KN, corresponding to 3× body weight was applied perpendicularly to the proximal end of the femur. FE analyses demonstrated a reduction of 67 % in principal stress in the knee joint following an opening wedge HTO surgery. HTO reduced stress in specific regions of the knee, which have been associated with OA progression (Mootanah, et al., 2009).

Yang et al. (2010) created three different subject-specific 3D FE models of the knee joint to study the effect of varus, neutral and valgus alignment on the stress and strain distribution in the knee. The subject with varus alignment had the largest stress in the medial compartment, whereas the stress in valgus alignment was found to be larger in

the lateral compartment. These results suggested that subjects with a varus or valgus alignment might be prone to developing medial or lateral OA, respectively (Yang, Nayeb-Hashemi et al. 2010).

Pressel et al. (2010) created an FE model of the tibia simulating different HTO wedges. It was concluded that the osteotomy angle largely affected the maximum stress in the bone. At 2.5° valgus, the stress at the medial and lateral tibial plateau were equivalent, while increasing valgus angles reduced medial stress and vice versa. However, this model did not include any of the soft tissues or any of the other bones (Pressel et al., 2010). None of the previous models have investigated the relationship between MAD and the stress in the tibial or femoral cartilage.

### **2.8.3. Model Validation**

Validation is an important step towards improving clinical utility of computational models (Li et al., 1999; Donahue et al., 2002; Beillas et al., 2004; Zhao et al., 2007). Once validated, a model may predict biomechanical parameters under complex loading conditions that cannot be measured experimentally. Unlike model validation, model verification implies that sensitivity analysis, comparison with other experimental data, or corroboration with another model or theoretical analysis was performed. Validation implies that an independent experimental data set was compared with model predictions for the same specimen (Henninger et al., 2010).

Yosibash et al. (2007 and 2010) developed a subject-specific FE model of a femur and validated strain and displacement using an Instron mechanical testing machine. However, only the femur was used in their study (Yosibash, Trabelsi and Milgrom, 2007; Yosibash, Tal and Trabelsi, 2010). Peña et al. (2006) and Li et al. (1999) verified their models using experimental and numerical results obtained by other authors. Mononen et al. (2013) also verified their model by comparing its varus-valgus rotation, contact pressures and meniscal movements to experimental findings of other studies (Komistek et al., 1997; Godest et al., 2002; Halloran, Petrella and Rullkoetter, 2005; Kozanek et al., 2009).

Chantarapanich et al. (2009) claimed that their results were accurate due to application of realistic boundary conditions and material assumptions. Miller et al. (2009) developed a subject-specific 2D computational knee model, using discrete element analysis, and validated the total load, peak load and peak load location with 4 human cadaveric knees within a root mean square error (RMSE) of 4% (Miller et al., 2009). Kiapour et al. (2014) validated their FE model with cadaveric specimens under quasi-static loadings. Strong linear correlations ( $r > 0.8$  and  $p < 0.0005$  for all comparisons) between model predictions and experimental data of 16 cadaveric models were reported (Kiapour et al., 2014).

Haut Donahue et al. (2003) validated their model by experimentally measuring the contact pressure distribution on the tibial plateau in the same knee used to create the model. An optimisation was performed under 1200 N of compressive load that involved changing the material properties of five parameters to minimise the difference between the experimental and model results to 5.4% (Haut Donahue et al., 2003).

Completo et al. (2007a) validated four FE models of intact and reconstructed synthetic tibiae against experimental cortex bone strains. The RMSE obtained for all results was less than 10% (Completo, Fonseca and Simoes, 2007a). The same analysis was carried out for the femur and similar conclusions were drawn (Completo, Fonseca and Simoes, 2007b).

The Stanmore knee simulator (Walker et al., 1997) was developed to objectively test cadaveric specimens with intact and prosthetic knees. Forces and moments were supplied as inputs while rotation and translations were the outputs. Several authors used experimental kinematic data of the Stanmore knee simulator to verify their models (Godest et al., 2002; Halloran, Petrella and Rullkoetter, 2005; Perillo-Marccone and Taylor, 2007). None of these models were built from the cadavers that were actually tested.

Beillas et al. (2004) compared model kinematics to experimental data from a different subject. Angular kinematics predicted by the model were within  $1.4^\circ$  RMSE of the experimental data and translations were within 1 mm RMSE (Beillas et al., 2004). Guess et al. (2010) compared tibiofemoral as well as patella-femoral kinematics of their multibody knee model to an identically loaded cadaver knee. RMSE between

model predicted and experimental kinematics during a walk cycle were less than 11 mm in translation and less than  $7^\circ$  in rotation (Guess et al., 2010). This multibody model could not predict joint stress.

Baldwin et al. (2011) conducted *in vitro* tests on three cadaveric specimens and validated the kinematics of their FE model with the results of the dynamic cadaveric tests. Model-predicted and experimental RMSE were averaged across all three specimens for each kinematic variable. Deep knee bend tibiofemoral flexion–extension had an average RMSE of  $3.8^\circ \pm 1.9^\circ$ , while internal–external and varus–valgus rotations had less than  $1.3^\circ \pm 0.7^\circ$ ; anterior–posterior, inferior–superior and medial–lateral translations matched within  $2.1 \text{ mm} \pm 1.2 \text{ mm}$ ,  $1.7 \text{ mm} \pm 1.2 \text{ mm}$  and  $0.9 \text{ mm} \pm 0.5 \text{ mm}$ , respectively (Baldwin et al., 2011).

Lanovaz et al. (2005) developed a 3D forward-dynamics model of a TKA, including both a tibiofemoral and a patellofemoral joint, which allowed 6 DOF kinematics. For validation, a unique experimental apparatus was constructed to simulate an open-chain extension motion under quadriceps control. The RMSE between experimental data and model predictions across all simulations were good for both the kinematics (angles:  $0.3^\circ$  -  $1.6^\circ$ , displacements: 0.1 mm - 0.8 mm) and kinetics (forces: 5 - 11 N, moments: 0.2 - 0.6 Nm) (Lanovaz and Ellis, 2005). Joint stress was not included in this model.

Blankevoort and Huiskes (1996) developed four 3D subject-specific models of knee soft tissues and validated them with the kinematics of the same joint specimens. RMSE for internal-external rotation was  $\leq 8^\circ$ , while posterior-anterior translation ranged from -5 mm to 3 mm (Blankevoort and Huiskes, 1996).

Tuncer (2013) developed four FE UKA models and validated them for bone strain across a range of specimen bone densities of ten fresh frozen cadaveric specimens. The quadratic correlation ( $r^2$ ) between predicted and measured cemented and cementless implant models was computed. The cemented UKA  $R^2$  values for predicted versus measured bone strains were 0.85 and 0.92 for the tibia and femur, respectively. The cementless UKA  $r^2$  values were slightly lower at 0.62 and 0.73 (Tuncer et al., 2013).

Akbar et al. (2012) developed a 3D dynamic patellofemoral joint model and validated patella kinematics with an *in vivo* experiment, involving MR imaging of a normal knee while performing isometric leg presses against a constant 140 N force. RMSE of 2 mm

for translations ( $< 0.7$  mm for patellar medio-lateral shift) and  $4^\circ$  for rotations ( $< 3^\circ$  for patellar tilt) were reported (Akbar et al., 2012).

Lundberg et al. (2013) compared FE model predicted TKA contact forces to *in vivo* forces from an instrumented prosthesis during normal walking and medial thrust gait. The percent difference between measured and predicted peak contact force was 2.89% (1<sup>st</sup> peak) and 9.36% (2<sup>nd</sup> peak) for normal walking and 3.94% (1<sup>st</sup> peak) and 14.86% (2<sup>nd</sup> peak) for medial thrust gait (Lundberg, Knowlton and Wimmer, 2013). Typical contact forces exhibit two peaks during the stance phase of gait.

Innocenti et al. (2014) developed an FE UKA model and validated it against experimentally-measured relative load distributions between the medial and lateral compartment of that same knee. It was reported that good agreement was observed between FE-predicted and *in vitro*-measured results. However, no percent error was reported (Innocenti et al., 2014).

#### **2.8.4. Concluding Remarks**

The above literature survey has demonstrated that 3D FE modelling is a powerful tool for understanding the contact mechanics of joints. Still, FE models are only estimates of the actual contact mechanics and have errors due to assumptions made in the modelling process. The accuracy of FE models depends on precise geometry and material properties (Peña et al., 2006). To quantitatively determine the accuracy of the model used in this study, a subject-specific validation with a cadaveric specimen was conducted.

## 2.9. Need for Improvement/ Gap in Knowledge

The aim of the proposed research was to predict joint contact mechanics before and after virtual HTO. This was conducted by developing an accurate computer simulation of the malaligned and reconstructed knee joint on a validated subject-specific model. The main motivation for this work was to provide the foundation for developing a tool to be used in surgical realignment planning for the treatment of OA, a debilitating disease associated with pain and reduced range of motion.

Knee OA reduces quality of life by hindering an individual's capability to work or perform activities of daily living. OA is a major burden to the economy due to direct health care costs, as well as indirect costs due to absence from work (Le Pen, Reygrobelle and Gerentes, 2005). In 2006, 8.5 million Britons were diagnosed with OA and £39 billion of NHS expenditure was used to treat these patients (Department of Health, 2006). The WHO reported that OA accounted for 2.2% of the total "years of life spent living with a disability" in high-income countries (National Institute for Health and Clinical Excellence, 2005). In 2002 the cost of OA exceeded 1.6 billion Euros in France (Le Pen, Reygrobelle and Gerentes, 2005). In the US the economic and societal impact of lower extremity OA is \$171 billion per annum in direct medical care with job-related costs of \$13.2 billion annually (Maetzel et al., 2004).

There are an increasing number of younger individuals experiencing knee OA because of obesity and, in part, due to a more active lifestyle (exercise, fitness and wellness). This has resulted in patients requiring joint replacements earlier in life. However, TKA in osteoarthritic patients younger than 55 years fail earlier than those in older patients who are less active (Ranawat, Padgett and Ohashi, 1989). To address the need of the younger OA population, while preserving the tissues within the diarthrodial joint, there is a need for HTO surgical outcomes to be more consistent, hence delaying the requirement for TKA.

A critical review of the literature showed that HTO is a well-accepted and often practiced surgery, yet outcome variability can be substantial. Research that connects the individual patient's realignment requirement with predicted compartmental stress, as a function of MAD is needed. When performing lower-limb realignment surgery, surgeons target an MAD of 0 mm or an intersection of the MA at 62% of the tibial



plateau width, which is referred to as the Fujisawa Point (Fujisawa, Masuhara and Shiomi, 1979; Dorsey et al., 2006). However, the ideal alignment to interrupt the vicious circle of joint degeneration and malalignment, described by Coventry (1965), remains controversial. Malalignment and resulting excessive joint stress are considered to be common factors that damage the tissues within the diarthrodial joint, irrespective of the specific biomechanical etiology (Sharma et al., 2001). Therefore, an understanding of the relationship between knee joint alignment and contact stress, before and after HTO, could help evaluate the relative effectiveness of different surgical interventions.

Given the anatomical variations amongst individuals with OA, it is possible that achieving an MAD of 0 mm or the Fujisawa Point does not present the minimum contact stress within the knee joint. While there have been many studies of osteotomy realignment (McKellop et al., 1991; Westrich et al., 1998; Agneskirchner et al., 2006) none has optimised the correction and assessed the effects on contact stress in a subject-specific manner.

Work in this area is attracting a lot of interest from biomedical researchers, orthopaedic surgeons, medical device companies and patients. Chao has developed a 2D surgical planning tool based upon long-leg x-rays which is limited to determining frontal plane alignment correction from joint force distribution, as opposed to stress, but has still yielded improved clinical outcomes (Chao and Sim, 1995).

Reinbolt's (2008) 3D computational gait model aimed to predict post-surgical outcomes, based on patients' pre-treatment gait pattern. In his approach, the patient's post-treatment gait pattern is predicted by a musculoskeletal model, which is scaled to the stature of the patient. The outcome of interest, peak knee adduction moment, was assumed to be a surrogate for medial knee joint loading (Reinbolt et al., 2008).

*In vitro* and *in vivo* studies to investigate all of the nuances of HTO surgery would be time consuming and expensive. This research, using computational biomechanical methods, identified factors to improve HTO joint contact mechanics and brought further insight on how to improve outcomes for knee OA patients. A unique aspect of this model is that it simulated joint contact mechanics for different varus and valgus deformities pre- and post- lower extremity realignment surgery in a subject-specific manner.

This model could ultimately be used to plan conservative surgical procedures to relieve damaged tissues from excessive loading, delaying the onset and progression of OA and the need for a TKA. Improved HTO surgical techniques are anticipated to lead to an improved quality of life of patients by reducing pain, risk for revision surgery, health costs and staff time and by increasing mobility. HTO offers the possibility of significantly delaying the more invasive knee replacement surgery whilst preserving bone stock and soft tissue structures (Meding et al., 2000).

## 2.10. Conceptual framework

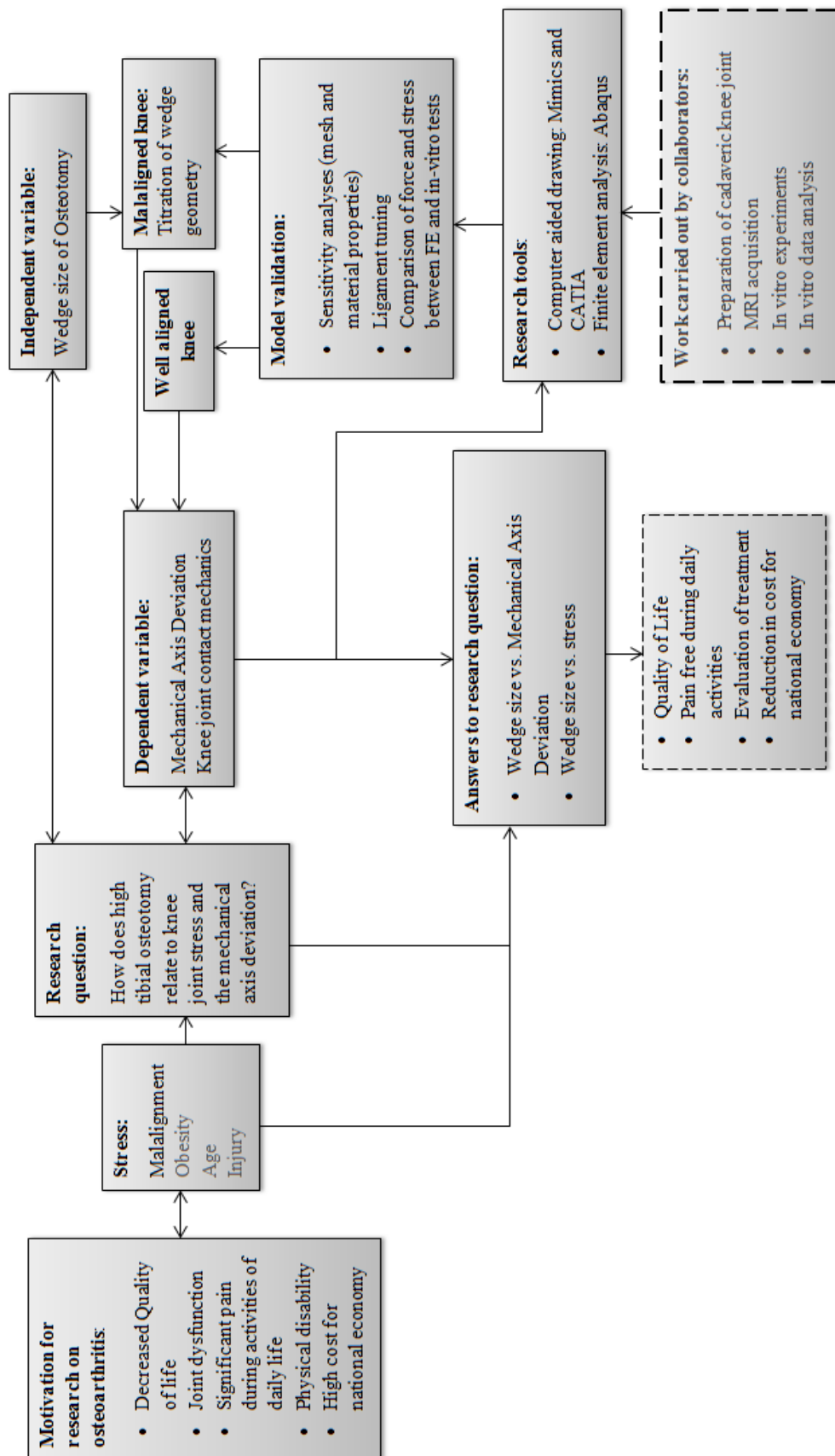


Figure 2.20: Conceptual Framework

## 2.11. Specific Aims and Hypotheses

The overarching purpose of this study was to find the relationship between peak tibiofemoral joint stress, compartment forces and MAD. A number of hypotheses were formulated and tested to achieve the specific aims and the study purpose:

**Specific aim 1: To determine the sensitivity of knee contact stress to material properties and different mesh sizes.**

**Hypothesis 1a:** The contact mechanics\* will vary more with different material properties of soft tissues compared to those of bone.

**Hypothesis 1b:** There is a threshold mesh size for bones and soft tissues below which the contact mechanics\* vary by less than 5% with additional mesh size reduction.

**Specific aim 2: To develop and validate a subject-specific finite element (FE) model with an *in vitro* experiment.**

**Hypothesis 2:** Tibiofemoral contact mechanics (normalised peak pressure, force and compartmental force ratio) of the *in vitro* experiment and corresponding FE model predictions will agree within 10% for the same boundary conditions.

**Specific aim 3: To perform virtual osteotomies on the validated knee model to predict the resulting contact mechanics\* for different knee alignments from 16° varus to 14° valgus.**

**Hypothesis 3a:** The HTO geometry that corresponds to an MAD of zero millimetres does not correspond to the minimum contact stress.

**Hypothesis 3b:** The HTO geometry that corresponds to the Fujisawa point (62 % of the distance from the medial to the lateral tibial plateau) does not correspond to the minimum contact stress.

**Specific aim 4: To find the correlation between the geometry (MAD) and the knee joint contact mechanics\*.**

**Hypothesis 4:** The 3D FE knee model will predict post-operative knee joint mechanics, as evidenced by a linear correlation of  $r > 0.8$  between surgical realignment geometry, MAD and knee joint contact mechanics.

\*contact mechanics = peak compartment stress, force and area.

It is anticipated that results of this study can be used to help improve the design and adjustment of HTO devices to improve knee joint contact mechanics. Given that HTO actually does not violate the joint, it may be considered a conservative procedure for treating the patient with knee OA, thereby improving the quality of life, reducing the need for revision surgery and reducing healthcare costs. This study is a first step towards the future development of a tool that will assist orthopaedic surgeons with surgical planning for the genuvarum or genuvalgum knee that minimises excessive stress to the tissues within the joint, thereby reducing the risk of OA progression.

### 3. Methods

A diverse set of geometries, material properties and loading and boundary conditions for computationally modelling the knee joint is discussed in the literature. This chapter covers the FE model development, method justification, problems arising in the process and the corresponding solutions, sensitivity analyses on mesh size, tuning of ligament material properties, and the model validation process.

An implicit quasi-static 3D model of the knee joint was constructed to simulate geometry, material properties and physiological loading and boundary conditions, which are important aspects of FE modelling (Yang, Nayeb-Hashemi and Canavan, 2009). This solid FE knee model was then used to simulate HTOs, by virtually removing different wedge geometries, for the correction of lower limb malalignment, as conducted in surgery. The effect of wedge geometry on knee joint stress was then investigated. The desirable wedge geometries were those that reduced peak joint contact mechanics. The load applied to the knee model, as in physiological conditions, was simulated on the natural and reconstructed knee joints. Physiological loading and boundary conditions, as well as material properties were applied to the knee model to provide accurate predictions of knee joint contact mechanics.

### 3.1. Flow chart of methods

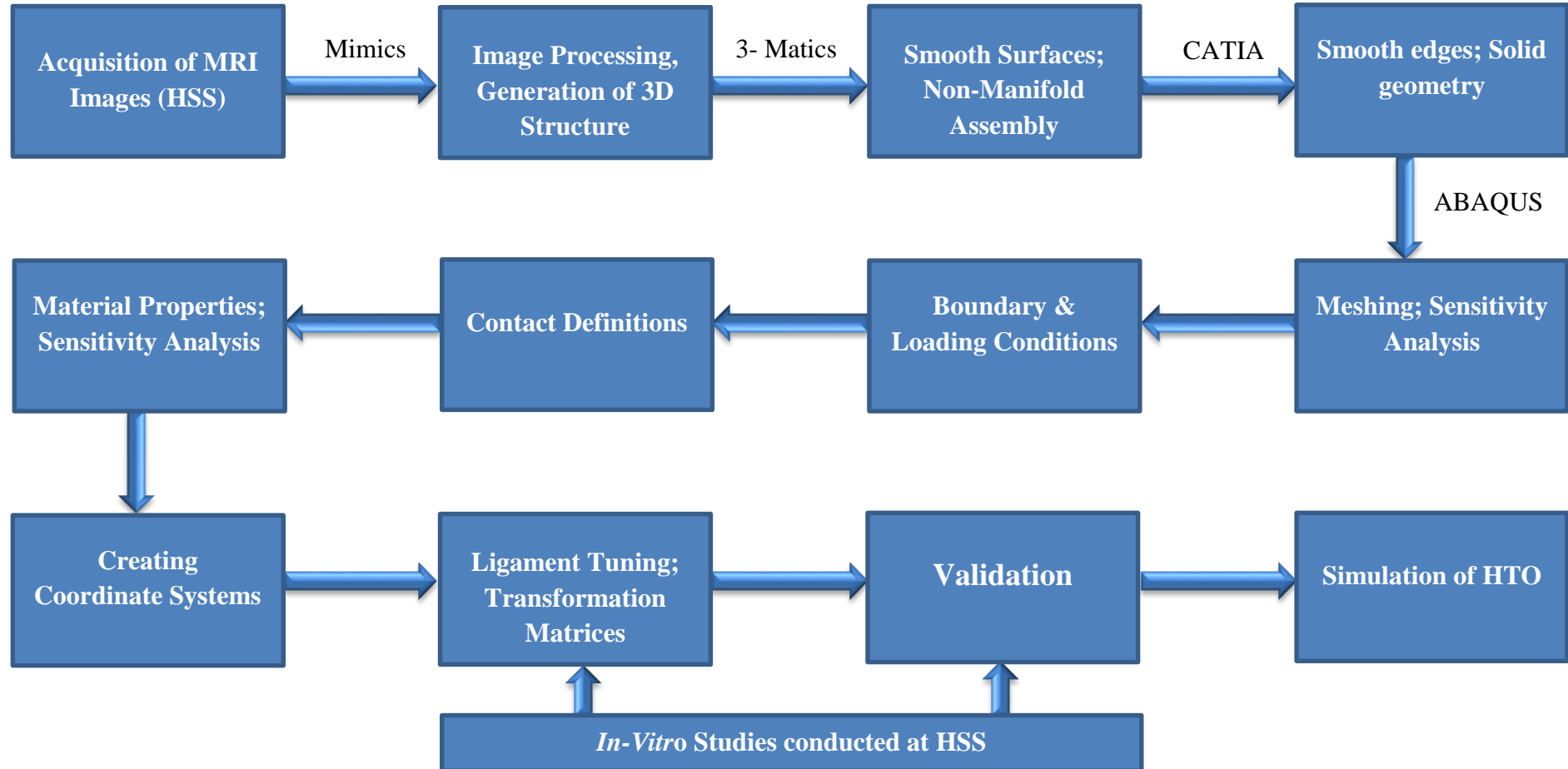
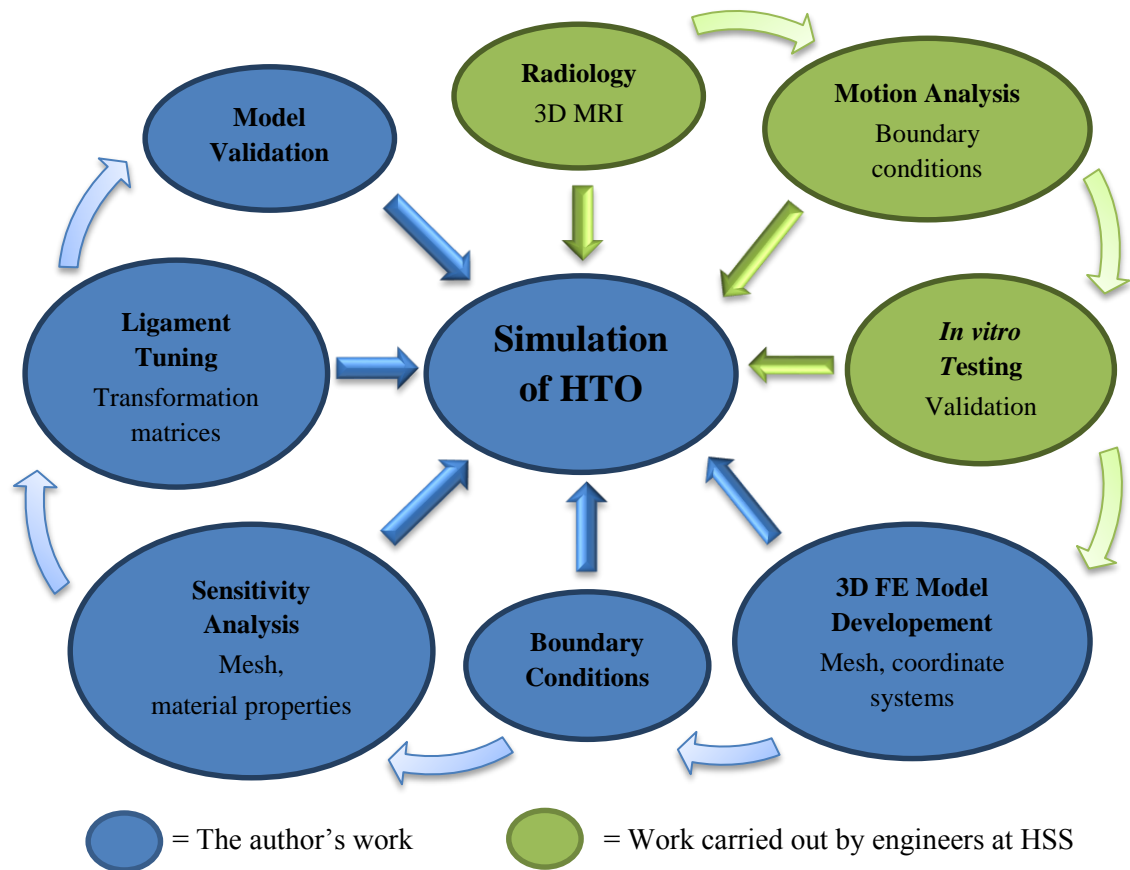


Figure 3.1: Flow Chart of Methods

### 3.2. Collaboration

MRI acquisition and a parallel *in vitro* study were conducted by our collaborators at the Hospital for Special Surgery (HSS) in New York. Data collection occurred before the author was involved in the study. However, the author actively contributed to every step of the FE knee model development and to all computations that were required for the validation process (Figure 3.2).



**Figure 3.2: Collaboration flow chart.** Boundary conditions from the Leon Root Motion Analysis Lab are to simulate the end of weight acceptance ( $F_{axial} = 811 \text{ N}$ ,  $M_{bending} = 20 \text{ Nm}$ ) for HTO assessment at the Medical Engineering Research Group; whereas boundary conditions for the Medical Engineering Research Group are to: (1) match those of the robot for model validation ( $F_{axial} = 374 \text{ N}$ ,  $M_{bending} = 0 \text{ to } 15 \text{ Nm}$ ) and (2) to simulate the end of weight acceptance to perform HTO assessments ( $F_{axial} = 811 \text{ N}$ ,  $M_{bending} = 20 \text{ Nm}$ ).



### 3.3. MRI scanner

A 3D T1-weighted frequency fat-suppressed spoiled gradient recalled echo (SPGR) sequence and a 3D CUBE scan sequence (sub-millimetre 3D data format) were used to generate a volumetric dataset for the segmentation of cartilage, bones, meniscus and ligament structures of a cadaveric specimen. Acquisition parameters for the 3D SPGR sequence were: echo time (TE): 3ms; repetition time (TR): 14.6ms, acquisition-matrix: 512×512; number of excitations: 2; field-of view: 15cm; slice thickness: 0.6 mm; receiver black and white:  $\pm 41.7$  kHz. Parameters for the 3D CUBE sequence were: TE: 33ms; TR: 2500ms; acquisition-matrix: 512×512; number of excitations: 0.5; field-of-view: 15cm; slice thickness: 0.6 mm; echo train length: 42; receiver black and white:  $\pm 41.7$  kHz. The in-plane resolution for both scans was 0.29 mm×0.29 mm.

Each of the 10 magnets in the MRI Centre of HSS is periodically calibrated by a physicist from the manufacturer (GE). The magnets undergo a major calibration when they are first installed. The first task is to obtain stability of the centre frequency. Then the field engineer can do a coarse adjustment of the field. Next, a passive shimming is performed using a passive shim camera. This is done with fiberglass rods that extend down the bore of the scanner (~4-5ft in length) that have > 40 attachment points for pieces of metal of known sizes and composition. Each rod has its own position around the bore (0-360°). The calibrator sweeps the passive shim camera around the bore, taking measurements of the centre frequency and then a computer program performs an optimisation to make the frequency at the isocentre within specification (5-10 ppm). This is an iterative process and is repeated until specification is met. Periodic proof-of-performance measurements are made with a precision phantom.

MRI has a superior soft tissue contrast and is considered the most accurate imaging modality available for assessment of articular cartilage (Andriacchi et al., 2000). Although CT images are commonly used to provide accurate geometry of bones (Keyak and Skinner, 1992; Bendjaballah, Shirazi-Adl and Zukor, 1995; Gardiner and Weiss, 2003), MRI can also give accurate geometrical representations of the osseous tissues within the knee joint when an appropriate scanning sequence is used and the joint line is positioned in the centre of the field of view (Mootanah, et al., 2011).

Although MRI is known to result in a shrinkage in the bony geometry (Bowers et al., 2007), the CUBE sequence causes only a 1.5% shrinkage at the joint line in a field of view of 15 cm (Mootanah, et al., 2011). The CUBE sequence gives accurate representation of meniscus and ligaments and the SPGR sequence gives accurate representations of bones and cartilage (Figure 3.3). Hence, these two MRI scanning sequences were used to create the 3D knee model.

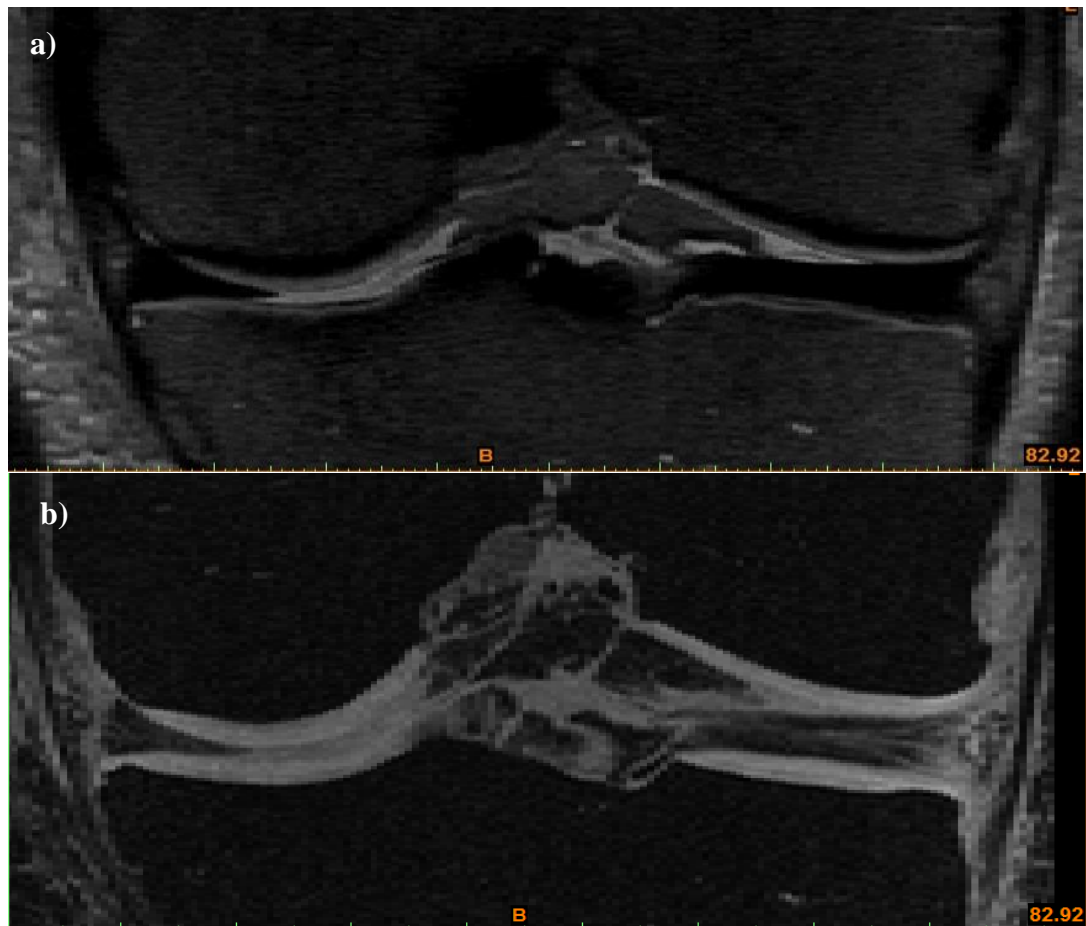


**Figure 3.3: MRI images of the coronal view of the knee joint in (a) CUBE sequence for accurate representation of meniscus and ligament and (b) SPGR sequence for accurate representation of cartilage and bone**

### **3.4. Cadaveric specimen**

The left lower extremity of an anonymous 50-year-old male (1.65 m; 68 kg) was obtained from a tissue bank (Appendix A-1), screened negative for blood-borne pathogens, and had no visible sign of tissue damage or disease within the knee. The fresh-frozen ( $-20^{\circ}\text{C}$ ) cadaveric specimen was truncated to 15 cm above and below the knee joint, secured in a sealed plastic bag and taken to the HSS Radiology Department.

The donor had a 1° varus knee alignment, which was within normal limits (Insall, Joseph and Msika, 1984; Moreland, Bassett and Hanker, 1987; Hsu et al., 1990; Chao et al., 1994). Ethical approval to carry out this study was obtained from HSS (Appendix A-2).

### **3.5. Six-Degree-of-Freedom Robot**

Parallel in-vitro studies were conducted using a 6 DOF robotic arm (ZX165U; Kawasaki, Tokyo, Japan). The robot used force feedback to determine the kinematic pathway to achieve the desired loading conditions within a prescribed tolerance of  $\leq 5$ -N force and  $\leq 0.5$ -Nm moment. Under worst case scenarios of maximum speed and payload, the position repeatability of the robot is  $\pm 0.3$ mm (Kawasaki Robotics cited in Imhauser et al., 2013, p. 816).

### **3.6. Development of an Accurate 3D FE Knee Model**

#### **3.6.1. Creation of 3D Osseous and Soft Tissues from MRI**

##### ***Tissue Visualisation***

DICOM images of the SPGR and CUBE MRI datasets of the cadaveric knee joint were imported into Mimics V14.2 (Materialise, Leuven, Belgium). Mimics is a specialised image processing software that interfaces 3D radiology with FE packages. The CUBE sequence was used to create accurate 3D representations of the medial and lateral menisci, the anterior and posterior cruciate ligaments and the medial and lateral collateral ligaments. The SPGR sequence (Figure 3.4) was used to create accurate representations of the tibia, femur, fibula, as well as the medial and lateral tibial and femoral cartilage. The 3D models were created using a number of image processing algorithms within Mimics, including 3D livewire, manual editing and non-manifold assembly, as detailed below.

Amadi et al. (2008) showed that the meniscomfemoral ligaments of the human knee, which connect the posterior horn of the meniscus to the medial femoral condyle, significantly contributed to lateral knee joint contact pressure (Amadi et al., 2008). However, these ligaments are found in only 50% of human knees (Gupte et al., 2002) and were not present in the cadaveric knee used in this study.

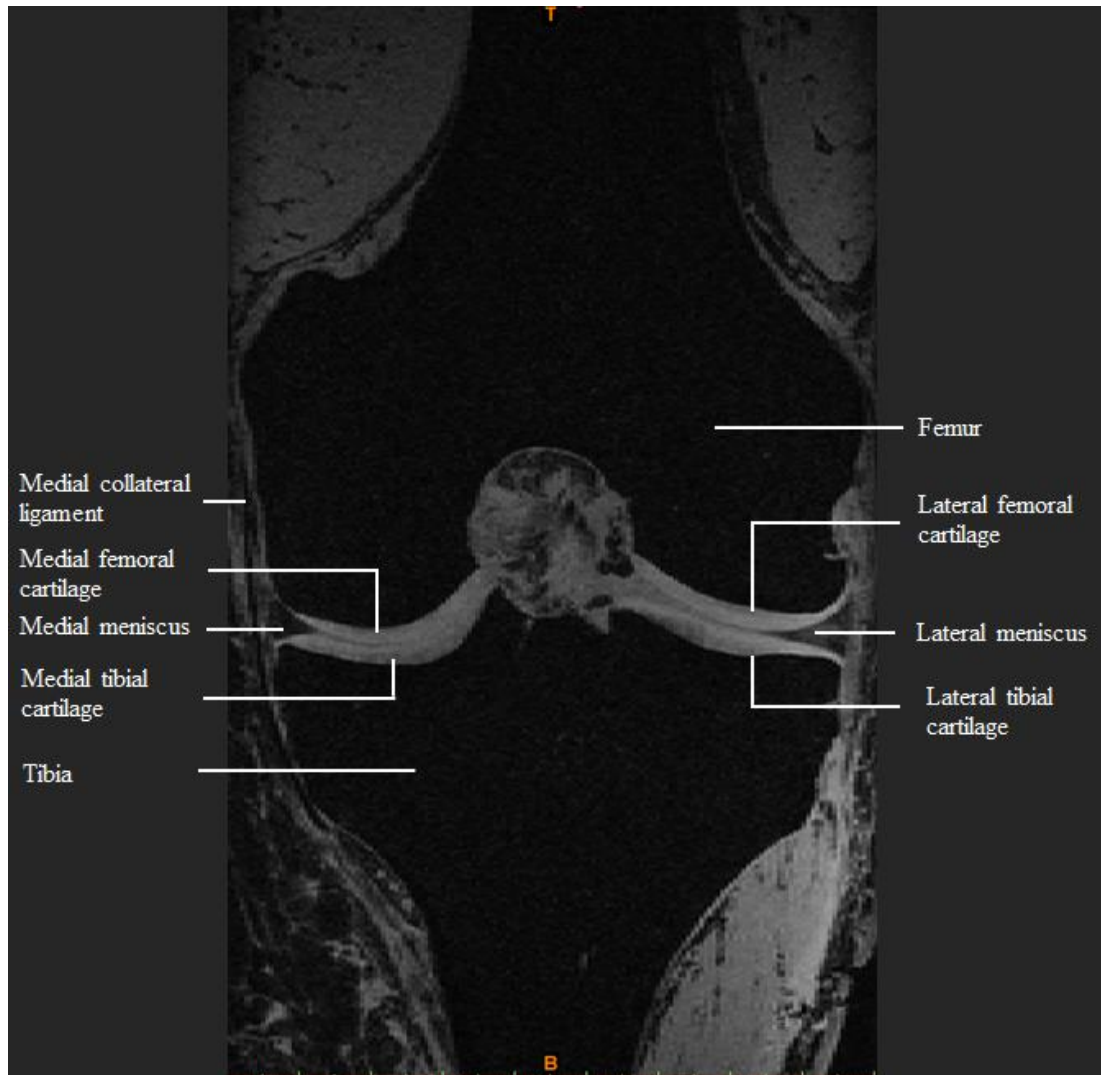


**Figure 3.4: MR image of the knee joint (coronal view)**

After setting the correct orientation (anterior, posterior, medial and lateral) according to the original MRI scan and selecting the region of interest, the data are displayed in the following views as shown in Figure 3.5:

- Axial (or Top) view
- Sagittal (or Side) view
- Coronal (or Front) view
- 3D view

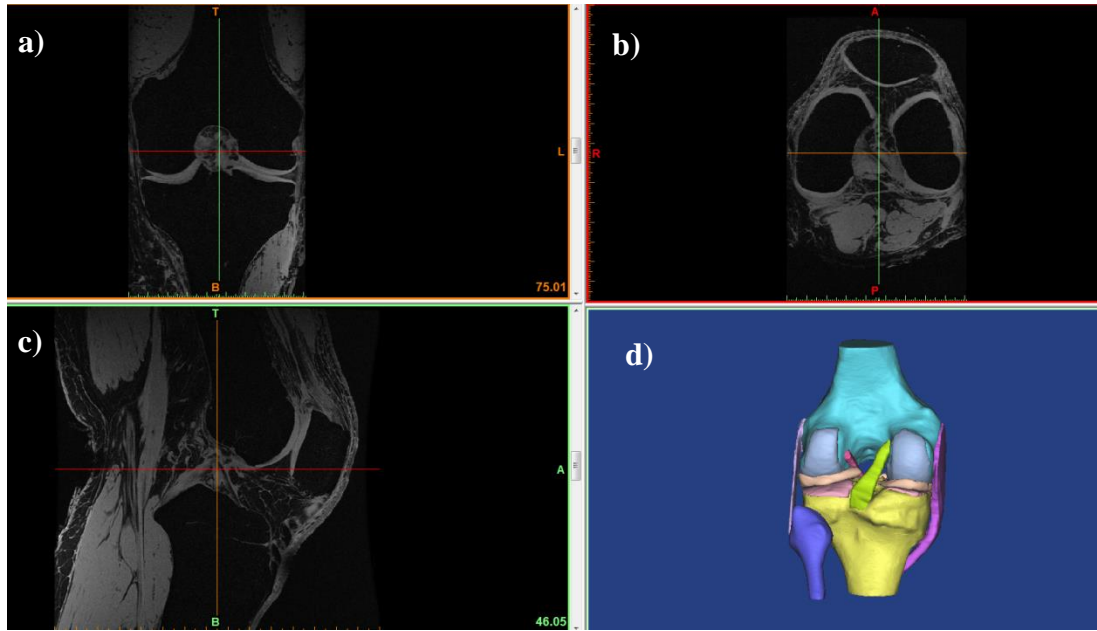


**Figure 3.5: Mimics workspace; a) coronal view; b) axial view; c) sagittal view and d) 3D view**

### *Tissue Segmentation*

The most straightforward procedure for bone (femur, tibia and fibula) and soft tissue (menisci, ligaments and cartilage) segmentation from MRI data, is to use the 3D LiveWire tool. This is an interactive segmentation method to identify points lying at the tissue boundaries in all three planes. A line was drawn between the points and snapped to the boundaries of the object (Figure 3.6a). Depending on the image gradient, the snapping is more or less accurate. Based on this information, a close contour was formed at the boundaries of the structure to be segmented and a mask was created (Figure 3.6b).

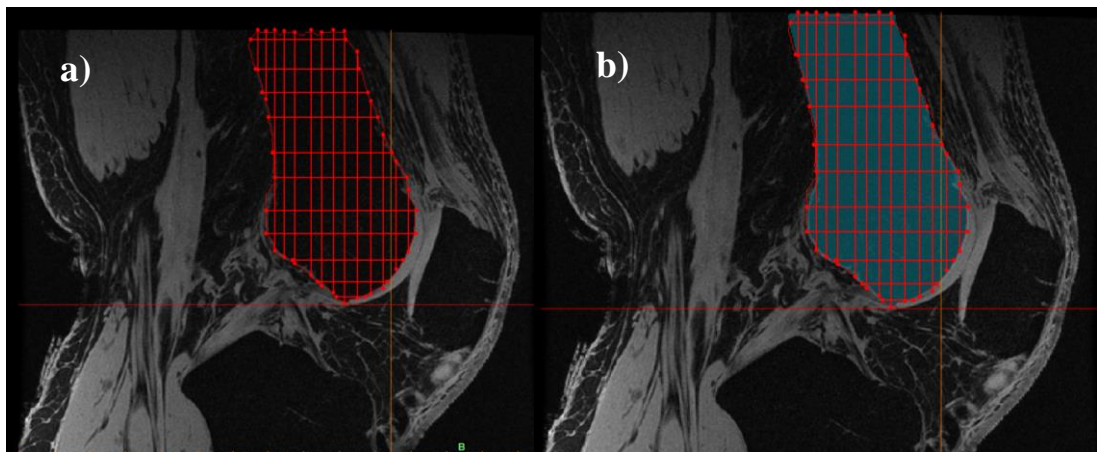


**Figure 3.6: The 3D Live Wire algorithm: a) to create geometries of the different tissues, b) 3D Live Wire with mask**

## ***Tissue Masking***

These masks were then used to create accurate 3D models of the different tissues comprising the knee joint. Each tissue was drawn to intersect the attached tissue in order to avoid gaps between them. These intersecting regions were then eliminated in the non-manifold assembly algorithm, described in Section 3.6.2.

## ***3D Model Development***

Any artefacts were removed from the 3D model using the “Edit mask in 3D” tool. This allowed visualising and editing the mask in 3D (Figure 3.7).

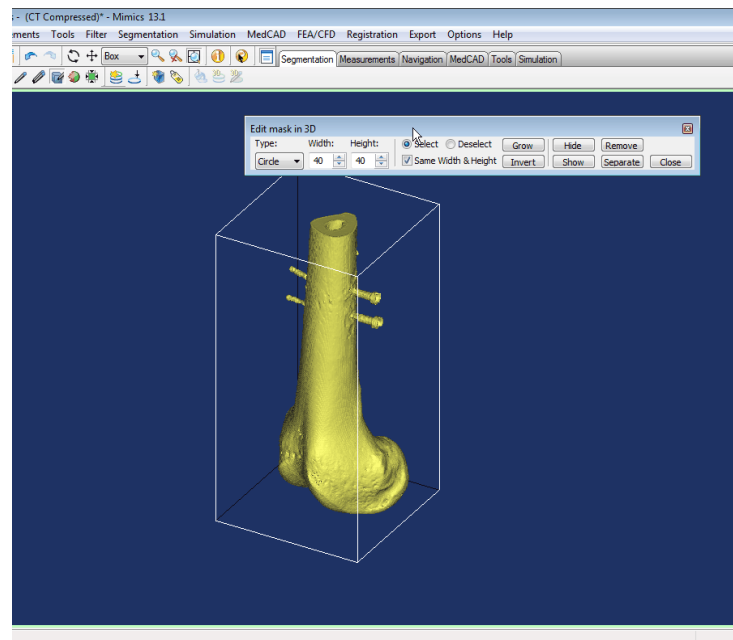


**Figure 3.7: Editing mask in 3D**

To fill the cavities in the simulated parts, the “Multiple Slice Editing” tool was used. This tool allowed manual editing on several slices of the mask so that a completely filled mask of the part could be produced in an efficient manner (Figure 3.8).

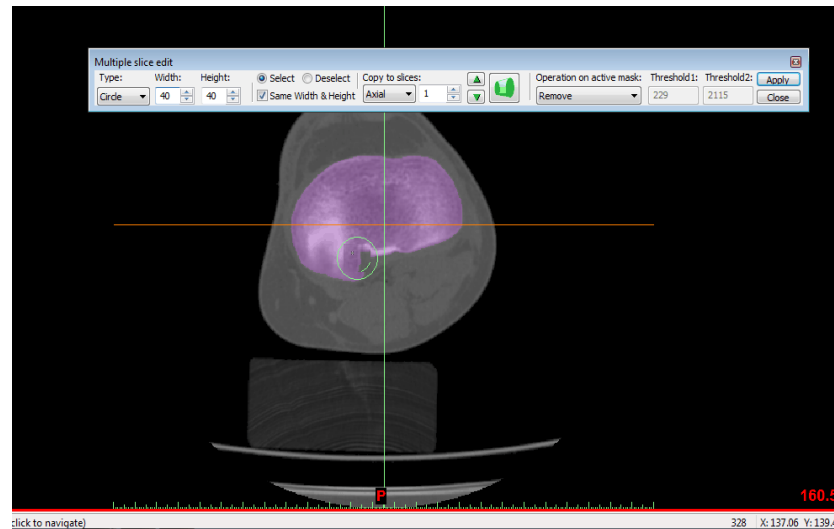


**Figure 3.8: Multiple slice editing**

Once the mask was completely edited, the 3D model of each part was generated (Figure 3.9).

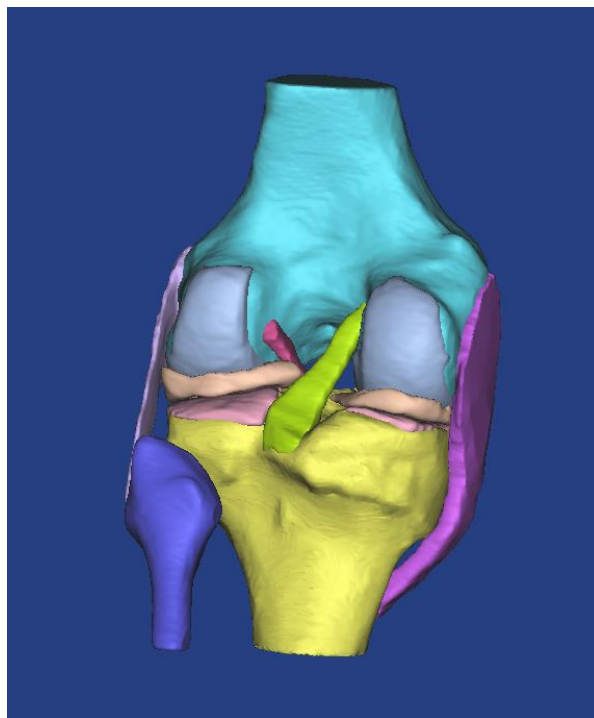


**Figure 3.9: Creating the 3D model**

Extensive effort was invested to ensure accurate geometry of the knee model. Beillas et al. (2004) stated that “errors as small as 1 mm on bone positions may have unacceptable effects on the predictions of loads”. Meakin et al. (2003) found that the geometry usually has a greater effect on the behaviour of the model than material properties. Results of their study indicated that inconsistent geometry between the



femur and the meniscus influenced the magnitude and distribution of meniscal and cartilage stress within the tissues (Meakin et al., 2003).

The surface mesh quality was improved, using the smoothing, reducing and re-meshing module of Mimics. This tool expedited the meshing process by deleting many sharp edges that were created during segmentation. This process promoted high quality 3D elements to be produced during the FE meshing stage. The smoothing operation decreases the “noise”, introduced during the scanning process. A smooth surface minimises high stress concentrations that may result in unreliable predictions.

### **3.6.2. Non-Manifold Assembly of Bone and Cartilage**

It is important to have common borders between the adjacent tissues to obtain FE model stability while solving. The creation of adjacent anatomical structures in any CAD package inevitably results in gaps or overlaps at surfaces in contact for reasons including: (i) quantification errors when approximating a continuous surface with discrete elements (voxels), (ii) low image gradient at the boundary between two anatomical structures and (iii) approximations caused by the smoothing process. To avoid contact boundary gaps or overlaps when creating the FE model, common borders between adjacent masks were created, using the ‘non-manifold assembly’ tool in Mimics, thereby allowing a straightforward workflow towards solving the FE model (Figure 3.10). This method is particularly useful for structures with complex and irregular geometries such as the knee joint. This procedure was repeated until all parts comprising the knee joint were included, one at a time.



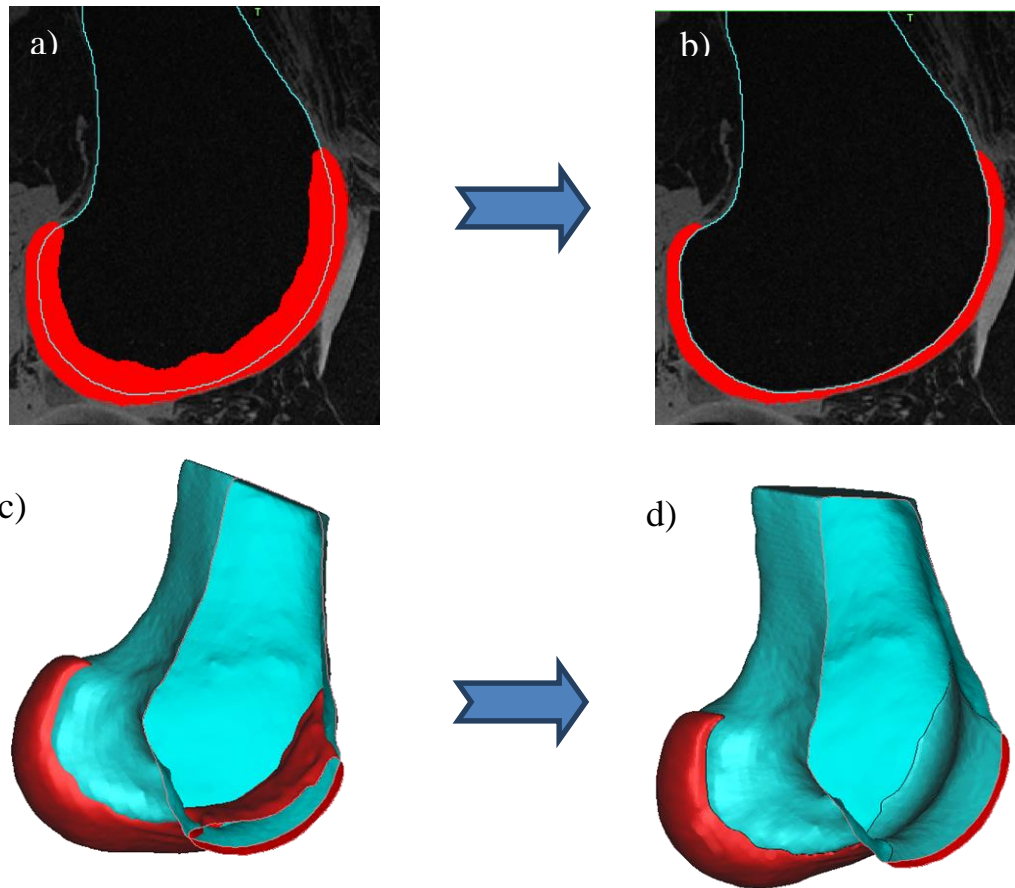


**Figure 3.10: The use of the ‘non-manifold algorithm’ to create common contact areas between adjacent tissue, such as the distal femur and femoral cartilage. a) The inner geometry of the cartilage (in pink) was overestimated to protrude into the femur (outlined in b in blue) and eliminate any gap at the femur-cartilage boundary. b) The non-manifold assembly technique superimposed the accurately-identified femur with the overestimated cartilage image to remove overlaps between the femur and cartilage, creating a common boundary between the adjacent femur and cartilage surfaces. c) 3D view of femur with cartilage before non-manifold algorithm. d) 3D view of femur with cartilage after non-manifold algorithm**

The remeshed knee joint surface assembly was then exported in stereolithography format (.stl) to the computer aided design package CATIA V5R18 (Dassault Systèmes, Vélizy-Villacoublay, France), where accurate solid geometries of the osseous and soft tissues were created (Figure 3.11) for the subsequent generation of a 3D FE knee model.

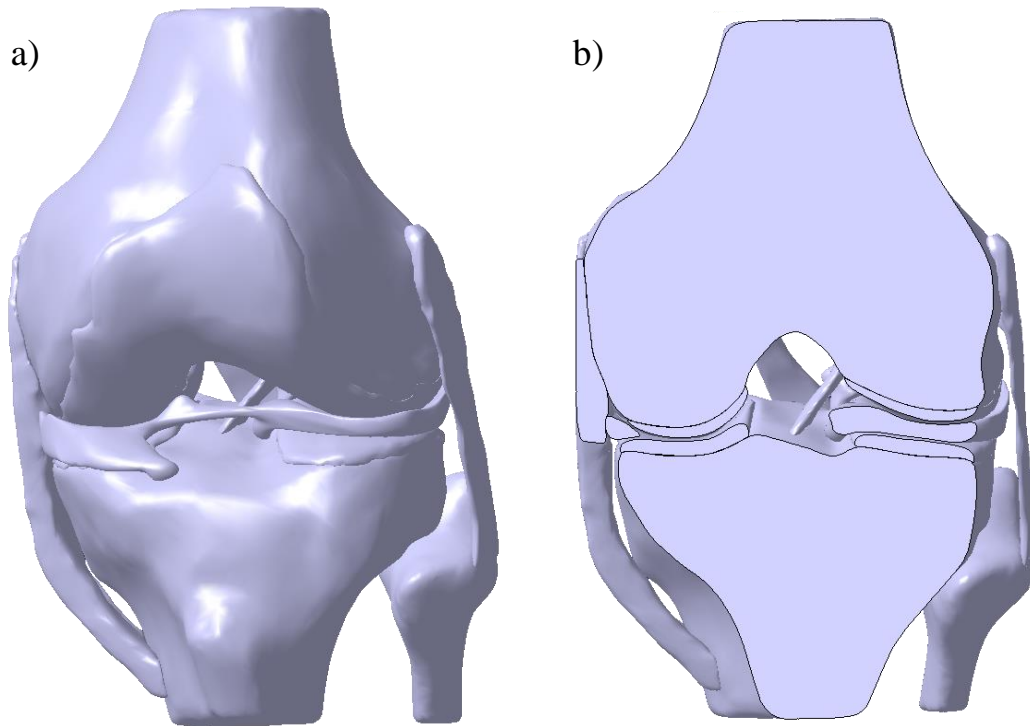


**Figure 3.11: Solid 3D geometry of the full knee assembly. a) anterior view; b) cross sectional view**

### ***Meshing Techniques***

In order to mesh the soft tissues using superior hexahedral elements, their edges had to be thickened in CATIA. This was accomplished by creating a 3D spline (Figure 3.12) around the edge of the structure, which was then employed to cut through the part to create a thick edge and enable the creation of hexahedral mesh. This method was repeated for all ligaments, cartilage and the meniscus and has been used by several authors (Keyak and Skinner, 1992; Perie and Hobatho, 1998; Donahue et al., 2002; Peña et al., 2006; Kazemi et al., 2011; Mononen, Jurvelin and Korhonen, 2013). The solid 3D knee joint assembly model was then exported to Abaqus V6.12-3 (Dassault Systemes Simulia Corp., Providence, RI, USA).

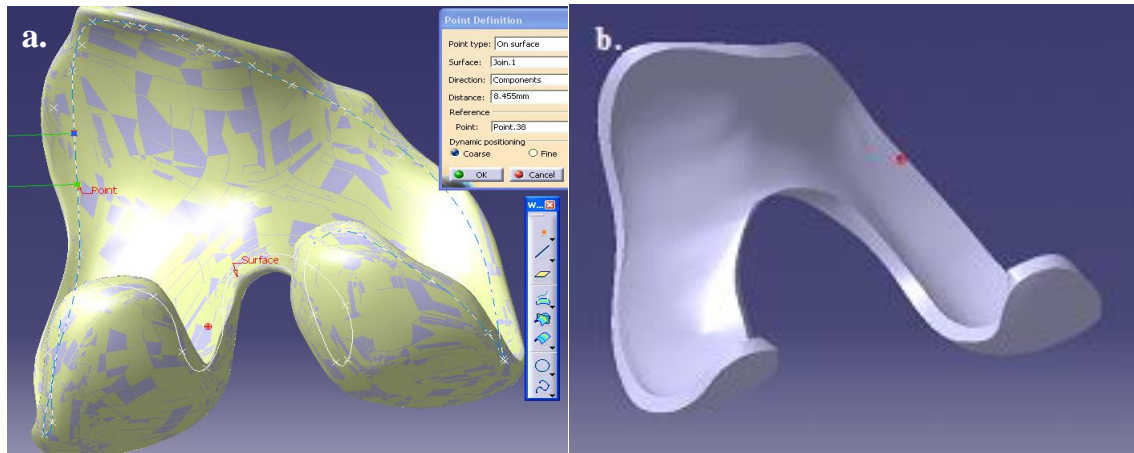


**Figure 3.12: Model preparation for hexagonal meshing a) A 3D spline was created near the edge of the cartilage surface. b) The 3D spline was used to truncate the very thin edge to produce a finite thickness that would accommodate hexahedral elements.**

### 3.7. Mesh Quality

In order to create a uniform mesh in Abaqus, a virtual topology technique, which merges several faces together, was employed (Figure 3.13).

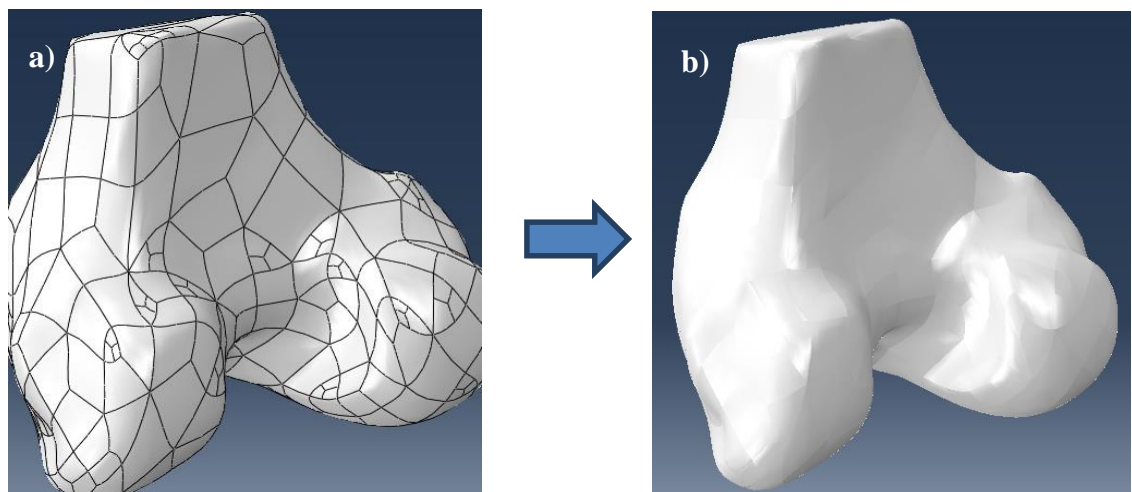


**Figure 3.13: 3D model of the femur a) before and b) after virtual topology technique**

It was difficult to fit hexagonal mesh elements in the bones, due to their many radii of curvature that form their irregular shape. Therefore, 4-noded tetrahedral elements were used, which still remain one of the most popular primitives for modelling complex geometry (Weiss and Gardiner, 2001). Even though hexahedral elements are noted for their high accuracy in FEA (Viceconti et al., 1998; Tadeipalli, Erdemir and Cavanagh, 2011), it was acceptable to use tetrahedral elements for the osseous tissues because the area of interest for the stress analysis was in the tibial and femoral cartilage, not the bones.

### ***Bone Meshing***

A sensitivity analysis was carried out to investigate whether 4-noded linear tetrahedral elements gave similar results to 10-noded quadratic elements. Force, contact pressure, maximum compressive stress and the shear stress in the tibial cartilage were compared when the bones were modelled with both mesh types. Full scale error (FSE) was less than 2% in all cases (Section 4.1), so 4-noded tetrahedral elements were used to mesh bony tissues. The FSE was obtained by expressing the RMSE as a percentage of the maximum corresponding value.

### ***Soft tissue meshing***

The soft tissues were meshed with 8-noded hexahedral elements. The ligaments were meshed with element sizes ranging from 0.5 mm to 1.5 mm. The largest mesh size for each element was then computed in Abaqus. The aim was to obtain the largest mesh size while maintaining accuracy and a minimum convergence time.

The cartilage and meniscus mesh were created as uniform and smooth as possible, using planes to generate even partitions. These were used to create a better mesh quality for each tissue (Figure 3.14).

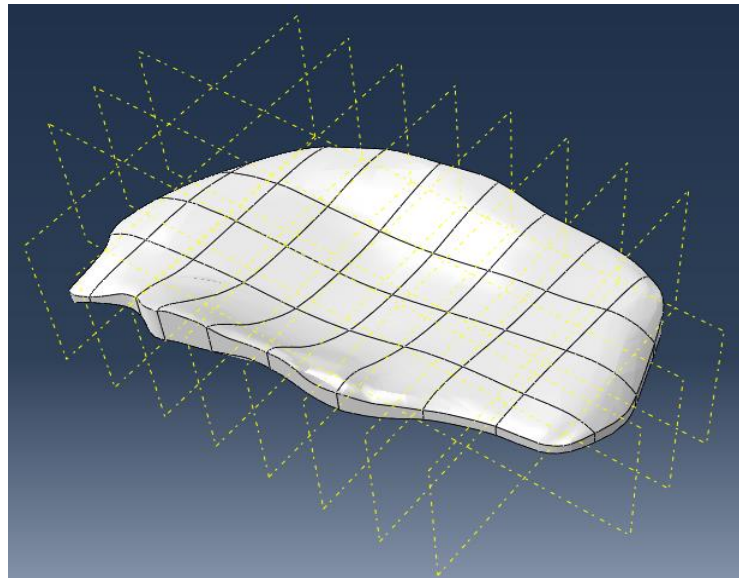


**Figure 3.14: Planes to generate even partitions and mesh distribution within soft tissues (e.g. tibial cartilage). Each grid represents a partition of the tissue.**

The cartilage and menisci were then meshed using a reference element size of 1 mm in two and three layers, respectively. Element validity was checked to obtain high-

quality mesh, using the “verify mesh” tool (Figure 3.15). Highlighted elements of high aspect ratio and poor quality were then manually edited to improve mesh quality, using the node dragging operation.

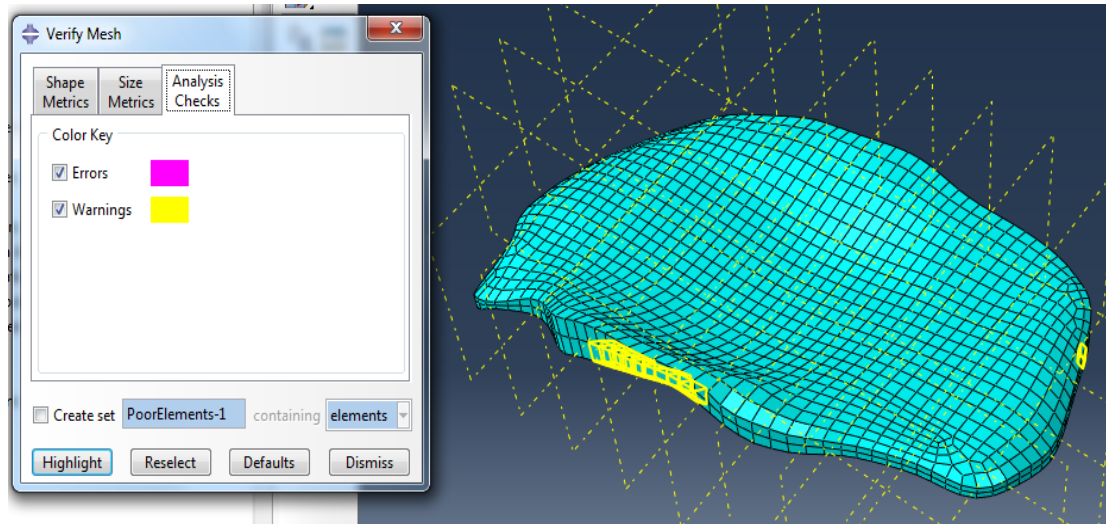


**Figure 3.15: Element validity check to obtain high-quality elements, using the “verify mesh” tool**

A sensitivity analysis, using refined meshes for femoral and tibial cartilage, as well as menisci, was conducted to ensure that peak joint pressure did not change by more than 5% (Section 4.2). From the analysis it was concluded that a mesh size of 1 mm for tibial and femoral cartilage, as well as menisci, provided minimal computational burden while ensuring acceptable accuracy.

FE model accuracy depends on mesh size, shape and quality. Therefore, the element aspect ratio, which represents the ratio of edge lengths, was evaluated. An aspect ratio of 1.0 is considered ideal. However, as the geometry of the cartilage and the inner periphery of the meniscus were very thin and uneven, an average aspect ratio of 3.0 was considered acceptable. Other investigators also consider this threshold acceptable (Kazemi et al., 2011). This is well below the default criteria of 10, which is considered acceptable within Abaqus software (Abaqus 6.13 Documentation). Table 3.1 summarises the average aspect ratio of femoral and tibial cartilage as well as menisci.

**Table 3.1: Aspect ratio of tibial and femoral cartilage and menisci**

<b>Tissue</b>	<b>Average Aspect Ratio</b>	<b>% of elements with average aspect ratio &gt; 3</b>
Femoral cartilage	1.70	1.62
Medial Tibial Cartilage	1.53	0.89
Lateral Tibial Cartilage	1.44	0.30
Menisci	2.96	32.24

Although 32.24% of the meniscus elements were above an aspect ratio of 3, the average aspect ratio was 2.96, which met acceptance criteria. Only 1.22% of the meniscus elements were above an aspect ratio of 10 (Abaqus default). These elements were not in the area of interest and no analysis errors were reported for the element quality within Abaqus. Therefore, the selected mesh was considered suitable. The final FE mesh of the intact knee joint was constructed with 158738 4-noded linear tetrahedral elements (C3D4) and 33827 8-noded linear hexahedral elements (C3D8R). This allowed an acceptable compromise between accuracy and computational cost. Table 3.2 summarises the element size and type of mesh for each component within the knee joint and Figure 3.16 shows the meshed knee assembly.

**Table 3.2: Final mesh sizes for the knee assembly**

<b>Part</b>	<b>Element size</b>	<b>Type</b>		<b>Number of elements</b>
ACL	0.5-1.5	Hex	8-node linear	597
LCL	0.5-1.5	Hex	8-node linear	1386
MCL	0.5-1.5	Hex	8-node linear	10810
PCL	0.5-1.5	Hex	8-node linear	688
Meniscus	1.0	Hex	8-node linear	4314
Femoral cartilage	1.0	Hex	8-node linear	11044
Lateral tibial cartilage	1.0	Hex	8-node linear	2982
Medial tibial cartilage	1.0	Hex	8-node linear	2006
Femur	2.5	Tet	4-node linear	86207
Fibula	2.0	Tet	4-node linear	14985
Tibia	2.5	Tet	4-node linear	57546



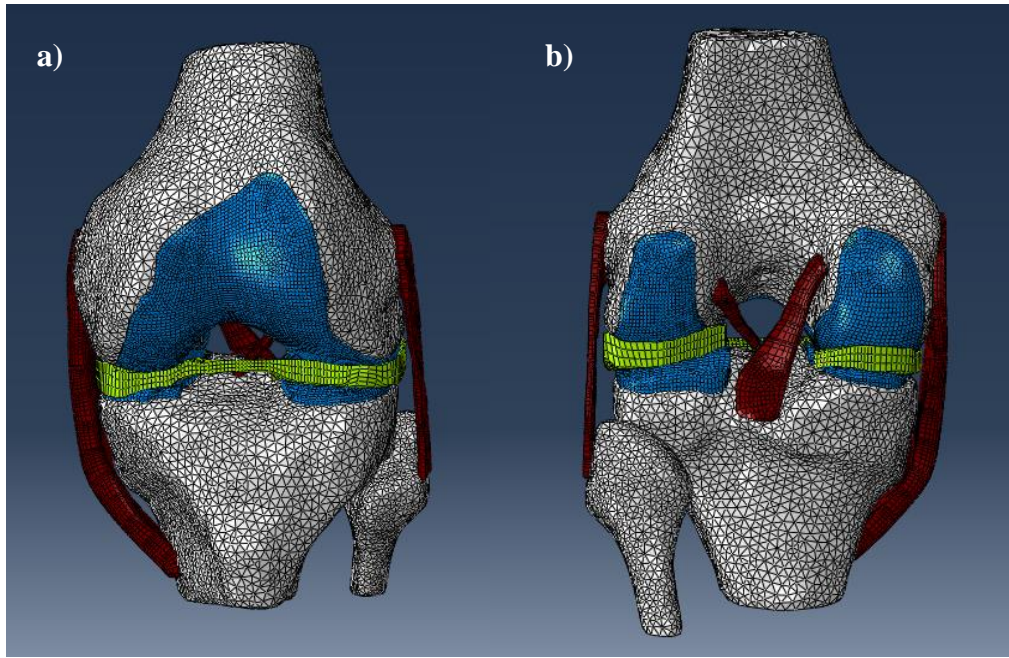


**Figure 3.16: Finite element mesh of the knee a) anterior view and b) posterior view**

It was noted that a few cartilage elements were distorted during the analysis. This effect is referred to as hourglassing as the elements distort into a shape of an hourglass (Figure 3.17).

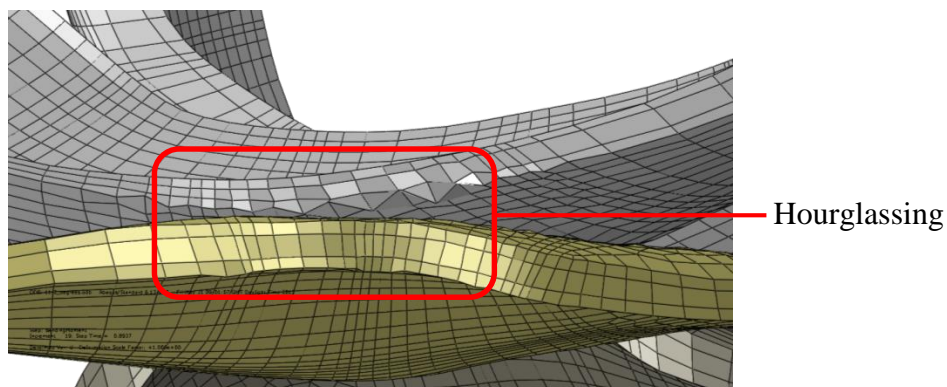


**Figure 3.17: Hourglassing between the femoral and tibial cartilage contact**

To overcome that problem, an enhanced hourglass control was applied. Hourglass controls are additional constraints applied to the element to help resist deformation to which they normally have no resistance. To ensure that the additional constraint did not affect the stress in the compartments, a comparison between the analysis with and without hourglass controls was conducted. Table 3.3 shows a summary of the results. The complete sensitivity analysis can be found in Appendix B.

**Table 3.3: The root mean square and percent full scale error between FE models with and without hourglass control**

	RMSE		% Full Scale Error	
	Lateral	Medial	Lateral	Medial
Force	0.13 N	0.08 N	0.02	0.03
Contact Pressure	0.10 MPa	0.05 MPa	2.31	1.92
Min. Principal Stress	0.06 MPa	0.02 MPa	1.28	0.72
Shear	0.12 MPa	0.04 MPa	3.72	2.38

The above results show that the hourglass control resulted in less than 3% FSE in stress and force within the medial and lateral compartments.

### 3.8. Joint Coordinate System

To evaluate the motions of the knee joint in all 6 DOF the Grood and Suntay knee joint coordinate system (1983) was created. This coordinate system (CS) was derived, using Euler angles as a precise mathematical description for joint rotational motions. The purpose of a CS is to specify the relative position between two bodies (Grood and Suntay, 1983).

In order to create the knee joint CS 1) the embedded femoral and tibial Cartesian coordinate frames; 2) a fixed axis for rotation and translation within the tibia and femur; and 3) a translational reference point (midpoint between the femoral epicondyles ( $ORG_{fem}$ )) were specified.

The directions of the fixed femoral and tibial axes were specified by unit base vectors  $e_1$  (a line connecting the femoral epicondyles, represented by points 8 and 9) and  $e_3$  (a line connecting the  $e_1$  bisection and most distal posterior tibia (point 7)) (Figure 3.18).



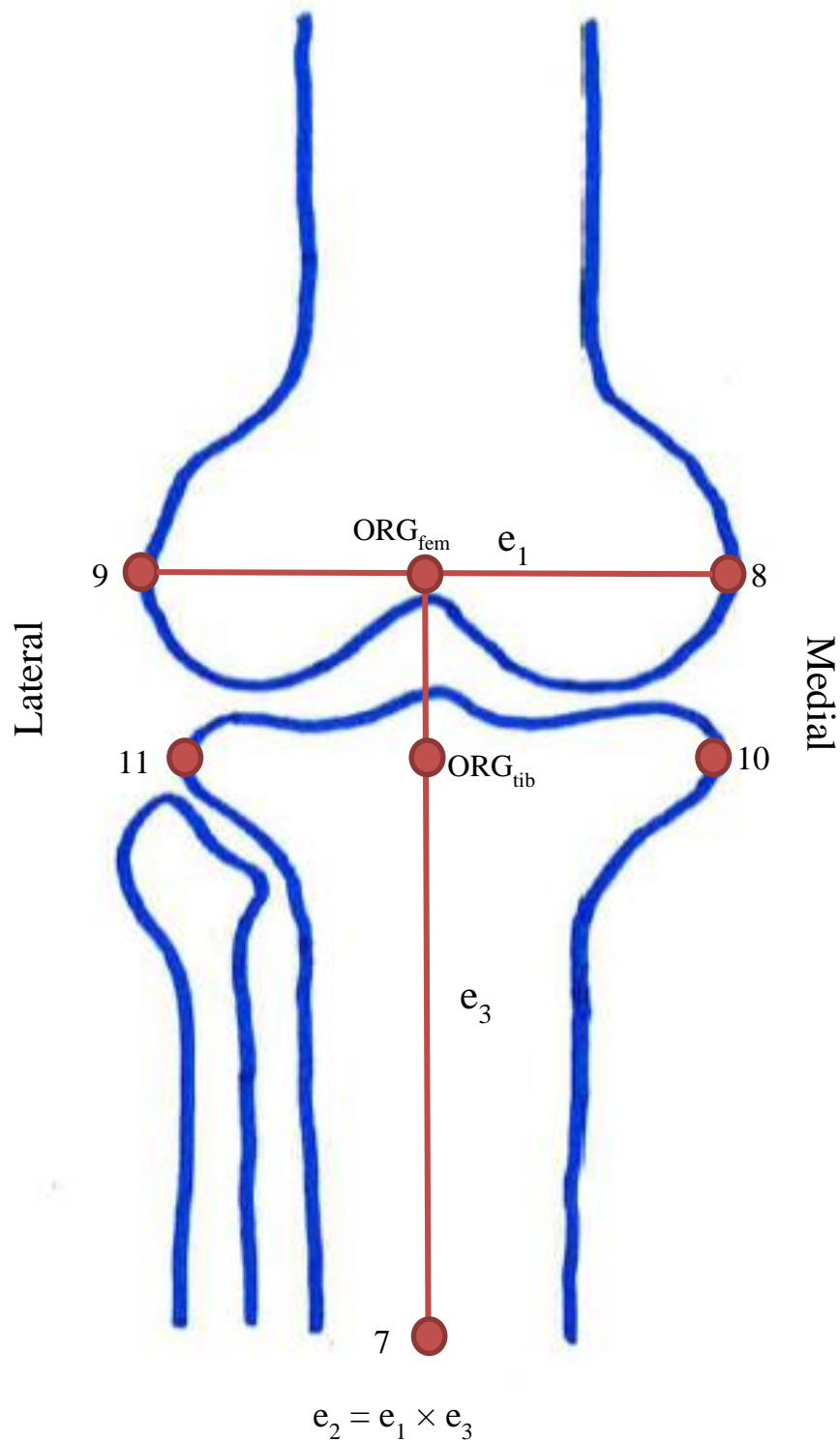


**Figure 3.18:** Femoral and tibial axes to represent the knee joint coordinate system.  $e_1$ = a line connecting the femoral epicondyles, represented by points 8 and 9;  $e_3$ = a line connecting the  $e_1$  bisection and most distal posterior tibia (point 7);  $e_2$ = cross product of  $e_1$  and  $e_3$

### ***The femoral embedded frame***

A temporary x-axis of the femoral embedded frame was created from the midpoint of the femoral epicondyles ( $ORG_{fem}$ ) to the most distal posterior tibia ( $e_3$ ). The fixed axis  $e_1$  was defined as the y-axis. The z-axis was the cross product of  $e_1$  and the temporary x-axis of the femoral embedded frame. The final x-axis was then calculated as the cross product of the y- and z-axes. Figure 3.19 illustrates the equations to calculate each axis of the femoral embedded frame.

$$ORG_{fem} = \frac{1}{2} (8 + 9) \quad \text{Equation 1}$$

$$X_{fem-temp} = \frac{7-ORG_{fem}}{7-ORG_{fem}} \quad \text{Equation 2}$$

$$Y_{fem} = \frac{8-9}{8-9} \quad \text{Equation 3}$$

$$Z_{fem} = X_{fem-temp} \times Y_{fem} \quad \text{Equation 4}$$

$$X_{fem} = Y_{fem} \times Z_{fem} \quad \text{Equation 5}$$

**Figure 3.19: Equations to calculate the femoral embedded frame**

### ***The tibial embedded frame***

A temporary y-axis of the tibial embedded frame was defined by a line connecting the tibial epicondyles represented by points 10 and 11 (Figure 3.18). The x-axis of the tibial embedded frame was represented by  $e_3$ . The z-axis of the tibial embedded frame was obtained from the cross product of the temporary y-axis and the body fixed axis  $e_3$ . The final y-axis was then calculated as the cross product between the z- and x-axes. Figure 3.20 illustrates the equations to calculate each axis of the tibial embedded frame.

$$y_{tib-temp} = \frac{10 - 11}{10 - 11} \quad \text{Equation 6}$$

$$ORG_{tib} = \frac{1}{2} (10 + 11) \quad \text{Equation 7}$$

$$x_{tib} = \frac{7 - ORG_{tib}}{7 - ORG_{tib}} \quad \text{Equation 8}$$

$$z_{tib} = x_{tib} \times y_{tib-temp} \quad \text{Equation 9}$$

$$y_{tib} = z_{tib} \times x_{tib} \quad \text{Equation 10}$$

**Figure 3.20: Equations to calculate the tibial embedded frame**

Figure 3.21 shows the position of the femoral and tibial embedded frame within the 3D knee model.

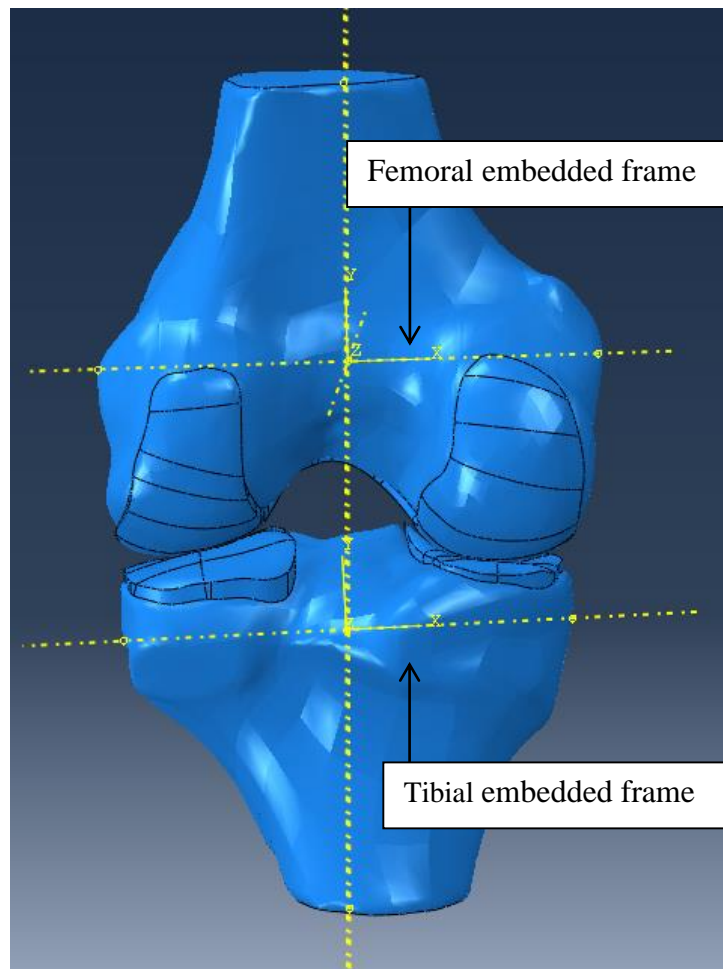


**Figure 3.21: Position of tibial and femoral embedded frames**

### ***The knee joint coordinate system***

The relative joint rotations between the two bones can be defined by creating the joint CS, which is composed of the femoral and tibial fixed axes  $e_1$  and  $e_3$  and their common perpendicular  $e_2$  (Figure 3.22). Flexion-extension occurs about  $e_1$ ; abduction-adduction occurs about  $e_2$ ; and internal-external rotation is about  $e_3$ . Medial-lateral tibial thrust is a motion of the tibial origin with respect to the femoral origin along the  $e_1$  axis; anterior-posterior tibial drawer is a motion along the  $e_2$  axis; and joint distraction-compression is designated by a motion along the  $e_3$  axis (Grood and Suntay, 1983).

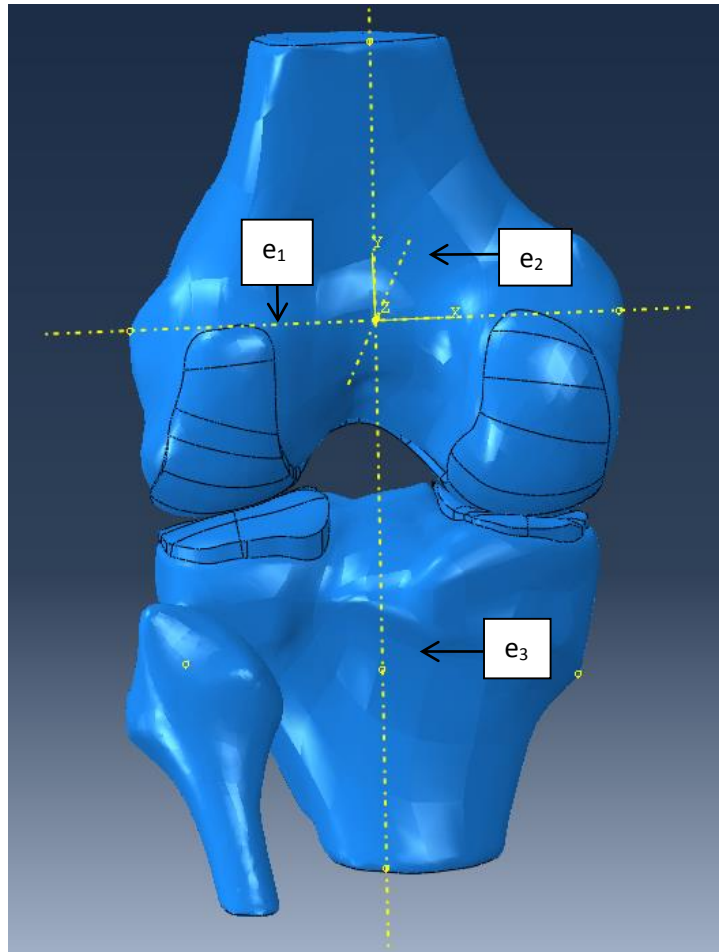


**Figure 3.22: Position of the knee joint coordinate system axes**

The five reference points (lateral and medial femoral epicondyles, lateral and medial tibial condyles and the most posterior distal aspect of the tibia) (Grood and Suntay, 1983; Woo et al., 1999; Standring, 2008; Liu et al., 2010) were identified in the FE model (Table 3.4) to calculate each axis of the joint coordinate system (Equation 11-13).

**Table 3.4: Coordinates of the five bony landmarks used to create the joint coordinate system**

	<b>X</b>	<b>Y</b>	<b>Z</b>
<b>Lateral femoral epicondyle</b>	74.33	-54.04	46.97
<b>Medial femoral epicondyle</b>	70.18	-52.65	-38.73
<b>Lateral tibial condyle</b>	80.61	-101.71	42.93
<b>Medial tibial condyle</b>	82.57	-97.26	-33.94
<b>Most posterior distal part of tibia</b>	64.69	-149.51	9.24

$$e_1 = \begin{pmatrix} 70.18 \\ -52.65 \\ -38.72 \end{pmatrix} - \begin{pmatrix} 74.33 \\ -54.04 \\ 46.97 \end{pmatrix} = \begin{pmatrix} -4.15 \\ 1.39 \\ -85.69 \end{pmatrix} \quad \text{Equation 11}$$

$$e_3 \text{ and } x_{fem-temp} = \frac{\begin{pmatrix} 70.18 \\ -52.65 \\ -38.72 \end{pmatrix} + \begin{pmatrix} 74.33 \\ -54.04 \\ 46.97 \end{pmatrix}}{2} - \begin{pmatrix} 64.69 \\ -149.51 \\ 9.24 \end{pmatrix} = \begin{pmatrix} 72.26 \\ -53.34 \\ 4.12 \end{pmatrix} -$$

$$\begin{pmatrix} 64.69 \\ -149.51 \\ 9.24 \end{pmatrix} = \begin{pmatrix} 7.56 \\ 96.17 \\ -5.12 \end{pmatrix} \quad \text{Equation 12}$$

$$e_2 = \begin{pmatrix} -4.15 \\ 1.39 \\ -85.69 \end{pmatrix} \times \begin{pmatrix} 7.56 \\ 96.17 \\ -5.12 \end{pmatrix} = \begin{pmatrix} 1.39 \times (-5.12) - 96.17 \times (-85.69) \\ (-85.69) \times 7.56 - (-5.12) \times (-4.15) \\ (-4.15) \times 96.17 - 7.56 \times 1.39 \end{pmatrix} =$$

$$\begin{pmatrix} 8233.01 \\ -669.13 \\ -409.99 \end{pmatrix} = \begin{pmatrix} 0.99 \\ -0.081 \\ -0.05 \end{pmatrix} \quad \text{Equation 13}$$

### 3.9. Material Properties

Inaccuracies in tissue properties influence stress values in the knee joint (Andriacchi et al., 2004). It is important that realistic constitutive tissue properties are used in FE models to accurately predict the stress distribution within the joint. However, it is not always feasible to measure these tissue properties and wide variations are reported in literature. Therefore, sensitivity analyses of the effect of variations in tissue material properties on knee joint contact pressure were conducted. This process allowed an identification of parameters that are critical to the behaviour of the knee joint and their degree of accuracy required for reliable predictions. Table 3.5 shows the range of properties for each tissue that was included in the analysis. The peak stress values and loading on the tibial cartilage were plotted for each condition (Section 4.3).

**Table 3.5: Range of properties applied to the FE model for each tissue**

<b>Tissues</b>	<b>Poisson's Ratio</b>	<b>Range of Young's Modulus investigated (MPa)</b>
Bone	0.3	100 – 5000
Cartilage	0.45	1 - 40
Meniscus	0.45	1 - 200

### **3.9.1. Bone Properties**

Following the sensitivity analyses and literature review, it was decided to consider the bone as homogenous linear elastic with a Young's modulus of 1000 MPa and a Poisson's ration of 0.3. This gave an average modulus of cortical and cancellous bone and has been used by many investigators (Wilson et al., 2003; Guo et al., 2009; Kubicek and Florian, 2009). In addition, the Young's modulus of subchondral bone, directly beneath the cartilage, is reported to be 1 GPa (Choi et al., 1990).

### **3.9.2. Cartilage Properties**

Cartilage material properties were modelled as homogenous, isotropic with linear elastic behaviour. This assumption can be justified because 1) cartilage mechanical response does not vary significantly with time at short loading conditions (Armstrong, Lai and Mow, 1984; Eberhardt et al., 1990; Donahue et al., 2002) and 2) a static analysis was conducted to simulate the end of weight acceptance during walking. Cartilage properties depend on healthy synovial fluid, age and activity level of the patient (Carter and Wong, 2003). A Young's modulus of 25 MPa was used for cartilage in this study, which is slightly higher than what other investigators have used. However, there is a wide range of Young's modulus reported in literature, which can be explained by the degradation in cartilage properties post-harvesting.

### **3.9.3. Meniscus Properties**

The meniscus was a homogeneous, linear elastic, transversely isotropic material. Donahue et al. (2003) demonstrated this material property was important to achieve a similar contact pressure on the tibial plateau as their *in vitro* investigations. In order

to identify the axial, radial and circumferential directions, coordinate systems were applied to each finite element of the meniscus. The directions necessary to describe the transversely isotropic behaviour were:

1= radial

2= circumferential

3= axial

Six independent parameters were required: (1) the circumferential modulus  $E_2=120$  MPa, (2) the axial and radial modulus  $E_1$  and  $E_3 = 20$  MPa, (3) the out-of-plane Poisson's ratios  $\nu_{11} = \nu_{13} = 0.3$ , (4) the in-plane (circumferential) Poisson's ratio  $\nu_{22} = 0.2$ , (5)  $G_{11} = G_{13} = 57.7$  and (6)  $G_{22} = 8.33$  which describe the shear modulus (Whipple, Wirth and Mow, 1984; Fithian et al., 1989; Skaggs, Warden and Mow, 1994; Tissakht and Ahmed, 1995; Donahue et al., 2002; Yang, Nayeb-Hashemi and Canavan, 2009). The meniscus is stiffer circumferentially because the collagen fibres are oriented primarily in this direction (Yang, Nayeb-Hashemi et al. 2010).

### 3.9.4. Ligament Properties

The ligaments were represented using neo-Hookean hyperelastic material properties. Due to the high ratio between the viscoelastic time constant of the ligaments and the loading time of interest in this study, the material characteristics dependent upon time were neglected. Other authors have used a similar approach (Hirokawa and Tsuruno, 2000). An average value of the posterior and anterior region of the MCL material properties was used. Gardiner and Weiss (2003) concluded that subject-specific FE knee models were not as sensitive to ligaments with distributed material properties.

The bulk ( $K_0$ ) and shear ( $\mu_0$ ) moduli describing the neo-Hookean properties were obtained from the modulus of elasticity ( $E$ ) and Poisson's ratio ( $\nu$ ) as follows:

$$K_0 = \frac{E}{3x(1-2\nu)} \quad \text{Equation 14}$$



$$\mu_0 = \frac{E}{2x(1+\nu)} \quad \text{Equation 15}$$

Neo-Hookean coefficients,  $D_1$  and  $C_{10}$ , were then calculated, using the bulk and shear moduli, respectively, and input to the strain energy density function within Abaqus to define the soft tissue properties.

$$C_{10} = \frac{\mu_0}{2} \quad \text{Equation 16}$$

$$D_1 = \frac{2}{K_0} \quad \text{Equation 17}$$

Ligament properties change with strain values (Chapter 2.8.1 Figure 2.20). During flexion and extension, ligament strain change independently as the ligaments engage at different knee positions, which may differ among individuals (Qi, et al., 2013). In order to match the FE model ligament material properties in each degree of flexion to those of the cadaver, a ligament tuning process was conducted.

### 3.10. Ligament Tuning

The model ligament properties were adjusted in an iterative process until an acceptable match between the kinematics of the tibia relative to the femur in the FE model and the cadaver was achieved. The six DOF Kawasaki robot and the FE model were passively flexed from 0° full extension to 65° of flexion and kinematics were compared. A 374-N axial load and varus / valgus bending moments, spanning 0 to 15 Nm, were then applied to the distal tibia and the model ligament properties were further adjusted until knee model kinematics matched those *in vitro* in all six DOF, using the Grood and Suntay coordinate system. Young's modulus for each ligament,

from full extension to 65° flexion and from 15 Nm valgus to 15 Nm varus bending moment were obtained from this process.

In order to change the material properties during a step, a predefined value was assigned to each ligament during the initial step. In step one the model executed with the initial material property definitions, which were then changed in the following step. The value is interpolated linearly between these two steps in Abaqus software.

### 3.10.1. Transformation Matrices

#### *Position of FE and cadaveric femur in space*

Because the translation and rotation of the FE model and cadaver were based on different coordinate systems, transformation matrices were calculated to match the results (Appendix C). First, a transformation matrix from the femur to the global coordinate system in Abaqus was calculated to understand the position of the FE femur in space ( $T_{fem}^{aba}$ ). This process was repeated for the cadaveric femur and the global coordinate system of the robot ( $T_{fem}^{glo}$ ).

The position of a point, represented by a vector, and the rotation matrix, comprised of three vectors to specify orientation, were used to create a 4×4 matrix, known as the homogenous transformation. The transformation matrix represented the position and orientation of a frame relative to another frame embedded in a body. The rotation matrix was defined by the unit vectors of the three femoral coordinate system axes. Translation was defined as the vector from the origin of the global coordinate system to origin of the femur for both the cadaver and FE model.

#### *Position of FE femur in relation to cadaveric femur*

A transformation matrix determining the position of the Abaqus (FE model) femur in relation to the global (cadaveric) femur was calculated ( $T_{glo}^{aba}$ ). This was done by multiplying the inverse of the femoral position in the robot ( $T_{glo}^{fem}$ ) with the position of the femur in Abaqus ( $T_{fem}^{aba}$ ).

$$T_{glo}^{aba} = T_{glo}^{fem} \times T_{fem}^{aba} \quad \text{Equation 18}$$

### ***Position of tibia in space for FE model***

A temporary transformation matrix was calculated, to define the position of the tibia within the Abaqus coordinate system ( $T_{tibtemp}^{aba}$ ). The three unit vectors of the tibial coordinate system served as the rotation matrix, while the vector between the origin of the Abaqus coordinate system and the midpoint between the tibial condyles formed the translation vector. The origins of the tibia ( $OT^{aba}$ ) and femur were then set as coincident. The next step was to calculate the transformation of the tibial origin with respect to the femoral origin during motion. A fixed tibial origin ( $OT^{tibtemp}$ ) was calculated by multiplying the inverse of the temporary tibial transformation matrix ( $T_{aba}^{tibtemp}$ ) with the tibial origin ( $OT^{aba}$ ) at full extension.

$$OT^{tibtemp} = T_{aba}^{tibtemp} \times OT^{aba} \quad \text{Equation 19}$$

The temporary tibial transformation matrix for any degree of flexion ( $T_{tibtemp}^{aba'}$ ) was then multiplied with the fixed tibial origin ( $OT^{tibtemp}$ ). The resulting vector ( $OT^{aba'}$ ) served as the new tibial origin after any rotation.

$$OT^{aba'} = T_{tibtemp}^{aba'} \times OT^{tibtemp} \quad \text{Equation 20}$$

$OT^{aba'}$  was defined as the translation vector for the final transformation matrix from tibia to Abaqus ( $T_{tib}^{aba}$ ). The purpose of establishing a temporary transformation matrix ( $T_{aba}^{tibtemp}$ ) is to solve the translation vector that is required in the transformation matrix ( $T_{tib}^{aba}$ ), so that the tibia can be located with respect to the femur after any rotation of the knee model.

### ***Position of tibia relative to femur***

Next the transformation matrix from tibia to femur was calculated ( $T_{tib}^{fem}$ ). This was done by multiplying the transformation matrix from Abaqus to femur ( $T_{aba}^{fem}$ ) with the transformation matrix from tibia to Abaqus ( $T_{tib}^{aba}$ ).

$$T_{tib}^{fem} = T_{aba}^{fem} \times T_{tib}^{aba} \quad \text{Equation 21}$$

### ***Identity check***

Once the transformation matrices from tibia to femur for the FE model and the cadaver were calculated, an identity check was performed to ensure that both positions were equal. The transformation from tibia to femur in the Abaqus (FE model) coordinate system ( $T_{tib}^{fem} \text{ Abaqus}$ ) was multiplied by the transformation of femur to tibia in the global (cadaveric) coordinate system ( $T_{fem}^{tib} \text{ robot}$ ). Identity (I) was confirmed.

$$T_{tib}^{fem} \text{ Abaqus} \times T_{fem}^{tib} \text{ robot} = \mathbf{I} \quad \text{Equation 22}$$

### ***Position at each degree of flexion***

A MATLAB program was written (Appendix D) to calculate the position of the tibia with respect to the femur for each degree of prescribed flexion in the remaining 5 DOF. The ligament properties were adjusted iteratively until the kinematics of the FE model tibia relative to the femur closely matched those of the cadaver for all DOF.

Literature was used as a guide to provide a basic understanding of how the ligaments behave during flexion and extension (Matsumoto et al., 2001; Amis et al., 2003; Shelburne, Pandy and Torry, 2004; Amis, Bull and Lie, 2005; Robinson et al., 2006; Amiri et al., 2007; Li et al., 2007; Shao et al., 2011; Adouni, Shirazi-Adl and Shirazi, 2012). Some studies have also used a ligament tuning process to ensure that the properties were similar to those of the specimen under study (Baldwin et al., 2011; Kiapour et al., 2013). Once the motions coincided for each angle of rotation, it was assumed that the ligament properties were close to those of the specimen. Results of the ligament tuning process for this model are summarised in Section 4.4.

### 3.11. Contact Definitions

The attachment of each ligament and cartilage to the bone was modelled by creating a surfaced-based tie contact (Figure 3.23). In order to define contact in Abaqus, a master surface and a slave surface were chosen. The material with a finer mesh or a higher stiffness was chosen to be the master surface to avoid deformations of the mesh. The tie contact constraints ensured that each node on the slave surface had the same displacement as the corresponding point on the master surface. The fibula was tied to the tibia to simulate a rigid connection.

To represent sliding motion, cartilage-cartilage and cartilage-meniscus contact surfaces were created, using the surface-to-surface contact option within Abaqus. This type of contact ensures that the selected surfaces don't intersect. Although, some penetration may be observed at individual nodes, large penetrations of master nodes into the slave surface do not occur. The option to gradually remove the slave node overclosure (intersecting contact points) during the step was selected to ensure convergence.

Scholes et al. (2004) measured the coefficient of friction in joints with synovial fluid to be 0.02, which is almost frictionless. In this model, all contacts were assumed to be frictionless with a finite sliding tracking approach. Frictionless sliding allows no fluid flow between the permeable tissues and non-contacting surfaces (Mononen, Jurvelin and Korhonen, 2013). The finite-sliding contact allows for separation, sliding and rotation of the contacting surfaces. Prior to analysis, a technique was used to adjust initial surfaces to move any node on the slave surface that was penetrating its master surface onto the master surface.

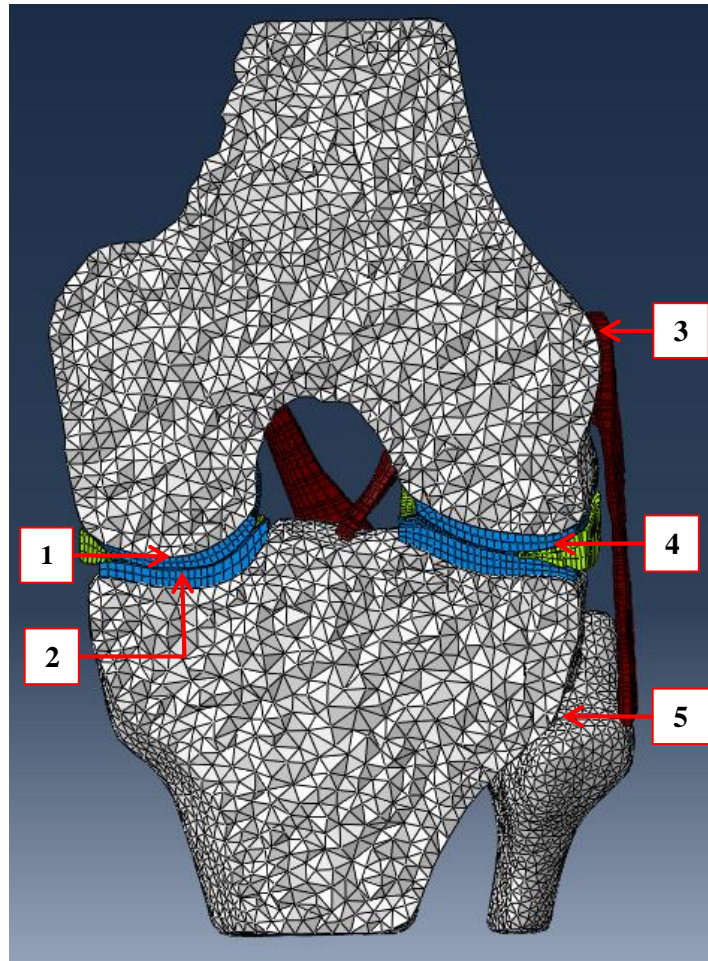


**Figure 3.23: Boundary conditions, showing contact pairs between (1.) femur – femoral cartilage, (2.) femoral cartilage – tibial cartilage, (3.) femur – LCL, (4.) femoral cartilage – meniscus, (5.) tibia – fibula**

A surface-to-surface contact was created between the MCL and the tibia to avoid penetration between them. Each meniscal horn was attached to the tibial plateau, using 1D linear spring elements with a stiffness of 2000 N/mm (Donahue et al., 2002). The external periphery of the meniscus was attached to the tibial plateau and the medial meniscus to the MCL, using 1D linear spring elements (Figure 3.24) to avoid excessive meniscus movement during rotation (Figure 3.25).



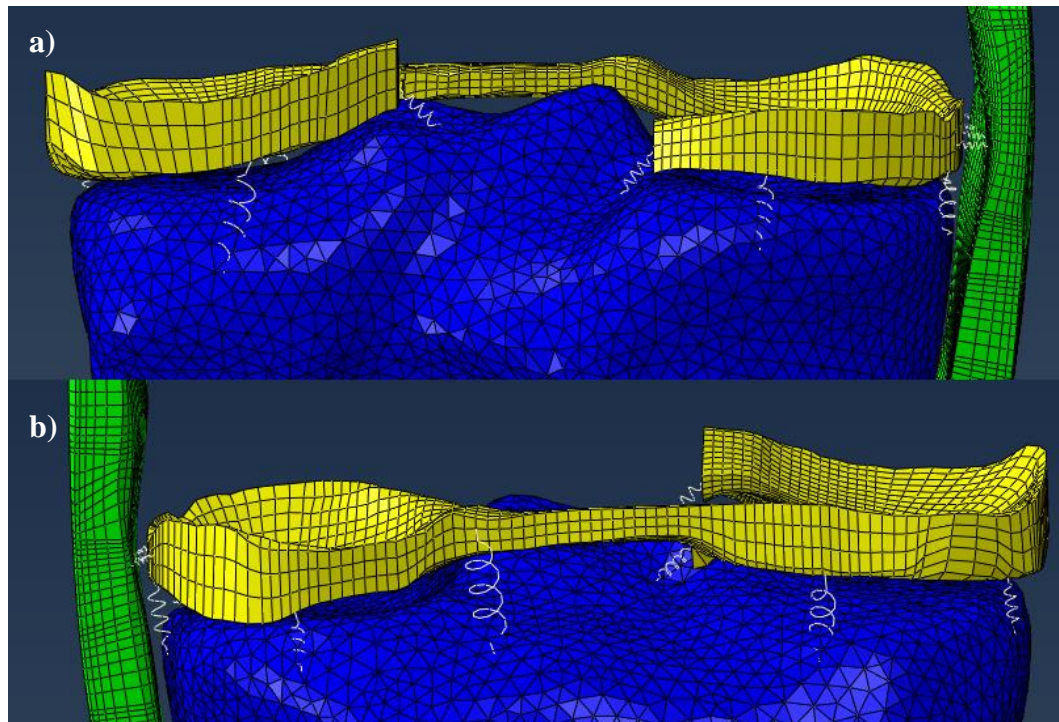


**Figure 3.24: Meniscal attachment with the tibia and the MCL; a) posterior view and b) anterior view**

The lateral meniscus was attached with fewer springs since it is not connected to the LCL and therefore moves more compared to the medial meniscus (Standring, 2008). These attachments simulated the joint capsule. Yao et al. (2006) proved that the peripheral attachments were necessary to avoid excessive translation of the meniscus.

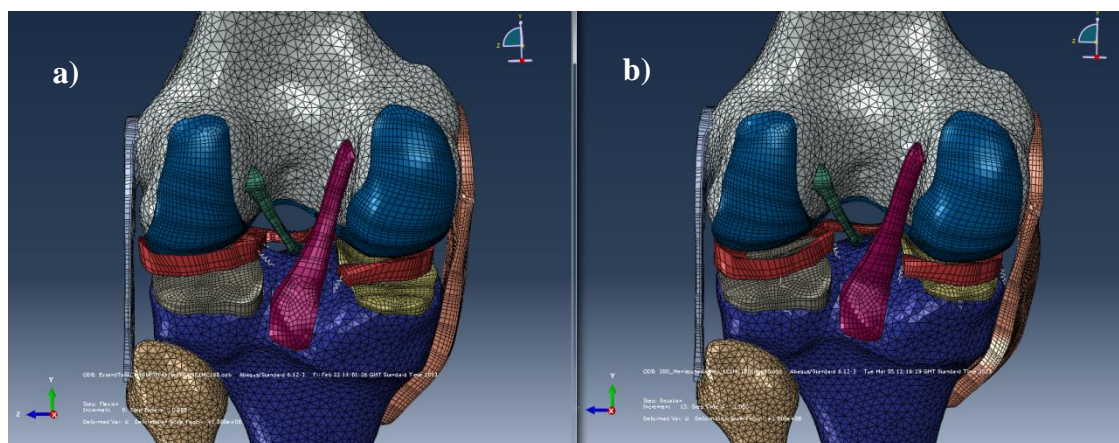


**Figure 3.25: Meniscus movement when the meniscus a) was not attached at peripheral borders and b) was attached at peripheral borders. Note the amount of exposed posterior medial tibial cartilage when the meniscus was not attached.**

### 3.12. Boundary and Loading conditions

The following steps were set up in Abaqus (Figure 3.26) to ensure that static equilibrium was achieved after each step.

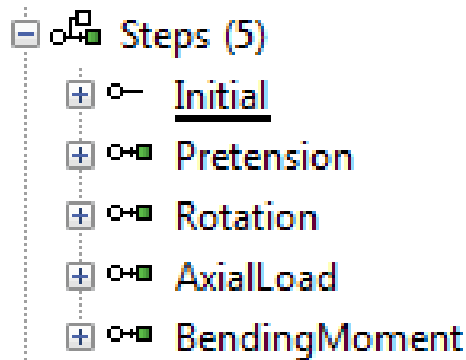


**Figure 3.26: Steps sequence used in Abaqus for analysis**

Boundary conditions were applied in the initial step and matched those of the *in vitro* tests on the cadaveric knee to validate the FE model. The proximal femur was mechanically grounded in all six DOF. To fix the proximal surface, a surface-based coupling constraint was set up. This constraint provided a coupling between a reference node and a group of nodes referred to as the “coupling nodes”. The motion of these nodes was coupled to the rigid motion of the reference point, which was created in the centre of the proximal femoral surface (Figure 3.27).



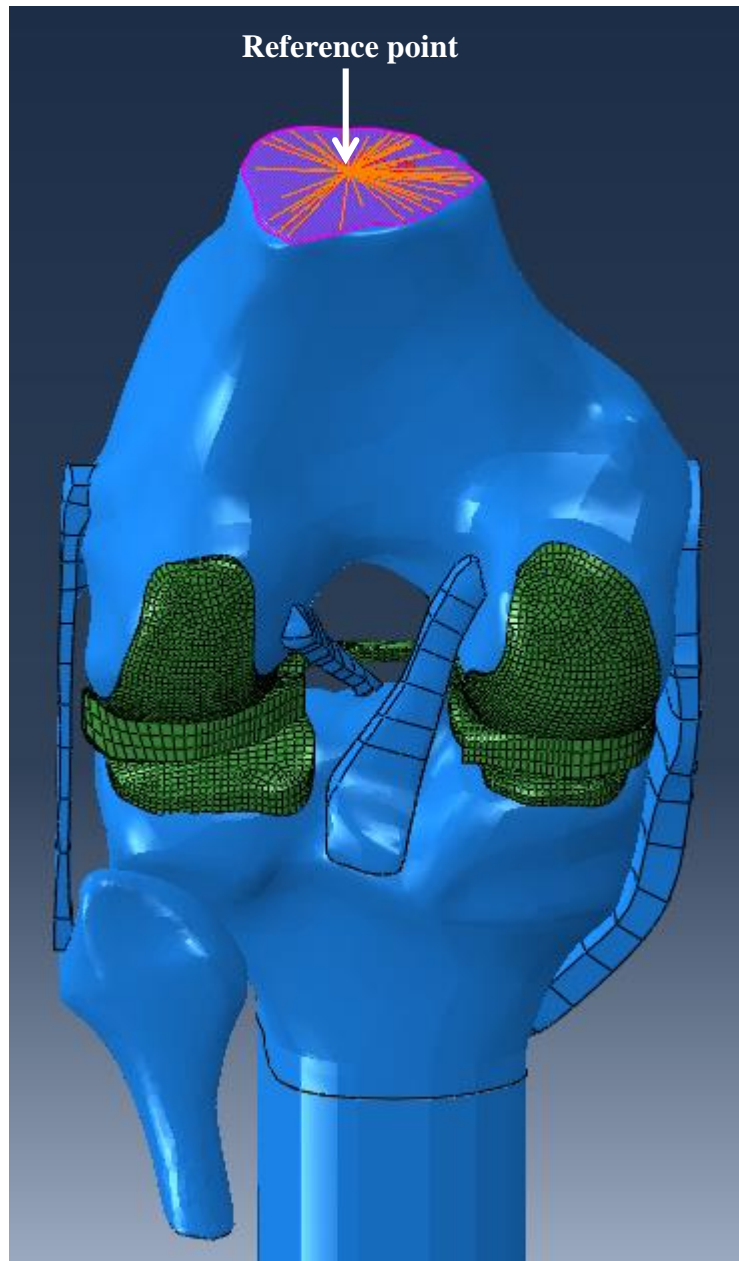


**Figure 3.27: Setting up boundary conditions for the femur**

A surface-based coupling constraint was applied to the distal surface of the tibia. The coupling nodes were attached to the reference point midway between the femoral epicondyles, to specify the motion of the tibia along the axes of the Grood and Suntay joint coordinate system (Figure 3.28). The nodes follow the motions that are entered in this boundary condition. Rotations were specified in radians and displacements were specified in mm. Flexion/extension was fixed at specific angles and all other DOF were left free. The motion of the ligaments, fibula, menisci and cartilage were specified by their respective contact models with the bony surfaces.

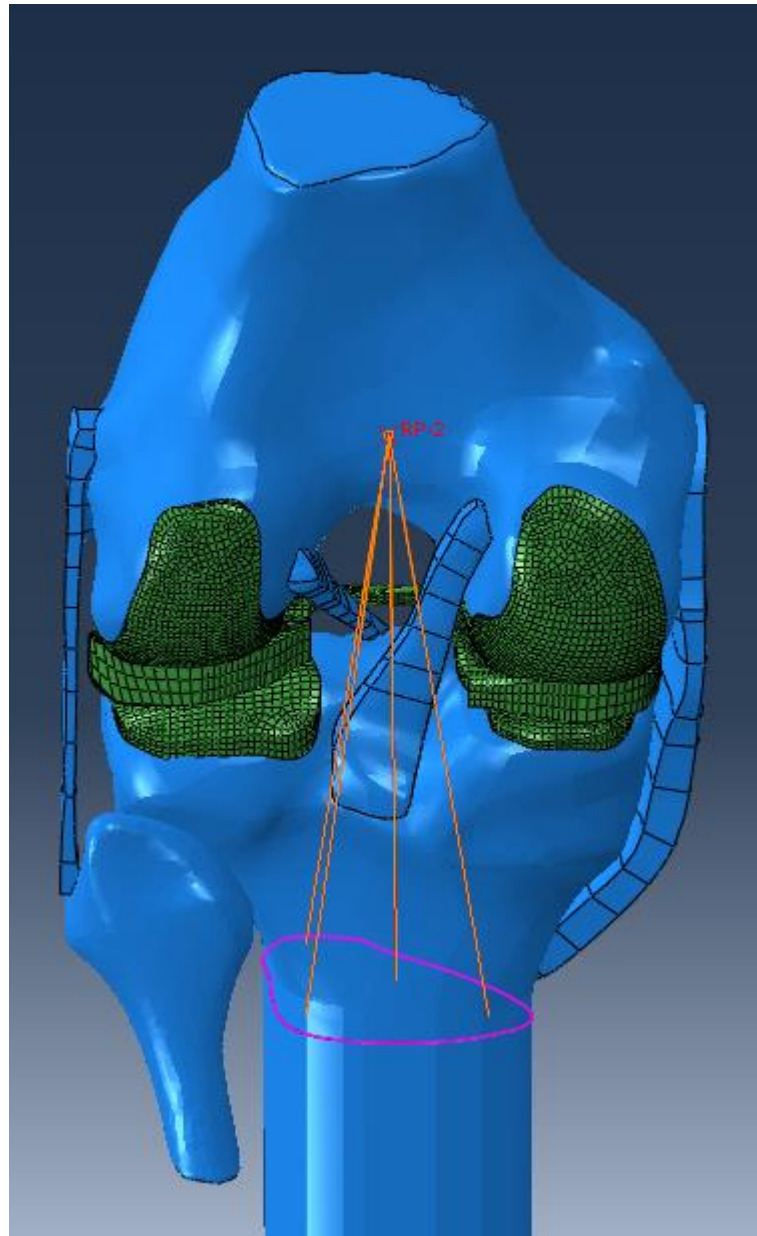


**Figure 3.28: Creating boundary conditions for tibia**

In the second step, a pretension to the ligaments was applied to eliminate any slack. This was performed by applying a fixed tensile load of 1N along the axis of each ligament. Limbert and Taylor (2001) mentioned that a pretension in the ligaments was essential to obtain realistic FE simulations. Peña et al. (2006) also mentioned that kinematic results were strongly dependant on the initial strain of the ligament. In the steps following the pretension, ligament forces changed automatically in accordance with the response of the model.

An axial load of 374 N was applied along the tibia as defined by the Grood and Suntay joint CS, to match the loading conditions of the *in vitro* tests. Although loads similar

to bodyweight could have been selected for the analysis of joint stress due to malalignment, the Kawasaki robot (model #ZX165U) did not converge for compressive loads greater than 374 N while in force control using the Broyden algorithm. The load was applied as a concentrated force to a reference point at the distal tibia. This ensured that forces were distributed across the nodes on the distal tibial surface. Varus and valgus bending moments, ranging from 0 Nm to 15 Nm, were then applied to the knee joint to simulate adduction and abduction (Figure 3.29). Most 3D knee FE studies have only simulated compressive knee force with axial loading (McKellop et al., 1991; Agneskirchner et al., 2007; Chantarapanich et al., 2009; Yang et al., 2010; Pressel et al., 2010). However, the adduction moment is a key determinant of load distribution at the knee and was incorporated into this FE model to provide a realistic stress distribution at the knee. Moments were applied to the reference point at the origin of the Grood and Suntay CS about the anterior/posterior axis. It is to be noted that, in addition to an axial compressive load, each knee experiences a bending moment due to the eccentrically loaded femur from the application of BW at the centre of mass (45 mm anterior from the second sequel vertebra) (Maquet, Van de Berg and Simonet, 1975).

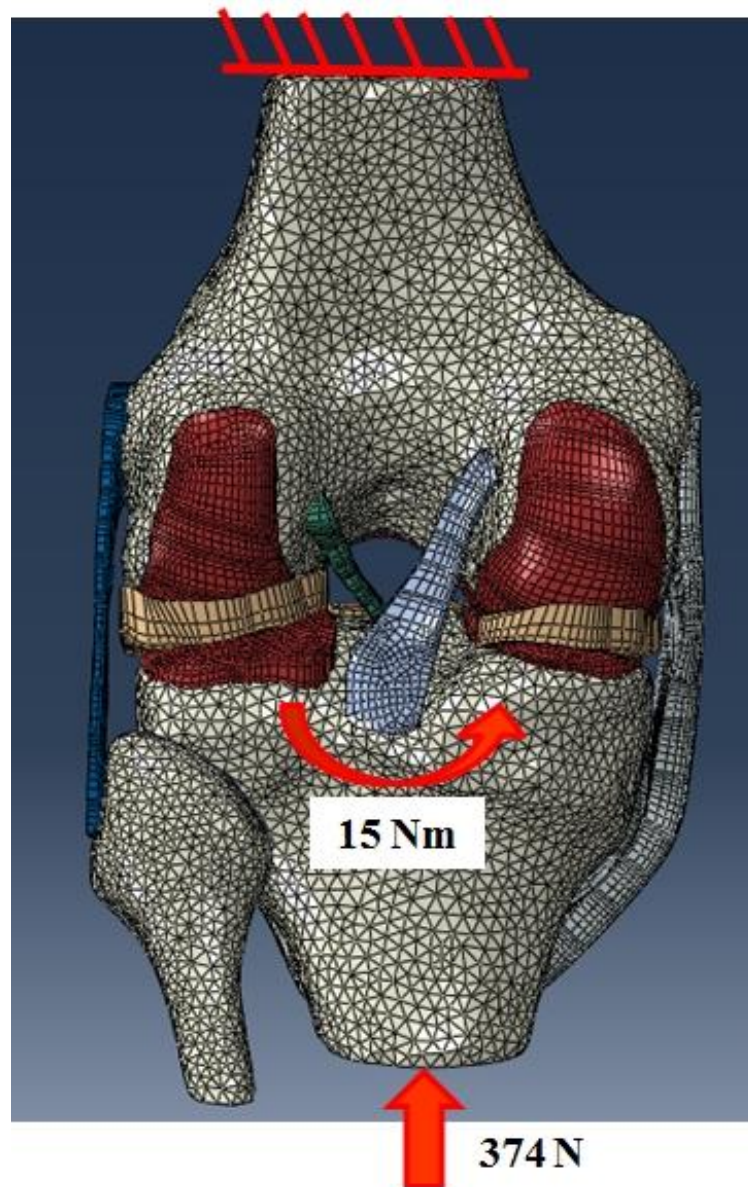


Figure 3.29: Loading conditions on the FE knee joint model

### 3.13. Validation

A unique aspect of this model is that it simulates joint contact mechanics from the same cadaveric knee that was used for experimental testing (Figure 3.30a). Results obtained in the FE analysis were validated with *in vitro* knee contact pressure. The prepared knee was positioned upside down in a six DOF robot, with the proximal femur mechanically grounded to a floor-mounted fixture and the tibia affixed to the robot gripper and load cell (Delta, ATI, Inc) (Figure 3.30 b, c). The specimen was oriented in accordance with normative movement data (obtained from the Leon Root, MD Motion Analysis Laboratory at HSS) in a position emulating weight acceptance



during stance (20° flexion). This occurs during maximum varus thrust just after the diagonal weight shift following heel strike. The applied axial load and bending moments were within the limits of the six DOF load cell.

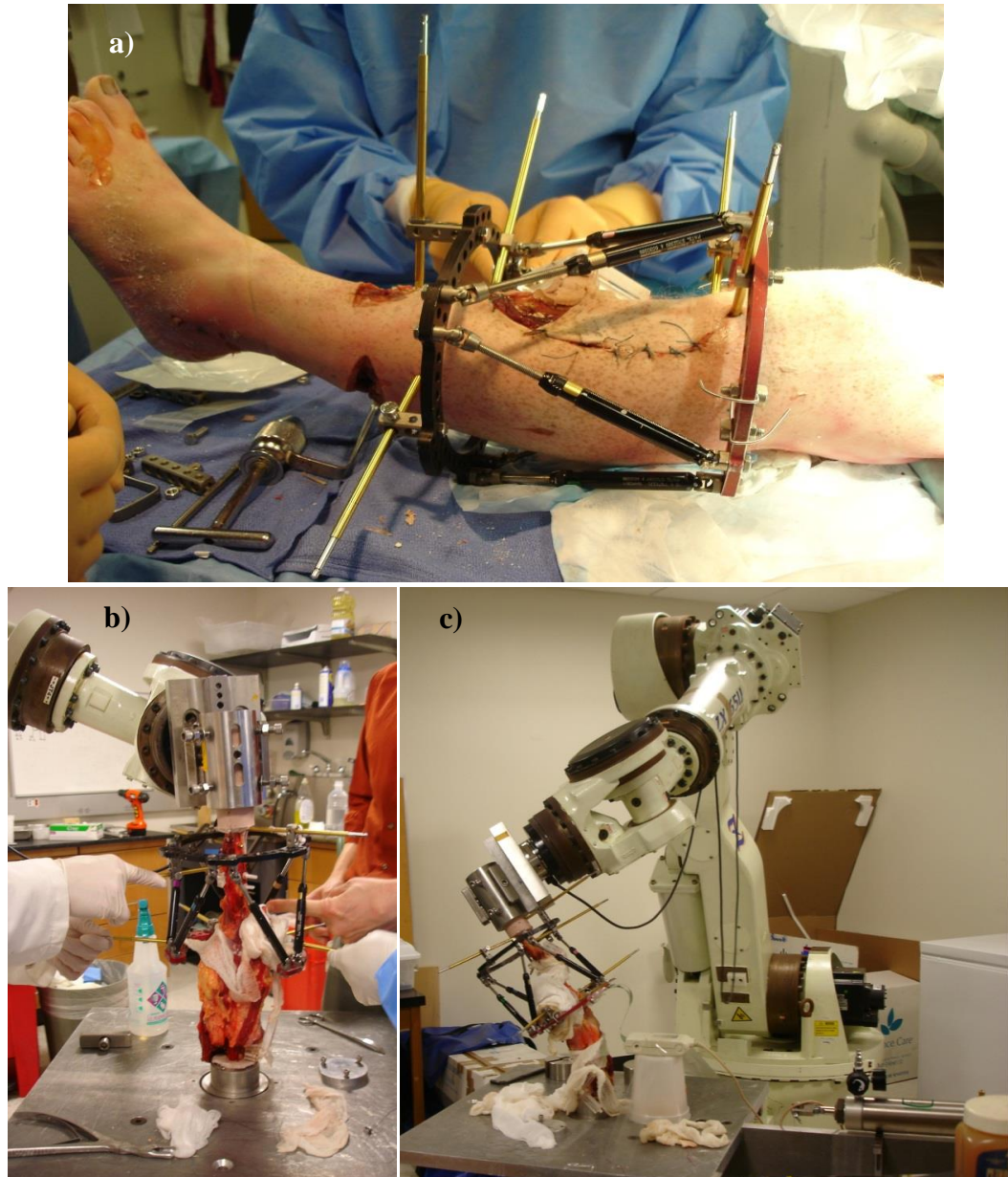


**Figure 3.30: Cadaveric knee a) with Taylor Spatial Frame for subsequent simulations of malalignment; b, c) mounted on a six degree-of-freedom robot for controlled loading (Courtesy of Hospital for Special Surgery, New York)**

Pressure at the tibial plateau was recorded using a 0.2-mm thick Kscan 4010 sensor (Tekscan Inc, South Boston, MA). The sensor consisted of two separate measurement areas, each with a total matrix width and height of 68.1 mm and 43.9 mm, respectively (Figure 3.31).

#### Sensor Model / Map: 4010N

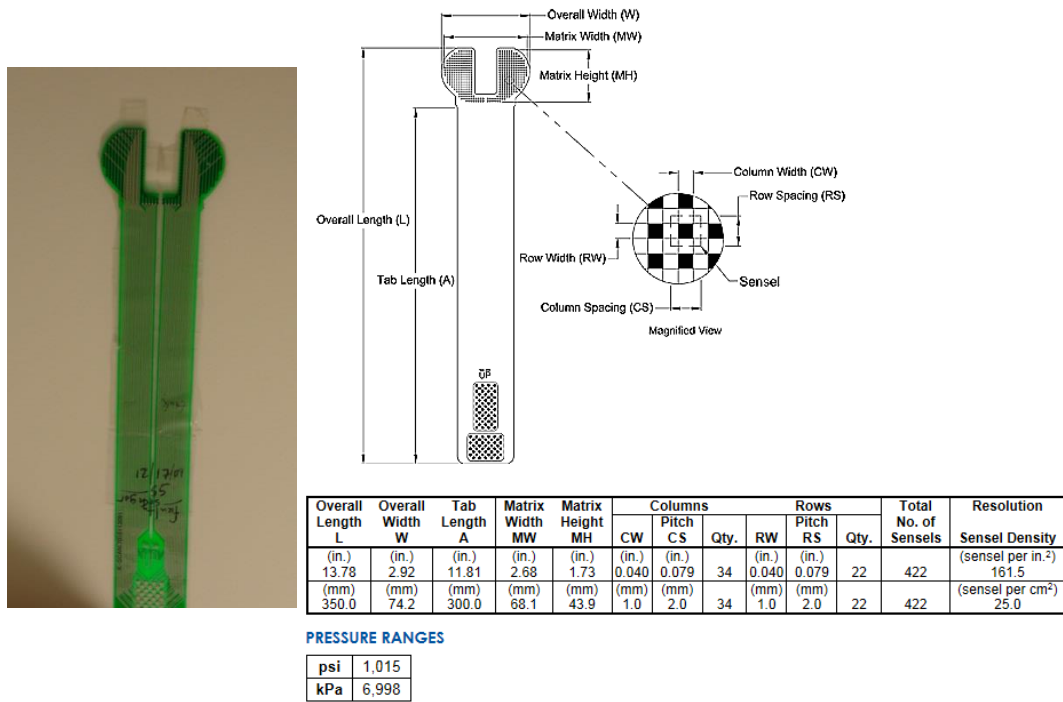


**Figure 3.31: Specification of the transducer**  
(Source: Tekscan Inc, 2014; Reprinted with permission)

The transducer resolution was 25 sensels/cm<sup>2</sup>. Following equilibration (Figure 3.32) and calibration, the pressure sensor was positioned on the tibial plateau and sutured to the base of the anterior cruciate ligament and the posterior capsule to record contact pressures in the tibiofemoral joint (Figure 3.33).

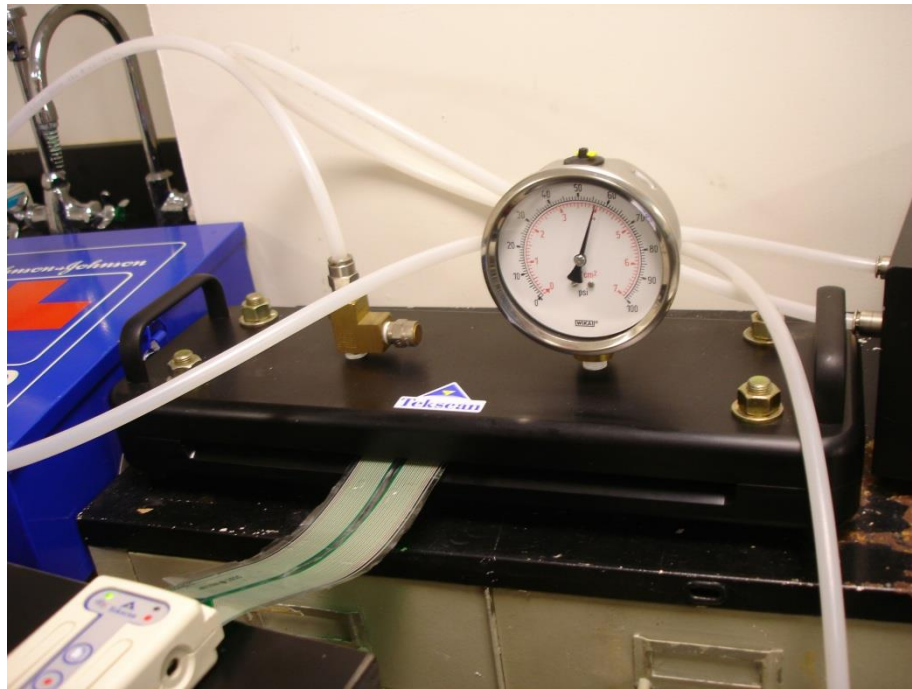


**Figure 3.32: Tekscan IScan sensor equilibration**  
(Courtesy of Hospital for Special Surgery, New York)

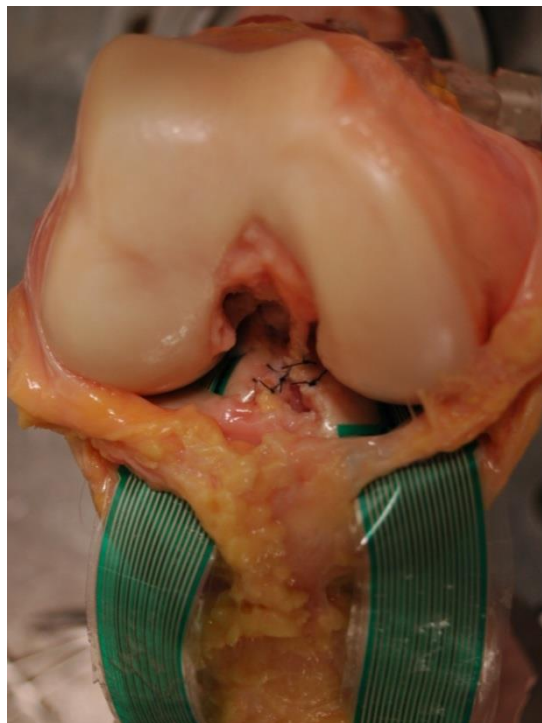


**Figure 3.33: Sensors fixed *in vitro* between the tibial cartilage and the femur. Note: A different specimen from that used in this study is depicted to show the positioning of the Tekscan sensor.**  
(Courtesy of Hospital for Special Surgery, New York)

Medial and lateral compartment pressures and forces were measured in response to the externally applied forces and moments by the robot. These experimental results were then compared with those predicted by the FE model of the knee joint for the same boundary conditions (374-N axial loads with varus bending moments ranging from 0 Nm to 15 Nm). The experimental data was collected for one trial for each condition (i.e. each level of bending moment).

In both cases, the model was fixed at 20° flexion in order to simulate the end of weight acceptance within the stance phase of gait. Since each sensel has an area of 4 mm<sup>2</sup>, the FE-predicted pressure was taken as an average of all nodes comprising this area size to achieve an accurate comparison between the tekscan measurements and the FE predictions.

A custom analysis program was developed in MATLAB by Mr Mark Lenhoff at the Hospital for Special Surgery (The MathWorks Inc., Natick, MA) to evaluate the cadaveric knee loading in the medial and lateral compartments. To compare the trends of FE-predicted and *in vitro*-measured peak pressure and compartmental force values, these loading parameters were normalised to the corresponding maximum compartmental value. The normalised FE-predicted and *in vitro*-measured values were compared for model validation (Section 4.5). The percentage load acting in the medial and lateral compartments of the knee were computed and compared with published data. Static equilibrium calculations were carried out to further verify the model (Section 4.5.4).

### 3.14. Analysis

Stress distributions in the medial-lateral compartment of the knee joint with alignments spanning from 14° valgus to 16° varus were predicted. This is the range of malalignments that occur in patients with medial and lateral knee OA (Cooke, Li and Scudamore, 1994). The end of weight acceptance during walking is where many patients exhibit their maximum adduction angle (referred to in orthopaedics as varus thrust), which is anticipated to correspond with the peak stress in the medial compartment of the joint. Hence, the end of weight acceptance was emulated in this computational model as a worst-case scenario during walking. Normalised knee joint rotations (Figure 3.34), forces (Figure 3.35) and moments (Figure 3.36) during the



stance phase of gait, for a subject with matching age, sex, weight, height and alignment as the cadaver, were obtained from the Leon Root, MD Motion Analysis Laboratory at HSS. The knee joint coordinate system utilised in the FE model was identical to that of the patient. The boundary conditions were the same as the validation study. Knee joint forces and moments at the end of weight acceptance during walking are summarised in Table 3.6.

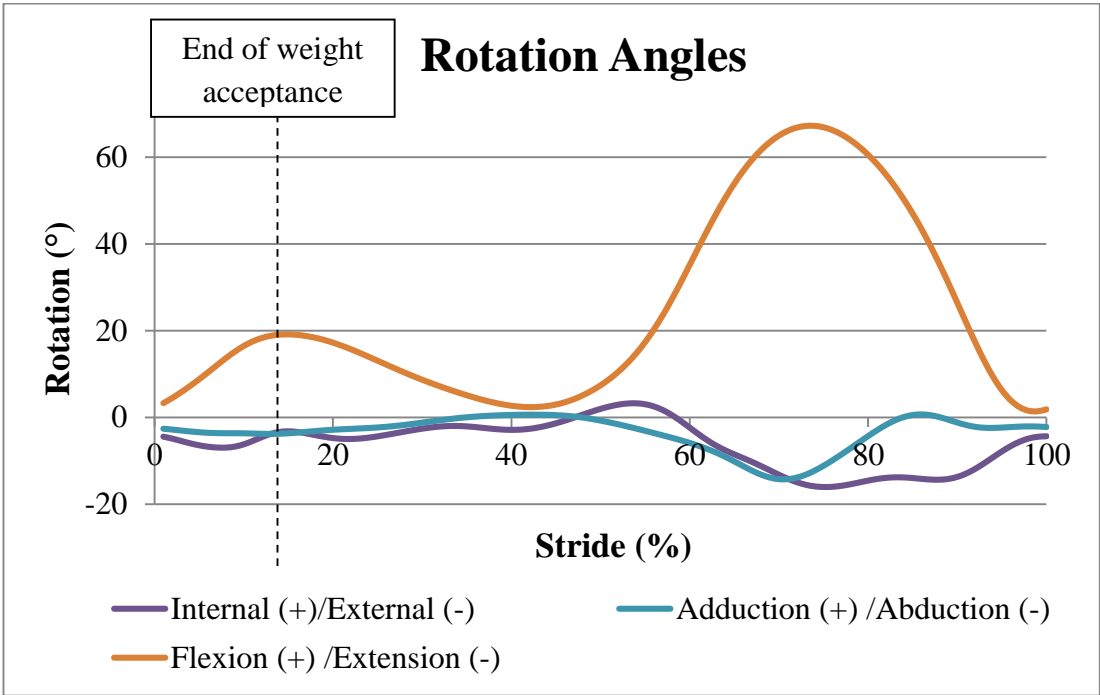


**Figure 3.34: Rotation angles during the gait cycle of level walking. The dashed line represents the end of weight acceptance.**

(Courtesy of Dr Hillstrom, Leon Root MD, Motion Analysis Lab, Hospital for Special Surgery, New York)

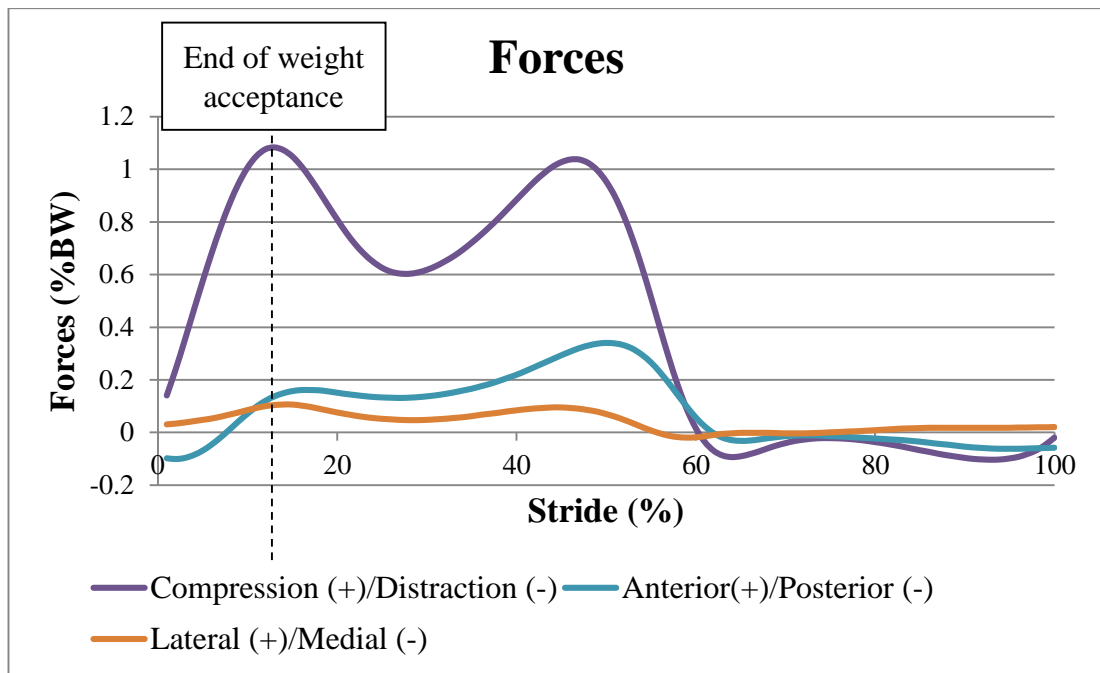


**Figure 3.35: Knee joint forces during the gait cycle of level walking. The dashed line represents the end of weight acceptance.**  
 (Courtesy of Dr Hillstrom, Leon Root MD, Motion Analysis Lab, Hospital for Special Surgery, New York)

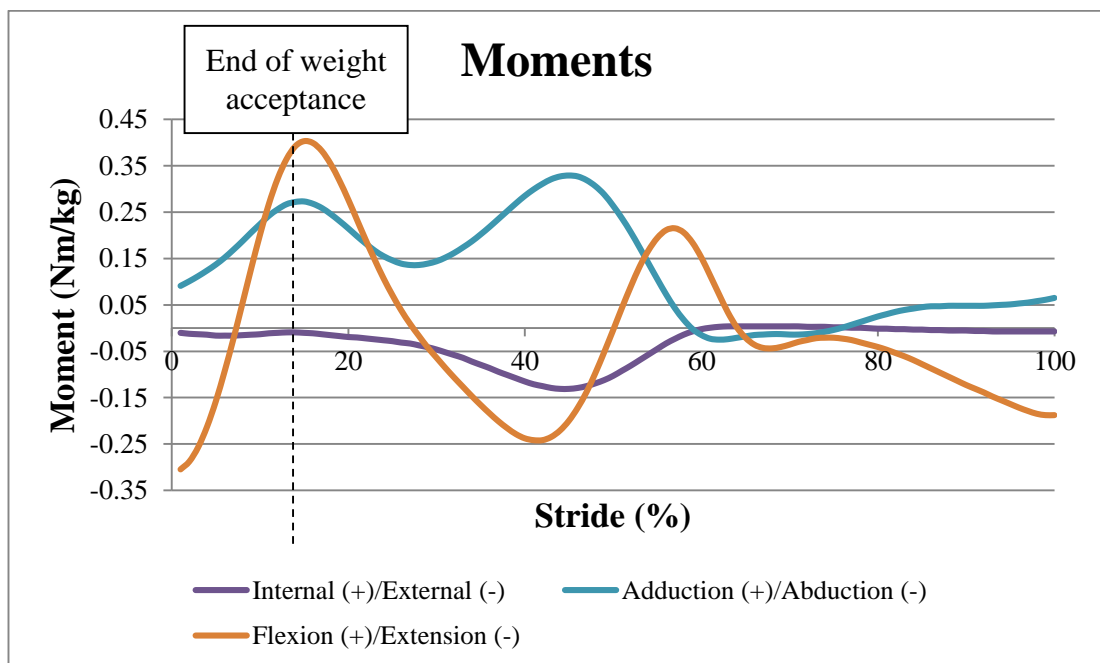


**Figure 3.36: Knee joint moments during the gait cycle of level walking. The dashed line represents the end of weight acceptance.**  
 (Courtesy of Dr Hillstrom, Leon Root MD, Motion Analysis Lab, Hospital for Special Surgery, New York)

**Table 3.6: Loading conditions of the knee model at the end of weight acceptance during walking applied to knee coordinate system.**

Flexion Angle	19.8°
Medial (+)/ Lateral (-) Force	-77.9 N
Compression (+)/Distraction (-) Force	811.4 N
Posterior (+)/ Anterior (-) Force	-102.6 N
Flexion (-)/ Extension (+) Moment	-27.81 Nm
Internal (-)/ External (+) Moment	6.88 Nm
Varus (+)/ Valgus (-) Moment	20.39 Nm

The model output included contact mechanics for both the medial and lateral compartments. Contact forces were transmitted through cartilage and meniscus. The maximum compressive stress is the force per unit area that is aligned with the joint coordinate system. The contact pressure is also a force per unit area, but acts perpendicular to the surface of interest. Since the tibial cartilage is relatively flat, these two parameters are very close in magnitude. FE-predicted contact pressures were compared with those measured *in vitro*, using pressure transducers.

Maximum shear stress has been related to cartilage degeneration (Donahue et al., 2002; Andriacchi et al., 2006; Wilson et al., 2006). Peña et al. (2008) reported a strong correlation between the increase in shear stress and cartilage degeneration and that maximum shear stress occurs at a subsurface region. Loading affects the stiffness of the deep chondral layer (calcified cartilage and subchondral plate) and high shear in the overlying cartilage results in splitting and degeneration at the cartilage base without disruption of the tangential layer at the articular surface (Radin et al., 1991). Hence, in this study, maximum shear stress of the cartilage centre was reported.

### 3.15. Malaligned Knee Joint

The relationship between MAD and alignment angle was obtained by creating a simple 2D CAD model. MAD is a function of the femur and tibia lengths and the alignment angle. The MA, FM and TM form a triangle and hence are trigonometrically related (Figure 3.37). The alignment angle in this study was defined as the angle of intersection between the TM and FM, known as the HKA angle (Prodromos, Andriacchi and Galante, 1985; Hsu et al., 1990; Tetsworth and Paley, 1994; Chao et al., 1994; Cooke, Sled and Scudamore, 2007). Positive and negative HKA angles refer to varus and valgus alignment, respectively.

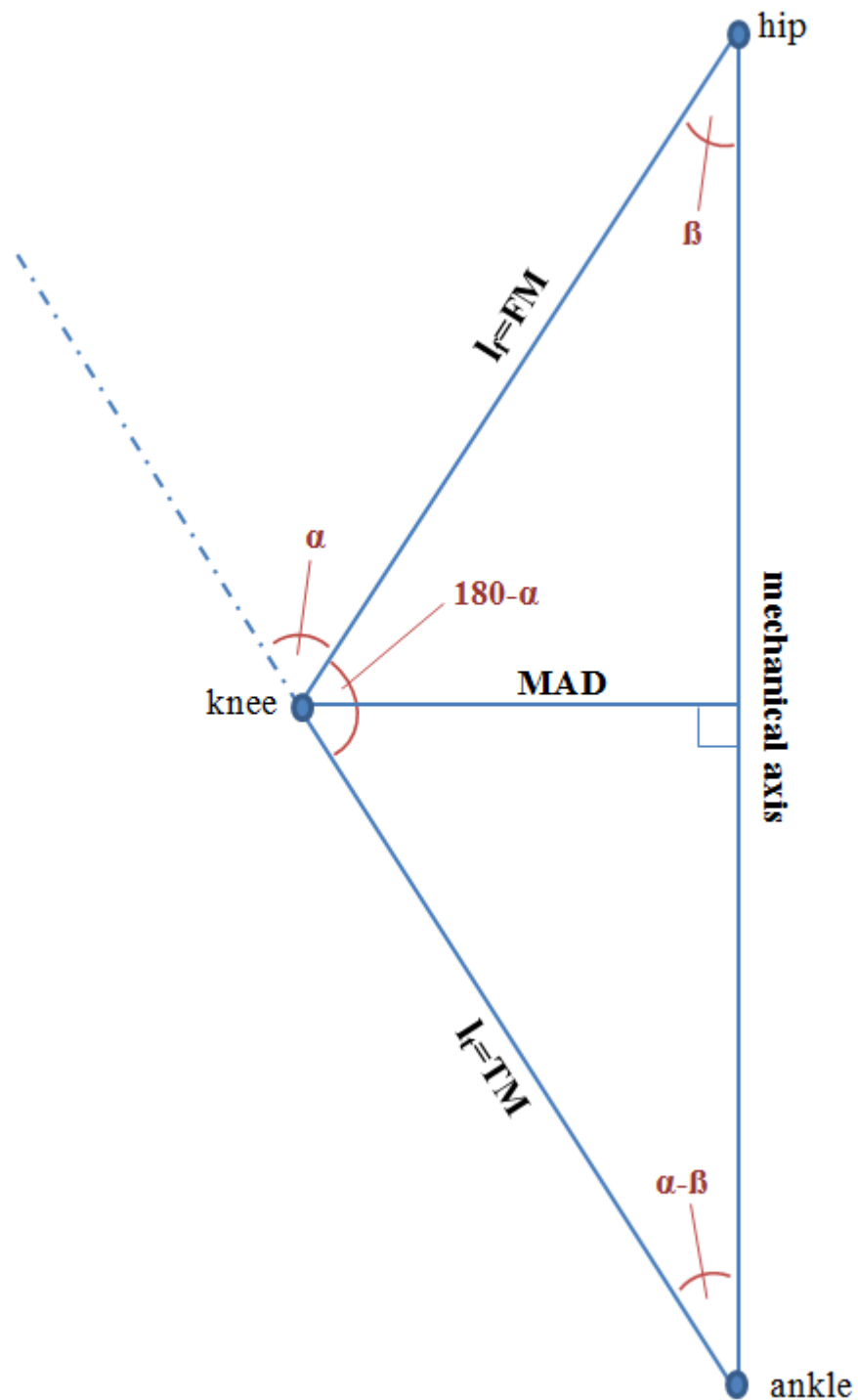


Figure 3.37: 2D scheme of the malaligned lower limb to determine the mechanical axis deviation (MAD) for various alignments; where  $\alpha$  = angle of alignment;  $l_f$  = length of femur (femoral mechanical axis FM);  $l_t$  = length of tibia (tibial mechanical axis TM); and  $\beta$  = angle between the mechanical axis and the femur.

$$\sin(\alpha - \beta) = \frac{MAD}{l_t} \quad \text{Equation 23}$$

$$\sin(\beta) = \frac{MAD}{l_f} \quad \text{Equation 24}$$

$$\text{substitute 24 into 23: } \frac{\sin(\beta) \times l_f}{l_t} = \sin(\alpha - \beta) \quad \text{Equation 25}$$

$$\frac{\sin(\beta) \times l_f}{l_t} = \sin(\alpha) \times \cos(\beta) - \cos(\alpha) \times \sin(\beta) \quad \text{Equation 26}$$

$$\left( \frac{l_f}{l_t} + \cos(\alpha) \right) \times \sin(\beta) = \sin(\alpha) \times \cos(\beta) \quad \text{Equation 27}$$

$$\left( \frac{l_f}{l_t} + \cos(\alpha) \right) \times \tan(\beta) = \sin(\alpha) \quad \text{Equation 28}$$

$$\tan(\beta) = \frac{\sin(\alpha)}{\left( \frac{l_f}{l_t} + \cos(\alpha) \right)} \quad \text{Equation 29}$$

$$\beta = \tan^{-1} \left( \frac{\sin(\alpha)}{\frac{l_f}{l_t} + \cos(\alpha)} \right) \quad \text{Equation 30}$$

$$\text{substitute 23 in 24: } MAD = \sin \left( \tan^{-1} \left( \frac{\sin(\alpha)}{\frac{l_f}{l_t} + \cos(\alpha)} \right) \right) \times l_f \quad \text{Equation 31}$$

Using the above equations, the MAD can be calculated for every tibia to femur ratio for any alignment angle. The full-length CT image was used to derive the length of the tibia (395 mm) and femur (432 mm). According to Dempster (1955) and Trotter et al. (1952) these values were those of an average man. Table 3.7 shows the FE model MAD for different alignments. The cadaveric knee had a 1° varus alignment when fixed in the robotically-loaded test jig at HSS. This represents the average HKA angle of a well-aligned individual (Insall, Joseph and Msika, 1984; Moreland, Bassett and Hanker, 1987; Hsu et al., 1990; Chao et al., 1994). The cadaver's alignment at the end of weight acceptance was derived from the 3D kinematics of the 6 degree-of-freedom robot under loading at 20° flexion and was measured as 0° in the frontal plane (HKA angle).

**Table 3.7: MAD for different alignments for a person with a tibial length of 395 mm and a femoral length of 432 mm**

for tibia 395 mm and femur 432 mm	
Angle of alignment (°)	Corresponding MAD (mm)
-14	-50.4
-11.5	-41.4
-9	-32.4
-6.5	-23.4
-4	-14.4
-1.5	-5.4
1	3.6
3.5	12.6
6	21.6
8.5	30.6
11	39.6
16	57.6

The MRI is limited to scanning  $\pm 7.5$  cm from the joint line, based on the size of the knee coil, whereas the full tibia is 40 cm long. To simulate osteotomies, the distal tibia was virtually extended in CATIA to simulate its original length. A full-length tibia was required to apply moments to the models during gait and derive appropriate loading conditions within the malaligned knees. Figure 3.38 shows the knee model with the extruded tibia. To ensure that the tibia was represented realistically, it was imported into Mimics and the direction of the extruded tibial shaft was compared to that of the long CT scan data (Figure 3.39). Differences in thickness of the distal tibia did not affect the stress at the joint line, where geometries were closely matched. A line was created along the centre of each tibial shaft. The angle between those two lines was less than  $1^\circ$  ensuring that the extruded tibia was represented realistically.

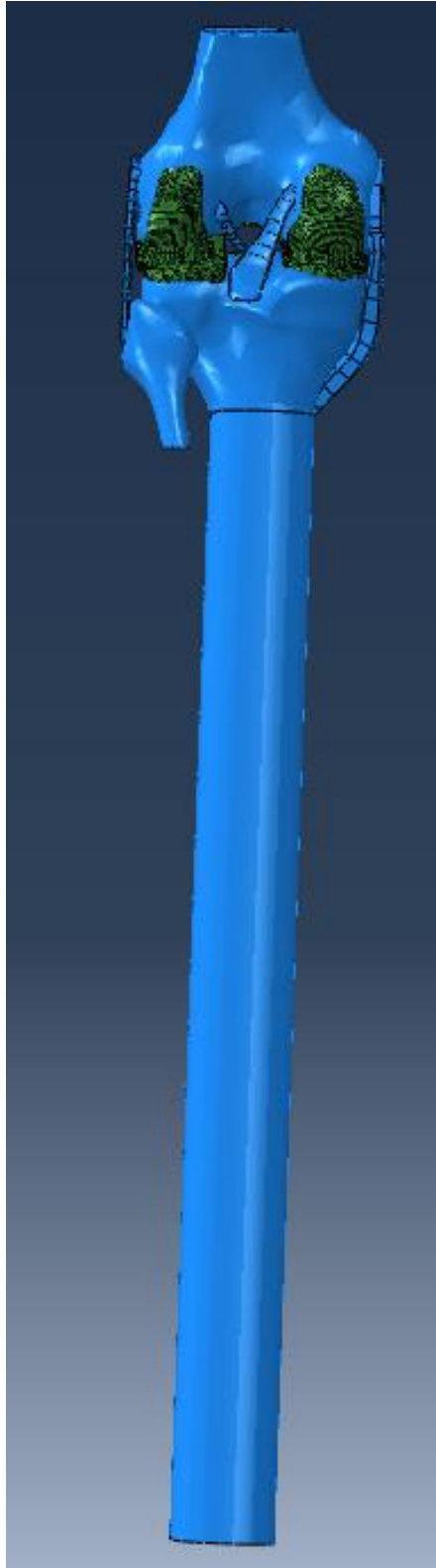
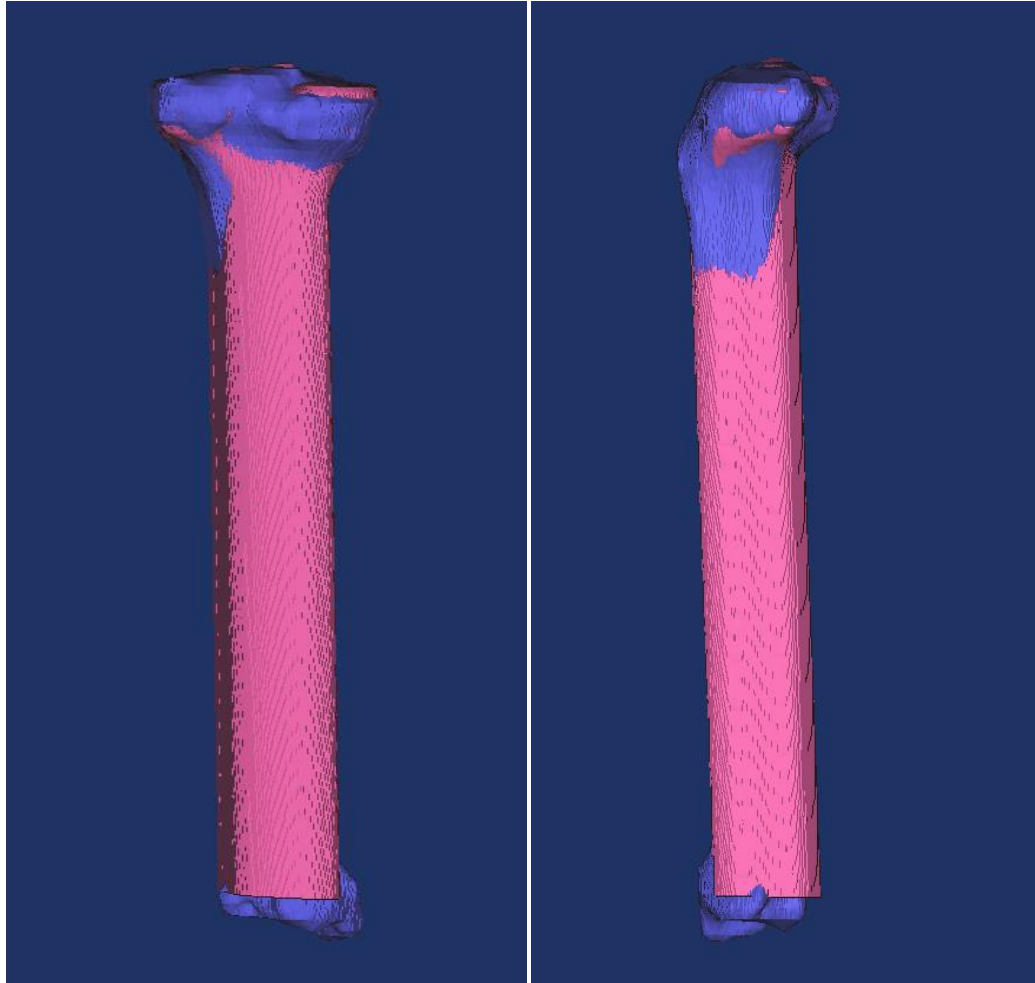


Figure 3.38: Knee joint with virtually extended tibia





**Figure 3.39: FE tibia (pink) shows similar alignment with CT scan (blue) for both the coronal (left) and sagittal (right) plane views.**

The knee joint coordinate system was projected to the centre of the distal tibia (Figure 3.40). As the forces were applied further away from the knee joint centre, larger moments would result. A matrix transformation was performed to counterbalance those additional moments.



**Figure 3.40: Extended tibia with the knee joint CS and the projected distal CS.**

To transform forces and moments from the knee joint CS to the distal tibial CS, the exact location and orientation of the distal tibial CS is required. The rotational displacement is such that the angles between the axes are given by  $\theta_{11}, \theta_{12}, \dots, \theta_{22}, \dots, \theta_{33}$ , where  $\theta_{ij}$  ( $i=1, 2, 3; j=1, 2, 3$ ) is the angle between the unit vector  $\vec{u}_i^1$  and  $\vec{u}_j^2$  of the two coordinate systems. The displacement of the origin of knee joint CS<sup>1</sup> with respect to the distal tibial CS<sup>2</sup> is given as the vector  $v = \{r_1 \ r_2 \ r_3\}$ , where  $v_1, v_2$  and  $v_3$  are measured in the distal CS. The measured forces and moments were transformed to the distal CS using the following relations:

$$\begin{pmatrix} F_x^2 \\ F_y^2 \\ F_z^2 \end{pmatrix} = [T] \times \begin{pmatrix} F_x^1 \\ F_y^1 \\ F_z^1 \end{pmatrix} \quad \text{Equation 32}$$

$$\begin{pmatrix} M_x^2 \\ M_y^2 \\ M_z^2 \end{pmatrix} = [T] * \begin{pmatrix} M_x^1 \\ M_y^1 \\ M_z^1 \end{pmatrix} + v \times \begin{pmatrix} F_x^2 \\ F_y^2 \\ F_z^2 \end{pmatrix} \quad \text{Equation 33}$$

$$\text{where } [T] = \begin{bmatrix} \cos(\theta_{11}) & \cos(\theta_{12}) & \cos(\theta_{13}) \\ \cos(\theta_{21}) & \cos(\theta_{22}) & \cos(\theta_{23}) \\ \cos(\theta_{31}) & \cos(\theta_{32}) & \cos(\theta_{33}) \end{bmatrix}$$

Using the above equations the following matrices were calculated:

$$T_{knee\ joint\ CS}^{distal\ tibial\ CS} = \begin{bmatrix} \cos(0) & \cos(-90) & \cos(90) \\ \cos(90) & \cos(0) & \cos(-90) \\ \cos(-90) & \cos(90) & \cos(0) \end{bmatrix} = \begin{bmatrix} 1 & 0 & 0 \\ 0 & 1 & 0 \\ 0 & 0 & 1 \end{bmatrix} \quad \text{Equation 34}$$

Since  $T_{knee\ joint\ CS}^{distal\ tibial\ CS}$  equals the identity matrix, forces applied to the knee joint CS will be identical to those applied to the distal tibial CS. However, there is a translation between the origins and therefore the moments will be different.

$$\text{origin knee joint CS} = \begin{pmatrix} 72.26 \\ -53.34 \\ 4.12 \end{pmatrix}$$

$$\text{origin distal tibial CS} = \begin{pmatrix} 174.44 \\ -524.052 \\ -7.55 \end{pmatrix}$$

Abaqus provided the origins with respect to the global CS which were transferred into the knee joint CS by computing the transformation matrix of the knee joint CS to the global CS.

$$T_{knee\ joint\ CS}^{global\ CS} = \begin{pmatrix} -0.05 & -0.25 & 0.97 & 72.26 \\ 0.02 & 0.97 & 0.24 & -53.34 \\ -0.99 & 0.0001 & -0.04 & 4.12 \\ 0 & 0 & 0 & 1 \end{pmatrix} \quad \text{Equation 35}$$

Next, the inverse of Transformation matrix  $T_{knee\ joint\ CS}^{global\ CS}$  was calculated in order to acquire the coordinates of the global CS with respect to the knee joint CS.

$$T_{global\ CS}^{knee\ joint\ CS} = \begin{pmatrix} -0.04 & -0.01 & -0.99 & 6.59 \\ -0.24 & 0.97 & 0.03 & 69.04 \\ 0.97 & 0.24 & -0.04 & -56.99 \\ 0 & 0 & 0 & 1 \end{pmatrix} \quad \text{Equation 36}$$

The origins with respect to the knee joint CS was obtained by multiplying the inverse of Transformation matrix ( $T_{knee\ CS}^{global\ CS}$ ) with the coordinates of the origins.

$$Origin\ knee\ joint\ CS = \begin{pmatrix} 0 \\ 0 \\ 0 \end{pmatrix}$$

$$Origin\ distal\ tibial\ CS = \begin{pmatrix} 12.21 \\ -481.79 \\ -14.09 \end{pmatrix}$$

$$\text{Translation } v, \text{ measured in the distal tibial CS, } v = \begin{pmatrix} -12.21 \\ 481.79 \\ 14.09 \end{pmatrix} \quad \text{Equation 37}$$

The above equations were used to calculate forces and moments that had to be applied to the distal tibial CS. Table 3.8 shows the loading conditions at the end of weight acceptance in the knee joint CS and transformed to the distal tibial CS.

**Table 3.8: Forces and moments acting in the knee joint CS (left) at the end of weight acceptance during level walking acquired from inverse dynamics. Corresponding forces and moments after transformation to the distal tibial CS (right).**

	<b>Knee Joint CS</b>		<b>Distal Tibial CS</b>	
	<b>Force (N)</b>	<b>Moment (Nm)</b>	<b>Force (N)</b>	<b>Moment (Nm)</b>
<b>x</b>	-77.92	-27.81	-77.92	-88.69
<b>y</b>	811.41	0.69	811.41	-1.66
<b>z</b>	-102.64	20.39	-102.64	48.03

Material properties for the tibial extension were set as 17 GPa, which equals the properties of cortical bone. A sensitivity analysis was conducted to investigate whether cortical, with or without cancellous bone, was appropriate for the model. A purely cortical extension was compared to an extension consisting of a cortical 6-mm-thick wall, filled with cancellous bone ( $E = 0.5$  GPa). Force and stress results were compared and summarised in Table 3.9. The full sensitivity analysis can be found in Appendix B.

**Table 3.9: The root mean square and percent full scale error between cortical and cortical/cancellous bone material properties for the tibial shaft.**

	<b>RMSE</b>		<b>%FSE</b>	
	<b>Lateral</b>	<b>Medial</b>	<b>Lateral</b>	<b>Medial</b>
<b>Force</b>	3.15 N	2.99 N	1.14	0.49
<b>Contact Pressure</b>	0.03 MPa	0.05 MPa	1.22	1.25
<b>Maximum Compressive Stress</b>	0.03 MPa	0.03 MPa	1.09	0.76
<b>Maximum Shear Stress</b>	0.01 MPa	0.02 MPa	0.74	1.15

To investigate whether a model with either a short or long tibia gave comparable results, another sensitivity analysis was conducted. The same loading conditions were applied to the knee joint with the short tibia and the one with the long tibia. Table 3.10 represents the %FSE for the models with the long and short tibia. The full sensitivity analysis is described in Appendix B. The short and long tibia gave slightly different results, indicating that the tibia is not rigid and experienced a slight bend during load application (Figure 3.41).

Therefore, a model with a fully-rigid tibial extension was analysed for force and contact pressure at the knee joints (Table 3.10).

**Table 3.10: Root means square and percent full scale error between the model with the short and longer tibias**

	<b>RMSE short compared to long</b>		<b>RMSE short compared to long with rigid extension</b>	
	<b>Medial</b>	<b>Lateral</b>	<b>Medial</b>	<b>Lateral</b>
<b>Force (N)</b>	12.02	11.48	0.22	0.23
<b>Contact Pressure (MPa)</b>	0.08	0.17	0.01	0.05
<b>Maximum Compressive Stress (MPa)</b>	0.07	0.06	0.01	0.01
<b>Maximum Shear Stress (MPa)</b>	0.02	0.84	1.54	1.44
	<b>%FSE short compared to long (%)</b>		<b>%FSE short compared to long with rigid extension (%)</b>	
	<b>Medial</b>	<b>Lateral</b>	<b>Medial</b>	<b>Lateral</b>
<b>Force</b>	6.27	1.71	0.13	0.03
<b>Contact Pressure</b>	3.18	0.13	0.32	1.11
<b>Maximum Compressive Stress</b>	2.75	0.32	0.35	0.32
<b>Maximum Shear Stress</b>	1.24	0.84	1.54	1.44

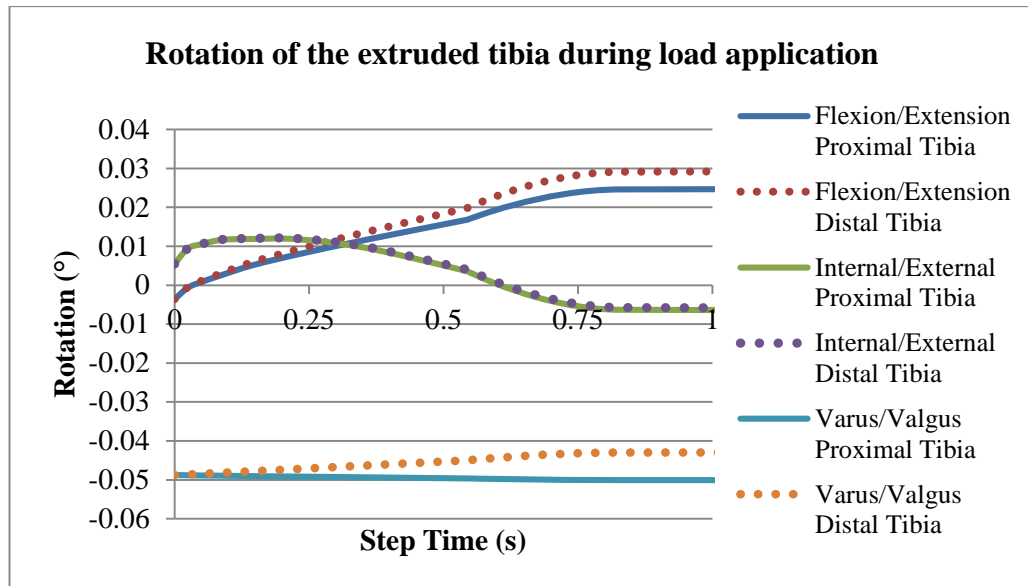


**Figure 3.41: Rotation of the tibial extension during the load application step.**

These results confirmed that the model with the rigid extension gave more accurate results than the model with the extension that had a Young's modulus of 17 GPa. This was expected because the tibia was subjected to a slight bending with the application of a high load. The model with a short tibia and the model with a long tibia gave similar results. Therefore, the knee joint with the long tibia was used for all analyses. Next, virtual osteotomies of 3.5°, 6°, 8.5°, 11° and 16° varus alignment and 1.5°, 4°, 6.5°, 9°, 11.5° and 14° valgus alignment were simulated by removing the appropriate wedge size from the extended tibia. Figure 3.42a and b show examples for 16° varus and 14° valgus, respectively.

Even though the osteotomy is often performed above the MCL insertion during surgery, for the purpose of this model, the osteotomy was simulated below the MCL attachment. This location permitted the assessment of alignment upon joint stress without requiring ligament tuning for each new alignment of the model.

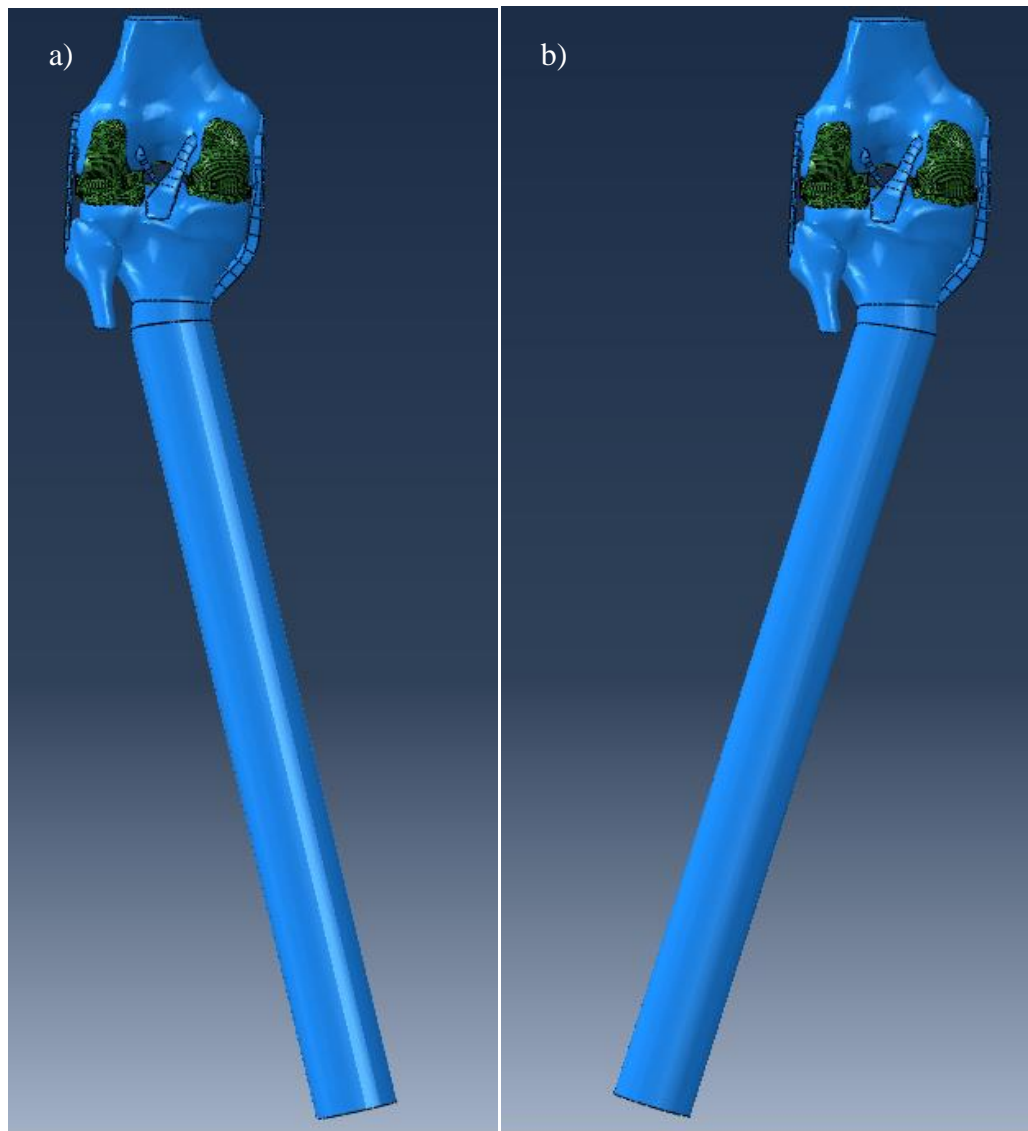


**Figure 3.42: Knee joint with a) 16° varus alignment and b) 14° valgus alignment**

A transformation was developed to compute the applied forces and moments acting about the distal tibia after surgical realignment. The frontal plane moment was maintained to simulate the primary effect of malalignment.

Knee joint contact stress patterns were predicted for varus, neutral and valgus alignments to investigate the relationship between osteotomy geometry, MAD and joint mechanics to determine the optimum knee alignment. Optimal HTO geometry was defined as the alignment that minimised peak knee joint stress for a specific applied load. Results of this study clarify the factors that increase knee joint stress and how surgical realignment can reduce these contact loads.

To specify the knee adduction moment that was applied to the knee joint centre due to malalignment, the tibial forces were transformed from the distal tibia to the knee joint



centre, using the same transformation matrix method as described above. Table 3.11 illustrates the knee adduction moments applied to the knee joint for each alignment angle.

**Table 3.11: Knee adduction moments applied to the knee joint due to varus (positive) and valgus (negative) alignments.**

<b>Alignment (°)</b>	<b>Knee adduction moment (Nm)</b>	<b>%BW×height</b>
-14	-59.00	-5.36
-11.5	-46.10	-4.19
-9	-33.05	-3.00
-6.5	-19.87	-1.81
-4	-6.56	-0.59
-1.5	6.86	0.62
1	20.40	1.85
3.5	34.49	3.13
6	47.78	4.34
8.5	61.43	5.58
11	75.03	6.82
16	102.07	9.27

### 3.16. Static Equilibrium

To conduct mathematical verifications of the computational model, a planar static equilibrium analysis was performed across the knee joint. The external loads are balanced by the internal anatomical forces and moments (Kutzner et al., 2010).

Figure 3.43 illustrates all forces and moment arms required for static equilibrium. Varus moment, as well as axial and medial/lateral forces during walking were obtained by investigators from HSS, on an individual who was anthropometrically matched to the cadaveric specimen. Moment arms from load application to joint centre were acquired from MRI data. The following static equilibrium equations were formulated:

1) Moments at the knee joint centre:

$$\sum \textit{Anticlockwise Moments} - \sum \textit{Clockwise Moments} = 0$$

$$F_{MCL} * d_{MCL} + F_M * d_M - F_{LCL} * d_{LCL} - F_L * d_L - M_{ext} = 0 \quad \textbf{Equation 38}$$

2) Horizontal forces:

$$\sum \textit{Horizontal Forces} = 0 \quad \textbf{Equation 39}$$

$$F_{med/lat} + F_{PCL} * \cos \beta - F_{ACL} * \cos \alpha = 0$$

3) Vertical forces:

$$\sum \textit{Vertical Forces} = 0 \quad \textbf{Equation 40}$$

$$F_{LCL} + F_{ACL} * \sin \alpha + F_{PCL} * \sin \beta + F_{MCL} + F_{axial} - F_L - F_M = 0$$

Where

$F_{MCL}$ = Force in the MCL

$F_{LCL}$ = Force in the LCL

$F_{ACL}$ = Force in the ACL

$F_{PCL}$ = Force in the PCL

$F_M$  = Force in the medial compartment of the knee joint

$F_L$ = Force in the lateral compartment of the knee joint

$F_{med/lat}$  = Medial/lateral force from gait analysis

$F_{axial}$ = Axial force from gait analysis

$M_{ext}$  = varus/valgus moment from gait analysis

$d_{MCL}$ = distance from the centre of the MCL to the centre of the knee

$d_{LCL}$ = distance from the centre of the LCL to the centre of the knee

$d_M$ = distance from the centre of the medial compartment to the centre of the knee

$d_L$ = distance from the centre of the lateral compartment to the centre of the knee.

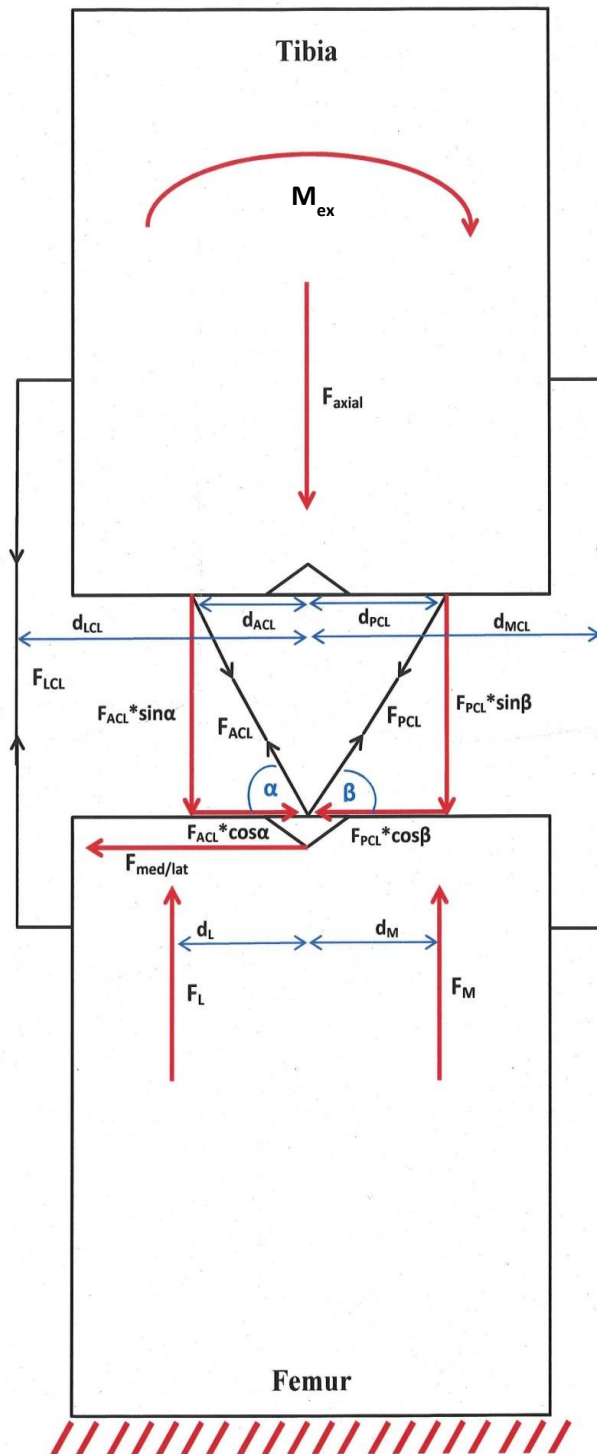


Figure 3.43: Static equilibrium; Where  $F_{MCL}$ = Force in the MCL;  $F_{LCL}$ = Force in the LCL;  $F_{ACL}$ = Force in the ACL;  $F_{PCL}$ = Force in the PCL;  $F_M$  = Force in the medial compartment of the knee joint;  $F_L$  = Force in the lateral compartment of the knee joint;  $F_{med/lat}$  = Medial/lateral force from gait analysis;  $F_{axial}$ = Axial force from gait analysis;  $M_{ext}$  = varus/valgus moment from gait analysis;  $d_{MCL}$ = distance from the centre of the MCL to the centre of the knee;  $d_{LCL}$ = distance from the centre of the LCL to the centre of the knee;  $d_M$ = distance from the centre of the medial compartment to the centre of the knee;  $d_L$ = distance from the centre of the lateral compartment to the centre of the knee.

## 4. Results and Analysis

In this chapter, sensitivity analyses results are presented to test Hypothesis 1a (H1a: The contact mechanics will vary more with different material properties of soft tissues compared to those of bone) and Hypothesis 1b (H1b: There is a threshold mesh size for bones and soft tissues below which the contact mechanics vary by less than 5% with additional mesh size reduction). Kinematics and contact pressure of the tibiofemoral joint were compared between the FE knee model and *in vitro* data to test Hypothesis 2 (H2: Tibiofemoral contact mechanics (normalised peak pressure, force and compartmental force ratio) of the *in vitro* experiment and corresponding FE model predictions will agree within 10% for the same boundary conditions).

The model was employed to determine the alignment that corresponds to minimum compartmental stress. Hypothesis 3a (H3a: The HTO geometry that corresponds to an MAD of zero millimetres does not correspond to the minimum contact stress) and Hypothesis 3b (H3b: The HTO geometry that corresponds to the Fujisawa point (62 % of the distance from the medial to the lateral tibial plateau) does not correspond to the minimum contact stress) were tested to examine if clinical alignment targets correspond to minimum knee stress. Hypothesis 4 (H4: The 3D FE knee model will predict post-operative knee joint mechanics, as evidenced by a correlation between surgical realignment geometry, MAD and knee joint contact mechanics) was tested to determine the subject-specific relationship between knee alignment and knee joint contact mechanics.

### 4.1. Effect of Mesh Type on Knee Joint Contact Mechanics

Force, contact pressure, maximum compressive stress and maximum shear stress were compared between linear and quadratic meshed models. Tables 4.1-4.4 and Figures 4.1-4.7 represent the results of the full sensitivity analysis.

**Table 4.1: Comparison of force between 4-noded (linear) and 10-noded (quadratic) meshed bones. Step interval 0 represents the initial loading of the knee joint and step interval 10 represents completion of the task.**

	Force (N)					
	Linear		Quadratic		Square Error	
Step Interval	Lateral	Medial	Lateral	Medial	Lateral	Medial
0	11.1	16.8	10.6	16.3	0.2	0.3
1	29.5	74.6	28.9	72.6	0.3	4.1
2	48.7	138.2	50.7	143.1	3.9	24.3
3	69.3	201.5	71.1	208.5	3.2	49.3
4	93.3	274.5	96.3	283.1	8.9	74.3
5	114.1	337.3	118.1	345.8	15.9	72.2
6	137.5	389.6	141.5	400.9	16.2	127.3
7	161.5	451.2	166.5	464.3	24.9	171.1
8	186.2	512.1	191.3	525.9	25.5	194.1
9	211.6	572.3	216.7	585.1	25.5	163.2
10	237.5	631.9	235.2	635.9	5.5	15.6
			<b>Mean Square Error</b>		<b>11.8</b>	<b>81.4</b>
			<b>RMSE (N)</b>		<b>3.4</b>	<b>9.0</b>
			<b>%FSE</b>		<b>1.5 %</b>	<b>1.4 %</b>

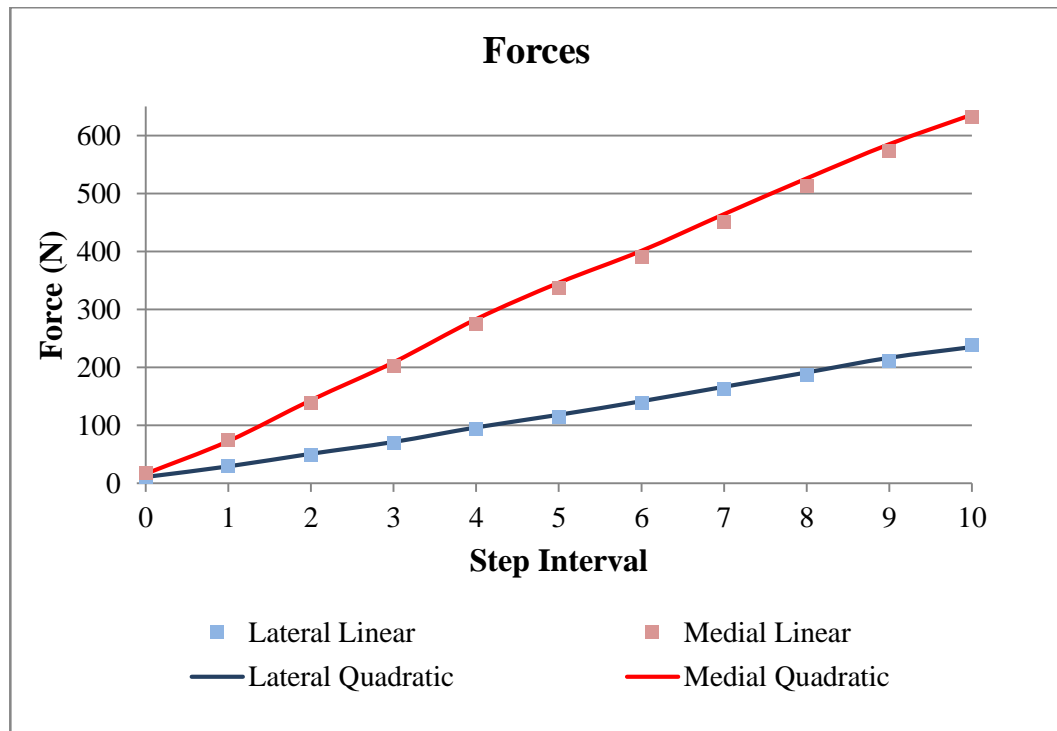


**Figure 4.1: Force distribution for a model with linear mesh elements compared to a model with quadratic mesh elements**

**Table 4.2: Comparison of contact pressure between linear and quadratic meshed bones. Step interval 0 represents the initial loading of the knee joint and step interval 10 represents completion of the task.**

	Contact Pressure (MPa)				Square error	
	Linear		Quadratic			
Step Interval	Lateral	Medial	Lateral	Medial	Lateral	Medial
0	0	0.34	0	0.34	0	0
1	0.33	0.72	0.32	0.69	0.0001	0.0009
2	0.49	1.76	0.53	1.82	0.0016	0.0036
3	0.93	2.53	0.91	2.6	0.0004	0.0049
4	1.19	2.7	1.22	2.73	0.0009	0.0009
5	1.4	2.88	1.41	2.95	0.0001	0.0049
6	1.59	3.19	1.57	3.27	0.0004	0.0064
7	1.74	3.44	1.72	3.53	0.0004	0.0081
8	1.9	3.67	1.85	3.73	0.0025	0.0036
9	2.05	3.76	2.03	3.82	0.0004	0.0036
10	2.22	3.9	2.18	3.94	0.0016	0.0016
			<b>Mean Square Error</b>		<b>0.0008</b>	<b>0.0035</b>
			<b>RMSE (MPa)</b>		<b>0.0276</b>	<b>0.0592</b>
			<b>%FSE</b>		<b>1.24 %</b>	<b>1.52 %</b>

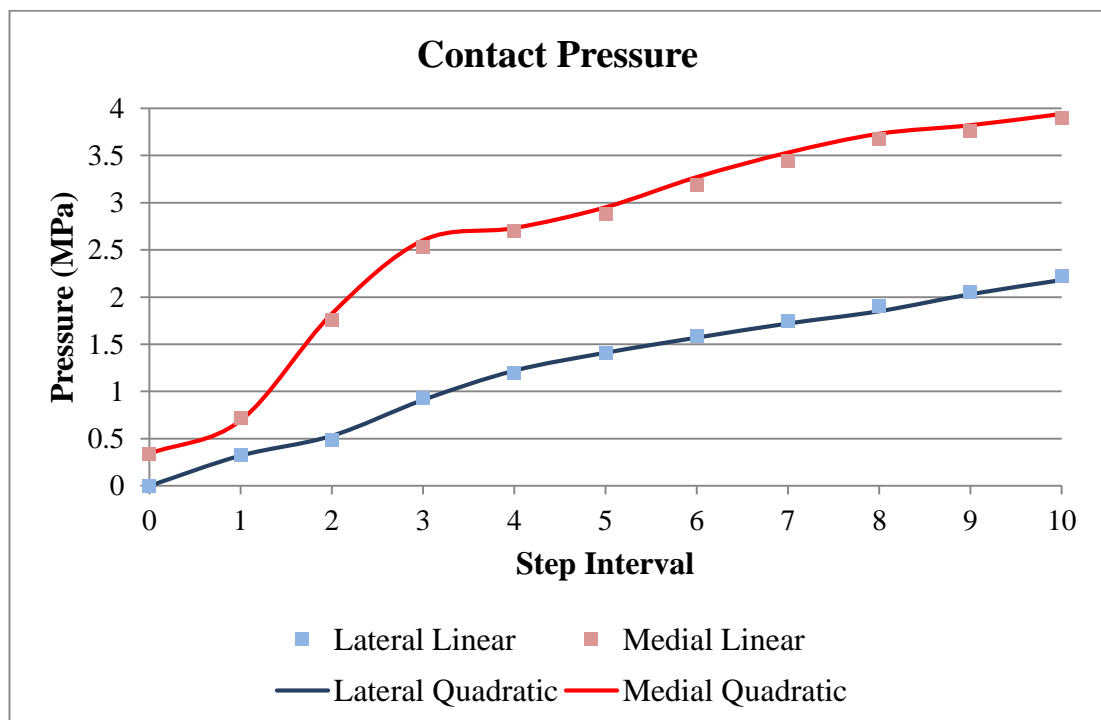


**Figure 4.2: Peak contact pressure for a model with linear mesh elements compared to a model with quadratic mesh elements**

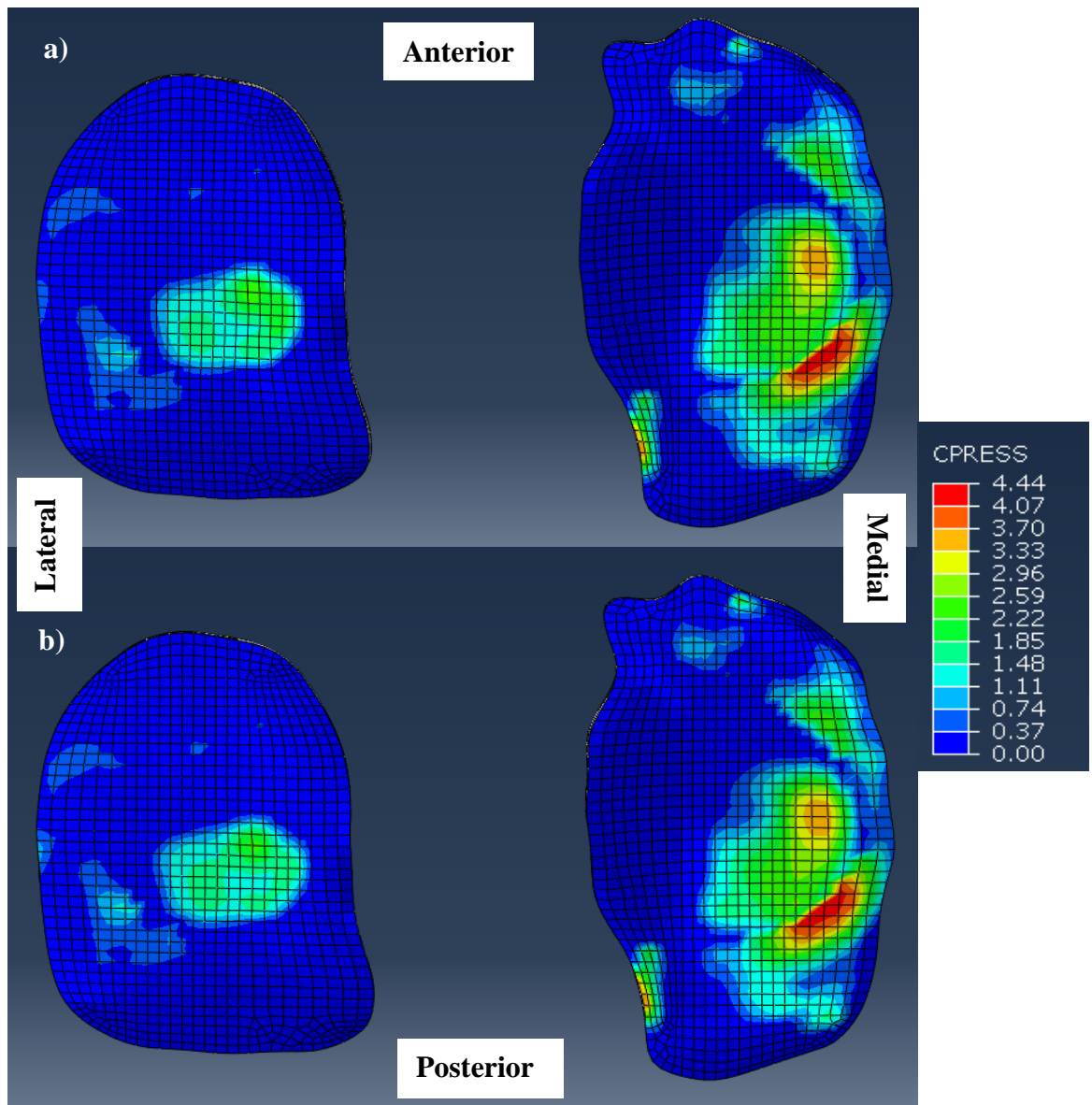
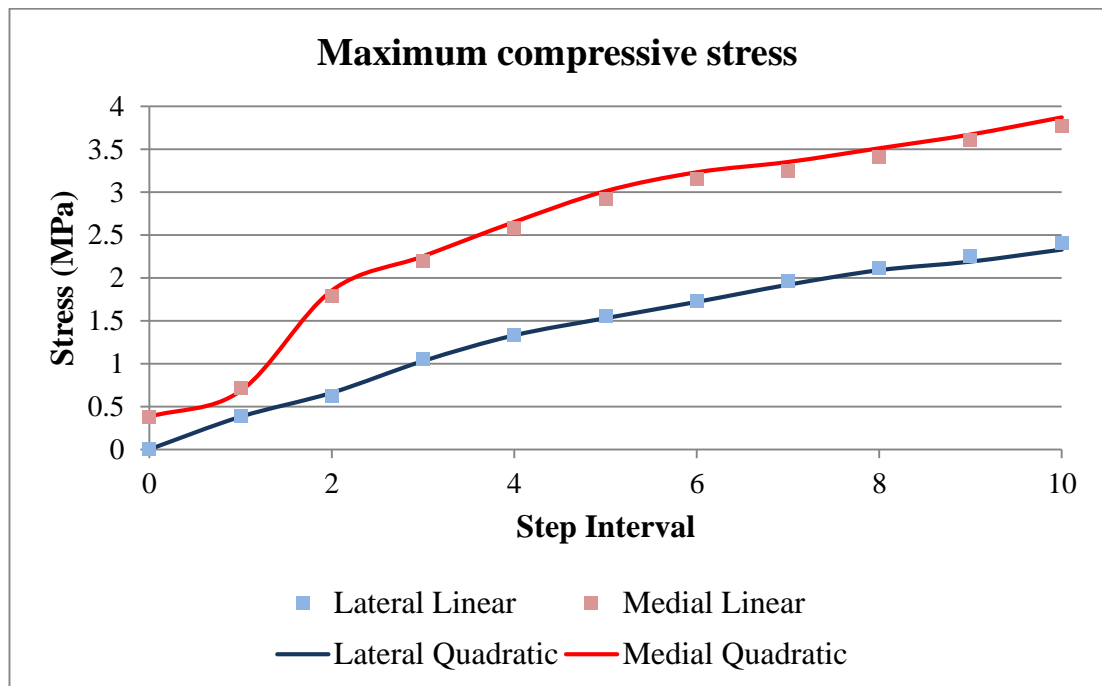


Figure 4.3: Contact pressure area a) model with linear mesh elements b) model with quadratic mesh elements

**Table 4.3: Comparison of maximum compressive stress between linear and quadratic meshed bones. Step interval 0 represents the initial loading of the knee joint and step interval 10 represents completion of the task.**

Step Interval	Maximum compressive stress (MPa)					
	Linear		Quadratic		Square error	
	Lateral	Medial	Lateral	Medial	Lateral	Medial
0	0	0.38	0	0.38	0.0000	0.0000
1	0.39	0.71	0.38	0.68	0.0001	0.0009
2	0.62	1.79	0.66	1.85	0.0016	0.0036
3	1.06	2.2	1.03	2.25	0.0009	0.0025
4	1.33	2.58	1.33	2.65	0.0000	0.0049
5	1.56	2.92	1.53	3.01	0.0009	0.0081
6	1.73	3.15	1.72	3.23	0.0001	0.0064
7	1.96	3.25	1.92	3.35	0.0016	0.0100
8	2.12	3.41	2.09	3.51	0.0009	0.0100
9	2.25	3.61	2.19	3.67	0.0036	0.0036
10	2.41	3.77	2.33	3.87	0.0064	0.0100
<b>Mean Square Error</b>					<b>0.0015</b>	<b>0.0055</b>
<b>RMSE (MPa)</b>					<b>0.0383</b>	<b>0.0738</b>
<b>%FSE</b>					<b>1.59 %</b>	<b>1.96 %</b>



**Figure 4.4: Peak maximum compressive stress for a model with linear mesh elements compared to a model with quadratic mesh elements**



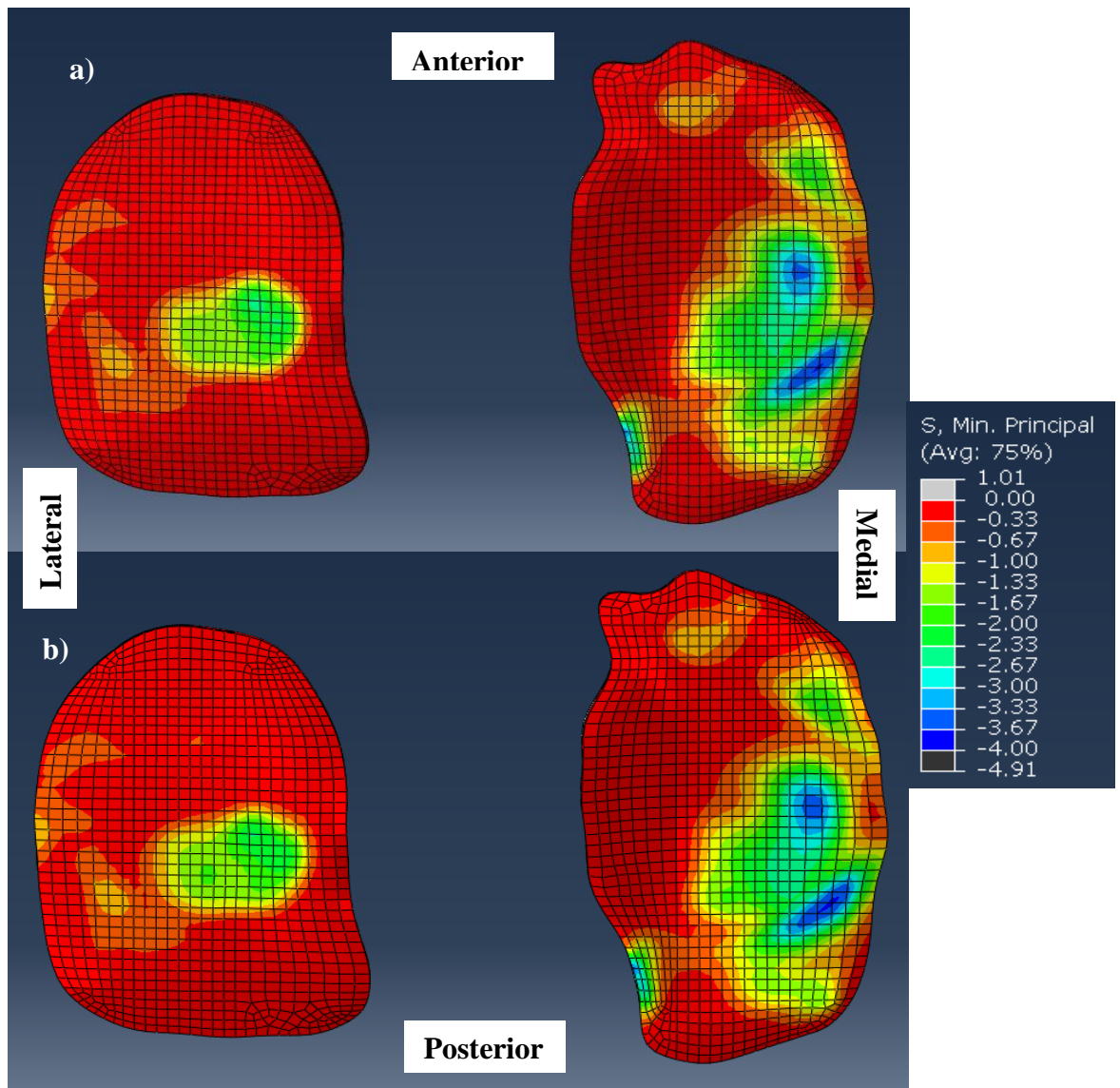
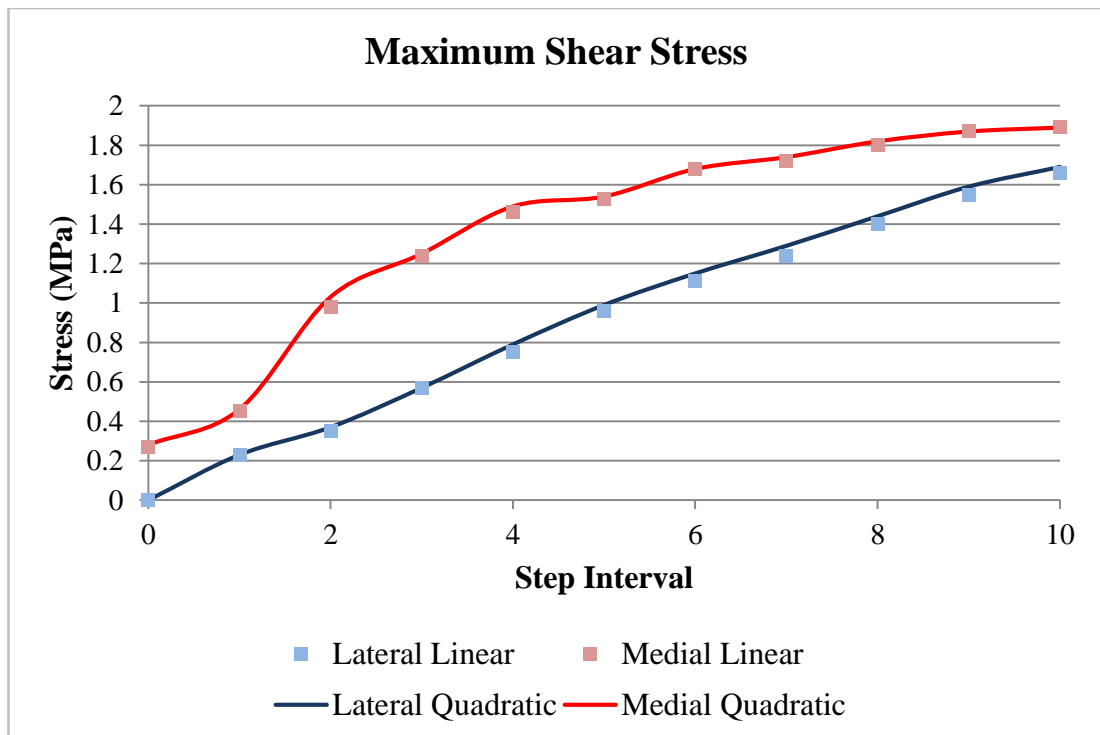


Figure 4.5: Maximum compressive stress area for a) model with linear mesh elements compared to b) model with quadratic mesh elements

**Table 4.4: Comparison of maximum shear stress between linear and quadratic meshed bones. Step interval 0 represents the initial loading of the knee joint and step interval 10 represents completion of the task.**

Step Interval	Maximum Shear Stress (MPa)				Square error	
	Linear		Quadratic			
	Lateral	Medial	Lateral	Medial	Lateral	Medial
0	0	0.27	0	0.28	0.0000	0.0001
1	0.23	0.45	0.23	0.46	0.0000	0.0001
2	0.35	0.98	0.37	1.03	0.0004	0.0025
3	0.57	1.24	0.57	1.25	0.0000	0.0001
4	0.75	1.46	0.79	1.49	0.0016	0.0009
5	0.96	1.53	0.99	1.54	0.0009	0.0001
6	1.11	1.68	1.15	1.68	0.0016	0.0000
7	1.24	1.72	1.29	1.74	0.0025	0.0004
8	1.4	1.8	1.44	1.82	0.0016	0.0004
9	1.55	1.87	1.59	1.87	0.0016	0.0000
10	1.66	1.89	1.69	1.89	0.0009	0.0000
			Mean Square Error		0.0010	0.0004
			RMSE (MPa)		0.0318	0.0205
			%FSE		1.91 %	1.08 %



**Figure 4.6: Peak maximum shear stress for a model with linear mesh elements compared to a model with quadratic mesh elements**

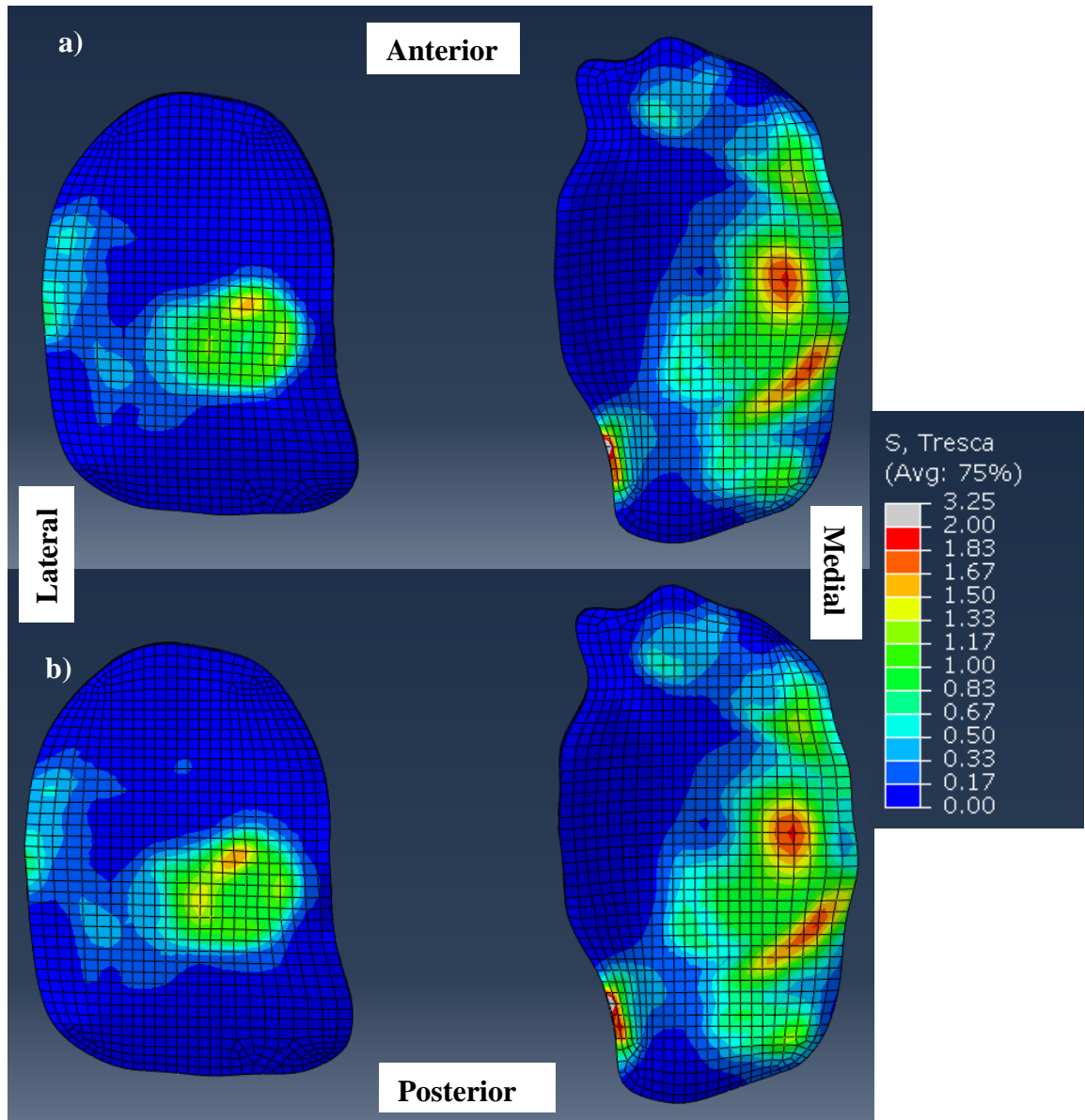


**Figure 4.7: Maximum shear stress area for a) model with linear mesh elements compared to b) model with quadratic mesh elements**

Tables 4.1- 4.4 show that the %FSE for all contact force and stress parameters is less than 2% between linear and quadratic mesh elements. This shows that there was no substantial difference between the 4-noded and 10-noded element models. It can be concluded that knee joint contact mechanics were not sensitive to mesh type in osseous tissues. Figures 4.1-4.7 further verify this assumption by showing that there is no difference in the pressure and stress distributions between the two models. Therefore, it was decided that the 4-noded element model would be used for all further analyses since this provided a faster convergence time.

## 4.2. Effect of Mesh Size on Contact Pressure

To optimise the mesh density and ensure the best mesh size with the least computation a mesh sensitivity analysis was performed. Throughout the analysis the term ‘contact pressure’ refers to both tibial and femoral compartments. Results were useful in determining how different element sizes affected contact mechanics and to select the coarsest acceptable mesh. Table 4.5 summarises percent change in contact pressure for different element sizes in the osseous tissues. Table 4.6 provides an overview of the percent change in contact pressure for different element sizes in the tibial and femoral cartilage and the menisci.

**Table 4.5: Mesh sensitivity analysis for element sizes in osseous tissues**

	Number of elements (element size)			Change in maximum contact pressure (%)
	Femur	Tibia	Fibula	
Reference Mesh	229792 (1.5 mm)	162121 (1.5 mm)	29531 (1.5 mm)	-
Case 1	121601 (2 mm)	85179 (2 mm)	14985 (2 mm)	0.08
<b>Case 2</b>	<b>86207</b> <b>(2.5 mm)</b>	<b>57546</b> <b>(2.5 mm)</b>	<b>14985</b> <b>(2 mm)</b>	<b>0.21</b>
Case 3	55567 (3 mm)	33478 (3 mm)	14985 (2 mm)	0.29
Case 4	13325 (5 mm)	11056 (5 mm)	4681 (3 mm)	7.58
Case 5	5764 (7 mm)	6563 (7 mm)	1614 (4.5 mm)	20.49
Case 6	2022 (10 mm)	4147 (10 mm)	1294 (4.5 mm)	34.47

**Table 4.6: Mesh sensitivity analysis for element sizes in soft tissues**  
(Source: (Mootanah et al., 2014))

	Number of elements (element size)			Change in maximum contact pressure (%)
	Femoral Cartilage	Tibial Cartilage	Menisci	
Reference mesh	29547 (0.75 mm)	36026 (0.5 mm)	38034 (0.5 mm)	-
Case 1	29547 (0.75 mm)	36026 (0.5 mm)	4314 (1 mm)	2.92
Case 2	29547 (0.75 mm)	4988 (1 mm)	4314 (1 mm)	3.63
<b>Case 3</b>	<b>11044 (1 mm)</b>	<b>4988 (1 mm)</b>	<b>4314 (1 mm)</b>	<b>4.56</b>
Case 4	2558 (1.5 mm)	1994 (1.5 mm)	1224 (1.5 mm)	15.68
Case 5	1455 (2 mm)	674 (2 mm)	936 (2 mm)	20.5

From Table 4.5 it can be concluded that contact pressure is relatively invariant to osseous mesh size until the mesh is so large that bony geometry is distorted (Case 4 and higher). The smallest mesh possible was set as the reference mesh and the percent change was calculated for each element size. Case 2 was selected for the final mesh because it required only 32 % of the computational time to solve while maintaining an error of less than 0.5 % compared to the reference model. A larger mesh size for bone would have created a high discrepancy from the cartilage element size. This would have resulted in distorted cartilage elements and unacceptable errors.

Table 4.6 shows that the contact pressure is very sensitive to soft tissue element size. The smallest mesh possible was set as the reference mesh and the percent change was calculated for each element size. Case 3 was selected for the final mesh because it

required only 10 % of the computation time to solve while maintaining an error of less than 5 % compared to the reference model. Coarser meshes gave unacceptable errors.

### 4.3. Effect of Material Properties on Knee Joint Contact Pressure

In order to understand how different material properties affect the contact mechanics of the knee joint, a probabilistic analysis technique was carried out. A 374 N axial load and a 15 Nm bending moment were applied to the knee joint. Different material properties were then selected for various tissues and the effect on contact pressure and compartmental forces was analysed. Figures 4.8-4.13 summarise the results of the sensitivity analysis.

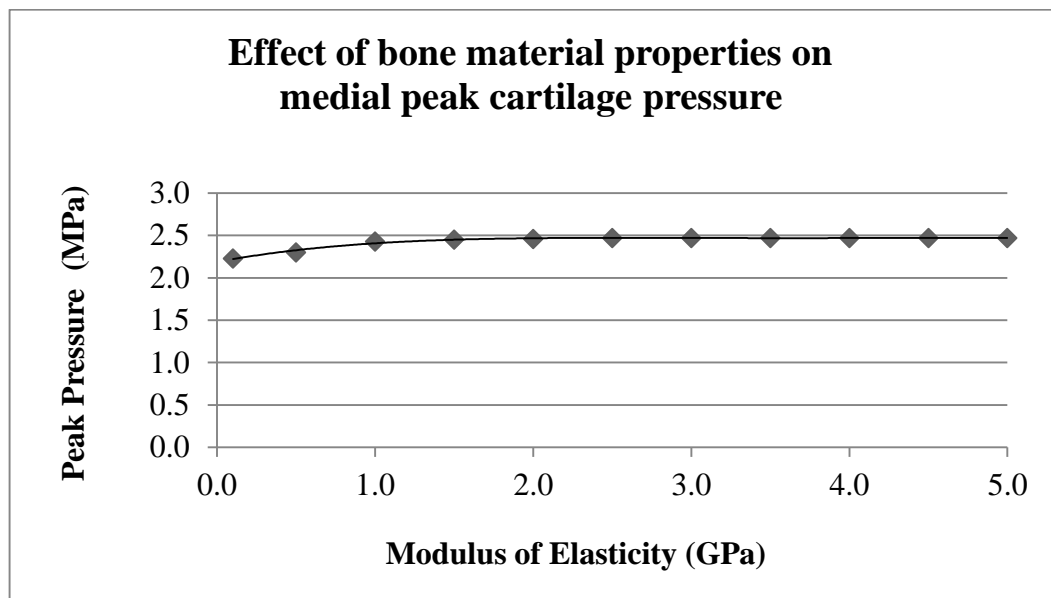


Figure 4.8: Effect of bone material properties on medial peak joint pressure

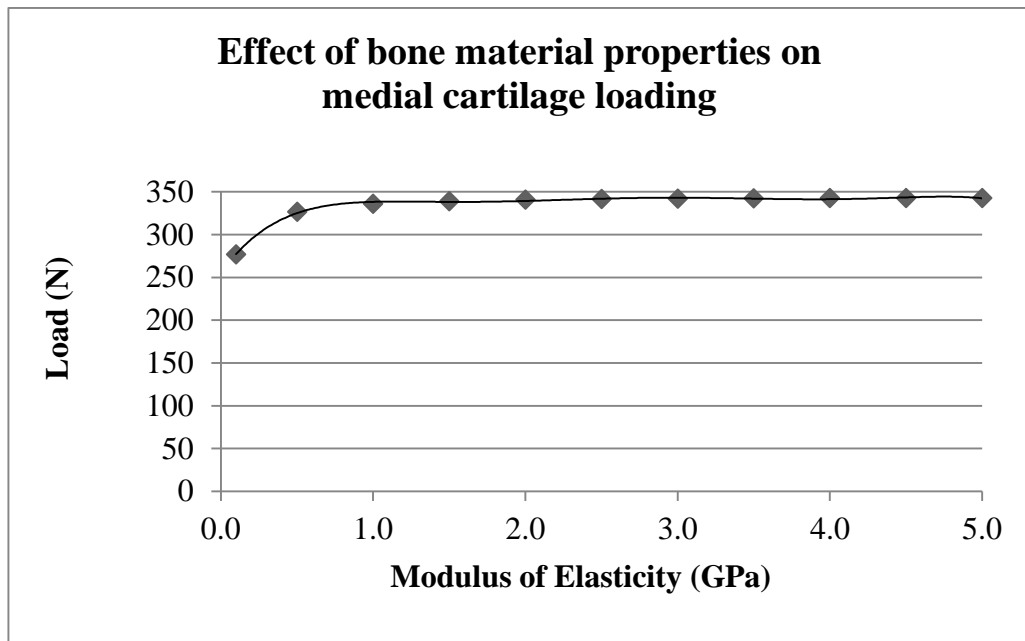


Figure 4.9: Effect of bone material properties on medial tibial cartilage loading

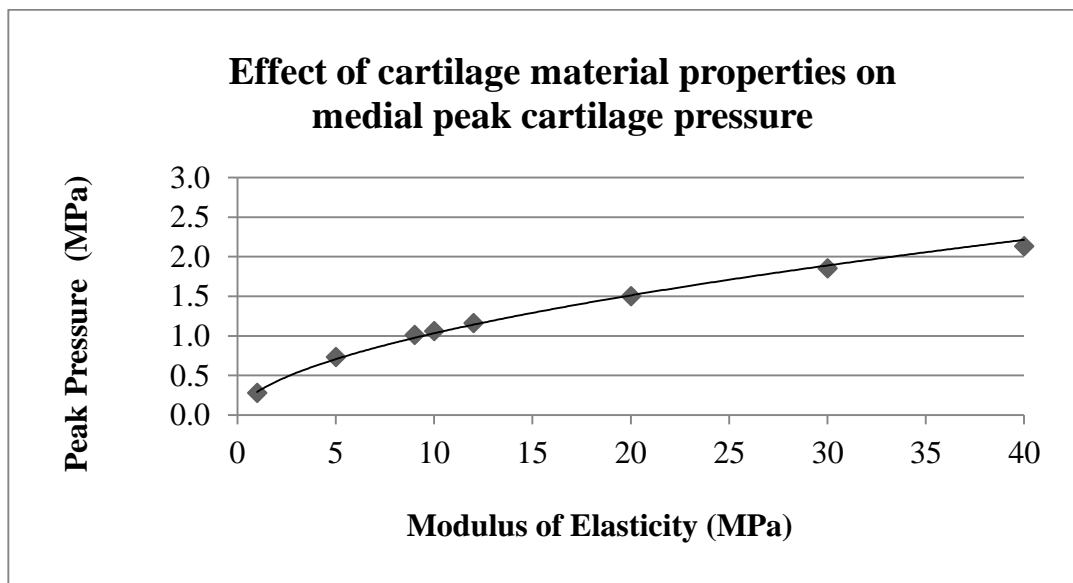
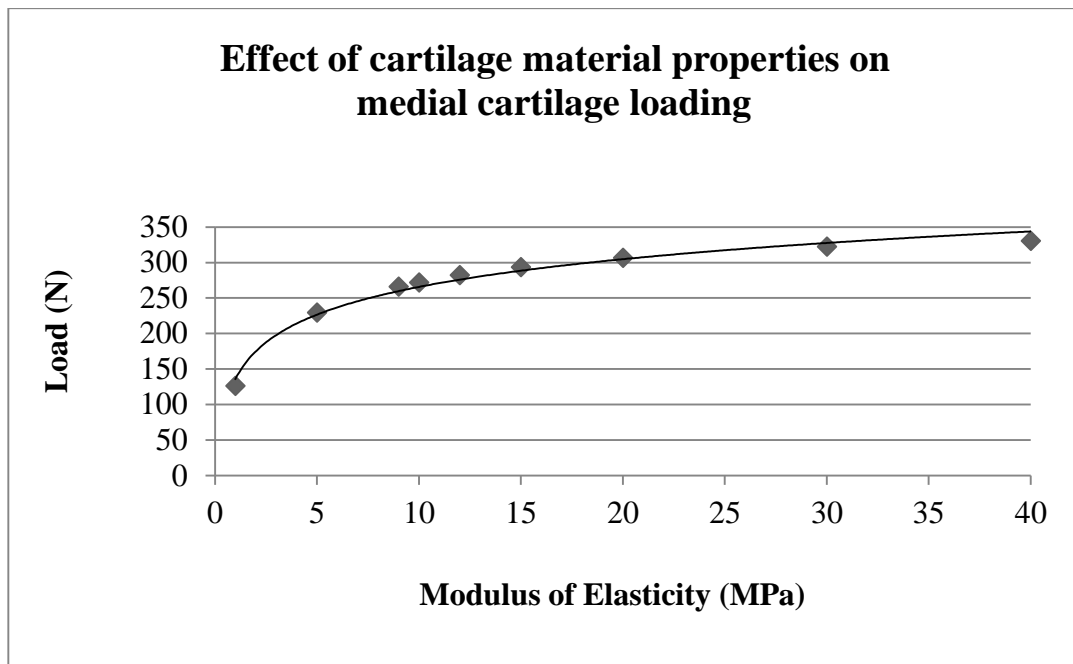
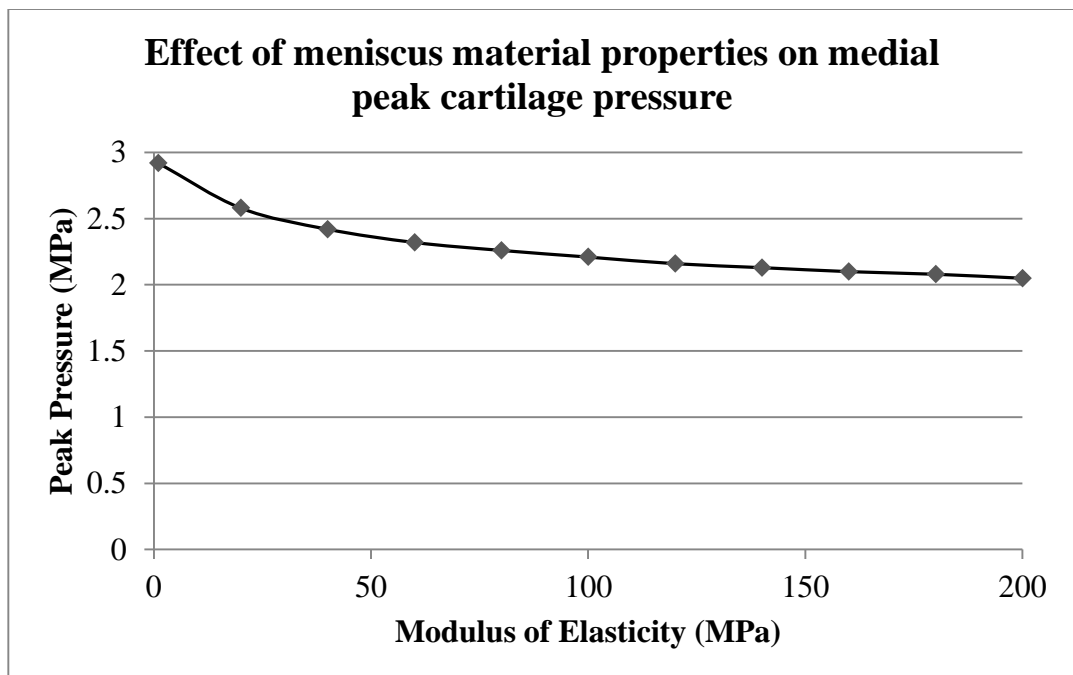


Figure 4.10: Effect of cartilage material properties on medial peak joint pressure



**Figure 4.11: Effect of cartilage material properties on medial tibial cartilage loading**



**Figure 4.12: Effect of meniscus material properties on medial peak joint pressure**



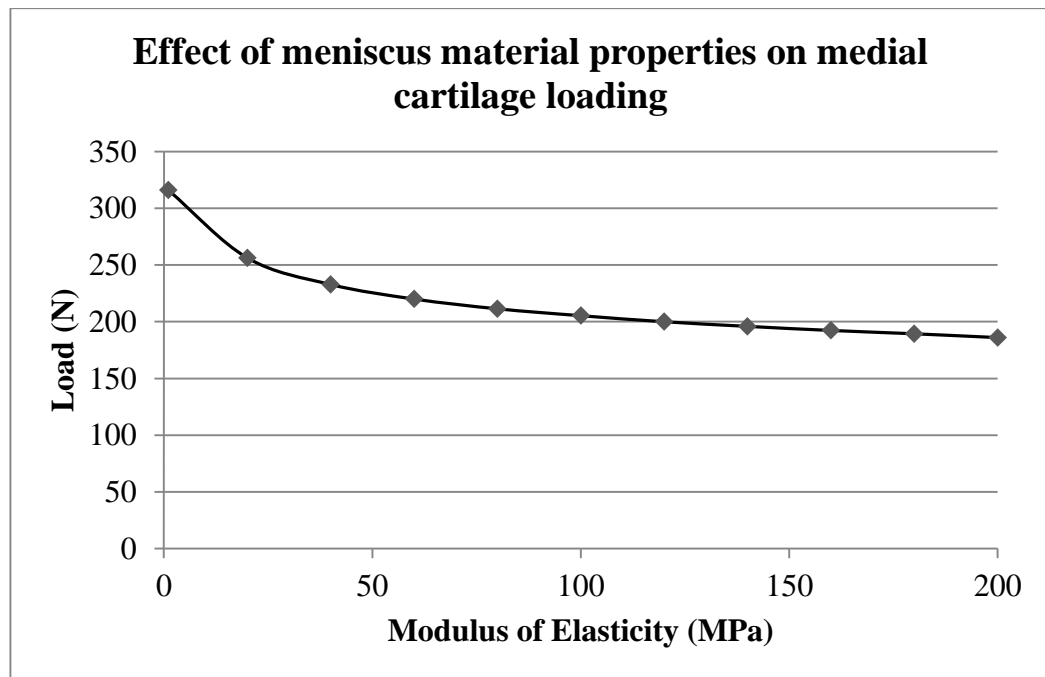


**Figure 4.13: Effect of meniscus material properties on medial tibial cartilage loading**

Figure 4.8 shows that an increase in the bone modulus from 0.5 GPa to 2 GPa resulted in an increase in contact pressure from 2.25 MPa to 2.55 MPa. Any further increase in the modulus did not affect the pressure and forces within the knee compartment. An increase in the cartilage modulus of elasticity from 5 MPa to 50 MPa consistently results in a substantial increase in peak stress in the medial cartilage from 0.73 MPa to 2.13 MPa (Figure 4.10).

An increase of the circumferential menisci modulus from 1 MPa to 200 MPa resulted in a decrease in contact pressure and load (Figures 4.12 and 4.13). This means that the meniscus was taking most of the load while preserving the cartilage. The meniscus transforms the direction of the load, converting the compressive stress to tensile stress (or hoop stress), which causes the meniscus to extrude, usually at the medial side (Nordin and Frankel, 2001).

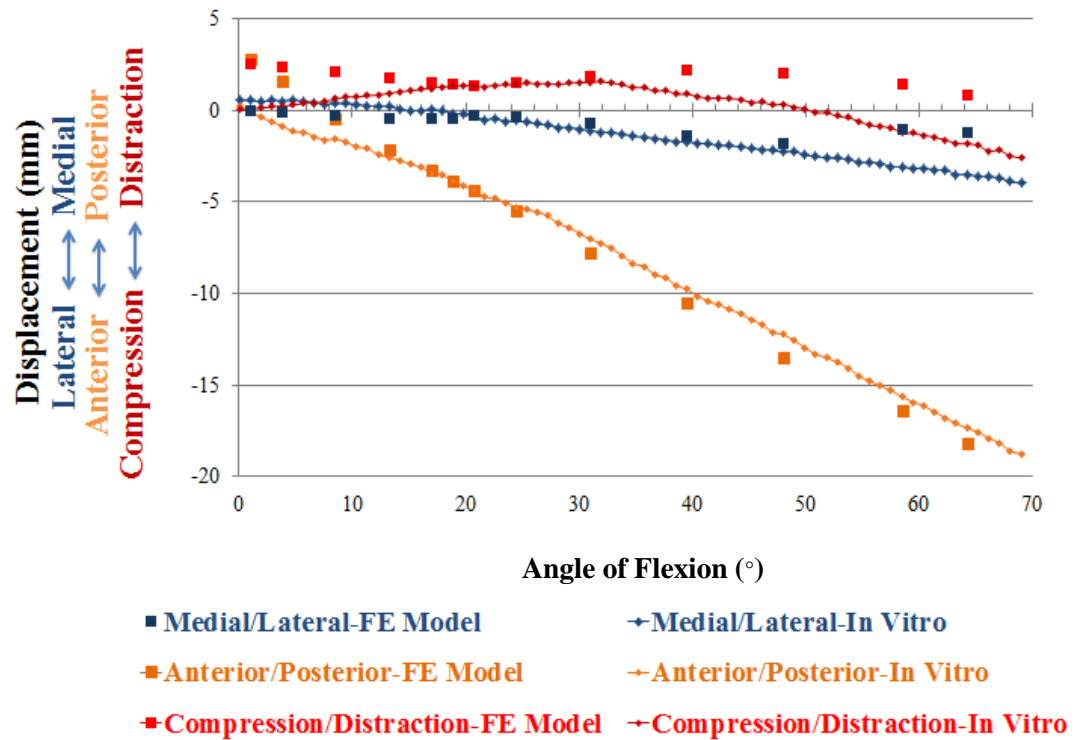
From these results, it can be concluded that the properties of the bone had little influence (2.5%), the properties of the meniscus had a substantial influence (3%-7% for every 20 MPa change) and the properties of cartilage had an even greater influence (40%-100% for every 10-20 MPa change) on joint stress and loading values.

## 4.4. Ligament Tuning

### 4.4.1. Matching Kinematics to Tune the Ligament Properties

To compare the kinematics between the FE model and the cadaver, the position of the tibia with respect to the femur was calculated for each model. Material properties of each ligament were tuned until the kinematics of the FE model matched those of the cadaveric specimen, positioned in a load controlled robot, in 5 degrees of freedom along a  $0^\circ$  to  $65^\circ$  flexion pathway. Figures 4.14 a, b show the rotational and translational kinematics of the tibia relative to the femur obtained from FE model prediction and *in vitro* experiments for the  $0^\circ$  to  $65^\circ$  flexion pathway. The RMSE of each remaining DOF was calculated. In addition, the sagittal plane position was fixed at  $20^\circ$ , simulating the end weight acceptance, while the ligament properties were tuned with an application of varus and valgus bending moments (Figures 4.15 a, b). Table 4.7 summarises the RMSE for each DOF between the FE model and the cadaver kinematics.

a) **Translational Kinematics of the Tibia Relative to the Femur**



b) **Rotational Kinematics of the Tibia Relative to the Femur**

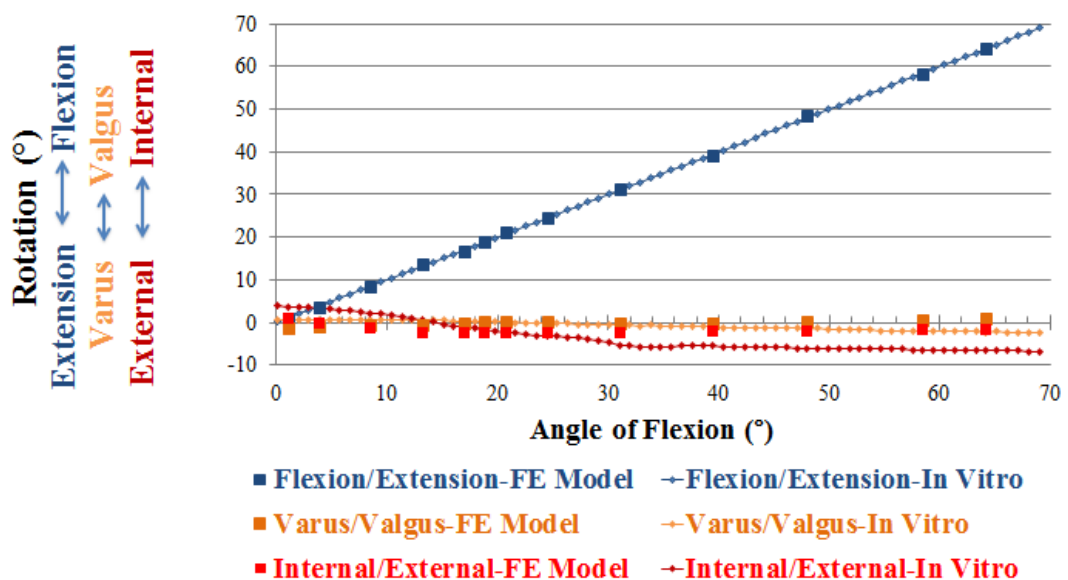


Figure 4.14: The ligament tuning process: the ligament properties were adjusted in an iterative process until the kinematics of the tibia relative to the femur in the model closely matched those *in vitro* in all six degrees of freedom for a) translational and b) rotational kinematics during a sagittal rotation from full extension to 65° flexion (Source: Mootanah et al., 2014)

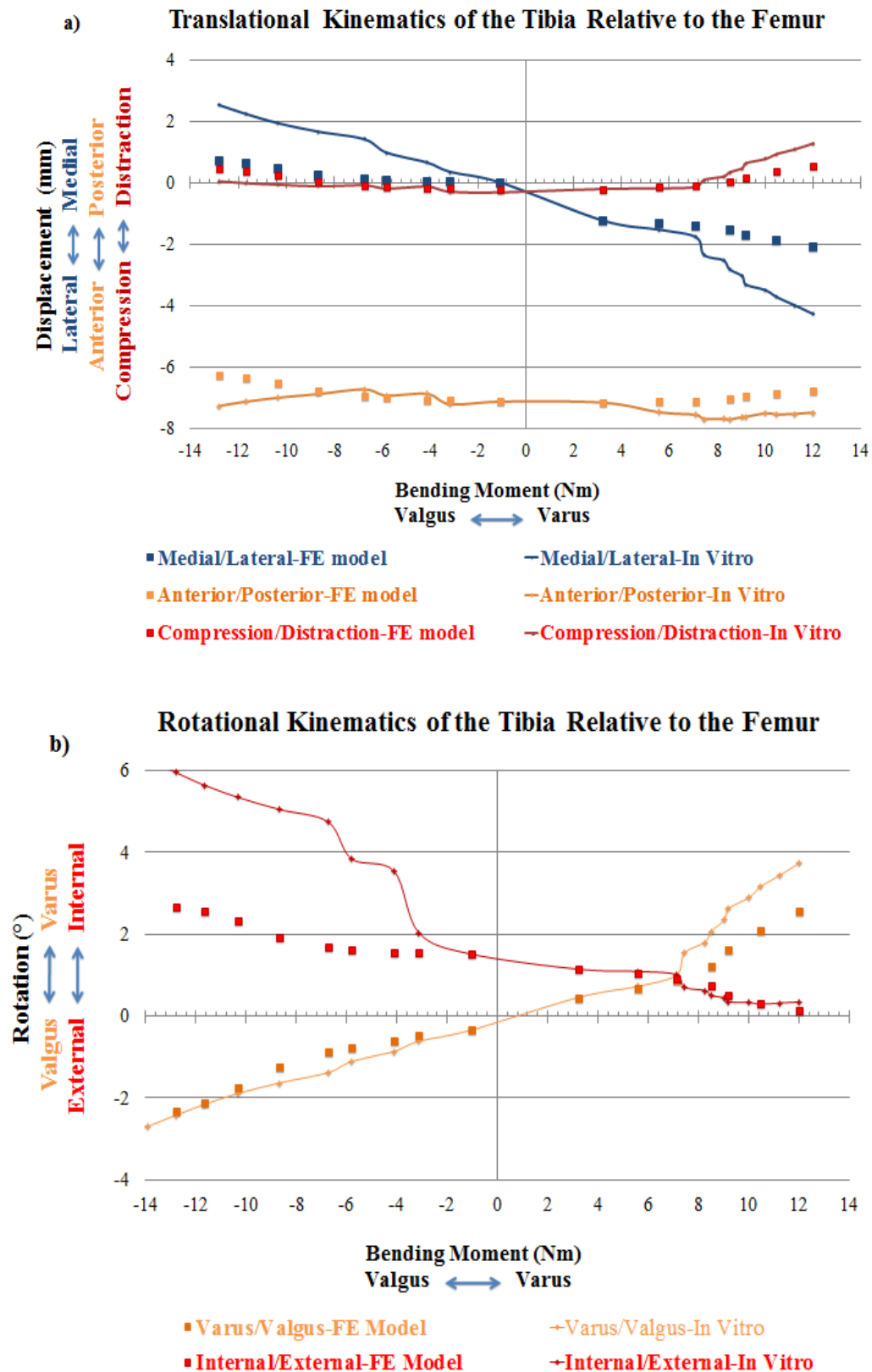


Figure 4.15: The ligament tuning process: the ligament properties were adjusted in an iterative process until the kinematics of the tibia relative to the femur in the model closely matched those *in vitro* in all six degrees of freedom for a) translational and b) rotational kinematics during 0–12 Nm valgus / varus bending moments.

(Source: Mootanah et al., 2014)

**Table 4.7: RMSE for each degree of freedom between finite element model predictions and *in vitro* results**

<b>Degree of freedom</b>	<b>RMSE passive flexion</b>	<b>RMSE varus</b>	<b>RMSE valgus</b>
Compression/Distracton	1.68	1.15	0.10
Medial/Lateral	0.93	2.51	1.58
Anterior/Posterior	1.44	0.56	0.55
Internal/External	3.08	0.65	2.97
Flexion/Extension	0.26	n/a	n/a
Varus/Valgus	1.54	0.87	0.58

Table 4.7 shows that kinematic results are in close agreement and therefore the model can be seen as moving in the same directions as the cadaver.

#### **4.4.2. Material Properties after Tuning**

After the tuning process, the material properties of the four ligaments at each degree of flexion were acquired. Figure 4.16 presents the material properties for each ligament at different angles of passive flexion. The material properties after an application of 374 N axial load and a 15 Nm varus / valgus bending moment are summarised in Table 4.8.

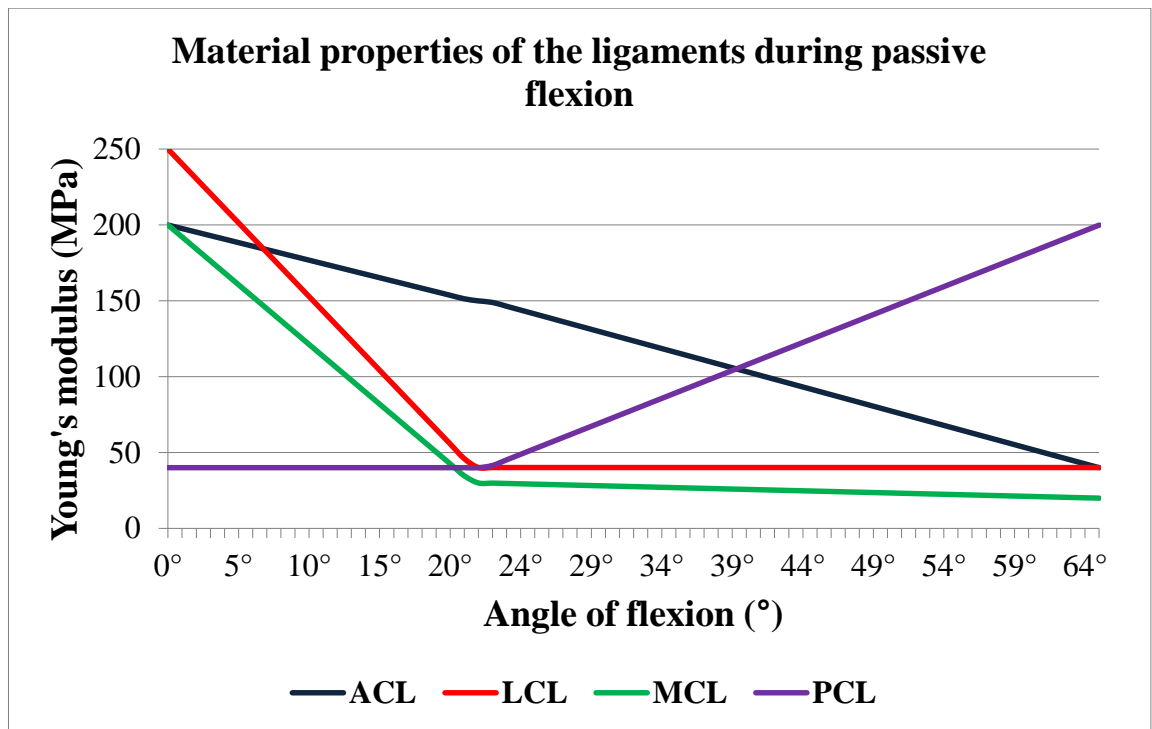


**Figure 4.16: Material properties for the lateral collateral ligament (LCL), medial collateral ligament (MCL), anterior cruciate ligament (ACL) and posterior cruciate ligament (PCL) at every angle of flexion, following the ligament tuning process.**  
(Source: Mootanah et al., 2014)

**Table 4.8: Young's modulus values of the medial collateral ligament (MCL), lateral collateral ligament (LCL), anterior cruciate ligament (ACL) and posterior cruciate ligament (PCL) before and after application of varus and valgus bending moments. Linear increments in ligament Young's moduli were applied in the model as bending moments increased from 0 Nm to 15 Nm varus and valgus.**  
(Source: Mootanah et al., 2014)

Bending Moment	Young's Modulus (MPa)			
	MCL	LCL	ACL	PCL
15 Nm varus	10	60	250	40
0 Nm	30	40	150	40
15 Nm valgus	60	5	150	40

Figure 4.16 shows how the material properties responded to passive joint kinematics. At full extension the PCL had a low modulus, which represents a slackened position. ACL, MCL and LCL had high moduli, which means that they were in tension. With

flexion, the moduli of the LCL and MCL rapidly decreased and became 40 and 30 MPa, respectively, at 20° flexion which corresponds to the end of weight acceptance. The ACL had a modulus of 150 MPa providing resistance for translation and rotation. After 20° the modulus of the PCL increased, the ACL decreased and the MCL and LCL stayed within the toe region of the stress-strain curve.

Table 4.8 shows that the modulus of the LCL increased, the MCL decreased and the ACL substantially increased in response to a varus bending moment. For a valgus bending moment the MCL increased in modulus (from 10 to 60 MPa), the LCL decreased (from 40 to 5 MPa) and the ACL and PCL had no change. It can be concluded that ligament modulus is very sensitive to rotations and translations. Therefore, special attention has been given to tune these moduli for each degree of flexion from 0° to 65°.

## 4.5. Validation

To compare the trends of FE-predicted and *in vitro*-measured peak pressure and compartmental force, all values were normalised to the corresponding maximum in each compartment. The normalised FE-predicted and *in vitro*-measured values were compared to validate the FE model. The percentage of total load acting in the medial and lateral compartment of the knee was computed and compared with the literature.

Figures 4.17a, b illustrate the intra-articular compartmental pressure distribution, measured by the Tekscan transducer (Figure 4.17a) and the corresponding results predicted by the FE model (Figure 4.17b) for a 374 N axial force with

- i) a 15 Nm varus bending moment
- ii) no bending moment
- iii) a 15 Nm valgus bending moment.

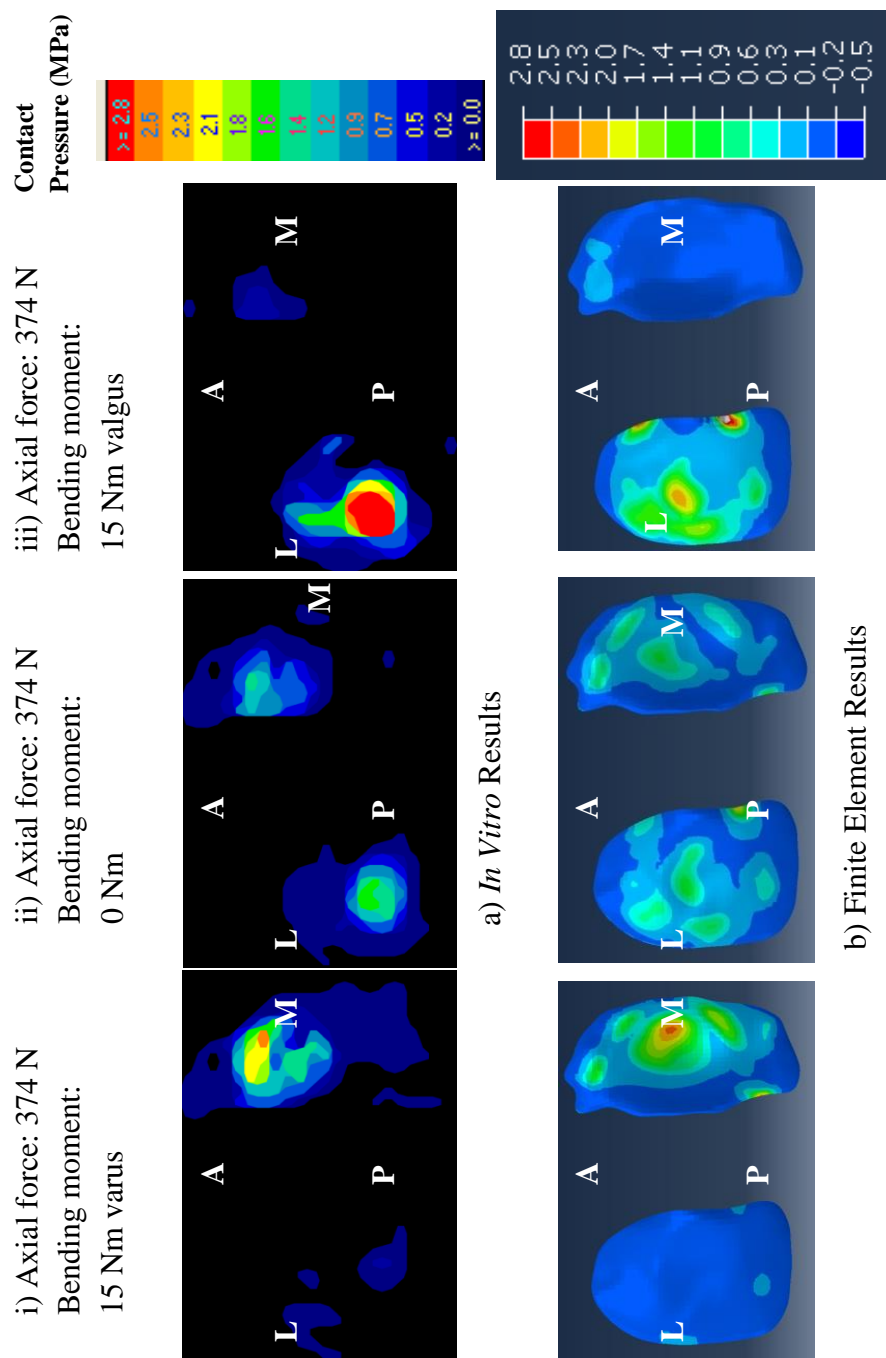
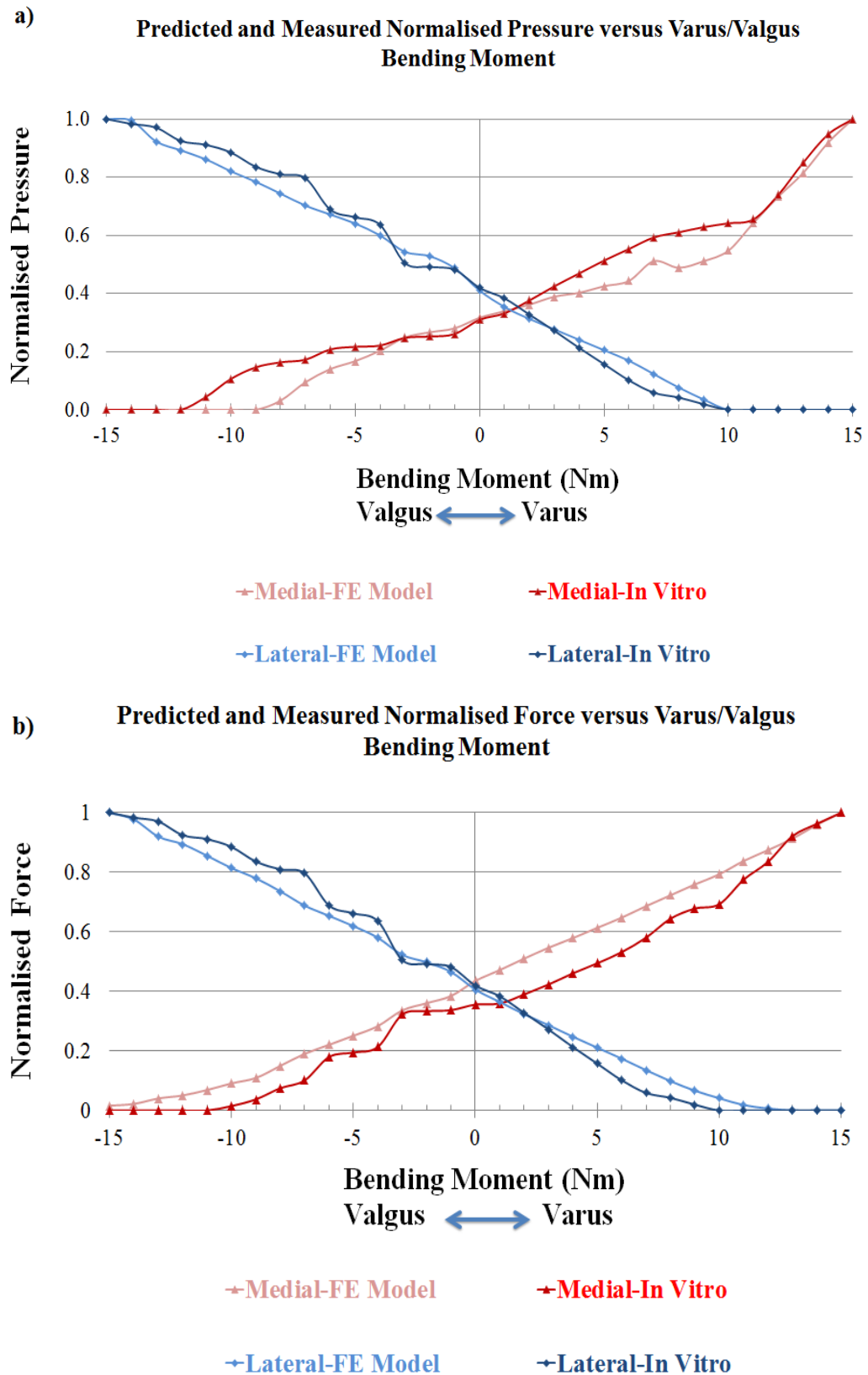


Figure 4.17: Evaluation of finite element (FE) model. Pressure distributions in the tibiofemoral joint in response to a 374 N axial load and a 15 Nm varus / valgus bending moment for a) *in vitro* testing and b) FE model predictions; A=Anterior, P=Posterior, L=Lateral, M=Medial (Source: Mootanah et al., 2014)

Figure 4.18a graphs the *in vitro* and computer-simulated normalised medial and lateral compartmental pressures during a 374 N axial load with a 0 to 15 Nm varus and valgus bending moment. Figure 4.18b shows the *in vitro* and computer simulated normalised compartment forces for the same loading conditions. The normalised force and peak pressure values were obtained by dividing each absolute loading value by the corresponding maximum in each compartment.





**Figure 4.18: *In vitro* and FE predicted medial and lateral compartment loading in response to a 374 N axial load and 0 to 15 Nm varus and valgus bending moments for a) normalised peak pressure and b) normalised force**  
(Source: Mootanah et al., 2014)

Table 4.9 presents the absolute and normalised *in vitro* and FE results of 1) the medial and lateral force, 2) the medial and lateral peak pressure values, 3) the corresponding RMSE and 4) the % FSE for peak pressure and force in the medial and lateral compartments.

**Table 4.9: Root mean square error (RMSE) and percentage full scale error (FSE) in medial and lateral force and peak pressure values between *in vitro* and FE results for axial load of 374 N and varus/valgus bending moments ranging from 0 to 15 Nm.**

Percentage FSE was obtained by expressing the RMSE as a percentage of the maximum corresponding value.

(Source: Mootanah et al., 2014)

	Bending Moment (Nm)	Medial Compartment				Lateral Compartment				Medial Compartment				Lateral Compartment			
		Absolute Force (N)		Normalised Force		Absolute Force (N)		Normalised Force		Absolute Pressure (MPa)		Normalised Pressure		Absolute Pressure (MPa)		Normalised Pressure	
		Exp	FE	Exp	FE	Exp	FE	Exp	FE	Exp	FE	Exp	FE	Exp	FE	Exp	FE
Valgus Bending Moment	-15	0	8	0.00	0.02	305	436	1.00	1.00	0.00	0.00	0.00	0.00	4.75	1.95	1.00	1.00
	-14	0	11	0.00	0.02	300	426	0.98	0.98	0.00	0.00	0.00	0.00	4.60	1.94	0.97	0.99
	-13	0	20	0.00	0.04	296	401	0.97	0.92	0.00	0.00	0.00	0.00	4.52	1.80	0.95	0.92
	-12	0	25	0.00	0.05	282	390	0.92	0.89	0.00	0.00	0.00	0.00	4.35	1.74	0.92	0.89
	-11	0	34	0.00	0.07	278	373	0.91	0.86	0.10	0.00	0.04	0.00	4.20	1.68	0.88	0.86
	-10	4	45	0.01	0.09	270	355	0.89	0.81	0.24	0.00	0.11	0.00	4.03	1.60	0.85	0.82
	-9	10	54	0.04	0.11	255	340	0.84	0.78	0.33	0.00	0.15	0.00	3.80	1.53	0.80	0.78
	-8	20	74	0.07	0.15	247	321	0.81	0.74	0.37	0.07	0.16	0.03	3.66	1.45	0.77	0.74
	-7	27	94	0.10	0.19	243	300	0.80	0.69	0.39	0.21	0.17	0.10	3.54	1.37	0.75	0.70
	-6	48	109	0.18	0.22	210	285	0.69	0.65	0.47	0.31	0.21	0.14	3.12	1.31	0.66	0.67
	-5	52	124	0.19	0.25	202	270	0.66	0.62	0.49	0.37	0.22	0.17	2.93	1.25	0.62	0.64
	-4	57	140	0.21	0.28	194	253	0.64	0.58	0.50	0.45	0.22	0.20	2.72	1.17	0.57	0.60
	-3	86	166	0.32	0.34	154	228	0.50	0.52	0.56	0.55	0.25	0.25	2.10	1.06	0.44	0.54
	-2	89	178	0.33	0.36	150	217	0.49	0.50	0.57	0.59	0.25	0.27	1.94	1.03	0.41	0.53
	-1	90	190	0.34	0.38	147	203	0.48	0.47	0.59	0.62	0.26	0.28	1.80	0.95	0.38	0.49
Varus Bending Moment	0	95	215	0.36	0.44	128	177	0.42	0.41	0.70	0.70	0.31	0.32	1.50	0.80	0.32	0.41
	1	96	233	0.36	0.47	117	159	0.38	0.36	0.75	0.75	0.33	0.34	1.30	0.69	0.27	0.35
	2	104	252	0.39	0.51	100	141	0.33	0.32	0.85	0.80	0.38	0.36	1.10	0.61	0.23	0.31
	3	113	270	0.42	0.55	83	125	0.27	0.29	0.96	0.86	0.42	0.39	0.90	0.54	0.19	0.28
	4	123	286	0.46	0.58	65	108	0.21	0.25	1.06	0.89	0.47	0.40	0.70	0.47	0.15	0.24
	5	132	303	0.49	0.61	48	92	0.16	0.21	1.16	0.94	0.51	0.43	0.51	0.40	0.11	0.21
	6	142	320	0.53	0.65	31	76	0.10	0.17	1.25	0.98	0.55	0.44	0.34	0.33	0.07	0.17
	7	155	339	0.58	0.69	18	59	0.06	0.14	1.34	1.13	0.59	0.51	0.22	0.24	0.05	0.12
	8	172	357	0.64	0.72	13	43	0.04	0.10	1.38	1.08	0.61	0.49	0.17	0.15	0.04	0.08
	9	181	375	0.68	0.76	6	29	0.02	0.07	1.42	1.13	0.63	0.51	0.09	0.07	0.02	0.04
	10	185	392	0.69	0.79	0	18	0.00	0.04	1.45	1.21	0.64	0.55	0.00	0.00	0.00	0.00
	11	207	414	0.78	0.84	0	8	0.00	0.02	1.48	1.42	0.65	0.64	0.00	0.00	0.00	0.00
	12	223	432	0.84	0.87	0	3	0.00	0.01	1.67	1.62	0.74	0.73	0.00	0.00	0.00	0.00
	13	246	451	0.92	0.91	0	0	0.00	0.00	1.92	1.80	0.85	0.81	0.00	0.00	0.00	0.00
	14	257	474	0.96	0.96	0	0	0.00	0.00	2.14	2.03	0.95	0.92	0.00	0.00	0.00	0.00
	15	267	494	1.00	1.00	0	0	0.00	0.00	2.26	2.21	1.00	1.00	0.00	0.00	0.00	0.00
RMSE		138.71 N		0.08		65.18 N		0.04		0.16 MPa		0.07		1.49 MPa		0.06	
FSE (%)		28.08		7.56		14.95		4.48		7.18		6.67		31.30		5.94	

#### 4.5.1. Peak Pressure in the Tibial Cartilage

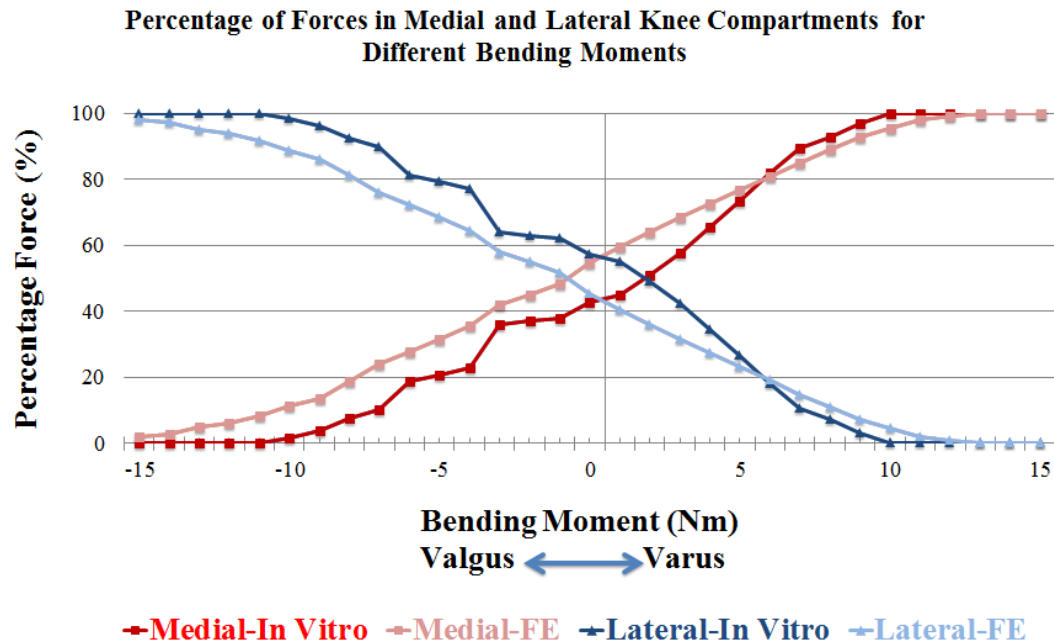
Figures 4.17a and 4.17b show that peak pressure locations, at 15 Nm varus, 0 Nm and 15 Nm valgus bending moments, were in quantitative agreement between *in vitro*-measured and FE-predicted pressure values. It can be seen that the meniscal horn attachments create an edge effect at the tibial cartilage, which is artificial and is therefore ignored in this study.

Figure 4.18a shows that normalised peak pressure increased monotonically in the medial compartment and decreased in the lateral compartment as varus bending moment increased from 0 to 15 Nm. The FE model consistently predicted normalised peak pressures similar to *in vitro*-measured values in the tibial cartilage throughout the application of varus bending moments from 0 to 15 Nm (Figure 4.18a). Consistent normalised peak pressures were also observed in each compartment when a 0 to 15 Nm valgus bending moment was applied. The RMSE between absolute FE-predicted and *in vitro*-measured peak pressures, in the medial and lateral compartments were 0.16 MPa and 1.49 MPa, resulting in 7% and 31% FSE, respectively. After normalisation, the %FSE between FE-predicted and *in vitro*-measured peak pressures, were 6.67% in the medial and 5.94% in the lateral compartments.

#### 4.5.2. Compartmental Forces in the Tibial Cartilage

With an axial force of 374 N, normalised force increased in the medial compartment and decreased in the lateral monotonically as varus moment increased from 0 to 15 Nm for both the FE-predicted and the *in vitro*-measured investigations (Figure 4.18b). The FE model consistently predicted normalised forces similar to *in vitro*-measured values. Consistent normalised forces were also observed in each compartment when a valgus moment was applied. The RMSE between absolute FE-predicted and *in vitro*-measured forces, in the medial compartment was 138 N (28.08 % FSE). In the lateral compartment the RMSE was 65 N (14.95 % FSE). After normalisation with the corresponding maximum compartmental forces the % FSE in FE-predicted and *in vitro*-measured forces was 7.56 % in the medial compartment and 4.48 % in the lateral.

As varus bending moment increased, the ratio of medial compartment to total force increased, while the ratio of the force in the lateral compartment to the total force decreased for both *in vitro* and FE studies. The reverse occurred as valgus moment increased as seen in Figure 4.19. The % FSE between FE-predicted and *in vitro*-measured for both medial and lateral force percentage values were 8.05%.



**Figure 4.19: *In vitro* and FE predicted forces in the medial and lateral compartments as percentages of the total axial force during 0 to 15 Nm varus and valgus bending moments**

(Source: Mootanah et al., 2014)

Based upon %FSE being less than the hypothesised 10%, FE-predicted normalised forces and peak joint pressures in the medial and lateral tibial cartilage agreed with those obtained from *in vitro* tests across the range of applied varus and valgus bending moments. FE-predicted absolute force values were higher than those measured during the *in vitro* tests (normalised medial and lateral force FSEs: 7.56% and 4.48%, respectively). This was expected because some of the anatomical structures bearing load were likely to have been physically outside the force transducer sensel areas and not recorded by the sensor matrix.

The validated FE knee model was then used to evaluate the relative performances of different knee alignments to predict surgical outcomes, thereby delaying OA progression and the need for TKA.

### 4.5.3. Static Equilibrium

The model was also verified by a simple frontal plane static equilibrium calculation (Table 4.10). The distances from the knee joint centre, measured from MRI scans, were 40 mm to the medial and lateral ends of the tibial plateau and 45 mm to the LCL and MCL. The points of contact between the distal femur and the proximal tibia were assumed to be in the middle of each compartment (20 mm) for the aligned knee joint. For the model with a varus/valgus bending moment the distances were assumed to be 35 mm as the contact area shifted medially for a varus knee and laterally for a valgus knee. Bending moments resulting from forces in the ACL and PCL were ignored because the distance of the line of force from the joint centre was negligible. Table 4.10 illustrates the results of static equilibrium for the validation study, using equations for horizontal forces, vertical forces and moments.

**Table 4.10: Static equilibrium for the validation of the subject-specific FE model**

	<b>15 Nm Valgus</b>	<b>Straight</b>	<b>15 Nm Varus</b>
<b>Inputs to static equilibrium equations</b>			
<b>F<sub>ACL</sub> (N)</b>	4.30	8.50	67.40
<b>F<sub>LCL</sub> (N)</b>	-0.80	4.10	53.50
<b>F<sub>MCL</sub> (N)</b>	25.60	2.70	-0.60
<b>F<sub>PCL</sub> (N)</b>	36.70	12.90	31.10
<b>F<sub>M</sub> (N)</b>	0.00	214.70	494.50
<b>F<sub>L</sub> (N)</b>	436.40	176.80	0.00
<b>F<sub>axial</sub> (N)</b>	374.00	374.00	374.00
<b>Moment (Nm)</b>	-15.00	0.00	15.00
<b>d<sub>LCL</sub> (mm)</b>	45.00	45.00	45.00
<b>d<sub>MCL</sub> (mm)</b>	45.00	45.00	45.00
<b>d<sub>M</sub> (mm)</b>	0.00	20.00	35.00
<b>d<sub>L</sub> (mm)</b>	35.00	20.00	0.00
<b>sin<math>\alpha</math> (51°)</b>	0.78	0.78	0.78
<b>cos<math>\alpha</math> (51°)</b>	0.63	0.63	0.63
<b>sin<math>\beta</math> (63°)</b>	0.89	0.89	0.89
<b>cos<math>\beta</math> (63°)</b>	0.45	0.45	0.45
<b>Results from static equilibrium equations</b>			
<b>Resultant vertical force (N)</b>	<b>-1.55</b>	<b>7.38</b>	<b>12.36</b>
<b>Resultant horizontal force (N)</b>	<b>13.97</b>	<b>0.58</b>	<b>-28.34</b>
<b>Resultant moment (Nm)</b>	<b>0.91</b>	<b>0.69</b>	<b>-0.13</b>

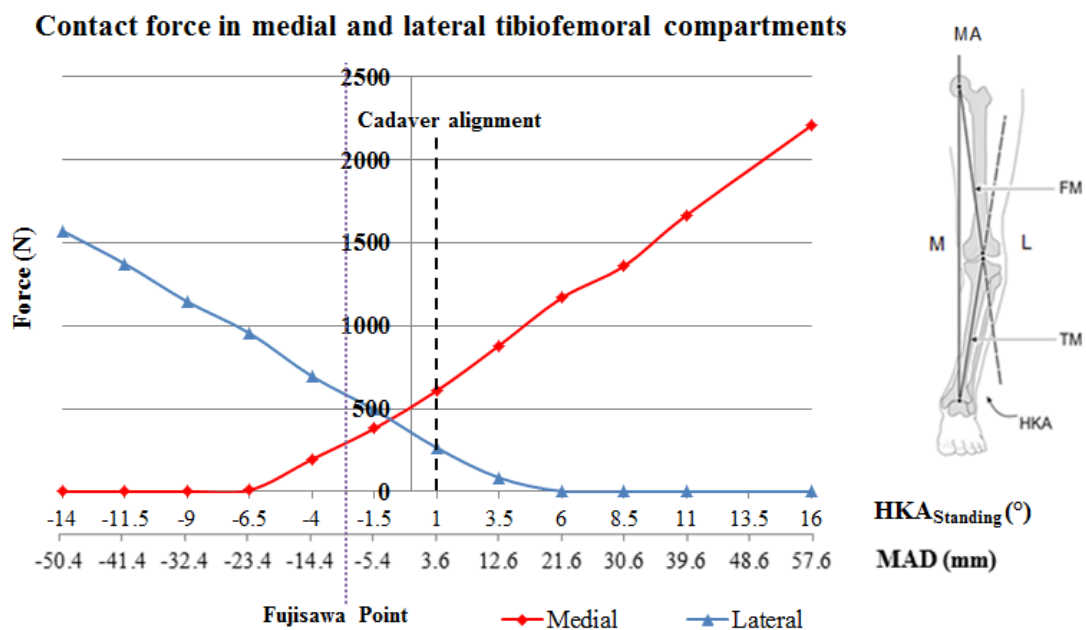
## 4.6. Malaligned Knee Joint Simulations

To compare the contact mechanics of different alignments various osteotomies were performed and the load, pressure and stress acting on the medial and lateral compartments of the knee were computed and analysed.

Figure 4.20 illustrates the force distribution in the medial and lateral compartments for the loading conditions at the end of weight acceptance during level walking for alignments spanning from  $14^\circ$  valgus to  $16^\circ$  varus. To normalise the force distribution the Fujisawa point was calculated (Figure 4.20). Figure 4.21 highlights the medial:lateral force ratio for each alignment with the corresponding MAD and HKA angle.

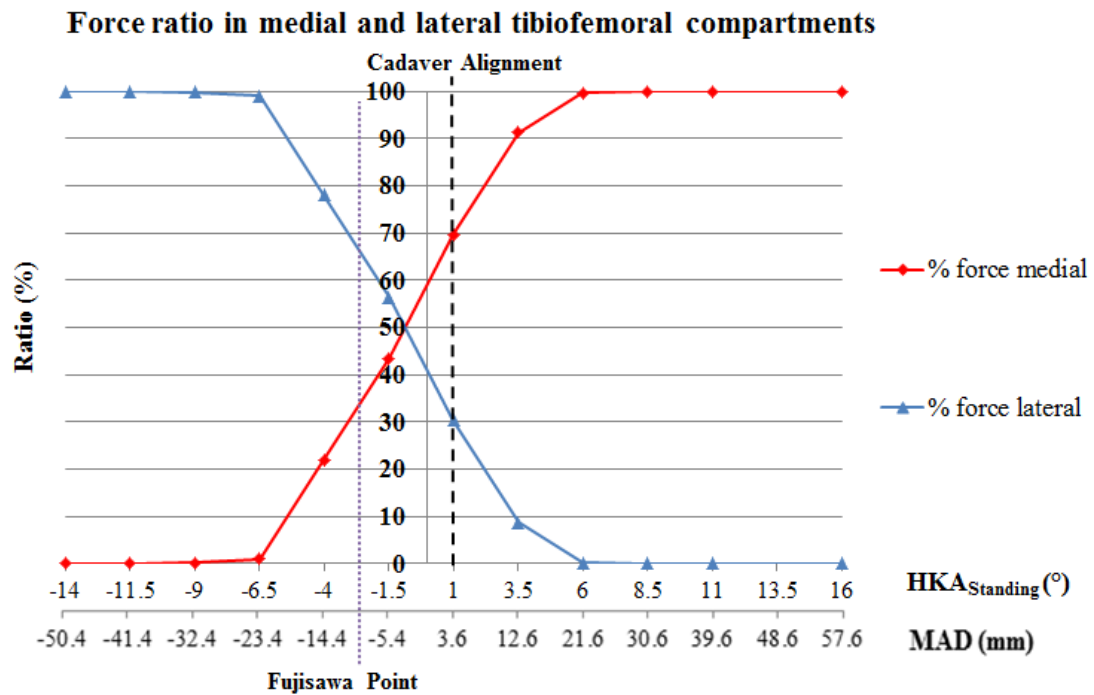
The effect of malalignment on contact pressure, maximum compressive stress and maximum shear stress in the medial and lateral tibial and femoral cartilage as predicted by the FE model is shown in Figures 4.22 to 4.24.

### 4.6.1. Forces in the Medial and Lateral Compartments



Note: Data from simulations are shown as symbols. The line represents a linear interpolation between these consecutive simulations.

**Figure 4.20: Tibiofemoral compartment contact forces during the end of weight acceptance for different alignments.**



Note: Data from simulations are shown as symbols. The line represents a linear interpolation between these consecutive simulations

**Figure 4.21: Medial to lateral force ratio for each alignment with the corresponding MAD and HKA angle**

Figure 4.21 shows that the native alignment of the cadaveric knee ( $1^\circ$  varus) gave a medial:lateral load ratio of 70%:30%. An increase in varus alignment substantially increased the load in the medial compartment while an increase of valgus angulation substantially increased the load in the lateral compartment.

An MAD of 0 mm resulted in a medial:lateral load ratio of 60%:40%. A Fujisawa point of 62% gave a medial:lateral load ratio of 34%:66%. There is a consensus in literature that slight overcorrection provides a good outcome (Section 2.2). However, there is a lack of consensus of how much the joint should be overcorrected. Therefore, Table 4.11 shows different load ratios with their corresponding MAD, HKA angle and the point where the MA intersects with the tibial plateau, illustrated as a percentage of the total tibial width measured from the medial to the lateral side.



**Table 4.11: Different load ratios with their corresponding mechanical axis deviation (MAD), hip-knee-ankle (HKA) angle and the point where the mechanical axis of the lower limb (MA) intersects with the tibial plateau. FM = mechanical axis of the femur; TM = mechanical axis of the tibia.**

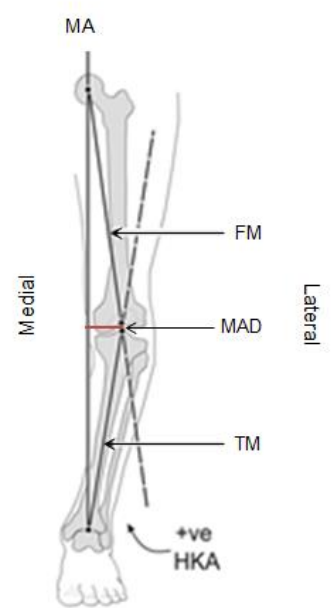
<b>Force ratio Medial (%): Lateral (%)</b>	<b>Intersection of the MA with the tibial plateau (%)</b>	<b>MAD (mm)</b>	<b>HKA angle (°)</b>	
<b>40:60</b>	58.4	-6.7	-1.9	
<b>45:55</b>	56.1	-4.9	-1.4	
<b>50:50</b>	54.0	-3.2	-0.9	
<b>55:45</b>	51.8	-1.5	-0.4	
<b>60:40</b>	50.0	0.0	0.0	

Table 4.11 shows that for this specific cadaver an MAD of 0 mm would have resulted in a 60%:40% medial:lateral load ratio. An MAD of -5 mm would have resulted in a 45%:55% medial:lateral compartment load ratio. Most surgeons target some level of overcorrection.

### 4.6.2. Pressure and Stress in the Medial and Lateral Compartments

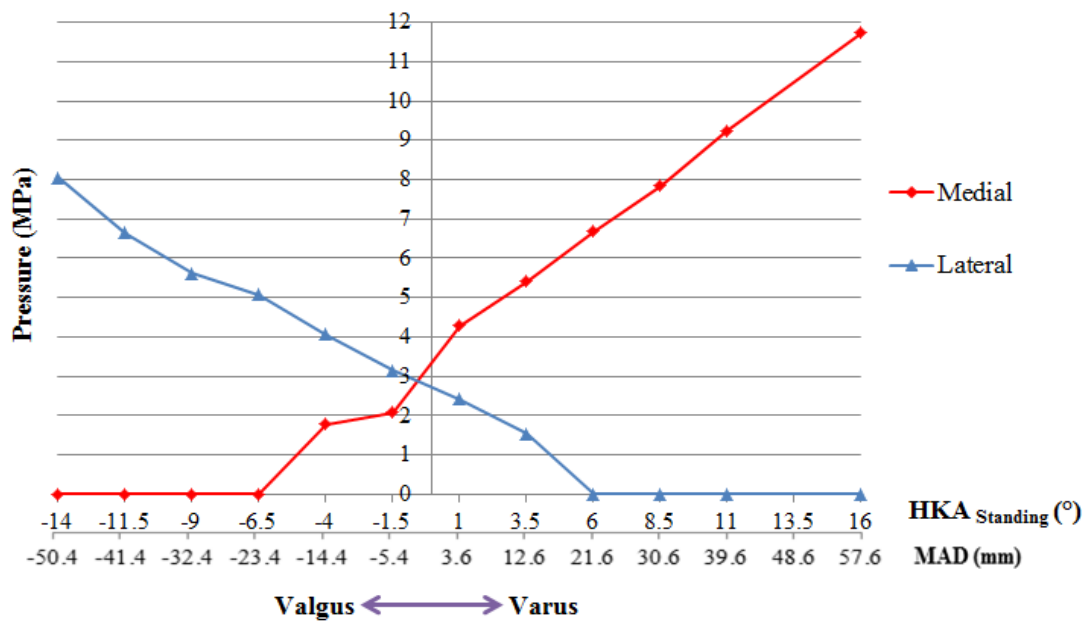
Peak contact pressure and stress for the native alignment (1° varus) of this cadaveric knee are shown in Table 4.12.

**Table 4.12: Peak contact pressure and stress for the intact knee joint**

	<b>Medial</b>	<b>Lateral</b>
<b>Contact Pressure (MPa)</b>	4.28	2.42
<b>Maximum compressive stress (MPa)</b>	4.02	2.72
<b>Maximum Shear stress tibial cartilage (MPa)</b>	2.04	1.71
<b>Maximum Shear stress femoral cartilage (MPa)</b>	1.67	1.32

Increasing varus angulation substantially increased medial and decreased lateral peak pressure and stress (Figure 4.22 - Figure 4.24). An increase in valgus angulation substantially increased lateral and decreased medial peak pressure and stress (Figure 4.22 - Figure 4.24). Exact values are tabulated in Appendix E.

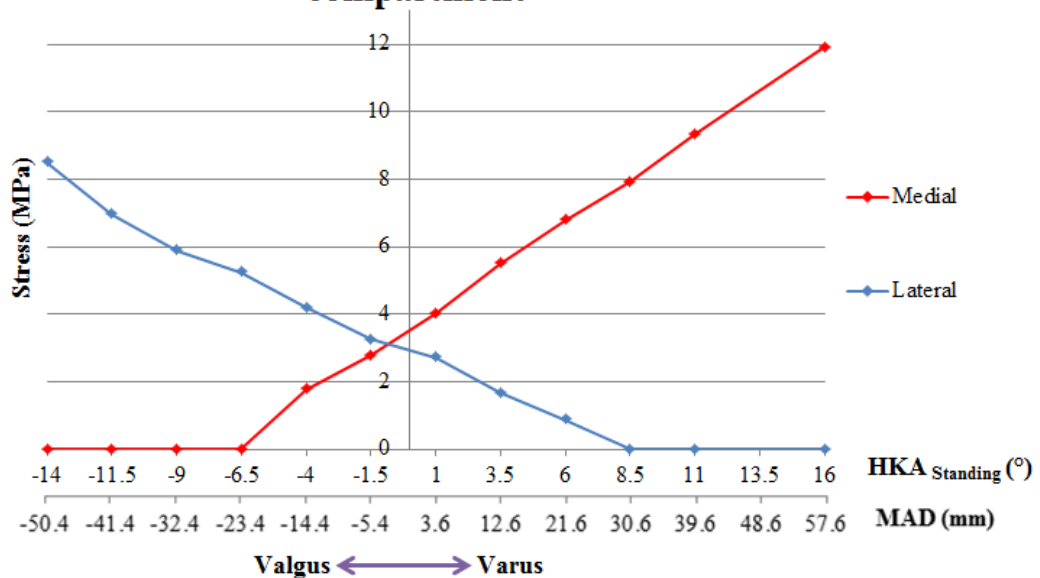
### Contact pressure in medial and lateral compartments



Note: Data from simulations are shown as symbols. The line represents a linear interpolation between these consecutive simulations

**Figure 4.22: Peak contact pressure in the tibial-femoral compartments during the end of weight acceptance for different alignments**

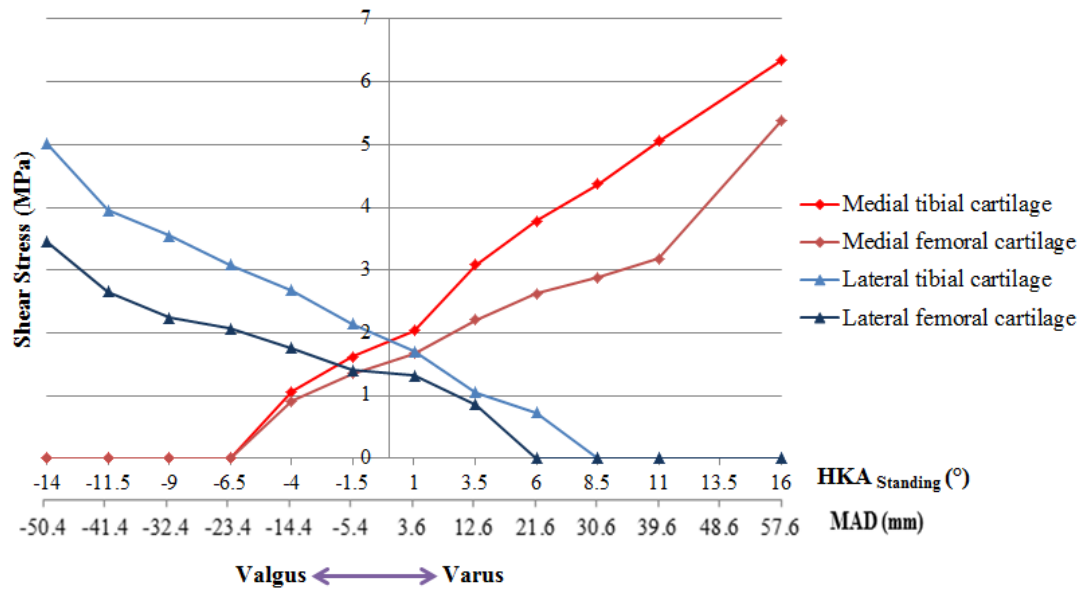
### Maximum compressive stress in medial and lateral compartment



Note: Data from simulations are shown as symbols. The line represents a linear interpolation between these consecutive simulations

**Figure 4.23: Peak maximum compressive stress in the tibial-femoral compartments during the end of weight acceptance for different alignments**

### Shear stress in medial and lateral compartments



Note: Data from simulations are shown as symbols. The line represents a linear interpolation between these consecutive simulations

**Figure 4.24: Peak maximum shear stress in the tibial-femoral compartments during the end of weight acceptance for different alignments**

A possible aim of the surgeon could be to provide an osteotomy geometry that achieves the minimum peak contact mechanics in the medial and lateral compartment. For this study the minimum peak pressure occurred at an HKA angle of  $-0.5^\circ$ , which corresponds to an MAD of  $-1.4$  mm (Figure 4.22). A correction that targets the Fujisawa point (62% of the medial to lateral plateau distance) would increase the pressure in the lateral compartment from 2.9 MPa to 3.6 MPa and decrease the pressure in the medial compartment from 2.9 MPa to 2 MPa. Corresponding results for maximum compressive stress and maximum shear stress are summarised in Table 4.13.

**Table 4.13: Peak pressure and stress values for different correction targets**

	Correction that targets minimum stress			
	Medial (MPa)	Lateral (MPa)	MAD (mm)	HKA (°)
Contact pressure tibial and femoral cartilage	2.9	2.9	-1.4	-0.5
Maximum compressive stress tibial and femoral cartilage	3.1	3.1	-2.9	-0.8
Maximum shear stress tibial cartilage	1.9	1.9	0.7	0.3
Maximum shear stress femoral cartilage	1.4	1.4	-4.3	-1.2
	Correction that targets Fujisawa point			
	Medial (MPa)	Lateral (MPa)	MAD (mm)	HKA (°)
Contact pressure tibial and femoral cartilage	2	3.6	-7.5	-2.1
Maximum compressive stress tibial and femoral cartilage	2.4	3.7	-9.0	-2.5
Maximum shear stress tibial cartilage	1.4	2.4	-9.0	-2.5
Maximum shear stress femoral cartilage	1.2	1.6	-8.2	-2.3

High peak maximum shear stress is one of the main causes for developing OA (Donahue et al., 2002; Andriacchi et al., 2006; Wilson et al., 2006; Peña et al., 2008). Therefore, special attention has to be paid to the change in maximum shear stress for different alignments. The reason for the difference in tibial and femoral cartilage maximum shear stress is the difference in the tissue thickness.

#### **4.6.3. Volumetric Stress Distribution**

A family of curves was developed that describe the percent of cartilage volume that experience stress up to a specific magnitude. Each curve represents a different knee alignment. This permits one to determine the effect of alignment upon the percent of cartilage volume that is exposed to a given magnitude of compressive or shear stress. Increasing varus alignment substantially increased the percent of medial cartilage volume at the tibia and femur that is exposed to a maximum compressive or shear stress (Figures 4.25-4.28). An increase in valgus alignment substantially increased the percent of lateral cartilage volume at the tibia and femur that is exposed to a maximum compressive or shear stress (Figures 4.29-4.32). Alignments that did not expose the cartilage to any stress (lift off) were not included in the graphs.

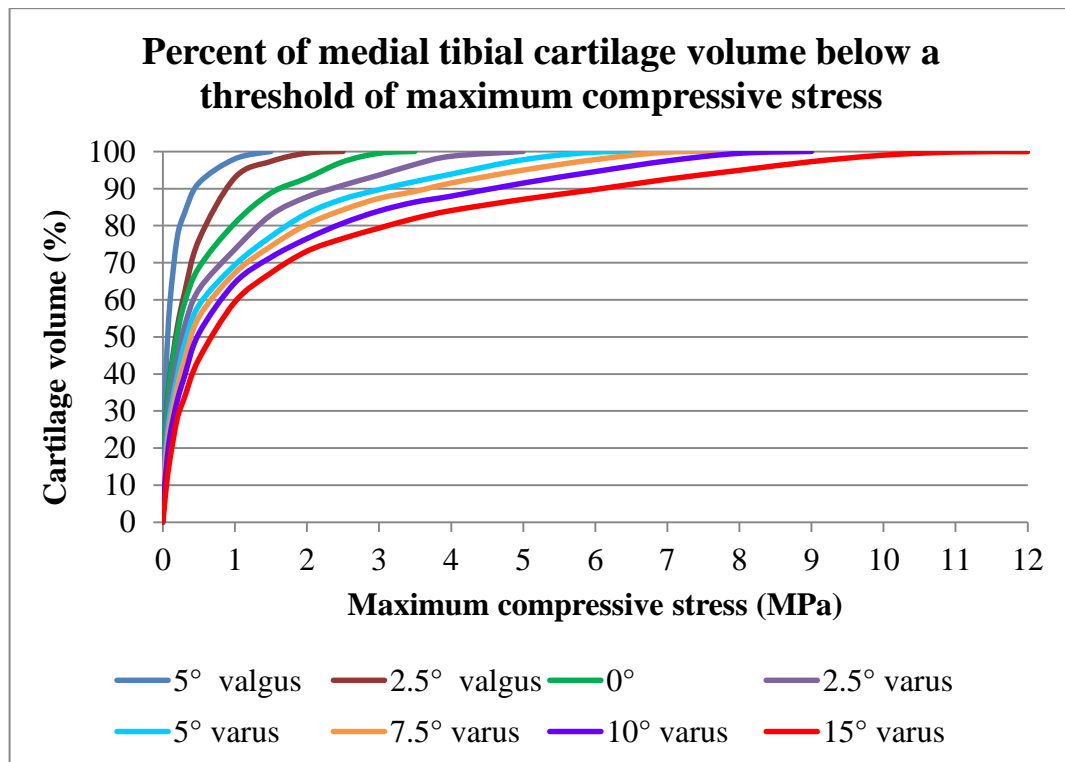


Figure 4.25: Percent of medial tibial cartilage volume below a threshold of maximum compressive stress.

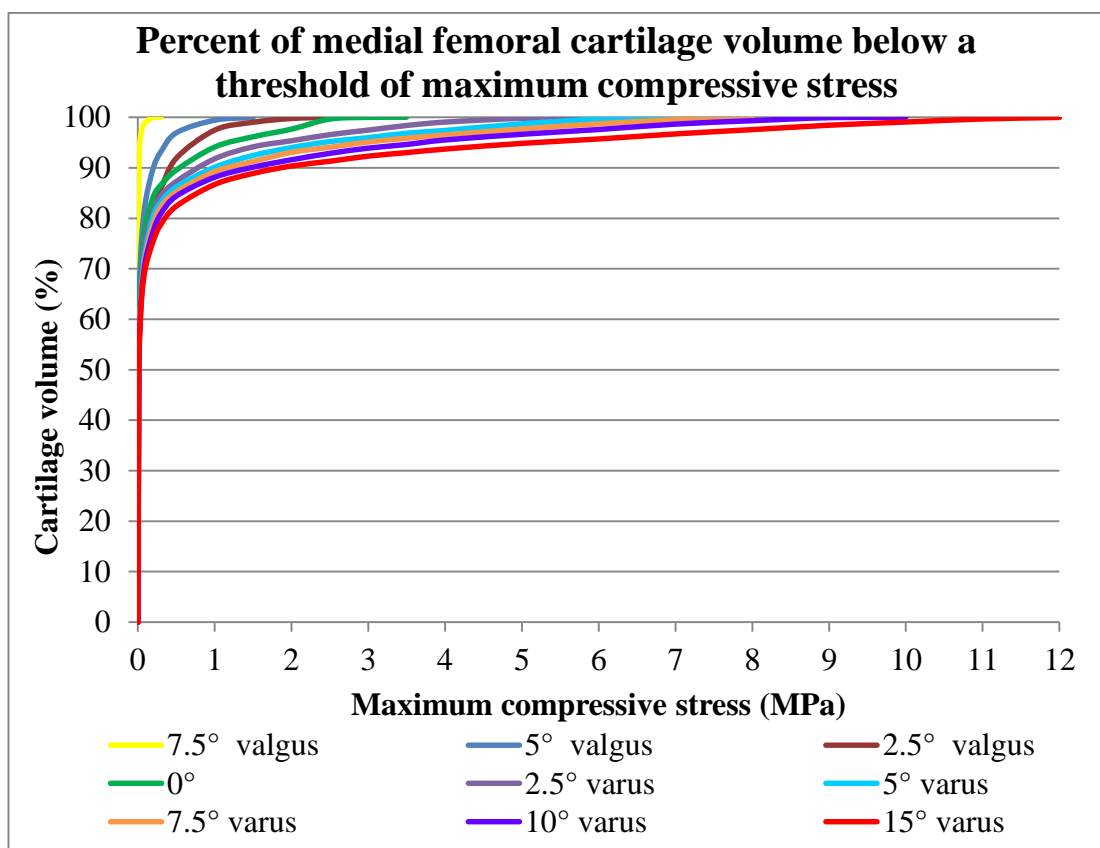


Figure 4.26: Percent of medial femoral cartilage volume below a threshold of maximum compressive stress.

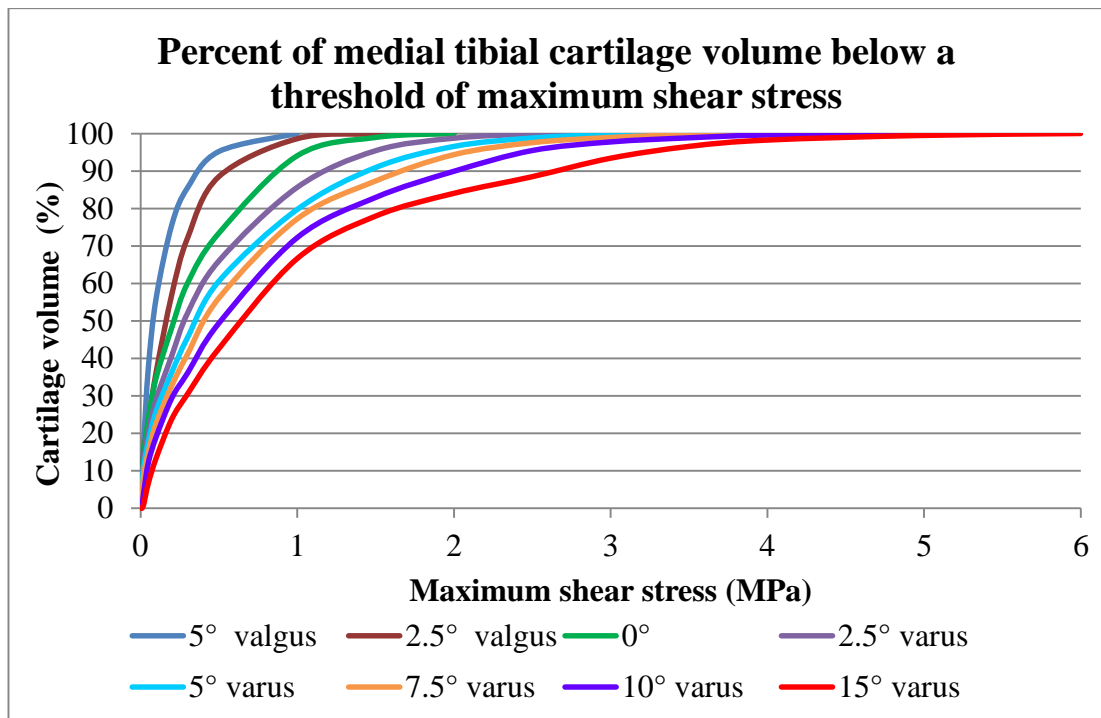


Figure 4.27: Percent of medial tibial cartilage volume below a threshold of maximum shear stress.

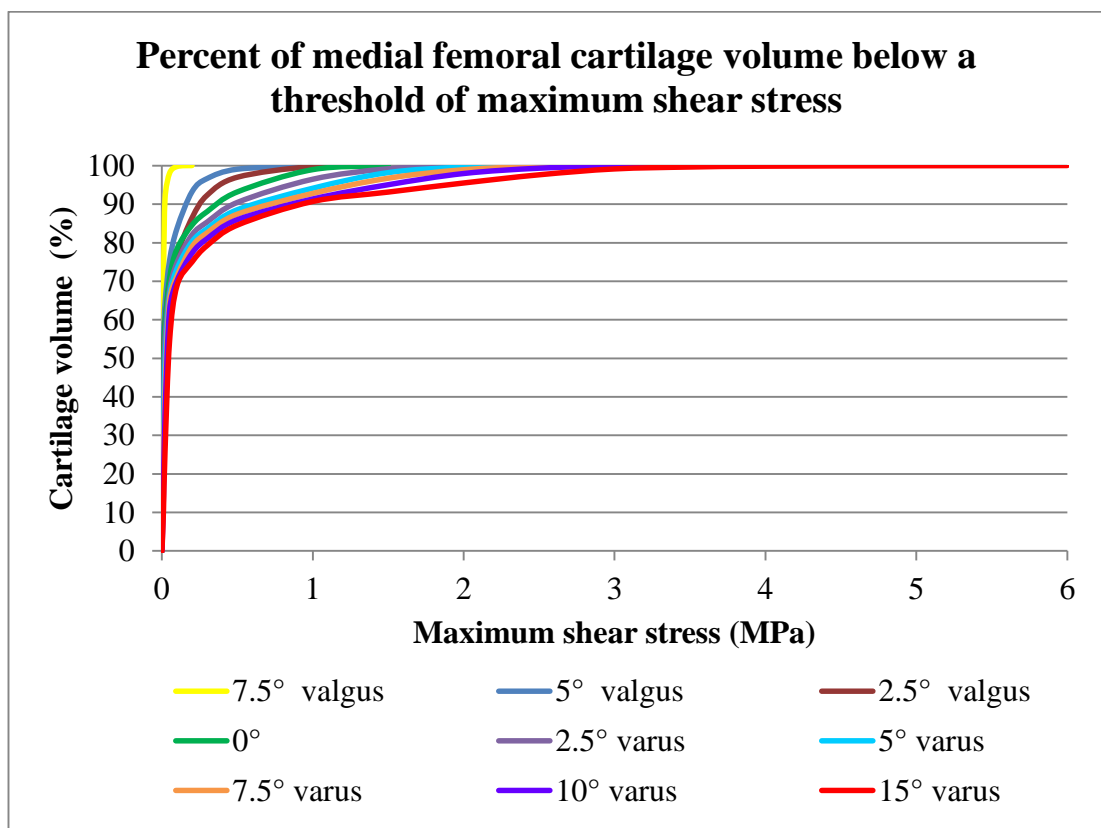
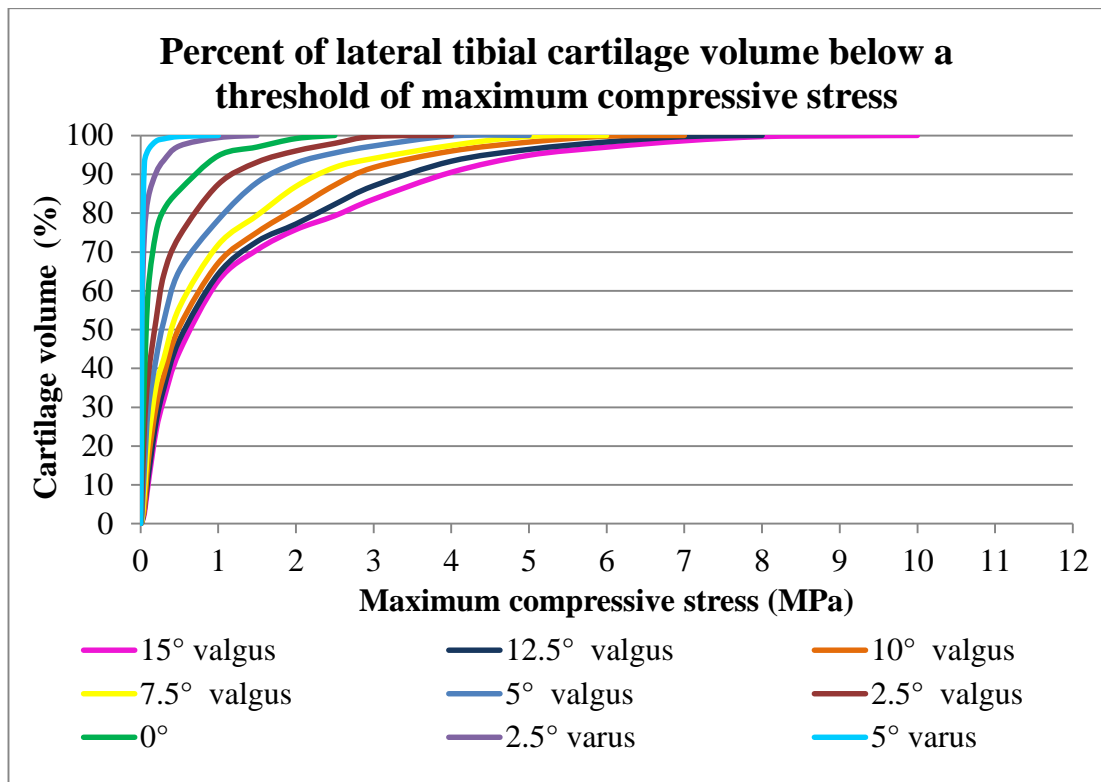
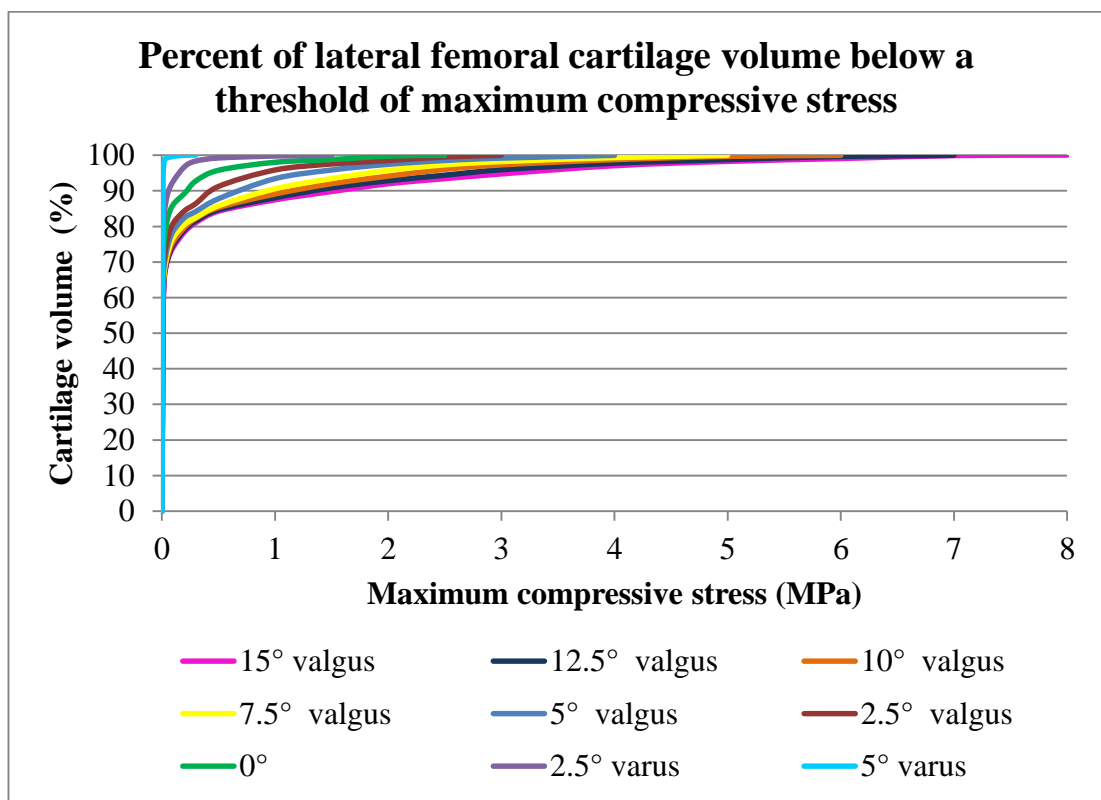


Figure 4.28: Percent of medial femoral cartilage volume below a threshold of maximum shear stress.





**Figure 4.29: Percent of lateral tibial cartilage volume below a threshold of maximum compressive stress.**



**Figure 4.30: Percent of lateral femoral cartilage volume below a threshold of maximum compressive stress.**

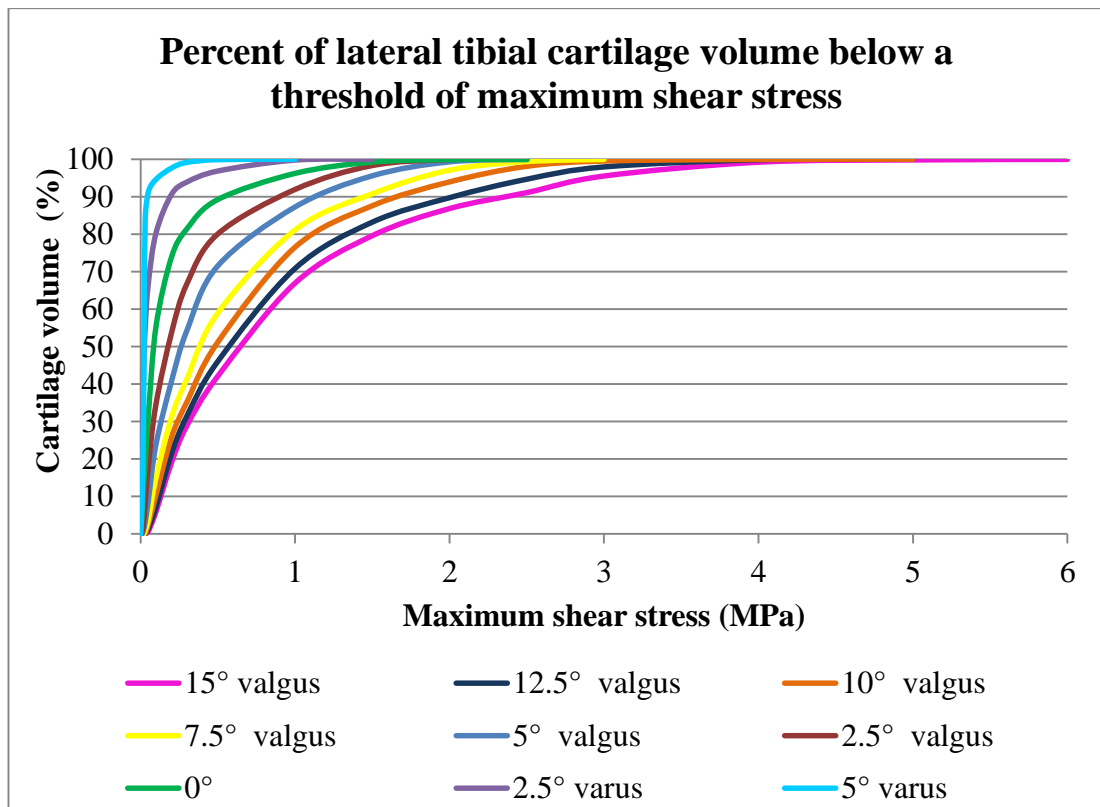


**Figure 4.31: Percent of lateral tibial cartilage volume below a threshold of maximum shear stress.**

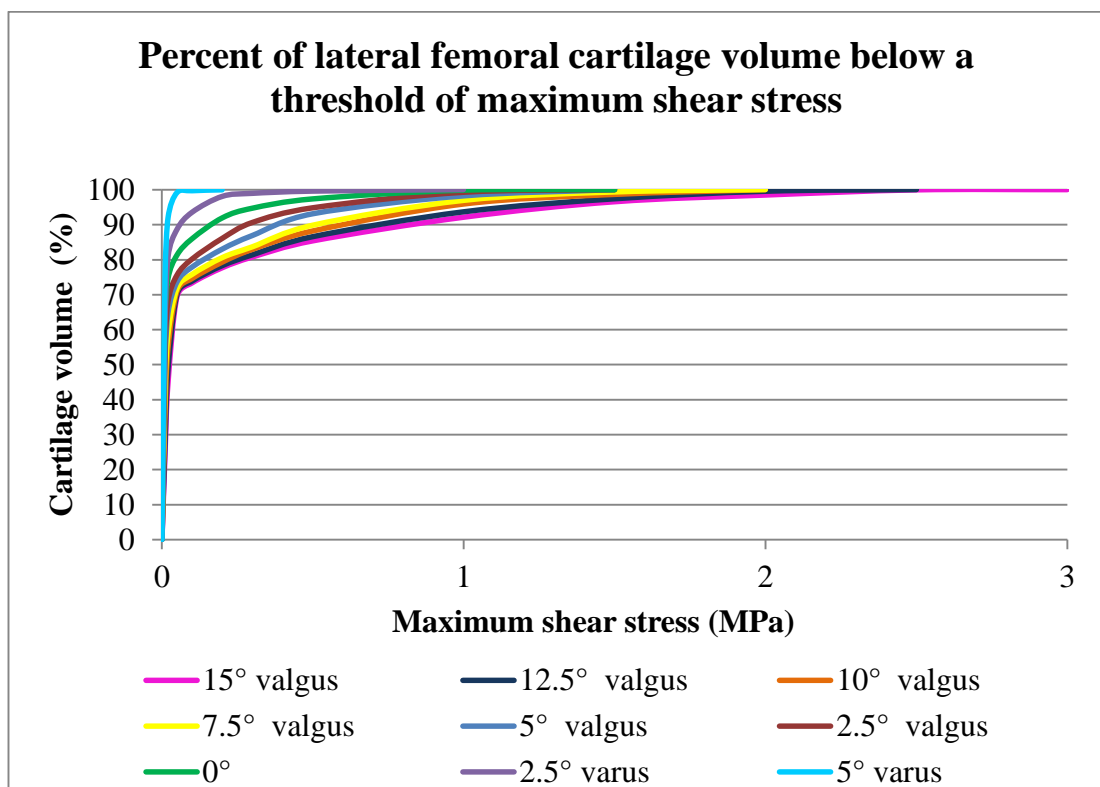


**Figure 4.32: Percent of lateral femoral cartilage volume below a threshold of maximum shear stress.**

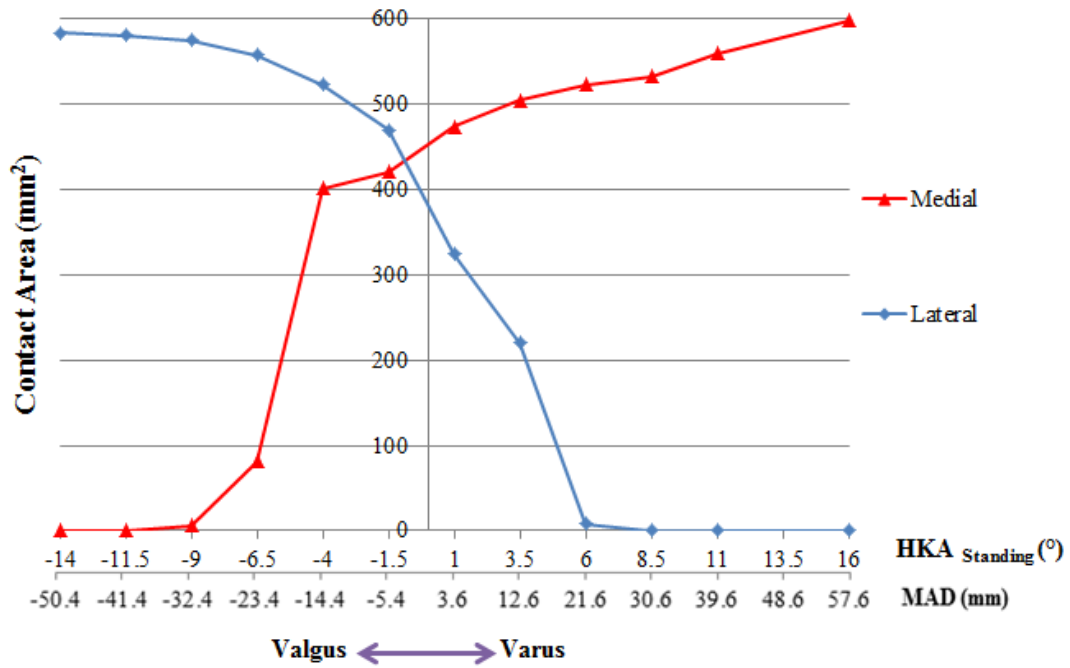
Cartilage exposed to 5 MPa or greater compressive stress is reported to be at high risk of developing knee OA (Clements et al., 2001; Chen et al., 2003). For the medial tibial cartilage, alignments ranging from 15° valgus to 2.5° varus did not expose the cartilage to a stress of 5 MPa or higher. At 5° varus, 2% of the medial cartilage was exposed to a stress higher than 5 MPa. This increased to 14% for 15° varus (Figure 4.25). At 5° valgus, 0.5% of the lateral cartilage was exposed to a stress higher than 5 MPa. This increased to 5% for 15° valgus (Figure 4.26).

For the medial femoral cartilage, an alignment of 5° varus exposed 1% to a pressure greater than 5MPa. This increased to 5% for an alignment of 15° varus. In the lateral compartment, 2% of the cartilage was exposed to a threshold above 5MPa at 15° valgus.

#### **4.6.3. Contact Area**

The native alignment of the cadaveric knee (1° varus) had a medial and lateral contact area of 473.5 mm<sup>2</sup> and 323.6 mm<sup>2</sup>, respectively (Figure 4.33). An increase in varus alignment substantially increased the medial contact area up to 583.4 mm<sup>2</sup>. Increasing the varus angulation increased the lateral contact area up to 598.0 mm<sup>2</sup>. An even distribution of the contact area between the medial and lateral compartment occurs at a valgus alignment of 0.9°, corresponding to an MAD of -3.2 mm (Figure 4.33).

### Contact Area in medial and lateral compartments



Note: Data from simulations are shown as symbols. The line represents a linear interpolation between these consecutive simulations

**Figure 4.33: Contact area in the tibial-femoral compartments during the end of weight acceptance for different alignments**

## 4.7. Correlation of Alignment with Joint Loading

The Pearson product-moment correlation coefficient is a measure of the similarity between two disparate variables and ranges from -1 to 1, where minus one is a perfect negative correlation, zero represents no correlation and one shows a perfect positive correlation. Equation 41 shows the formula used to calculate the Pearson product-moment correlation coefficient. Table 4.14 shows the correlation coefficients between joint geometry (different MAD values) and the corresponding knee joint contact mechanics.

$$r = \frac{\sum (x - \bar{x})(y - \bar{y})}{\sqrt{\sum (x - \bar{x})^2 \sum (y - \bar{y})^2}}$$

**Equation 41**

**Table 4.14: Pearson product-moment correlation coefficients and corresponding p-values between knee joint contact mechanics and joint geometry (MAD)**

<b>Dependent Variable (y)</b>	<b>Independent Variable (x)</b>	<b>Medial</b>	<b>Lateral</b>	<b>p-value medial</b>	<b>p-value lateral</b>
Force	MAD	0.97	-0.94	<0.0001	<0.0001
Contact Pressure Tibial Cartilage	MAD	0.98	-0.97	<0.0001	<0.0001
Contact Pressure Femoral Cartilage	MAD	0.98	-0.97	<0.0001	<0.0001
Max Shear Stress Tibial Cartilage	MAD	0.98	-0.98	<0.0001	<0.0001
Max Shear Stress Femoral Cartilage	MAD	0.97	-0.96	<0.0001	<0.0001
Max Compressive Stress Tibial Cartilage	MAD	0.98	-0.97	<0.0001	<0.0001
Max Compressive Stress Femoral Cartilage	MAD	0.98	-0.97	<0.0001	<0.0001

Table 4.14 shows that there is a strong correlation (Portney and Watkins, 2008) between the geometry and knee joint contact mechanics.

## **4.8. Static Equilibrium**

Joint force as a function of alignment was assessed with a simple frontal plane static equilibrium analysis (Table 4.15). Distances from the centre of the knee to the centre of contact between distal femur and proximal tibia were measured in the FE models. Bending moments resulting from forces in the ACL and PCL were ignored due to negligible moment arms. Table 4.15 illustrates the results of static equilibrium using equations for horizontal forces, vertical forces and moments. For small malalignments the sum of moments and sum of forces are close to zero. For larger malalignments the discrepancies increased because the PCL and ACL may have contributed. Additionally, distances that were originally measured on MRI may have significantly changed with malalignment. Model results for small malalignments were consistent with static equilibrium analyses (Table 4.15). Formulae and a sketch of the frontal plane static equilibrium can be found in Section 3.12.

Table 4.15: Static equilibrium for the analysis of different alignment simulations

	Valgus					Straight	Varus				
	-14°	-9°	-6.5°	-4°	-1.5°	1°	3.5°	6°	8.5°	11°	16°
<b>Inputs to static equilibrium equations</b>											
<b>F<sub>ACL</sub> (N)</b>	190.8	138.5	120.9	105.1	99.1	86.7	129.2	198.2	279.9	392.8	592.2
<b>F<sub>LCL</sub> (N)</b>	-3.2	-3.1	-2.9	-2.8	-2.6	-3.3	17.5	125.4	230.4	388.1	647.2
<b>F<sub>MCL</sub> (N)</b>	427.9	160.9	49.7	5.8	-0.9	0.2	-1.5	-5.5	-9.6	-14.7	-21.9
<b>F<sub>PCL</sub> (N)</b>	210.9	96.3	35.7	13.4	11.1	5.8	69.9	109.4	159.2	228.3	356.5
<b>F<sub>M</sub> (N)</b>	0	1.7	8.9	195.1	380.2	607.7	880.6	1167	1359.2	1665	2205
<b>F<sub>L</sub> (N)</b>	1571	1144.8	954.3	694.8	493.3	264.3	83.9	2.8	0	0	0
<b>F<sub>axial</sub> (N)</b>	811.4	811.4	811.4	811.4	811.4	811.4	811.4	811.4	811.4	811.4	811.4
<b>F<sub>med/lat</sub> (N)</b>	77.9	77.9	77.9	77.9	77.9	77.9	77.9	77.9	77.9	77.9	77.9
<b>Moment (Nm)</b>	-59.01	-33.05	-19.87	-65.62	68.63	20.39	34.49	47.78	61.43	75.03	102.07
<b>d<sub>LCL</sub> (mm)</b>	45	45	45	45	45	45	45	45	45	45	40
<b>d<sub>MCL</sub> (mm)</b>	40	45	45	45	45	45	45	45	45	45	40
<b>d<sub>M</sub> (mm)</b>	0	1	5	10	20	30	35	40	40	40	40
<b>d<sub>L</sub> (mm)</b>	40	40	23	15	15	15	10	0	0	0	0
<b>Results from static equilibrium equations</b>											
<b>Resultant Force<sub>vertical</sub> (N)</b>	<b>1.5</b>	<b>16.3</b>	<b>20.8</b>	<b>18.2</b>	<b>21.2</b>	<b>8.8</b>	<b>25.7</b>	<b>13.2</b>	<b>32.4</b>	<b>28.6</b>	<b>9.6</b>
<b>Resultant Force<sub>horizontal</sub> (N)</b>	<b>53.6</b>	<b>34.5</b>	<b>17.9</b>	<b>17.9</b>	<b>20.6</b>	<b>26.1</b>	<b>28.4</b>	<b>2.8</b>	<b>-25.9</b>	<b>-65.6</b>	<b>-132.9</b>
<b>Resultant Moment (Nm)</b>	<b>13.42</b>	<b>-5.36</b>	<b>0.34</b>	<b>-1.52</b>	<b>-6.58</b>	<b>-5.97</b>	<b>-5.36</b>	<b>-6.99</b>	<b>-17.87</b>	<b>-26.56</b>	<b>-43.99</b>

## 5. Discussion

In this chapter, a critical review of the results acquired in this study is presented. An evaluation of outcomes is given through a comparison with *in vitro* data acquired from the validation study and with results of other investigators. Additionally, the limitations of the study are discussed and future improvements proposed. The discussion of the results will help to understand how HTO can be better planned in order to improve post-operative outcomes. This will ensure that the evidence-based knowledge resulting from this study is transferred to clinicians for patient benefit.

The primary aim of this study was to investigate the relationship between peak tibiofemoral joint stress, compartment forces and MAD. This was done by

- (1) carrying out empirical research in order to establish what is already known in the area and to identify which methods have been used by previous researchers,
- (2) creating a full 3D subject-specific FE model, comprising the collateral and cruciate ligaments, femoral and tibial cartilage, meniscus, tibia, femur and fibula,
- (3) validating the FE model with a parallel *in vitro* study,
- (4) simulating HTO surgery spanning from 14° valgus to 16° varus
- (5) proposing the ideal MAD for the subject-specific model.

To my knowledge no subject-specific 3D FE knee model with ligament tuning, force and stress validation and the effect of alignment on compartmental stress has been previously reported in the literature. The FE model has allowed for examination of different alignments to investigate the relationship between MAD, wedge geometry, Fujisawa point and compartment mechanics.

## **5.1. Discussion of Sensitivity Analyses**

### **5.1.1. Mesh**

From the sensitivity analysis of the mesh, it was concluded that contact mechanics were not sensitive to mesh type for bones. Tetrahedral elements (4-noded) were used to create the osseous tissues while hexahedral elements (8-noded) were used to create all soft tissues. Many authors used 8-noded elements to represent their geometry (Perie and Hobatho, 1998; Limbert and Taylor, 2001; Donahue et al., 2002; Bratianu, Rinderu and Gruionu, 2004; Peña et al., 2006; Guo et al., 2009; Yang, Nayeb-Hashemi and Canavan, 2009; Hopkins et al., 2010; Kiapour et al., 2013; Mattei et al., 2014).

The mesh sensitivity analysis indicated that contact pressure in the knee joint was not significantly affected by mesh size of the osseous tissues. However, the contact pressure was very sensitive to element size of the soft tissues. Papaioannou et al. (2008) indicated that changing the mesh size from 1×1 mm to 4×4 mm increased all but one of the contact variables by up to 45% (Papaioannou et al., 2008). Keyak et al. (1992) found that use of larger elements decreased predicted stress.

Ideally, the smallest element size possible should be used to accurately represent tissue geometry. However, it was decided that a larger mesh, as indicated in Table 4.5 and Table 4.6, was valid as it gave an error of less than 5%. Several other investigators who have conducted convergence studies have considered a 5% error acceptable (Donahue et al., 2002; Anderson et al., 2005; Jones and Wilcox, 2008; Yang, Nayeb-Hashemi and Canavan, 2009; Kazemi et al., 2011; Bae et al., 2012; Kiapour et al., 2014).

### **5.1.2. Material Properties**

The sensitivity analysis revealed that bone modulus of elasticity (E) had little influence on peak pressure in the tibial cartilage (2.5% maximum change for  $E > 1\text{GPa}$ ). The properties of the meniscus had a substantial influence (3%-7% for every 20 MPa change) and cartilage properties had an even greater influence on peak pressure (40% - 100% for every 10 – 20 MPa change in E).



## *Cartilage*

Although FE knee model tissue geometries were subject-specific, the material properties were acquired from the literature. Cartilage material properties can substantially influence knee joint contact mechanics (Shirazi and Shirazi-Adl, 2008; Mattei et al., 2014).

The wide range of Young's moduli reported in literature can be explained by the degradation in cartilage properties post harvesting. In order to determine the true mechanical properties of the cartilage, the time taken between harvesting and testing is critical. Tests to determine the true properties of cartilage are usually carried out in saline solution, but to preserve mechanical properties, the specimen should not be stored in saline solution for a long period of time. In this study, the average of the published cartilage material properties is used ( $E = 25 \text{ MPa}$ ).

Despite the substantial influence of cartilage properties on knee mechanics, the linear elastic model is widely adopted in the literature for several FE knee models to investigate stress and strain of native and diseased joints (Bendjaballah, Shirazi-Adl and Zukor, 1995; Bendjaballah, Shirazi-Adl and Zukor, 1997; Donahue et al., 2002; Beillas et al., 2004; Peña et al., 2006; Papaioannou et al., 2008; Peña et al., 2008; Guo et al., 2009; Yang et al., 2010; Kiapour et al., 2014). An isotropic linear elastic behaviour was chosen because the time of load application was very short ( $< 1 \text{ sec}$ ) minimising the opportunity for viscoelastic effects (stress relaxation or creep compliance). The assumption of isotropy was made to simplify the solution and reduce computation time in lieu of not having the precise subject-specific constitutive relationship for the cartilage structures within the cadaveric specimen. Developing subject specific constitutive relationships for cartilage is further complicated by the presence or absence of disease (e.g. OA).

Recently, sophisticated biphasic constitutive models of articular cartilage have been implemented in human FE knee models. The fibril-reinforced model proposed by Li et al. (2009) has been implemented in FE knee models to investigate the effect of pore pressure and fibre orientation upon contact mechanics within both healthy and meniscectomised knee joints. The effect of fibril pattern has also been investigated by Mononen et al. (2012) for both healthy and osteoarthritic cartilage in the human knee.

However, these models were not subject-specific. Acquiring subject-specific constitutive relationships for cartilage are complicated by the variable thickness of these structures within a joint, the effects of age, gender, and disease state upon that relationship, the influence of body versus room temperature, and the lack of high quality methods to develop such relationships in vivo. Furthermore, implementation of a non-linear viscoelastic constitutive relationship is not computationally efficient to solve.

In this study, linear elastic properties were used to represent the cartilage. Magnitudes of the absolute medial and lateral force and pressure values were influenced by soft tissue material properties. However, relative values, where loading was normalised to the peak value in each respective compartment, were not affected. In future versions different material properties for the deep, intermediate and superficial zones of cartilage will be assigned to the model to ensure more realistic behaviour of the knee joint. Weiss et al. (2005) stated that “all material properties, whether adopted from literature or derived from experiments, include some degree of error”.

### ***Meniscus***

An increase in the circumferential meniscal material properties decreased the contact mechanics in this study (3% -7% for every 20 MPa increase). A higher Young’s modulus would make the tissue stiffer and therefore less deformable. The circumferential structure of the meniscus transfers load radially. Donahue et al. (2003) also found that contact pressure is sensitive to meniscal properties.

Meniscal attachments were modelled using linear elastic spring elements. A lack of information on the function and structural properties of these attachments made it difficult to select an appropriate stiffness (Masouros et al., 2008). It is important to conduct sensitivity analyses on the stiffness and position of the springs that attach the meniscus to the MCL, tibia and to each other, to investigate the effect of spring stiffness and position on knee joint contact mechanics.

For this study, which simulated the end of weight acceptance during gait (a short time duration event), the assumption of modelling the meniscus as transversely isotropic has been widely adopted in the literature (Donahue et al., 2002; Vaziri et al., 2008; Yang, Nayeb-Hashemi and Canavan, 2009; Netravali et al., 2011; Kiapour et al.,

2014). Longer duration loading conditions, such as posture, would invoke creep and require simulations that include viscoelastic material properties.

### ***Ligaments***

Kiapour et al. (2013) showed that ligaments with anisotropic hyperelastic properties resulted in realistic kinematics. However, subject-specific anisotropic ligament properties could not be obtained from cadaver used in the current study without destroying the specimen. To ensure that correct tissue properties were employed in the FE model, collateral and cruciate ligaments were tuned to obtain matching computational and experimental kinematics of the tibia relative to the femur. For practical reasons (i.e. manual optimisation of the ligament properties throughout the range of motion), neo-Hookean hyperelastic material properties were used for the ligaments in this model.

Baldwin et al. (2011) tuned the LCL, MCL, anterior lateral capsule, medial and posterior lateral capsule and popliteofibular ligaments in three TKA models by minimising the differences in kinematics between the FE and cadaveric models. However, these investigators used three cadaveric knee joints with a TKA, hence excluding the ACL and PCL. Although the patella tendon was included in the model, ligaments were represented as 2D structures.

Ligament properties obtained from the tuning process in this study were in good agreement with other studies where linear elastic material properties were used. Quapp et al. (1998) conducted a uniaxial tensile test at 0° flexion on the human MCL and suggested a Young's modulus of  $332.2 \pm 58.3$  MPa. Butler et al. (1986) conducted tensile tests on ACL, PCL and LCL and suggested a maximum Young's modulus of  $345 \pm 22.4$  MPa. The tensile test for the LCL was carried out at 15° flexion whereas for the ACL and PCL a flexion angle of 30° was chosen. Other studies have adopted those ligament properties for their 3D FE knee models (Chantarapanich et al., 2009; Kubicek and Florian, 2009). The material properties obtained in this study, after tuning, were within this range.

It is worth mentioning that the material properties in the ACL and PCL in this study may have been underestimated during passive motion. A load-bearing joint may be subjected to higher sliding motion and shear forces than those during passive motion.

### 5.1.3. Concluding Remarks

Since this was a comparative study all results were expressed relative to each other. Any error that occurred due to unrealistic material properties would have occurred in each analysis. Due to computational costs, the material properties described in this investigation were chosen to obtain useful results within a realistic timescale of approximately two to six hours (using a PC with a 64-bit Operating system, 32GB RAM, 3.07 GHz), which were adequate for a comparative basis.

In future models, it will be important to implement viscoelastic material properties for soft tissues and consider each ligament as a bundle of multiple tensile structures. This will be more feasible with more powerful processors. Since I focussed upon one position of the gait cycle (end of weight acceptance), viscoelastic material properties were not included in this model.

## 5.2. Discussion of Validation Study

A method for development and validation of a subject-specific FE model of the tibiofemoral joint is presented. The FE model of the knee employed tissue-specific MRI scanning sequences and Mimics-based image processing to represent the 3D geometry of the bony and soft tissues comprising the diarthrodial joint. Geometries of bone, meniscus, cartilage and ligaments are likely to influence resulting force and pressure values (Beillas et al., 2004). To reduce the number of variables and increase accuracy, the subject-specific FE knee model was created from 3D MRI datasets of the knee. The same *in vitro* specimen that was used to build the FE model was subjected to controlled loading in a robotic-based joint testing system. The same loading conditions were applied to the FE model and the cadaveric specimen to assess model performance.

The coordinate system used to describe the kinematic motions of the tibia with respect to the femur, in both the FE model and the cadaver, was adapted from Grood and Suntay (1983). This system uses the epicondylar axis, which connects the medial and lateral femoral epicondyles, as the axis of rotation. Most studies have used the same coordinate system to describe knee motion (Blankevoort and Huiskes, 1996; Beillas et al., 2004; Baldwin et al., 2011; Kiapour et al., 2013). Other studies approximated the

posterior femoral condyles by spherical surfaces. The axis of rotation was then defined by a line connecting the midpoints of the spheres (Kurosawa et al., 1985; Eckhoff et al., 2001; Walker et al., 2011).

Most et al. (2004) conducted a study to compare knee joint motion using these two different rotation axes. Kinematics were sensitive to the selection of the flexion axis. While the epicondylar axis resulted in higher posterior translation in the medial femoral condyle, the spherical axis led to higher tibial rotation. It was concluded that both methods give reliable results and could be used to describe knee motion as long as a clear definition of the flexion axis was given (Most et al., 2004).

### **5.2.1. Forces and Pressure between FE Model and *In Vitro* Study**

Normalised forces and peak joint pressure in the medial and lateral tibial cartilage, predicted by the FE model, were in good agreement with those obtained from *in vitro* tests across the range of applied varus and valgus bending moments. Absolute force values, predicted by the FE model, were higher than those measured during the *in vitro* tests (normalised medial and lateral force FSEs: 7.56% and 4.48%, respectively). This was expected because some of the load-bearing anatomical structures were likely to have been physically outside the force transducer sensel areas and not recorded by the sensor matrix. In addition, it has been reported that measurement errors on the order of 1-4% could occur when using Tekscan sensors (Fregly and Sawyer, 2003; Baer, et al., 2005; Brimacombe, et al., 2005). Results of the validation study confirmed Hypothesis 2 because peak joint stress magnitude and location as well as compartment forces, predicted by the 3D subject-specific FE model were within 10% of the *in vitro* results.

Compartmental force results are in accordance with several investigations on knee joint contact mechanics. Application of a 15 Nm varus moment resulted in a 279 N increase in medial contact force and a 15 Nm valgus moment resulted in a 259 N increase in lateral contact force (Table 4.10). Bendjaballah et al. (1997) applied varus and valgus moments up to 15 Nm, simulating different alignments, and observed the resulting load and stress at the tibial plateau. Results suggested that compressive stress in the tibial plateau became much greater with higher applied moments. A 15 Nm varus moment resulted in a 250 N increase in medial contact force. A 15 Nm valgus moment

resulted in a 320 N increase in lateral contact force (Bendjaballah, Shirazi-Adl and Zukor, 1997).

As shown in Figure 4.19, a 4-Nm varus bending moment in a well-aligned knee provided *in vitro* measured and FE predicted medial:lateral force ratios of 65%:35% and 73%:27%, respectively. Medial compartmental loading ranging from 60%-70% of total load has been reported by a number of investigators (Schipplein and Andriacchi, 1991; Tetsworth and Paley, 1994; Agneskirchner et al., 2004; Thambyah, 2007). This is because the MA passes medially to the knee joint centre in well-aligned knees and results in an adduction moment.

Figure 4.18b shows that, as the varus bending moment was increased, which represents a greater varus knee malalignment, medial compartmental force increased and lateral compartmental force decreased. In particular, FE results in Figure 4.19 show that a small increase in varus bending moment from 4 Nm to 8 Nm resulted in an increase in medial compartmental percent force from 73% to 89%. This agrees Tetsworth and Paley (1994), who reported that as little as 5° of varus malalignment increases medial compressive loading from 70% to 90% (Tetsworth and Paley, 1994). Medial load transfer, resulting from an increase in adduction moment, or varus malalignment, has also been reported (Tetsworth and Paley, 1994; Zhao et al., 2007; Kutzner et al., 2010).

FE model predictions for peak pressure values in the medial and lateral compartments in this validation study ranged from 0 to 2.51 MPa with a 374 N axial force and 15 Nm maximum bending moment. This is consistent with other experimental and FE studies, in which corresponding contact pressures between 2.4 MPa and 34 MPa have been reported for higher axial loads of 700 – 2000 N on simulated intact, injured, or reconstructed knee joints (Donahue et al., 2002; Marzo and Gurske-DePerio, 2009; Morimoto et al., 2009; Mononen et al., 2012; Adouni, Shirazi-Adl and Shirazi, 2012).

Applied loading conditions and FE-predicted compartment and ligament forces were input into the static equilibrium analysis (Table 4.10). Resultant forces and moments were close to zero, demonstrating that static equilibrium conditions were met. Small discrepancies can be explained as follows: 1) there may be some contribution of ligament forces in the moment equation which were not accounted for; 2) the actual moment arms may be slightly different than those measured manually in Mimics and Abaqus; 3) the angles of the cruciate ligaments might change with alignment. These

calculations further support the validation of the FE model, which adds to the sparse validation available in the knee modelling literature.

Other investigators have validated their models by comparing their results to subject specific cadaveric knee kinematics, kinematics from a different specimen, published kinematics, subject-specific *in vitro* contact mechanics, *in vitro* contact mechanics from other cadavers, or published contact mechanics (Table 5.1). This investigational team is the only group to have provided a subject-specific stress validation of their FE knee model (Mootanah et al., 2014).

**Table 5.1: Summary of FE-model validations in the literature**  
(Source: Mootanah et al., 2014)

<b>Authors and date</b>	<b>Parameters validated</b>	<b>Type of specimen</b>
Blankevoort, Huiskes, 1996	Kinematics of the knee soft tissue finite element model	<i>In vitro</i> tests from other cadaveric knee specimens
Li et al., 1999	Joint contact pressures of an FE knee model	Experimental findings from other investigators
Godest et al., 2002	Kinematics of an FE knee model	Previously published experimental kinematic data
Beillas et al., 2004	Kinematics of an FE knee model	<i>In vitro</i> tests from other cadaveric knee specimens
Halloran, Petrella and Rullkoetter, 2005	Kinematics of an FE knee model	Previously published experimental kinematic data
Peña et al., 2006	Joint contact pressures of an FE knee model	Experimental findings from other investigators
Perillo-Marcone, Taylor, 2007	Kinematics of an FE knee model	Previously published experimental kinematic data
Miller et al., 2009	Total load, peak load and peak load location for axial, varus and valgus loading conditions of a 2D discrete element analysis model	<i>In vitro</i> study from 4 human cadaveric knees
Shirazi and Shirazi-Adl, 2009	Joint contact pressures of an FE knee model	<i>In vitro</i> results from other cadavers
Yosibash, Trabelsi and Milgrom, 2007; Yosibash, Tal and Trabelsi, 2010	Strain and displacement of an FE femur model	<i>In vitro</i> tests from subject-specific cadaveric femur
Guess et al., 2010	Kinematics of a multibody knee model	Identically-loaded cadaveric knee
Baldwin et al., 2011	Kinematics of 3 subject-specific FE TKA models	<i>In vitro</i> dynamic tests from three cadaveric specimens



Authors and date	Parameters validated	Type of specimen
Tuncer et al., 2013	Strain in tibia and femur of an FE knee model with a UKA	<i>In vitro</i> tests from 10 different cadaveric knee specimens
Mononen, Juvelin and Korhonen, 2013	Knee joint stresses and strains–musculoskeletal multibody dynamics	Experimental findings from other investigators
Bahraminasab et al., 2013	Joint contact pressures of an FE knee model	Experimental findings from other investigators
Kiapour et al., 2014	Ligaments strain/force and centre of articular cartilage pressure and tibiofemoral kinematics	<i>In vitro</i> tests from 16 different cadaveric leg specimens
Innocenti et al., 2014	Force ratio in medial and lateral compartment of FE model with a UKA	<i>In vitro</i> test from subject-specific cadaver
Mootanah et al., 2014	Joint contact pressures of an FE model	Experimental findings from subject-specific knee joint

### 5.2.2. Ligament Tuning

Some investigators have conducted kinematic validations (Blankevoort and Huiskes, 1996; Beillas et al., 2004; Guess et al., 2010; Kiapour et al., 2014). However, the precise length-tension relationship and slack length of each subject-specific ligament is not known. To solve that problem, Baldwin et al. (2011) and Mootanah et al. (2014) tuned the ligaments by minimising the kinematic differences between their FE models and subject-specific specimens. Tuning the ligaments is an important feature to validate the model, as stress values were different before and after the procedure. Baldwin reported RMS differences from experimental measurements of  $3.8 \pm 1.9^\circ$ , while internal–external and varus–valgus rotations had differences of  $<1.3 \pm 0.7^\circ$ ; anterior–posterior, inferior–superior and medial–lateral translations matched within  $2.1 \pm 1.2$  mm,  $1.7 \pm 1.2$  mm and  $0.9 \pm 0.5$  mm, respectively (Baldwin et al., 2011). However, even though Baldwin et al. (2011) conducted a tuning procedure, their ligaments were represented as 2D structures.

Ligaments consist of many bundles with fibres that behave differently at different flexion angles (Qi et al., 2013). Data for ligament properties at each flexion angle is sparse in the literature, most likely subject specific and difficult to measure. In this study, ligament material properties were permitted to vary across different flexion angles (Figure 4.16). This practical approach describes the more complex behaviour of each ligament over the entire range of motion and permits tuning the model values to minimise kinematic errors with the cadaver. In this matter, an approximation to the subject-specific material properties could be obtained.

*In-vitro* kinematics for the ligament tuning were initially acquired during passive (unloaded) flexion-extension, using a 6DOF robot. In the loaded condition, a different translation in compression-distraction is expected. This necessitated a second phase of ligament tuning with axial loads and bending moments (Figure 4.15).

### 5.2.3. Validation

Results of the validation show good agreement with published data. Miller et al. (2009) reported RMS errors of < 4% for most loading conditions. However, for some applied loads, the predicted results overestimated the peak plateau force. For the locations of the peak medial plateau force, differences between predicted and experimental values were < 10%. For the lateral location of peak force, 2 out of 7 loading conditions had differences > 10% (Miller et al., 2009).

Kiapour et al. (2014) validated their FE knee model against ligament strain and force and centre of articular cartilage pressure. Results showed good agreement with experimental data on 16 cadaveric knees. Reported RMSE were 1% for ACL and MCL strain, 17 N of ACL load and 1 mm of tibiofemoral centre of pressure. However, this validation was not subject-specific and actual values of the contact pressure were not reported (Kiapour et al., 2014).

Donahue et al. (2003) built an FE model from the same knee that was used in testing and minimised differences in contact pressure between experimental and model results to 5.4%. Since contact pressure was minimised by altering cartilage and menisci properties, this model could not be validated for stress and did not include a kinematic validation (Haut Donahue et al., 2003).

The percent differences between measured and predicted peak total axial force in Lundberg et al.'s study (2013) were 2.89% at the first peak and 9.36% at the second peak contact force for normal walking. For medial thrust gait, the percent differences were 3.94% at the first peak and 14.86% at the second peak contact force. This model gave promising results but did not consider the contact pressure and shear stress across the joint (Lundberg, Knowlton and Wimmer, 2013).

Although there has been some effort to validate knee replacement models (Lanovaz and Ellis, 2005; Baldwin et al., 2011; Tuncer et al., 2013; Innocenti et al., 2014), these are not of the native knee.

#### **5.2.4. Concluding Remarks**

Despite the large number of publications on FE knee models, to my knowledge, no one has validated their model by comparing their contact force and stress predictions with measurements from the same cadaveric specimen. A validated FE knee joint model is a powerful tool for understanding the contact mechanics in weight bearing activities. The knee specimen used in this study was obtained from a fresh-frozen cadaver to ensure minimum changes in material properties during storage. Although the validation of joint stress and force was for the loading conditions of 375 N of axial force and 0-15 Nm bending moment, it is possible to emulate a variety of functional tasks and compute the corresponding contact mechanics.

The Tekscan transducer, being a resistive sensor, has an inherently higher hysteresis and lower accuracy than capacitive sensors. Capacitive transducers could have been used to measure contact pressure and forces in the cadaver more precisely. However, capacitive transducers are thicker and would have increased the joint space, which, in turn, increases the force in the ligaments and hence contact forces between the tibia and femur. This measurement would have influenced the contact pressures. Papaioannou et al. (2008) compared the results of an FE model with and without a transducer. Differences in contact mechanics were as large as 14%.

The transducer was calibrated on a flat surface whereas the knee anatomy is curved. This could have affected force and pressure measurements. To insert the transducer within the cadaveric knee joint, the posterior capsule had to be sliced open. This might

also have affected outcomes. To strengthen this validation, additional subject-specific models from different sized cadavers will be compared in future research.

### **5.3. Discussion of Analysis of Intact Knee**

*In vivo* 3D kinematic and kinetic data, supplied by the Leon Root, MD Motion Analysis Laboratory at HSS, was used to provide realistic position and loading input to the FE knee model from the end of weight acceptance during walking. Previously developed FE models provide insight into contact mechanics at the knee and have been used to investigate several pathologies. However, most FE studies apply only simple loading conditions.

Yang et al. (2010) applied loading conditions from gait analysis but did not include the medial/lateral force, which may substantially influence cartilage stress (Yang, Nayeb-Hashemi et al. 2010). A large medial/lateral force imposes a shear force and stress upon the knee joint cartilage surface, which is considered an important promoter of cartilage matrix breakdown (Donahue et al., 2002; Andriacchi et al., 2006; Wilson et al., 2006). A large axial force on the medial compartment is often imposed by a higher adduction moment, which has been reported to be highly correlated to knee joint stress (Prodromos, Andriacchi and Galante, 1985; Andriacchi, 1994; Blecha et al., 2005).

Other studies apply only an axial load and ignore other loading conditions (Papachristou, 2004; Chantarapanich et al., 2009; Pressel et al., 2010). These studies typically report forces and pressures during one-legged posture. Nevertheless, data provided by HSS clearly showed that, even during one-legged posture, there are tri-planar forces and moments acting on the knee (Table 5.2). During walking, these forces and moments vary throughout the gait cycle. To emulate the end of weight acceptance during the stance phase of walking, human movement data was employed from an individual with the same weight, alignment and height as the cadaver to provide a realistic representation of these loading conditions.

**Table 5.2: Movement data for posture (Courtesy of Dr Hillstrom, Leon Root MD, Motion Analysis Lab, Hospital for Special Surgery, New York)**

Knee Varus Angle	1.423°
Knee Flexion Angle	0.534°
Knee External Angle	2.172°
Knee Compression Force	0.487 %BW
Knee Anterior Force	0.033 %BW
Knee Lateral Force	0.022 %BW
Knee Extension Moment	0.001 %BW ×ht
Knee Varus moment	0.006 %BW ×ht
Knee External Moment	0.027 %BW ×ht

Andriacchi et al. (1994) reported that the loads generated during dynamic activities were substantially greater than the loads due to static posture (Andriacchi, 1994). A static knee radiograph cannot provide an estimate of the load distribution during gait (Johnson, Leitzl and Waugh, 1980). In bi-pedal standing radiographs, the MA is approximately coincident with the GR vector and typically used by orthopaedic surgeons as the basis for alignment correction (Prodromos, Andriacchi and Galante, 1985; Cooke, Sled and Scudamore, 2007). However, during walking, the GR vector and MA are not collinear (Figure 5.1), making it extremely difficult to predict how a surgical alignment change will affect gait. Johnson et al. (1980) confirmed the lack of correlation between the MA and the GR vector during walking. The end of weight acceptance was selected as the most important aspect of gait to evaluate, because it represents the maximum varus thrust during level walking.

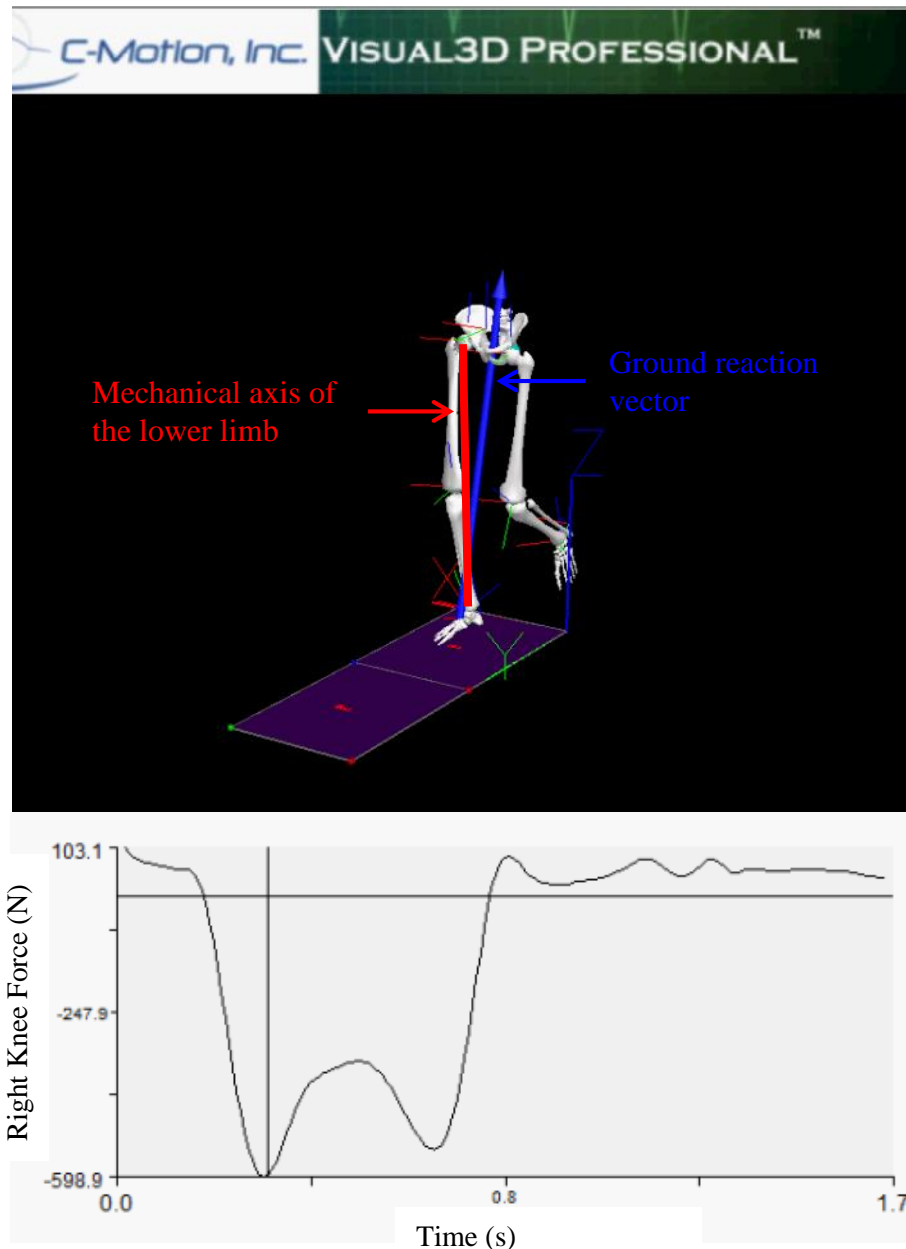


**Figure 5.1:** Illustration of the ground reaction vector (blue) and the mechanical axis of the lower limb (red) during the end of weight acceptance in walking

### 5.3.1. Pressure and Forces in the Intact Joint

Peak compressive stress in the intact knee was 4.05 MPa in the medial and 2.63 MPa in the lateral compartment. These values are within the same range as the medial (3.43 MPa) and lateral (4.88 MPa) compressive stress reported by Peña et al. (2008). The higher stress reported by Peña et al. (2008) could be due to application of a higher anterior load and inclusion of the patella and patella tendon in their model, which

might have increased the shear force. The higher stress in the lateral compartment was due to the lack of a varus bending moment, which is inherently present in standing and walking due to the eccentric loading of the femur (Maquet, Van de Berg and Simonet, 1975).

Hopkins et al. (2010) reported that, with a 200 N axial load, the percent cartilage surface exposed to a stress < 2 MPa was 80%. This was slightly lower than the volumetric stress reported in this study (93% for a stress < 2MPa). However, Hopkins et al. did not include any ligaments in their model, which would have increased their compressive stress.

Mattei et al. (2014) report a shear stress of 2.38 MPa in the femoral cartilage and 2.64 MPa in the tibial cartilage during the end of weight acceptance phase of the gait cycle. This is similar to the shear stress reported in this study (2.04 MPa in the tibial cartilage and 1.67 MPa in the femoral cartilage).

Several investigators have predicted knee joint contact pressure, using computational models. However, loading and boundary conditions vary extensively between studies, making it difficult to compare results (Donahue et al., 2002). Still, results for peak contact pressure lie within the range of published data (2-8 MPa) (Bratianu, Rinderu and Gruionu, 2004; Zielinska and Donahue, 2006; Thambyah, 2007; Morimoto et al., 2009; Shirazi and Shirazi-Adl, 2009; Marzo and Gurske-DePerio, 2009; Guo, Zhang and Chen, 2009).

In this study, the well-aligned knee joint gave a medial:lateral force ratio of 70%:30%. It is well documented that the distribution of force between the medial and lateral compartments is approximately 70% medial and 30% lateral (Hsu et al., 1990; Schipplein and Andriacchi, 1991; Andriacchi, 1994). Thambyah et al. (2007) applied an axial load of 1144 N to 4 cadavers and reported a medial load of 806.3 N (70%) and a lateral load of 337.5 N (30%) (Thambyah, 2007). As long as the GR is medial to the joint centre a bending moment is imposed, which will combine with compressive forces to increase the medial compartment load during standing and walking (Maquet, Van de Berg and Simonet, 1975).

## 5.4. The Malaligned Knee

In this investigation, FE analyses were conducted to predict knee joint contact mechanics for different HTO correction angles. Although, during surgical reconstruction, the osteotomy is performed proximally to the MCL attachment, for the purposes of this FE study, the virtual osteotomy was created distally to the MCL attachment. By not surgically altering the MCL, this provided a method of assessing the effects of knee alignment upon joint stress without the confounding variable of MCL status. Shim et al. (2013) studied 37 knees and concluded that an HTO distal to the tibial tubercle leads to significant improvements in radiographic parameters and knee function without changes in patellar height or posterior slope (Shim et al., 2013).

### 5.4.1. Load Application

The initial KAM, which corresponded to a  $1^\circ$  varus knee alignment, was 20.4 Nm from the gait data, which was anthropometrically matched to the cadaver. To calculate the new KAM at each frontal plane alignment, the initial forces and moments (in all 6 DOF) were transformed using the previously described transformations (Equations 32-34) and summarised in Table 3.11. The knee adduction moments applied to the model as a function of tibiofemoral angle are in agreement with several studies. Weidenhielm et al. (1993) reported a peak knee adduction moment of 64 Nm for  $9.2^\circ$  varus. Muendermann et al. (2005) measured a peak knee adduction moment of 3% BW $\times$ ht on a subject with well-aligned knees. Patients with severe OA had an alignment of up to  $5.7^\circ$  varus and a peak knee adduction moment of 3.8% BW $\times$ ht.

Prodromos (1985) carried out gait analyses of patients pre- and post-HTO and reported a peak adduction moment of 4% BW $\times$ ht for a pre-operative alignment of  $9^\circ$  varus and 2.8% BW $\times$ ht for a post-operative alignment of  $1.8^\circ$  valgus. Lind et al. (2010) carried out a similar investigation and also measured a peak knee adduction moment of 4% BW $\times$ ht, preoperatively, for a varus alignment of  $8^\circ$ . With an average of 2.3% BW $\times$ ht for an alignment of  $0^\circ$ , the postoperative knee adduction moment in Lind et al.'s study was slightly lower than that stated by Prodromos.

In Bhatnagar et al.'s study, the average peak knee adduction moment for a varus knee was 3% BW $\times$ ht. This was reduced to 1.25% BW $\times$ ht 6 months after HTO. Miyazaki et



al. also measured the knee adduction moment in different alignments and found 4.6 % BW×ht for 4° varus and 6.1 % BW×ht for 6.3° varus.

The KAM applied to this model (Table 3.11) were in agreement with other investigators and, hence, considered reasonable. However, in future studies the FE model could be enhanced by inputting subject-specific 3D kinetic data during gait preoperatively for surgical realignment planning and compare outcomes with 3D postoperative kinematics and kinetics.

It is worth noting that inverse dynamic measurements are an underestimate of contact forces within the knee joint, since ligament and muscular forces are not accounted for. Hillstrom et al. (2013) conducted a gait analysis on a subject with an instrumented TKA (e-tibia), capable of measuring force in-vivo. Contact force magnitude was 100% higher than intersegmental forces (inverse dynamics) of the same patient while performing level walking (Hillstrom, et al., 2013). This indicates the importance of including muscle forces into future models to realistically represent joint loading, as experienced during functional tasks.

#### **5.4.2. Forces in the Malaligned Models**

Joint force and stress, as a function of tibiofemoral alignment, was analysed in this investigation. With a varus alignment of 5° a load ratio of 99%:1% was achieved (Figure 4.21). This corresponds with the studies of Yagi and Sasaki (1986) and Tetsworth and Paley (1994) who noted that as little as 5° of varus malalignment increased the medial compressive loading from 70% to 90%.

Ogden et al. (2009) looked at changes in the load distribution after opening and closing wedged HTO. An axial load of 2000 N was applied, resulting in 830±122 N medial and 1207±116 N lateral compartment forces. The higher load in the lateral compartment was due to the cadaver knees being in slight valgus as well as not applying a varus bending moment. For a valgus realignment of 5° the force in the medial compartment was reduced to 773.43 N and the lateral force increased to 1247.68 N. A 10° valgus realignment decreased the medial load to 542.45 N, while the force in the lateral compartment increased to 1466.41 N (Ogden et al., 2009).

In this study, where the knee model was neutrally aligned and loaded with 811 N of axial force and 20 Nm of varus bending moment, different compartmental force ratios

were observed. For a 5° valgus realignment medial contact force decreased from 607.7 N to 195.1 N, while the lateral force increased from 264.3 N to 694.8 N. For a 10° valgus realignment the medial load decreased to 9 N while a lateral load of 954.3 N was recorded (Figure 4.20). These differences with respect to Odgen et al. (2009) are predominantly due to a lack of bending moment during loading conditions. The presence of a varus bending moment is important for achieving a 70%:30% compartment loading ratio.

For this particular model the physiological load ratio of 70%:30% (Hsu et al., 1990; Schipplein and Andriacchi, 1991; Andriacchi, 1994) was achieved for an initial alignment of 1° varus or an MAD of 3.6 mm. As this initial knee alignment may vary between subjects, data was normalised by calculating the intersection of the MA with the tibial plateau in percent. According to Fujisawa, the ideal alignment is when the MA passes the tibial plateau at 62% of the tibial width (Fujisawa, Masuhara and Shiomi, 1979). Figure 4.21 shows that, for this particular subject, the Fujisawa point resulted in a higher load in the lateral compartment (66%). An intersection of the MA with the tibial plateau at 54% showed a medial:lateral force ratio of 50%:50% which had an equivalent knee alignment of 1° valgus.

Based upon results of the OASIS surgical planning tool for malalignment correction, Babis et al. (2008) investigated the results of 54 lateral closing wedge osteotomies and found that patients with a medial compartment force ratio between 40% and 60% achieved a 100% ten-year survivorship after HTO. The average age of patients was 53 year (range 19-71) (Babis et al., 2008). A wide variety of postsurgical alignments was reported in the literature. Several investigators suggested that outcomes were best when the MA passed the tibial plateau between 50% and 70% (Miniaci et al., 1989; Dugdale, Noyes and Styer, 1992; Niemeyer et al., 2010; El-Azab et al., 2011; Reising et al., 2013). MAD is a function of patient size. If surgeons target the same MAD in mm for each tibia, then different post-operative alignments could result, dependent upon the lengths and widths of each individual tibia and femur (Dugdale, Noyes and Styer, 1992). Other surgeons focused on postsurgical HKA angle and reported a span of 3°-6° of valgus as their target alignment.

Table 5.3 shows a summary of the lowest and highest post-operative alignment targets with their equivalent MAD, HKA angle, medial:lateral force ratio and the point where the MA crosses the tibial plateau for this cadaveric specimen.

**Table 5.3: Summary of lowest and highest targets from literature with their equivalent mechanical axis deviation, hip-knee-ankle angle and the point where the mechanical axis of the lower limb intersects the tibial plateau.**

	<b>Lower limit from literature</b>	<b>Upper limit from literature</b>
<b>Intersection of MA with the tibial plateau</b>	<b>50%</b>	<b>70%</b>
Equivalent MAD	0 mm	-16 mm
Equivalent HKA angle	0.0°	-4.4°
Equivalent medial:lateral force ratio	60:40	18:82
<b>HKA angle</b>	<b>3° valgus</b>	<b>6° valgus</b>
Equivalent intersection of MA with tibial plateau	63.75 %	76.88 %
Equivalent medial : lateral force ratio	30:70	4:96
Equivalent MAD	-11.0 mm	- 21.5 mm

Table 5.3 demonstrates that the upper limit of 70% for the intersection of the MA with the tibial plateau would overcorrect this cadaver. A medial:lateral force ratio of 18%:82% would most likely overload the lateral cartilage. The lower limit of 50% might not sufficiently offload the medial compartment. The surgeon must select a target within this published range of corrections that will improve function and reduce pain, based upon the patient's alignment and disease severity.

Post-operative HKA angles span from 3° valgus to 6° valgus in the literature. The purpose for this overcorrection is to provide more offloading of the medial compartment. However, for the cadaver in this study, 3° of valgus corresponds to a medial:lateral force ratio of 30%:70%. This extreme of overcorrection falls outside the range reported by Chao et al. (2003). If the centre of Chao et al.'s (2003) correction range were established as the target (50% medial compartment loading), 1° of valgus would achieve this goal for the cadaveric specimen of this study.

Figure 4.21 shows that even a small change in alignment causes a significant shift in the medial:lateral load ratio and the pressure distribution in the medial and lateral compartments. This is consistent with the findings of Hsu et al. (1990). Adouni and Shirazi-Adl (2014) investigated the effect of frontal plane alignment on the medial:lateral load ratio and reported a 12% drop in medial contact load with a decrease in varus alignment of 1.5°.

The target MAD can provide substantially different medial to lateral force distributions. An MAD of 0 mm provided a medial:lateral force ratio of 60%:40%, whereas the Fujisawa point of 62% results in a medial:lateral force ratio of 34%:66%. Table 4.11 shows a summary of medial:lateral force ratios and their corresponding intersection of the MA with the tibial plateau, MAD and HKA angle. This table provides subject-specific alignment criteria to achieve a targeted medial:lateral force ratio which may be considered in the surgical treatment plan.

It is also important to consider the severity of articular cartilage damage. If a patient has severe medial OA, then a larger postoperative valgus angle should be considered to unload the medial compartment. Several investigators (Jakob and Murphy, 1992; Müller and Strecker, 2008) have recommended strategies to determine the amount of realignment by the severity of cartilage damage. In Babis et al.'s study (2008), they

was able to identify that those individuals who resulted in a 40% to 60% medial compartment load, had a 100% survivorship over ten years. By creating 3D subject-specific FE models, as presented in this study, the severity of articular cartilage and meniscal damage for each patient will be accounted for and an accurate realignment target angle determined.

### **5.4.3. Pressure in the Malaligned Models**

Given the anatomical variations amongst individuals, it is possible that achieving the targeted force ratio may not correspond to the minimum contact stress within the knee joint. Therefore, understanding the relationship between contact stress, MAD and wedge geometry is important. Segal et al. (2009) conducted a study on 3000 subjects and concluded that contact stress was a strong predictor of articular changes associated with pain.

Minimum contact stress in the medial and lateral compartments was achieved for an alignment of  $0.5^{\circ}$  valgus, which corresponds to a medial:lateral load ratio of 56%:44%. The corresponding intersection of the MA with the tibial plateau was 51.75% from medial to lateral, which was within the suggested post-operative alignment range and could be considered the target correction for this specific cadaver. Applying the Fujisawa point as the target correction would increase the lateral compartment stress, which may exacerbate the risk of lateral cartilage degeneration. Therefore, the Fujisawa point would be considered a substantial overcorrection for this cadaver.

Shear stress has been associated with articular cartilage degenerations (Donahue et al., 2002; Andriacchi et al., 2006; Wilson et al., 2006). Although difficult to measure, especially within a joint, 3D computational models may estimate the shear stress present. Surgeons may also consider, in their treatment planning, alignments that may reduce shear stress in the involved compartment. The alignment that minimises compartment shear stress may not correspond to the alignment that minimises contact stress. Furthermore, surgeons must be cautious not to overload the other compartment, in shear or contact stress, and promote OA development in that region. Computational models of the knee are expected to serve as powerful research tools to study the role

of shear stress in conjunction with contact stress in degeneration of the diarthrodial joint.

### ***Computational models***

The direct effect of lower limb malalignment on contact force and pressure within the knee has been documented in several computational studies. Chao and Sim (1995) emphasised the importance of accurate preoperative HTO planning to properly correct joint alignment. Chao and Sim's OASIS software, although limited to a 2D static standing posture via long-leg x-rays, linear elastic elements for cartilage and ligaments and a uniplanar osteotomy wedge angle, has yielded to an increased HTO success rate (Chao and Sim, 1995). However, joint cartilage stress is, not only determined by the magnitude and direction of the contact force, but also by the size and shape of the articular surface. To estimate joint stress (contact and shear), it is important to account for the articular geometry. Chao's study, although an important contribution in altering load distribution, is limited by being 2D and incapable of predicting joint stress.

Reinbolt et al. (2008) created a 3D musculoskeletal gait model to investigate the effect of an HTO on individual patients' knee adduction moment, based on their pre-treatment gait pattern. Compared to the well-aligned knee, the percentage of post-operative peak knee adduction moment increased monotonically with pre-operative severity of varus alignment (Table 5.4). This investigation was conducted on one patient, and did not evaluate joint contact stress (Reinbolt et al., 2008).

**Table 5.4: Results of Reinbolt et al.'s (2008) study. The percent increase of peak knee adduction moment with the corresponding HKA angle.**

<b>Varus alignment</b>	<b>%increase in peak adduction moment</b>
3°	0.71 % BW×ht
5°	1.2 % BW×ht
7°	1.7 % BW×ht

Yang et al. (2010) created three subject-specific 3D FE knee models to study the effect of frontal plane tibiofemoral angle on the stress and strain distribution within cartilage during the stance phase of gait. A simulated axial load of  $2.8 \times \text{BW}$  was applied along the femur of each subject. Table 5.5 summarises the results obtained at the end of weight acceptance during walking (Yang, Nayeb-Hashemi et al. 2010).

**Table 5.5: Summary of results obtained by Yang et al. (2010)**

		Maximum compressive stress (MPa)			
		Femoral cartilage		Tibial Cartilage	
	Knee Angle	Medial	Lateral	Medial	Lateral
Subject 1	Varus	14	2	13	1
Subject 2	Neutral	14.5	3	12.5	3
Subject 3	Valgus	12.5	7	10	6

Values obtained by Yang are significantly higher than those predicted in this study. This is due to the higher axial loads as well as muscle forces (Morrison, 1970; Schipplein and Andriacchi, 1991) that were included in their FE model. Yang et al.'s FE model was not validated and medial/lateral forces were not applied, which could have influenced the results.

Chantarapanich et al. (2009) created six 3D knee models: three in normal and three in varus alignment. Vertical forces of 768.45 N and 780.18 N were applied to the femoral head of the well-aligned and varus knees, respectively, to simulate single-leg standing. Predicted medial and lateral compartment stress was 2.42 MPa and 3.88 MPa, respectively, for the well-aligned knee. The corresponding, medial and lateral compartment stress for the varus knee was 3.87 MPa and 1.25 MPa, respectively (Chantarapanich et al., 2009). Chantarapanich et al.'s study indicates that varus knee joints experience higher peak normal stress in the medial compartment compared to well-aligned knees. However, only an axial load and no bending moment was applied to their model, which resulted in a higher peak normal stress in the lateral compartment compared to the medial. A varus moment, experienced during single-legged standing, would shift the peak lateral pressure towards the medial compartment.

Mootanah et al. (2009) conducted a pilot study to examine the feasibility of developing a 3D subject-specific FE knee stress model to predict post HTO joint loading. An axial load of 2100 N, corresponding to 3×BW, was applied perpendicularly to the proximal end of the femur. Results of FE analyses show a reduction of 67% in principal stress in the knee joint following a virtual opening wedge HTO surgery (Mootanah, et al., 2009).

Pressel et al. (2010) created FE models of the tibia with different osteotomies and applied an axial load of 1591 N to the proximal tibia. They observed equivalent stress

in the medial and lateral compartments after removing a 2.5° varus wedge of bone. In this thesis, minimum medial and lateral compartment peak stress was achieved at a valgus alignment of 0.8°. At 0° alignment, Pressel et al.'s knee model produced a medial peak stress of 3.4 MPa and lateral peak stress of 2.9 MPa. A 5° valgus osteotomy increased lateral stress to 3.5 MPa and decreased medial stress to 2.9 MPa. A 10° valgus osteotomy increased lateral stress to 3.8 MPa and decreased medial stress to 2.1 MPa (Pressel et al., 2010). Even though the study only included the tibia and soft tissues, their results between 0° and 5° of valgus corroborate with ours. In the model of this thesis, following a 10° valgus osteotomy, pressure in the medial compartment was reduced to 0 MPa, indicating lift-off. Pressel et al. did not include the femur in their model and, therefore, could not simulate lift-off.

### ***Cadaveric Models***

Agneskirchner et al. (2007) reported a strong correlation between the frontal plane axis of loading and the tibiofemoral cartilage pressure distribution. In response to a 1000-N valgus-oriented load, the medial tibiofemoral mean contact pressure changed from 0.71 ( $\pm 0.35$ ) MPa to 0.52 ( $\pm 0.25$ ) MPa, while a varus-oriented load of the same magnitude changed the pressure to 0.94 ( $\pm 0.44$ ) MPa. The lateral tibiofemoral mean contact pressure changed from 0.83 MPa to 0.50 ( $\pm 0.16$ ) MPa in response to a varus-oriented load, while a valgus-oriented load of the same magnitude changed the pressure to 0.88 ( $\pm 0.27$ ) MPa (Agneskirchner et al., 2007).

Results of Agneskirchner et al.'s study were significantly lower than the results presented in this thesis. The loading conditions and knee angles were different as well as the specimens from which the two datasets were obtained. It is expected that stress distributions in different cadavers may be different due to the subject-specific geometry, the presence of osteophytes and the integrity of the soft tissues. However, Agneskirchner et al. (2007) has shown that a varus alignment indicated a higher pressure in the medial compartment, which corresponds with results of this thesis.

McKellop et al. (1991) measured the effects of angular deformities of 5°, 10°, 15° and 20° of varus and valgus on knee cartilage contact pressure. An axial load of 2400 N was applied at full extension and all ligaments were left intact (McKellop et al., 1991).



Peak maximum pressure in the medial and lateral cartilage are summarised in Table 5.6.

**Table 5.6: Results of McKellop et al.'s (1991) study in comparison to the current investigation. Peak maximum pressure in the medial and lateral compartments for varus and valgus alignments of the knee.**

	Maximum pressure (MPa) in varus				Maximum pressure (MPa) in valgus			
HKA angle	McKellop et al. (1991)		Reisse et al. (2014)		McKellop et al. (1991)		Reisse et al. (2014)	
	Medial	Lateral	Medial	Lateral	Medial	Lateral	Medial	Lateral
0°	4.10	4.60	4.28	2.42	4.10	4.60	4.28	2.42
5°	4.80	3.10	6.68	0	2.90	6.70	1.78	4.06
10°	6.70	1.90	9.24	0	2.00	7.30	0	5.62
15°	7.70	0.90	11.74	0	0.80	8.80	0	8.05
20°	8.70	0.60	n/a	n/a	0.40	9.30	n/a	n/a

Results presented by McKellop et al. are similar to those presented in this study. McKellop et al.'s data shows a higher pressure in the lateral compartment for the well-aligned knee due to the lack of an applied bending moment. Although McKellop et al. demonstrated a relationship between angular deformity magnitude and increased contact pressure, the direct relationship between MAD and contact mechanics was not established.

Bruns et al. (1993) used a pressure-sensitive film in a cadaveric knee in response to 500 N of axial femoral load to measure joint contact stress. All ligaments were intact. For a well-aligned knee, the contact pressure was 3.68 MPa in the medial compartment and 2.9 MPa in the lateral. A 10° varus alignment increased the medial pressure to 5.33 MPa and decreased the lateral pressure to 2.04 MPa. A 10° valgus alignment increased the lateral pressure to 4.18 MPa and decreased the medial pressure to 2.77 MPa (Bruns, Volkmer and Luessenhop, 1993). Results presented by Bruns et al. corroborate well with those presented in this study.

Riegger-Krugh et al. (1998) studied the contact pressure of six human cadaver tibiofemoral joints with articular cartilage degeneration in neutral, 5° varus, 5° valgus alignment and after closing wedge osteotomy. Medial average contact pressure in the

neutral knee was  $2.52 \pm 0.49$  MPa. This increased to  $3.20 \pm 0.68$  MPa for  $5^\circ$  varus and decreased to  $2.22 \pm 0.18$  MPa for  $5^\circ$  valgus. In the lateral compartment, the average contact pressure was  $3.86 \pm 0.96$  MPa. This decreased to  $3.02 \pm 0.84$  MPa for  $5^\circ$  varus and increased to  $4.76 \pm 0.66$  MPa for  $5^\circ$  valgus. After a closing wedge osteotomy, contact pressure was restored close to that of the neutral alignment ( $2.77 \pm 1.16$  MPa medial and  $3.97 \pm 0.70$  MPa lateral) (Riegger-Krugh et al., 1998).

## 5.5. Static Equilibrium

Table 4.15 shows that the forces generated by the FE model corroborate well with the static equilibrium analysis. Kettelkamp and Chao (1972) showed that the medial and lateral compressive forces at the knee might be computed from measurements taken from full-length radiographs.

However, 2D analysis cannot be used to assess 3D function of the knee. Johnson and Waugh (1980) compared the method used by Kettelkamp et al. to subject-specific gait analysis results. They concluded that the examination of a static radiograph would not provide a good approximation of load distribution during gait (Johnson, Leitzl and Waugh, 1980). Chao (1995) showed that, even when using simple 2D calculations, accurate knee joint forces could be calculated (Chao and Sim, 1995). However, 2D calculations cannot accurately predict stress experienced in the cartilage since the actual contact area is not known.

## 5.6. The broader field of OA research

Although the precise mechanism for OA onset and progression has not been proven, several risk factors have been identified, which support both the longstanding debate between biomechanical (high BMI, soft tissue injury, and malalignment) and biochemical (genetics, inflammation, and enzymatic breakdown of cartilage) theories. Consistent with the biomechanical theory, this research has focussed on lower limb malalignment correction to reduce peak knee contact stress with the goal of reducing OA onset and progression.

Many investigators have focused upon the molecular mechanism of OA (arcOGEN Consortium et al., 2012; Bonnet et al., 2013; Kelly et al., 2013; Reynard et al., 2014). Other investigators have developed disease-modifying drugs (Wildi et al., 2013; Reginster et al., 2013; Shah, Mirza and Patel, 2014). Stem cell research has shown

promise, with the aim of regenerating cartilage, using the body's own cells, as a treatment option for OA. Jo et al. (2014) injected stem cells into 18 patients with knee OA and arthroscopy showed that cartilage defect size decreased in the medial femoral and tibial condyles of all patients.

Other researchers have investigated the gait characteristics of patients with knee OA. Kaufman et al. (2001) demonstrated that inverse dynamics used to calculate intersegmental forces, could elucidate gait adaptations used by patients with knee OA. However, recent studies on patients with instrumented TKAs revealed that inverse dynamics substantially underestimate joint contact forces experienced during functional activities (Hillstrom et al., 2013). Still, Mootanah et al. (2013) used gait, plantar pressure, radiological and patient self-assessed pain data to determine if gait patterns and plantar loading asymmetries differed among individuals with knee OA with and without pain. They found that the asymmetry of stance and single support times were greatest in participants with unilateral knee OA (Mootanah, et al., 2013).

It is certainly possible that biomechanical factors, such as excessive joint stress, may trigger aberrant biochemical pathways (e.g. degradation of synovial fluid (Neu et al., 2010)) that damage cartilage matrix. Alternatively, enzymatic breakdown of cartilage matrix and meniscal extrusion may cause malalignment and excessive joint stress. It is likely that many of these factors are co-existing and contributory to the onset and progression of OA.

This thesis contributes to the body of knowledge by predicting stress within the knee joint in a subject-specific manner. The advantage of the computational method is that joint stress can be predicted, without being affected by other biochemical variables which may not be possible *in vivo*. This research, using computational biomechanical methods, has identified realignment as a key factor to improve joint contact mechanics and has provided a basic foundation from which to develop a pre-surgical planning tool to improve clinical outcomes of knee OA patients. Much research remains to be done before accomplishing this goal and confirmation amongst a cohort of patients with knee OA and the associated biochemical markers of pathophysiology is essential.

## 5.7. Limitations

This thesis has demonstrated the ability to predict stress changes within both compartments of the knee, following varus and valgus knee alignment simulations. Even though computational methods are widely accepted, they are based on simplifications and assumptions. The following section discusses the limitations of the present study.

The main limitation of this study is that only one FE model was created and validated. Therefore, current results cannot be generalised for every patient. It is necessary to create additional models in order to account for the variability in knee geometry and material properties within the population.

Ligaments were represented using isotropic neo-Hookean hyperelastic material properties. The primary structural role for knee ligaments is to maintain joint stability while in tension. The material model selected exhibits the assigned properties and generates forces in tension and compression. Each ligament has an anatomical position that places the structure in slack (e.g. PCL in full extension or MCL in varus). The isotropic neo-Hookean ligament models resist compressive stress which is clearly not possible anatomically when ligaments are in a slackened position. As part of the ligament tuning process each ligament's material properties were obtained across 0 to 65 degrees of knee flexion and in response to varus and valgus loading. The criterion for tuning a ligament was to obtain the material property values that minimised kinematic differences between the model and the *in vitro* specimen. Once a ligament achieved a minimum modulus of 5-10 MPa then no lower moduli (to emulate the slackened state) would alter joint kinematics. This finding supported the use of this material model since ligaments in slack were unable to change joint kinematics due to their negligible force contributions in compression. For future generations of this model anisotropic ligament properties will be explored.

The assumption of using the same properties for medial and lateral cartilage in the malaligned knee may not give an accurate representation. The cartilage on the affected side might become stiffer due to higher wear rates. In turn, the cartilage on the unaffected side might become less stiff since it is not loaded as severely as the involved

side. Cartilage material properties may be a function of knee malalignment, which should be explored in future studies.

There are errors at each stage of model development and validation. A Table has been formed (Table 5.7) to summarise these errors and put this in perspective. Error specifications were provided when known but the magnitudes of certain errors (e.g. material properties) was beyond the scope of this thesis. Every opportunity to minimise a known source of error was taken.

**Table 5.7: Estimated errors during the model development**

<b>Task</b>	<b>Error Source</b>	<b>Comments</b>
MRI Acquisition	MRI served as the source for all 3D anatomy data to build the FE knee model. A magnification error of 2%, due to geometry shrinkage, was expected at the isocentre (Mootanah et al., 2011). This error was approximately half of typical from the literature (Bowers et al., 2007). The position of the Grood and Suntay coordinate system could be affected by this error. The ability to see the boundaries of each tissue is related to image resolution (0.29mm x 0.29mm in plane; slice thickness 0.6mm) and signal to noise ratio, which in turn is related to the scanning sequence (SPGR; CUBE) and magnetic field strength (3T). Two different scanning sequences were used to ensure that each part could be represented accurately.	The tibiofemoral joint space was positioned in the ISO centre, which was identified by lasers. Since the tare of interest (tibiofemoral joint space) was position at the isocentre, the magnification error is anticipated to have a negligible effect upon contact mechanics. Experts from the radiology department at HSS ensured that high quality images were provided.

<b>Task</b>	<b>Error Source</b>	<b>Comments</b>
MRI Segmentation	The MRI segmentation was conducted using the previously described 3D-livewire technique. Each view was magnified up to the maximum size of the screen to illustrate the boundary of each tissue and reduce error from visual inspection. Li and Lopez (1999) found FE models constructed from MRI to be reliable for cartilage stress analysis with the caveat that a 10% variation in results might be attributed to the manual digitisation.	
Smoothing	During the model development the image was processed with a smoothing filter. If the volume had a minor modification, this could have induced a small error.	
Mesh size	After the appropriate mesh geometry was selected (tetrahedral for bone; hexahedral for soft tissues) an initial element size was chosen and fit to the irregular shaped tissue geometries. This approximate fit is known as tessellation and is a source of error.	A mesh sensitivity analysis was conducted to reduce the errors due to tessellation by determining the most appropriate mesh size.
Tissue Thickness	The resolution of the MRI was set to as small a voxel size as possible (0.29 mm x 0.29 mm x 0.6 mm) to permit visualisation of thin tissues such as cartilage.	
Material Properties	Material models were selected to be consistent with the research questions posed. Material properties for each model could not be obtained from subject-specific tissues, but were selected from the peer-reviewed literature. Errors could have occurred due to a difference between the material properties employed and those of the cadaveric specimen.	To reduce errors associated with material properties, a sensitivity analysis and a ligament tuning process were conducted.

Task	Error Source	Comments
Grood & Suntay Coordinate System	Bony landmarks were picked by visual inspection to match those of the cadaver. Note that the original selection of these landmarks on the cadaver was by palpation, which also could have induced small errors.	The most medial and lateral protuberances were picked for the femoral and tibial, landmarks. Even though an error may have occurred during visual inspection, the position of the tibia with respect to the femur (as calculated within the Grood and Suntay coordinate) of the model matched closely with the cadaver as shown by the identity matrix. To further verify the position of the anatomical landmarks, the distances between each point were calculated compared between the model and the cadaver.
Boundary and Loading conditions	The cadaveric femur and model representation of the femur were both mechanically grounded. The cadaver and model were both constrained in one degree of freedom (sagittal) and unconstrained in all other degrees of freedom. The accuracy for application of axial loads and bending moments were within the errors of defining the coordinate systems.	
Gait data	A subject that anthropometrically matched the cadaver was selected to acquire gait data. However, this was not the same individual from which the MRI and, hence, FE model were created.	In future studies, FE models will be developed for in-vivo subjects who have undergone gait analysis to eliminate this potential error.

Task	Error Source	Comments
Validation	Calibration of the sensor was conducted on a flat surface. However, the cartilage is slightly curved so registration of the transducer to the anatomy in the model is not perfect. It has been reported that measurement errors on the order of 1-4% could occur when using Tekscan sensors (Baer et al. 2005, Brimacombe et al. 2005, Fregly, Sawyer 2003). The sensor was sutured to the corners of the knee capsule to try and minimise movement (Tent stake approach). However, it is possible that the sensor might still have moved during testing.	

Additionally, the patella-femoral joint, iliotibial band, muscles and tendons were not included in the model. Recent research (Kutzner et al., 2010; Hillstrom, et al., 2013) has shown that the muscle tendon systems and inverse dynamic intersegmental forces contribute similar amounts of load to form the joint contact forces. For this reason, developing musculoskeletal models in conjunction with stress models could provide a more comprehensive solution for how contact forces are derived and distributed across the surfaces of the knee joint. In future investigations, a musculoskeletal model will be implemented to generate physiological forces and moments and permit the simulation of surgeries on both osseous and soft tissues.

The asynchronous contractions of the knee musculature, as well as passive tension band contributions to knee stability (iliotibial band), will affect the magnitude and direction of joint contact forces in each compartment. However, in the development of this new joint contact mechanics model, muscle-tendon forces may be considered a confounding variable. Building a subject-specific knee joint model, inclusive of its anatomical complexity, requires appropriate geometries of the anatomical components, mesh structures and sizes, material properties, and boundary conditions. By applying a lump sum axial force and moment, one can focus on validating the contributions of these anatomical structures and perform static equilibrium based techniques to assist with parameterisation, such as ligament tuning. Once a model is



valid at this level, then replacing the lump sum loading conditions with muscle-tendon models makes sense if your research question requires that anatomical detail. Note that one could always apply the magnitude and direction of the contact forces, instead of inverse dynamic intersegmental forces, in a lump sum manner to an FE knee model if this data were available.

Another limitation might be the accuracy of meniscus geometry used in this model, because the edges of the soft tissues were cut to enable smooth mesh creation. Meniscal horn attachments were therefore represented using linear elastic spring elements. Sensitivity analyses of the stiffness and position of the springs that attach the meniscus to the MCL, tibia and to each other could be conducted, to investigate the effect of spring stiffness and position on knee joint contact mechanics. The challenge to represent these meniscal attachments is the lack of information about their function and structural properties (Masouros et al., 2008).

The robot could withstand a maximum load of 380 N and a bending moment of 15Nm. Therefore, the model could only be validated for those *in vitro* loading conditions. Using larger loading values, as experienced during the end of weight acceptance *in vivo* (axial force of 811 N and bending moment of 20 Nm), may result in errors larger than those described in the validation study.

The cadaveric specimen was healthy and had a varus alignment of 1°, which is considered normal. Therefore, malalignment had to be simulated. In addition, the cadaveric cartilage was healthy and smooth and therefore simulated using frictionless contact. Neu et al. (2010) reported an  $r^2 = 0.99$  between OA severity and the coefficient of friction. It is a limitation of this study to have not considered the increase in coefficient of friction associated with the severity of OA. Most patients with malalignment would typically demonstrate some level of OA. In future studies this should be accounted for.

This investigation was conducted in only one position of the gait cycle (end of weight acceptance during the stance phase of gait). Gait data was used from a subject with matching age, alignment, gender, weight and height to the cadaver. In future studies, loads at different phases of the gait cycle, using subject-specific gait data will be

investigated. Although these limitations might influence the absolute values of knee joint contact mechanics, the relative values are not expected to change.

## 6. Case Study

Although the classic HTO is considered a frontal plane wedge-based correction it is possible to perform the correction in all three planes simultaneously. A tri-planar osteotomy is reported to permit such a correction, thereby improving the function of a malaligned and unstable knee (Savarese et al., 2011; Khalilollah, Fouladi and Chinigarzadeh, 2013). The validated FE knee model can be used to simulate such a tri-planar osteotomy to predict knee joint contact mechanics. Standing radiographs or 2D approaches, such as the OASIS software, would not be able to predict the outcome of such a surgery, as they are limited to the frontal plane.

As an example, a 5° wedge was virtually removed in the sagittal and coronal planes from the FE knee model (Figure 6.1). Boundary conditions, mesh sizes and material properties matched those previously employed (Section 3).

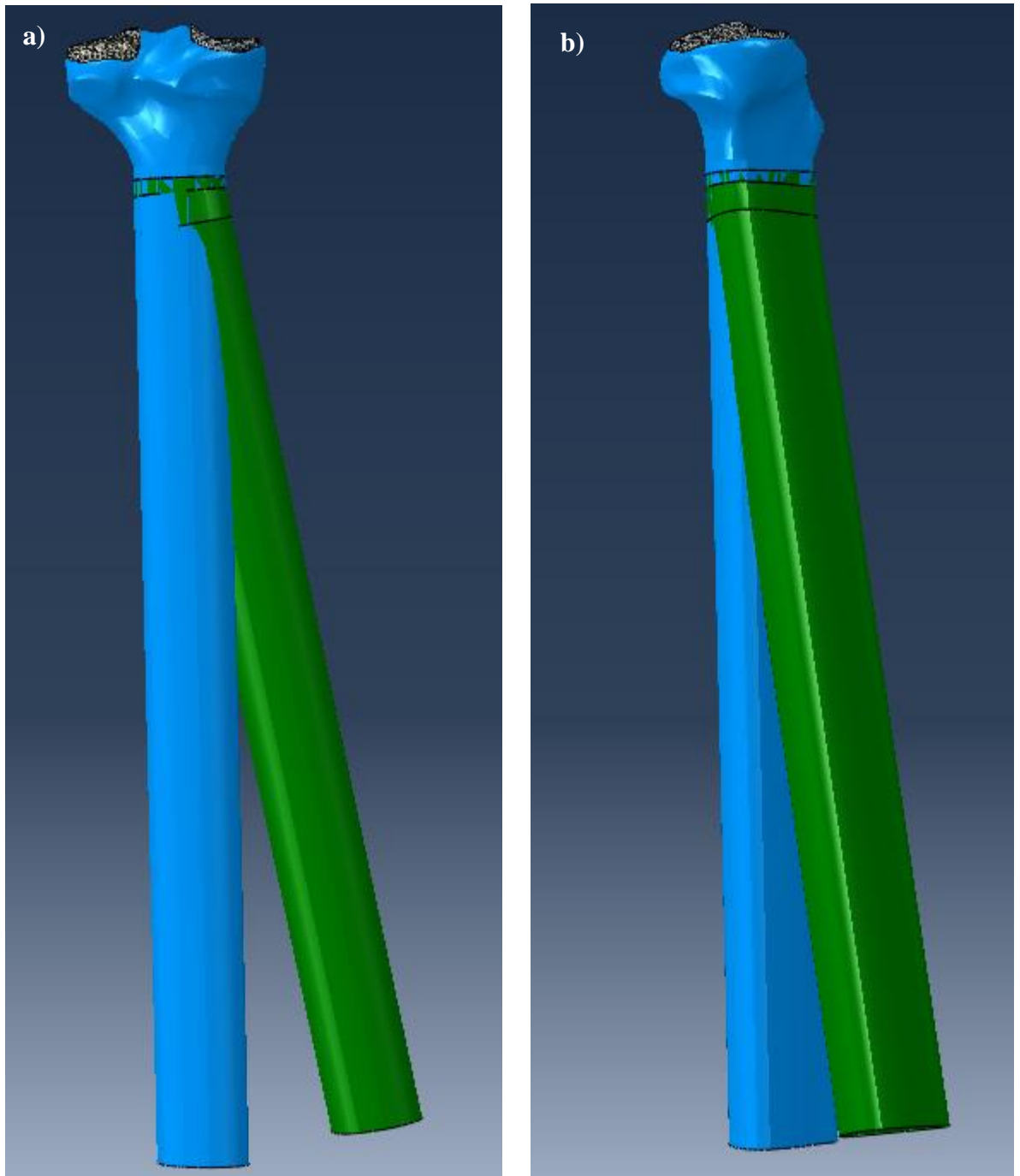


**Figure 6.1: Simulated tri-planar osteotomy a) frontal plane view and b) sagittal plane view. Blue tibia= well aligned knee; Green tibia= knee with 5° malalignment in the sagittal and coronal planes**

With a 5° varus and anterior alignment, the medial contact pressure increased by 60.9%; the medial compartmental force increased from 607.7 N to 1138.5 N, an 87.3% increase; and the medial:lateral force ratio changed from 70%:30% to 100%:0% (Table 6.1).

**Table 6.1: Knee joint contact pressure and force values before and after a 5° varus-anterior tri-planar osteotomy**

	Tri-planar osteotomy			
	Pressure (MPa)		Force (N)	
	Medial	Lateral	Medial	Lateral
Straight	2.82	2.14	607.7	264.3
5° varus 5° anterior	4.54	0	1138.5	2.8

Results of this case study indicate the importance of understanding tri-planar malalignment in order to accurately plan surgical realignment. The FE knee model predicted the outcomes of tri-planar surgery. In the future, this could help surgeons plan knee realignment by tri-planar osteotomy to improve survivorship. 2D surgical planning tools cannot predict such results.

## 7. Conclusions

In this study, a subject-specific FE model of the human knee joint was developed and validated. Sensitivity analyses were conducted to understand how different mesh sizes and material properties affect knee joint contact mechanics. The main objective was to understand how different malalignments influence loading and stress distributions in the tibiofemoral compartments and the relationship between MAD, HKA angle and knee joint contact mechanics.

Virtual osteotomies were conducted from 14° valgus to 16° varus. Knee joint contact mechanics in the aligned and malaligned knees were investigated at 20° flexion to simulate end of weight acceptance during gait.

### 7.1. Hypothesis 1

Knee joint contact mechanics were not substantially influenced by bone properties (2.5%). Contact mechanics were substantially affected by cartilage properties (40%-100% for every 10-20 MPa change) and meniscus properties (3%-7% for every 20 MPa change). The ligament tuning process showed that ligament properties varied widely with flexion angle. Hypothesis 1a, stating that knee joint contact mechanics will vary more with different material properties of soft tissues compared to those of bone, is accepted.

The effect of mesh element sizes on knee joint contact mechanics was investigated. It was found that, for osseous tissues, a mesh size of 3 mm resulted in a 0.29% change in contact pressure compared to the reference mesh (1.5 mm). For soft tissues, a mesh size of 1 mm resulted in a 4.56% change in contact pressure compared to the reference mesh (0.5 mm). Hypothesis 1b, stating that there is a threshold mesh size for bones and soft tissues below which the contact mechanics vary by less than 5% with additional mesh size reduction, is confirmed.

### 7.2. Hypothesis 2

Once the mesh and material property sensitivity analyses were completed, the knee model was validated. Predicted kinetic results were similar to those of the *in vitro* tests.

After normalising the data with maximum force and pressure values, the %FSE between FE-predicted and *in vitro*-measured peak pressures, were 6.67% in the medial and 5.94% in the lateral compartments. The %FSE between normalised FE-predicted and *in vitro*-measured forces was 7.56 % in the medial compartment and 4.48 % in the lateral. Hypothesis 2, stating that tibiofemoral contact mechanics of the *in vitro* experiment and corresponding FE model predictions will agree within 10% for the same boundary conditions, is confirmed.

### 7.3. Hypothesis 3

Virtual osteotomies, spanning from 14° valgus to 16° varus, were conducted and the resulting contact mechanics were investigated. An increase in varus alignment substantially increased contact forces in the medial compartment. An increase in valgus alignment substantially increased contact forces in the lateral compartment. A 6.5° varus alignment led to lift off of the lateral compartment. A similar result was obtained for medial compartment lift off. An MAD of 0 mm resulted in a medial:lateral force ratio of 60%:40%. Minimum peak contact pressure occurred at an MAD of -1.44 mm; minimum peak shear stress occurred at an MAD of 0.7 mm. Therefore, Hypothesis 3a, stating that the HTO geometry that corresponds to an MAD of zero millimetres does not correspond to the minimum contact stress, is confirmed.

A Fujisawa point of 62%, which is targeted by many surgeons, corresponded to a medial:lateral force ratio of 34%:66% for this knee specimen. Minimum contact pressure occurred at an intersection of the MA with the tibial plateau at 51.8% measured from the medial to lateral side. Minimum shear stress occurred at an intersection of the MA with the tibial plateau at 49.1% from medial to lateral. Therefore, Hypothesis 3b, stating that the HTO geometry that corresponds to the Fujisawa point does not correspond to the minimum contact stress, is confirmed.

### 7.4. Hypothesis 4

There was a strong correlation ( $r > 0.94$ ) between MAD, the intersection of the MA with the tibial plateau and knee joint contact mechanics. Therefore, Hypothesis 4, stating that the 3D FE knee model will predict post-operative knee joint mechanics, as evidenced by a correlation between surgical realignment geometry, MAD and knee

joint contact mechanics, is confirmed. Understanding the effect of surgical realignment techniques on knee joint contact mechanics is clinically important to surgeons when making decisions on malalignment correction.

## 7.5. Outcomes of the Study

This study demonstrated the ability of a subject-specific model to predict changes in the magnitude and location of peak pressure and loads within the knee as a function of malalignment. A subject-specific FE knee model was created from the same cadaveric specimen that was used for the *in vitro* investigations to measure contact forces and pressure distribution. Using the same knee in both the computational and *in vitro* studies enabled direct comparison of *in vitro*-measured force and pressure values with FE-predicted ones.

In addition, a tri-planar osteotomy was simulated. The FE knee joint model was capable of predicting contact mechanics for the more complicated tri-planar surgery. This cannot be predicted by standard long leg radiographs or 2D software.

Despite previous studies on the effect of alignment on knee contact mechanics, no investigation to date has optimised malalignment correction nor assessed the effect of malalignment on contact stress in a subject-specific manner. Even though many studies indicate the importance of MAD in the clinical decision-making process, to my knowledge, no one has clarified the relationship between MAD, compartment loading and peak joint stress, which is considered to promote OA onset. There is a general lack of objective criteria to specify the alignment that minimises excessive joint stress. It is important to know the effect of knee alignment on joint pressure distribution in a subject-specific manner, given the wide variation in knee joint morphology and material properties. Such information would help surgeons make an informed decision for knee malalignment correction.

Results obtained in this study refer to the knee joint stress at end of weight acceptance. It is this portion of the gait cycle where the maximum varus thrust, peak ground reaction force and adductory knee moment occurs. The osteotomy geometry that reduces the peak medial compartment stress while not excessively increasing the lateral compartment stress could serve as a target realignment for the surgeon. The effect of HKA angle and MAD upon the subject-specific medial and lateral

compartment stress is illustrated in Figures 4.22-4.24. The compromise between medial and lateral compartment stress as a function of knee joint alignment is clearly indicated in these Figures, and with additional clinical information, is expected to provide the surgeon with a target osteotomy geometry.



## 8. Future Investigations

The subject-specific model developed in this study is a first step towards a more sophisticated model, which will allow the prediction of knee joint contact mechanics during functional activities. The model will include:

- the patella and quadriceps musculo-tendinous forces, as well as hamstrings and gastrocnemius muscles to generate more physiological forces and moments
- a simulation of different knee joint angles during gait to evaluate the effect of surgical realignment
- the use of more sophisticated material property models for soft tissues (cartilage, ligaments and menisci).
- Inclusion of the iliotibial band
- Repeatability study on mechanical tests

Subject-specific *in vivo* gait and functional activity data will then be applied to the model to assess its utility in predicting contact mechanics after surgical reconstruction. Model kinematics could then be compared to *in vivo* fluoroscopy kinematics in order to further validate the model.

The ultimate aim is to create a subject-specific HTO planning tool to improve surgical outcomes. Future research will identify factors that enhance HTO surgical outcomes and bring new insights on how these techniques may be improved for treating knee OA. In addition, more FE models are needed to determine the importance of being subject specific as opposed to generic. These models will be categorised by size, age and gender. Joint contact mechanics in these different knee models will be used to evaluate the feasibility of having a generalised computer method to predict pre- and post-surgical joint stress to improve surgical planning.

## References

1. Adouni, M. & Shirazi-Adl, A. 2014, "Partitioning of knee joint internal forces in gait is dictated by the knee adduction angle and not by the knee adduction moment", *Journal of Biomechanics*, vol. 47, no. 7, pp. 1696-1703.
2. Adouni, M., Shirazi-Adl, A. & Shirazi, R. 2012, "Computational biodynamics of human knee joint in gait: from muscle forces to cartilage stresses", *Journal of Biomechanics*, vol. 45, no. 12, pp. 2149-2156.
3. Aglietti, P., Baldini, A., Buzzi, R., Lup, D. & De Luca, L. 2005, "Comparison of Mobile-Bearing and Fixed-Bearing Total Knee Arthroplasty: A Prospective Randomized Study", *The Journal of Arthroplasty*, vol. 20, no. 2, pp. 145-153.
4. Aglietti, P., Buzzi, R., Vena, L.M., Baldini, A. & Mondaini, A. 2003, "High tibial valgus osteotomy for medial gonarthrosis: a 10- to 21-year study", *The Journal of Knee Surgery*, vol. 16, no. 1, pp. 21-26.
5. Agneskirchner, J.D., Freiling, D., Hurschler, C. & Lobenhoffer, P. 2006, "Primary stability of four different implants for opening wedge high tibial osteotomy", *Knee Surgery, Sports Traumatology, Arthroscopy*, vol. 14, no. 3, pp. 291-300.
6. Agneskirchner, J.D., Hurschler, C., Wrann, C.D. & Lobenhoffer, P. 2007, "The effects of valgus medial opening wedge high tibial osteotomy on articular cartilage pressure of the knee: a biomechanical study", *Arthroscopy: The Journal of Arthroscopic & Related Surgery*, vol. 23, no. 8, pp. 852-861.
7. Agneskirchner, J., Hurschler, C., Stukenborg-Colsman, C., Imhoff, A. & Lobenhoffer, P. 2004, "Effect of High Tibial Flexion Osteotomy on Cartilage Pressure and Joint Kinematics: A Biomechanical Study in Human Cadaveric Knees", *Archives of Orthopaedic and Trauma Surgery*, vol. 124, no. 9, pp. 575-584.
8. Ahlback, S. 1968, "Osteoarthritis of the knee. A radiographic investigation", *Acta Radiologica: Diagnosis*, vol. 277, pp. 7-72.
9. Akbar, M., Farahmand, F., Jafari, A. & Saadat Foumani, M. 2012, "A Detailed and Validated Three Dimensional Dynamic Model of the Patellofemoral Joint", *Journal of Biomechanical Engineering*, vol. 134, no. 4, pp. no pagination.
10. Akizuki, S., Shibakawa, A., Takizawa, T., Yamazaki, I. & Horiuchi, H. 2008, "The long-term outcome of high tibial osteotomy A ten-to 20-year follow-up", *Journal of Bone & Joint Surgery, British Volume*, vol. 90, no. 5, pp. 592-596.
11. Alonso-Vázquez, A., Lauge-Pedersen, H., Lidgren, L. & Taylor, M. 2004, "Initial stability of ankle arthrodesis with three-screw fixation. A finite element analysis", *Clinical Biomechanics*, vol. 19, no. 7, pp. 751-759.

12. Amadi, H.O., Gupte, C.M., Lie, D.T., McDermott, I.D., Amis, A.A. & Bull, A.M. 2008, "A biomechanical study of the meniscomfemoral ligaments and their contribution to contact pressure reduction in the knee", *Knee Surgery, Sports Traumatology, Arthroscopy*, vol. 16, no. 11, pp. 1004-1008.
13. Amendola, A., Rorabeck, C.H., Bourne, R.B. & Apyan, P.M. 1989, "Total knee arthroplasty following high tibial osteotomy for osteoarthritis", *The Journal of Arthroplasty*, vol. 4, pp. S11-S17.
14. Amendola, L., Fosco, M., Cenni, E. & Tigani, D. 2010, "Knee joint arthroplasty after tibial osteotomy", *International Orthopaedics*, vol. 34, no. 2, pp. 289-295.
15. Amiri, S., Cooke, D., Kim, I. & Wyss, U. 2007, "Mechanics of the passive knee joint. Part 2: interaction between the ligaments and the articular surfaces in guiding the joint motion", *Proceedings of the Institution of Mechanical Engineers, Part H: Journal of Engineering in Medicine*, vol. 221, no. 8, pp. 821-832.
16. Amis, A.A. 2012, "Biomechanics of High Tibial Osteotomy", *Knee Surgery, Sports Traumatology, Arthroscopy*, vol. 21, no. 1, pp. 197-205.
17. Amis, A., Bull, A., Gupte, C., Hijazi, I., Race, A. & Robinson, J. 2003, "Biomechanics of the PCL and related structures: posterolateral, posteromedial and meniscomfemoral ligaments", *Knee Surgery, Sports Traumatology, Arthroscopy*, vol. 11, no. 5, pp. 271-281.
18. Amis, A.A., Bull, A.M. & Lie, D.T. 2005, "Biomechanics of rotational instability and anatomic anterior cruciate ligament reconstruction", *Operative Techniques in Orthopaedics*, vol. 15, no. 1, pp. 29-35.
19. Anderson, A.E., Peters, C.L., Tuttle, B.D. & Weiss, J.A. 2005, "Subject-specific finite element model of the pelvis: development, validation and sensitivity studies", *Transactions of the ASME-K-Journal of Biomechanical Engineering*, vol. 127, no. 3, pp. 364-373.
20. Andrews, S., Shrive, N. & Ronsky, J. 2011, "The shocking truth about meniscus", *Journal of Biomechanics*, vol. 44, no. 16, pp. 2737-2740.
21. Andriacchi, T.P., Lang, P.L., Alexander, E.J. & Hurwitz, D.E. 2000, "Methods for evaluating the progression of osteoarthritis", *Development*, vol. 37, no. 2, pp. 163-170.
22. Andriacchi, T.P., Mikosz, R.P., Hampton, S.J. & Galante, J.O. 1983, "Model studies of the stiffness characteristics of the human knee joint", *Journal of Biomechanics*, vol. 16, no. 1, pp. 23-29.
23. Andriacchi, T.P., Mündermann, A., Smith, R.L., Alexander, E.J., Dyrby, C.O. & Koo, S. 2004, "A framework for the in vivo pathomechanics of osteoarthritis at the knee", *Annals of Biomedical Engineering*, vol. 32, no. 3, pp. 447-457.

24. Andriacchi, T.P., Briant, P.L., Beville, S.L. & Koo, S. 2006, "Rotational changes at the knee after ACL injury cause cartilage thinning", *Clinical Orthopaedics and Related Research*, vol. 442, pp. 39-44.
25. Andriacchi, T.P. 1994, "Dynamics of knee malalignment", *The Orthopedic clinics of North America*, vol. 25, no. 3, pp. 395-403.
26. arcOGEN Consortium, arcOGEN Collaborators, Zeggini, E., Panoutsopoulou, K., Southam, L., Rayner, N.W., Day-Williams, A.G., Lopes, M.C., Boraska, V., Esko, T., Evangelou, E., Hoffman, A., Houwing-Duistermaat, J.J., Ingvarsson, T., Jonsdottir, I., Jonsson, H., Kerkhof, H.J., Kloppenburg, M., Bos, S.D., Mangino, M., Metrustry, S., Slagboom, P.E., Thorleifsson, G., Raine, E.V., Ratnayake, M., Ricketts, M., Beazley, C., Blackburn, H., Bumpstead, S., Elliott, K.S., Hunt, S.E., Potter, S.C., Shin, S.Y., Yadav, V.K., Zhai, G., Sherburn, K., Dixon, K., Arden, E., Aslam, N., Battley, P.K., Carluke, I., Doherty, S., Gordon, A., Joseph, J., Keen, R., Koller, N.C., Mitchell, S., O'Neill, F., Paling, E., Reed, M.R., Rivadeneira, F., Swift, D., Walker, K., Watkins, B., Wheeler, M., Birrell, F., Ioannidis, J.P., Meulenbelt, I., Metspalu, A., Rai, A., Salter, D., Stefansson, K., Stykarsdottir, U., Uitterlinden, A.G., van Meurs, J.B., Chapman, K., Deloukas, P., Ollier, W.E., Wallis, G.A., Arden, N., Carr, A., Doherty, M., McCaskie, A., Willkinson, J.M., Ralston, S.H., Valdes, A.M., Spector, T.D. & Loughlin, J. 2012, "Identification of new susceptibility loci for osteoarthritis (arcOGEN): a genome-wide association study", *Lancet*, vol. 380, no. 9844, pp. 815-823.
27. Armstrong, C.G., Lai, W.M. & Mow, V.C. 1984, "An analysis of the unconfined compression of articular cartilage", *Journal of Biomechanical Engineering*, vol. 106, no. 2, pp. 165-173.
28. Arokoski, J., Jurvelin, J., Väänänen, U. & Helminen, H. 2000, "Normal and pathological adaptations of articular cartilage to joint loading", *Scandinavian Journal of Medicine & Science in Sports*, vol. 10, no. 4, pp. 186-198.
29. Arthritis Research UK 2014, 01/05/2014-last update, *Osteoarthritis of the knee* [Homepage of Arthritis Research UK], [Online]. Available: <http://www.arthritisresearchuk.org/arthritis-information/conditions/osteoarthritis/which-joints-are-affected/knees.aspx> [2014, 06/24].
30. Babis, G.C., An, K.N., Chao, E.Y.S., Larson, D.R., Rand, J.A. & Sim, F.H. 2008, "Upper tibia osteotomy: long term results—realignment analysis using OASIS computer software", *Journal of Orthopaedic Science*, vol. 13, no. 4, pp. 328-334.
31. Bae, D., Song, S. & Yoon, K. 2009, "Closed-wedge high tibial osteotomy using computer-assisted surgery compared to the conventional technique", *Journal of Bone & Joint Surgery, British Volume*, vol. 91, no. 9, pp. 1164-1171.

32. Bae, J.Y., Park, K.S., Seon, J.K., Jeon, I. & Song, E.K. 2012, "Biomechanical analysis of the effects of medial meniscectomy on degenerative osteoarthritis", *Medical & Biological Engineering & Computing*, vol. 50, no. 1, pp. 53-60.
33. Baer, T., Pederson, D., Rudert, M., Kallemeyn, N., Grosland, N. & Brown, T. 2005, "Calibration and monitoring of piezoresistive contact stress sensor arrays using a traveling pressure wave protocol", *Proceedings of the 20th International Society of Biomechanics*. International Society of Biomechanics, Cleveland, 31/07-05/08.
34. Baldwin, M.A., Clary, C.W., Fitzpatrick, C.K., Deacy, J.S., Maletsky, L.P. & Rullkoetter, P.J. 2011, "Dynamic finite element knee simulation for evaluation of knee replacement mechanics", *Journal of Biomechanics*, vol. 45, no. 3, pp. 474-483.
35. Barrios, J.A., Davis, I.S., Higginson, J.S. & Royer, T.D. 2009, "Lower extremity walking mechanics of young individuals with asymptomatic varus knee alignment", *Journal of Orthopaedic Research*, vol. 27, no. 11, pp. 1414-1419.
36. Beillas, P., Papaioannou, G., Tashman, S. & Yang, K.H. 2004, "A new method to investigate in vivo knee behavior using a finite element model of the lower limb", *Journal of Biomechanics*, vol. 37, no. 7, pp. 1019-1030.
37. Bellemans, J., Colyn, W., Vandenuecker, H. & Victor, J. 2012, "The Chitranjan Ranawat Award: is neutral mechanical alignment normal for all patients? The concept of constitutional varus", *Clinical Orthopaedics and Related Research*, vol. 470, no. 1, pp. 45-53.
38. Bendjaballah, M.Z., Shirazi-Adl, A. & Zukor, D.J. 1995, "Biomechanics of the human knee joint in compression: reconstruction, mesh generation and finite element analysis", *The Knee*, vol. 2, no. 2, pp. 69-79.
39. Bendjaballah, M.Z., Shirazi-Adl, A. & Zukor, D. 1997, "Finite element analysis of human knee joint in varus-valgus", *Clinical Biomechanics*, vol. 12, no. 3, pp. 139-148.
40. Berman, A.T., Bosacco, S.J., Kjrshner, S. & Avolio Jr, A. 1991, "Factors influencing long-term results in high tibial osteotomy", *Clinical Orthopaedics and Related Research*, vol. 272, no. 272, pp. 192-198.
41. Bhatnagar, T. & Jenkyn, T.R. 2010, "Internal kinetic changes in the knee due to high tibial osteotomy are well-correlated with change in external adduction moment: An osteoarthritic knee model", *Journal of Biomechanics*, vol. 43, no. 12, pp. 2261-2266.
42. Bi, X., Yang, X., Bostrom, M.P.G. & Camacho, N.P. 2006, "Fourier transform infrared imaging spectroscopy investigations in the pathogenesis and repair of cartilage", *Biochimica et Biophysica Acta (BBA)-Biomembranes*, vol. 1758, no. 7, pp. 934-941.

43. Billings, A., Scott, D.F., Camargo, M.P. & Hofmann, A.A. 2000, "High Tibial Osteotomy with a Calibrated Osteotomy Guide, Rigid Internal Fixation, and Early Motion. Long-Term Follow-up", *The Journal of Bone & Joint Surgery*, vol. 82, no. 1, pp. 70-79.
44. Blankevoort, L., Kuiper, J.H., Huiskes, R. & Grootenboer, H.J. 1991, "Articular contact in a three-dimensional model of the knee", *Journal of Biomechanics*, vol. 24, no. 11, pp. 1019-1031.
45. Blankevoort, L. & Huiskes, R. 1996, "Validation of a three-dimensional model of the knee", *Journal of Biomechanics*, vol. 29, no. 7, pp. 955-961.
46. Blecha, L.D., Zambelli, P.Y., Ramaniraka, N.A., Bourban, P.E., Manson, J.A. & Pioletti, D.P. 2005, "How plate positioning impacts the biomechanics of the open wedge tibial osteotomy; A finite element analysis", *Computer Methods in Biomechanics and Biomedical Engineering*, vol. 8, no. 5, pp. 307-313.
47. Bonnet, C.S., Williams, A.S., Gilbert, S.J., Harvey, A.K., Evans, B.A. & Mason, D.J. 2013, "AMPA/kainate glutamate receptors contribute to inflammation, degeneration and pain related behaviour in inflammatory stages of arthritis", *Annals of the Rheumatic Diseases*, vol. 0, pp. 1-10.
48. Bonnin, M.P., Laurent, J., Zadegan, F., Badet, R., Archbold, H.P. & Servien, E. 2013, "Can patients really participate in sport after high tibial osteotomy?", *Knee Surgery, Sports Traumatology, Arthroscopy*, vol. 21, no. 1, pp. 64-73.
49. Börjesson, M., Weidenhielm, L., Mattsson, E. & Olsson, E. 2005, "Gait and clinical measurements in patients with knee osteoarthritis after surgery: a prospective 5-year follow-up study", *The Knee*, vol. 12, no. 2, pp. 121-127.
50. Borrelli Jr, J., Zhu, Y., Burns, M., Sandell, L. & Silva, M.J. 2004, "Cartilage tolerates single impact loads of as much as half the joint fracture threshold", *Clinical Orthopaedics and Related Research*, vol. 426, pp. 266-273.
51. Bowers, M.E., Tung, G.A., Fleming, B.C., Crisco, J.J. & Rey, J. 2007, "Quantification of meniscal volume by segmentation of 3T magnetic resonance images", *Journal of Biomechanics*, vol. 40, no. 12, pp. 2811-2815.
52. Bratianu, C., Rinderu, P. & Gruionu, L. 2004, "A 3D finite element model of a knee for joint contact stress analysis during sport activities", *Key Engineering Materials*, vol. 261, pp. 513-518.
53. Brimacombe, J.M., Anglin, C., Hodgson, A.J. & Wilson, D.R. 2005, "Validation of calibration techniques for tekscan pressure sensors", *Proceedings of International Society of Biomechanics XXth congress*. International Society of Biomechanics, Cleveland, 31/05-05/08.
54. Broom, N.D. & Marra, D.L. 1986, "Ultrastructural evidence for fibril-to-fibril associations in articular cartilage and their functional implication.", *Journal of Anatomy*, vol. 146, pp. 185-200.

55. Brouwer, G., Van Tol, A., Bergink, A., Belo, J., Bernsen, R., Reijman, M., Pols, H. & Bierma-Zeinstra, S. 2007, "Association between valgus and varus alignment and the development and progression of radiographic osteoarthritis of the knee", *Arthritis & Rheumatism*, vol. 56, no. 4, pp. 1204-1211.
56. Brown, G.A. & Amendola, A. 2012, "Radiographic Evaluation and Preoperative Planning for High Tibial Osteotomies", *Operative Techniques in Sports Medicine*, vol. 20, no. 1, pp. 93-102.
57. Bruns, J., Volkmer, M. & Luessenhop, S. 1993, "Pressure distribution at the knee joint", *Archives of Orthopaedic and Trauma Surgery*, vol. 113, no. 1, pp. 12-19.
58. Buckwalter, J. & Mankin, H. 1998, "Articular cartilage: degeneration and osteoarthritis, repair, regeneration, and transplantation.", *Instructional Course Lectures*, vol. 47, pp. 487-504.
59. Buckwalter, J.A., Saltzman, C. & Brown, T. 2004, "The impact of osteoarthritis: implications for research", *Clinical Orthopaedics and Related Research*, vol. 427, pp. S6-S15.
60. Burstein, A. & Wright, T. 2001, "Basic biomechanics", *Surgery of the Knee*, vol. 1, pp. 215-231.
61. Butler, D.L., Kay, M.D. & Stouffer, D.C. 1986, "Comparison of material properties in fascicle-bone units from human patellar tendon and knee ligaments", *Journal of Biomechanics*, vol. 19, no. 6, pp. 425-432.
62. Carter, D.R. & Wong, M. 2003, "Modelling cartilage mechanobiology", *Philosophical transactions of the Royal Society of London. Series B, Biological sciences*, vol. 358, no. 1437, pp. 1461-1471.
63. Chang, W. & Bennett, C.H. 2005, "High tibial osteotomy and related surgeries", *Current Opinion in Orthopaedics*, vol. 16, no. 2, pp. 77-81.
64. Chantarapanich, N., Nanakorn, P., Chernchujit, B. & Sitthiseripratip, K. 2009, "A Finite Element Study of Stress Distributions in Normal and Osteoarthritic Knee Joints", *Journal of the Medical Association of Thailand*, vol. 92, no. 6, pp. 97-103.
65. Chao, E. 2003, "Graphic-based musculoskeletal model for biomechanical analyses and animation", *Medical Engineering & Physics*, vol. 25, no. 3, pp. 201-212.
66. Chao, E.Y. & Sim, F.H. 1995, "Computer-aided preoperative planning in knee osteotomy.", *The Iowa Orthopaedic Journal*, vol. 15, pp. 4-18.
67. Chao, E., Neluhani, E., Hsu, R. & Paley, D. 1994, "Biomechanics of malalignment.", *The Orthopedic Clinics of North America*, vol. 25, no. 3, pp. 379-386.

68. Chen, C., Bhargava, M., Lin, P.M. & Torzilli, P.A. 2003, "Time, stress, and location dependent chondrocyte death and collagen damage in cyclically loaded articular cartilage", *Journal of Orthopaedic Research*, vol. 21, no. 5, pp. 888-898.
69. Chen, C., Burton-Wurster, N., Lust, G., Bank, R.A. & Tekoppele, J.M. 1999, "Compositional and metabolic changes in damaged cartilage are peak-stress, stress-rate, and loading-duration dependent", *Journal of Orthopaedic Research*, vol. 17, no. 6, pp. 870-879.
70. Chen, W.P., Tai, C.L., Shih, C.H., Hsieh, P.H., Leou, M.C. & Lee, M.S. 2004, "Selection of fixation devices in proximal femur rotational osteotomy: clinical complications and finite element analysis", *Clinical Biomechanics*, vol. 19, no. 3, pp. 255-262.
71. Choi, K., Kuhn, J.L., Ciarelli, M.J. & Goldstein, S.A. 1990, "The elastic moduli of human subchondral, trabecular, and cortical bone tissue and the size-dependency of cortical bone modulus", *Journal of Biomechanics*, vol. 23, no. 11, pp. 1103-1113.
72. Clements, K., Bee, Z., Crossingham, G., Adams, M. & Sharif, M. 2001, "How severe must repetitive loading be to kill chondrocytes in articular cartilage?", *Osteoarthritis and Cartilage*, vol. 9, no. 5, pp. 499-507.
73. Coggon, D., Croft, P., Kellingray, S., Barrett, D., McLaren, M. & Cooper, C. 2000, "Occupational physical activities and osteoarthritis of the knee", *Arthritis & Rheumatism*, vol. 43, no. 7, pp. 1443-1449.
74. Completo, A., Fonseca, F. & Simoes, J.A. 2007a, "Finite element and experimental cortex strains of the intact and implanted tibia", *Transactions-American Society of Mechanical Engineers Journal of Biomechanical Engineering*, vol. 129, no. 5, pp. 791.
75. Completo, A., Fonseca, F. & Simoes, J. 2007b, "Experimental validation of intact and implanted distal femur finite element models", *Journal of Biomechanics*, vol. 40, no. 11, pp. 2467-2476.
76. Cooke, T.D.V., Scudamore, A. & Greer, W. 2003, "Varus knee osteoarthritis: whence the varus?", *Journal of Rheumatology*, vol. 30, no. 12, pp. 2521-2523.
77. Cooke, T.D.V., Sled, E.A. & Scudamore, R.A. 2007, "Frontal plane knee alignment: a call for standardized measurement", *Journal of Rheumatology*, vol. 34, no. 9, pp. 1796-1801.
78. Cooke, T.D., Li, J. & Scudamore, R.A. 1994, "Radiographic assessment of bony contributions to knee deformity", *The Orthopedic Clinics of North America*, vol. 25, no. 3, pp. 387-393.



79. Coventry, M.B. 1973, "Osteotomy about the knee for degenerative and rheumatoid arthritis indications, operative technique, and results", *The Journal of Bone and Joint Surgery (American)*, vol. 55, no. 1, pp. 23-48.
80. Coventry, M.B. 1965, "Osteotomy of the Upper Portion of the Tibia for Degenerative Arthritis of the Knee a Preliminary Report", *The Journal of Bone and Joint Surgery (American)*, vol. 47, no. 5, pp. 984-990.
81. Coventry, M.B., Ilstrup, D.M. & Wallrichs, S.L. 1993, "Proximal tibial osteotomy. A critical long-term study of eighty-seven cases", *The Journal of Bone and Joint Surgery*, vol. 75, no. 2, pp. 196-201.
82. Coventry, M.B. 1979, "Upper tibial osteotomy for gonarthrosis. The evolution of the operation in the last 18 years and long term results", *The Orthopedic Clinics of North America*, vol. 10, no. 1, pp. 191-210.
83. Cushnaghan, J. & Dieppe, P. 1991, "Study of 500 patients with limb joint osteoarthritis. I. Analysis by age, sex, and distribution of symptomatic joint sites.", *Annals of the Rheumatic Diseases*, vol. 50, no. 1, pp. 8-13.
84. Dar, F. & Aspden, R. 2003, "A finite element model of an idealized diarthrodial joint to investigate the effects of variation in the mechanical properties of the tissues", *Proceedings of the Institution of Mechanical Engineers, Part H: Journal of Engineering in Medicine*, vol. 217, no. 5, pp. 341-348.
85. De Peretti, F., Lacroix, R., Bourgeon, A., Argenson, C. & Richelme, H. 1983, "Geometry of the facies articularis superior tibiae and rotation of the knee", *Surgical and Radiologic Anatomy*, vol. 5, no. 1, pp. 3-7.
86. Demiray, H. 1972, "A note on the elasticity of soft biological tissues", *Journal of Biomechanics*, vol. 5, no. 3, pp. 309-311.
87. Department of Health 2006, 7 December 2006-last update, *NHS reference costs 2005-06* [Homepage of Department of Health], [Online]. Available: [http://webarchive.nationalarchives.gov.uk/+/www.dh.gov.uk/en/publicationsandstatistics/publications/publicationspolicyandguidance/DH\\_062884](http://webarchive.nationalarchives.gov.uk/+/www.dh.gov.uk/en/publicationsandstatistics/publications/publicationspolicyandguidance/DH_062884) [2010, September/25].
88. Dettoni, F., Bonasia, D.E., Castoldi, F., Bruzzone, M., Blonna, D. & Rossi, R. 2010, "High tibial osteotomy versus unicompartmental knee arthroplasty for medial compartment arthrosis of the knee: a review of the literature", *The Iowa Orthopaedic Journal*, vol. 30, pp. 131-140.
89. Donahue, T.L.H., Hull, M.L., Rashid, M.M. & Jacobs, C.R. 2002, "A finite element model of the human knee joint for the study of tibio-femoral contact", *Journal of Biomechanical Engineering*, vol. 124, no. 3, pp. 273-280.
90. Donzelli, P.S., Spilker, R.L., Ateshian, G.A. & Mow, V.C. 1999, "Contact analysis of biphasic transversely isotropic cartilage layers and correlations with tissue failure", *Journal of Biomechanics*, vol. 32, no. 10, pp. 1037-1047.

91. Dorsey, W.O.P., Miller, B.S., Tadjé, J.P. & Bryant, C.R. 2006, "The stability of three commercially available implants used in medial opening wedge high tibial osteotomy", *Journal of Knee Surgery*, vol. 19, no. 2, pp. 95-98.
92. Dowd, G.S.E., Somayaji, H.S. & Uthukuri, M. 2006, "High tibial osteotomy for medial compartment osteoarthritis", *The Knee*, vol. 13, no. 2, pp. 87-92.
93. Dugdale, T.W., Noyes, F.R. & Styer, D. 1992, "Preoperative planning for high tibial osteotomy: the effect of lateral tibiofemoral separation and tibiofemoral length", *Clinical Orthopaedics and Related Research*, vol. 274, pp. 248-264.
94. Dunbar, W., Un, K., Donzelli, P. & Spilker, R. 2001, "An evaluation of three-dimensional diarthrodial joint contact using penetration data and the finite element method", *Transaction-American Society of Mechanical Engineers Journal of Biomechanical Engineering*, vol. 123, no. 4, pp. 333-340.
95. Eberhardt, A., Keer, L., Lewis, J. & Vithoontien, V. 1990, "An analytical model of joint contact.", *Journal of Biomechanical Engineering*, vol. 112, no. 4, pp. 407-413.
96. Eckhoff, D.G., Dwyer, T.F., Bach, J.M., Spitzer, V.M. & Reinig, K.D. 2001, "Three-dimensional morphology of the distal part of the femur viewed in virtual reality", *The Journal of Bone & Joint Surgery*, vol. 83, no. 1, pp. S43-50.
97. Efe, T., Heyse, T., Boese, C., Timmesfeld, N., Fuchs-Winkelmann, S., Schmitt, J., Theisen, C. & Schofer, M. 2010, "TKA following high tibial osteotomy versus primary TKA-a matched pair analysis", *BMC Musculoskeletal Disorders*, vol. 11, no. 1, pp. 1-6.
98. El-Azab, H.M., Morgenstern, M., Ahrens, P., Schuster, T., Imhoff, A.B. & Lorenz, S.G.F. 2011, "Limb alignment after open-wedge high tibial osteotomy and its effect on the clinical outcome", *Orthopedics*, vol. 34, no. 10, pp. 1-8.
99. Englund, M. 2010, "The role of biomechanics in the initiation and progression of OA of the knee", *Best Practice & Research Clinical Rheumatology*, vol. 24, no. 1, pp. 39-46.
100. Esenkaya, I., Misirlioglu, M., Kelestemur, M.H., Elmali, N. & Fadillioglu, E. 2007, "Biomechanical evaluation of different fixation plates in medial opening upper tibial osteotomy", *The Knee*, vol. 14, no. 1, pp. 46-50.
101. Federico, S., La Rosa, G., Herzog, W. & Wu, J.Z. 2004, "Effect of fluid boundary conditions on joint contact mechanics and applications to the modeling of osteoarthritic joints.", *Journal of Biomechanical Engineering*, vol. 126, no. 2, pp. 220-225.
102. Fithian, D., Schmidt, M., Ratcliffe, A. & Mow, V. 1989, "Human meniscus tensile properties: regional variation and biochemical correlation", *Transactions of the Orthopedic Research Society*, vol. 35, pp. 205-217.

103. Flecher, X., Parratte, S., Aubaniac, J.M. & Argenson, J.N.A. 2006, "A 12-28-year followup study of closing wedge high tibial osteotomy", *Clinical Orthopaedics and Related Research*, vol. 452, pp. 91-96.
104. Floerkemeier, S., Staubli, A.E., Schroeter, S., Goldhahn, S. & Lobenhoffer, P. 2013, "Outcome after high tibial open-wedge osteotomy: a retrospective evaluation of 533 patients", *Knee Surgery, Sports Traumatology, Arthroscopy*, vol. 21, no. 1, pp. 170-180.
105. Foroughi, N., Smith, R. & Vanwanseele, B. 2009, "The association of external knee adduction moment with biomechanical variables in osteoarthritis: a systematic review", *The Knee*, vol. 16, no. 5, pp. 303-309.
106. Fox, A.J.S., Bedi, A. & Rodeo, S.A. 2009, "The basic science of articular cartilage: structure, composition, and function", *Sports Health: A Multidisciplinary Approach*, vol. 1, no. 6, pp. 461-468.
107. Fragomen, A.T., Ilizarov, S., Blyakher, A. & Rozbruch, S.R. 2005, "Proximal tibial osteotomy for medial compartment osteoarthritis of the knee using the Ilizarov Taylor spatial frame", *Techniques in Knee Surgery*, vol. 4, no. 3, pp. 173-185.
108. Freeman, M., Swanson, S. & Todd, R. 1973, "Total replacement of the knee using the Freeman-Swanson knee prosthesis", *Clinical Orthopaedics and Related Research*, vol. 94, pp. 153-170.
109. Fregly, B.J., Reinbolt, J.A., Rooney, K.L., Mitchell, K.H. & Chmielewski, T.L. 2007, "Design of patient-specific gait modifications for knee osteoarthritis rehabilitation", *Biomedical Engineering, IEEE Transactions on*, vol. 54, no. 9, pp. 1687-1695.
110. Fregly, B.J. & Sawyer, W.G. 2003, "Estimation of discretization errors in contact pressure measurements", *Journal of Biomechanics*, vol. 36, no. 4, pp. 609-613.
111. Frost, H.M. 1994, "Wolff's Law and bone's structural adaptations to mechanical usage: an overview for clinicians", *The Angle Orthodontist*, vol. 64, no. 3, pp. 175-188.
112. Fu, D., Li, G., Chen, K., Zhao, Y., Hua, Y. & Cai, Z. 2013, "Comparison of High Tibial Osteotomy and Unicompartmental Knee Arthroplasty in the Treatment of Unicompartmental Osteoarthritis: A Meta-Analysis", *The Journal of Arthroplasty*, vol. 28, no. 5, pp. 759-765.
113. Fujisawa, Y., Masuhara, K. & Shiomi, S. 1979, "The effect of high tibial osteotomy on osteoarthritis of the knee. An arthroscopic study of 54 knee joints.", *The Orthopedic clinics of North America*, vol. 10, no. 3, pp. 585-608.

114. Fukubayashi, T. & Kurosawa, H. 1980, "The contact area and pressure distribution pattern of the knee: a study of normal and osteoarthrotic knee joints", *Acta Orthopaedica*, vol. 51, no. 1-6, pp. 871-879.
115. Fung, Y. 1967, "Elasticity of soft tissues in simple elongation", *American Journal of Physiology*, vol. 213, no. 6, pp. 1532-1544.
116. Gardiner, J.C. & Weiss, J.A. 2003, "Subject-specific finite element analysis of the human medial collateral ligament during valgus knee loading", *Journal of Orthopaedic Research*, vol. 21, no. 6, pp. 1098-1106.
117. Gasser, T.C., Ogden, R.W. & Holzapfel, G.A. 2006, "Hyperelastic modelling of arterial layers with distributed collagen fibre orientations", *Journal of the Royal Society Interface*, vol. 3, no. 6, pp. 15-35.
118. Giagounidis, E. & Sell, S. 1999, "High tibial osteotomy: factors influencing the duration of satisfactory function", *Archives of Orthopaedic and Trauma Surgery*, vol. 119, no. 7, pp. 445-449.
119. Godest, A., Beaugonin, M., Haug, E., Taylor, M. & Gregson, P. 2002, "Simulation of a knee joint replacement during a gait cycle using explicit finite element analysis", *Journal of Biomechanics*, vol. 35, no. 2, pp. 267-275.
120. Griffin, T.M. & Guilak, F. 2005, "The role of mechanical loading in the onset and progression of osteoarthritis", *Exercise and Sport Sciences Reviews*, vol. 33, no. 4, pp. 195-200.
121. Grood, E.S. & Suntay, W.J. 1983, "A joint coordinate system for the clinical description of three-dimensional motions: application to the knee", *Journal of Biomechanical Engineering*, vol. 105, no. 2, pp. 136-144.
122. Gross, K.D. & Hillstrom, H.J. 2008, "Noninvasive devices targeting the mechanics of osteoarthritis", *Rheumatic diseases clinics of North America*, vol. 34, no. 3.
123. Gstöttner, M., Pedross, F., Liebensteiner, M. & Bach, C. 2008, "Long-term outcome after high tibial osteotomy", *Archives of Orthopaedic and Trauma Surgery*, vol. 128, no. 1, pp. 111-115.
124. Guccione, A.A., Felson, D.T., Anderson, J.J., Anthony, J.M., Zhang, Y., Wilson, P.W., Kelly-Hayes, M., Wolf, P.A., Kreger, B.E. & Kannel, W.B. 1994, "The effects of specific medical conditions on the functional limitations of elders in the Framingham Study.", *American Journal of Public Health*, vol. 84, no. 3, pp. 351-358.
125. Guess, T.M., Thiagarajan, G., Kia, M. & Mishra, M. 2010, "A subject specific multibody model of the knee with menisci", *Medical Engineering & Physics*, vol. 32, no. 5, pp. 505-515.

126. Guo, H., Maher, S.A. & Spilker, R.L. 2013, "Biphasic finite element contact analysis of the knee joint using an augmented Lagrangian method", *Medical Engineering & Physics*, vol. 35, no. 9, pp. 1313-1320.
127. Guo, Y., Zhang, X. & Chen, W. 2009, "Three-Dimensional Finite Element Simulation of Total Knee Joint in Gait Cycle", *Acta Mechanica Solida Sinica*, vol. 22, no. 4, pp. 347-351.
128. Guo, L.X., Wang, Z.W., Zhang, Y.M., Lee, K.K., Teo, E.C., Li, H. & Wen, B.C. 2009, "Material property sensitivity analysis on resonant frequency characteristics of the human spine", *Journal of Applied Biomechanics*, vol. 25, no. 1, pp. 64-72.
129. Gupta, H., Dahiya, V., Vasdev, A. & Rajgopal, A. 2013, "Outcomes of total knee arthroplasty following high tibial osteotomy", *Indian Journal of Orthopaedics*, vol. 47, no. 5, pp. 469-473.
130. Gupte, C.M., Smith, A., McDermott, I.D., Bull, A.M., Thomas, R.D. & Amis, A.A. 2002, "Meniscomfemoral ligaments revisited. Anatomical study, age correlation and clinical implications", *The Journal of Bone and Joint Surgery.British Volume*, vol. 84, no. 6, pp. 846-851.
131. Halloran, J.P., Petrella, A.J. & Rullkoetter, P.J. 2005, "Explicit finite element modeling of total knee replacement mechanics", *Journal of Biomechanics*, vol. 38, no. 2, pp. 323-331.
132. Hankemeier, S., Mommsen, P., Krettek, C., Jagodzinski, M., Brand, J., Meyer, C. & Meller, R. 2010, "Accuracy of high tibial osteotomy: comparison between open-and closed-wedge technique", *Knee Surgery, Sports Traumatology, Arthroscopy*, vol. 18, no. 10, pp. 1328-1333.
133. Hart, A., Minns, R., Nabhani, F. & Muckle, D. 1999, "An examination of the internal stresses in articular cartilage of the human patella", *The Knee*, vol. 6, no. 3, pp. 171-174.
134. Haut Donahue, T.L., Hull, M.L., Rashid, M.M. & Jacobs, C.R. 2003, "How the stiffness of meniscal attachments and meniscal material properties affect tibio-femoral contact pressure computed using a validated finite element model of the human knee joint", *Journal of Biomechanics*, vol. 36, no. 1, pp. 19-34.
135. Henninger, H.B., Reese, S.P., Anderson, A.E. & Weiss, J.A. 2010, "Validation of computational models in biomechanics", *Proceedings of the Institution of Mechanical Engineers, Part H: Journal of Engineering in Medicine*, vol. 224, no. 7, pp. 801-812.
136. Hernigou, P., Medevielle, D., Debeyre, J. & Goutallier, D. 1987, "Proximal tibial osteotomy for osteoarthritis with varus deformity. A ten to thirteen-year follow-up study.", *The Journal of Bone and Joint Surgery.American Volume*, vol. 69, no. 3, pp. 332-354.

137. Hernigou, P., Ovadia, H. & Goutallier, D. 1992, "Mathematical modelling of open-wedge tibial osteotomy and correction tables", *Revue de Chirurgie Orthopedique et Reparatrice de l'Appareil Moteur*, vol. 78, no. 4, pp. 258-263.
138. Hillstrom, H.J., Minacori, R., Kirane, Y., D'Lima, D.D., Fregly, B.J., Lenhoff, M., Backus, S., Kraszewski, A., Garisson, G., Bido, J. & Kontaxis, A. 2013, "In-vivo Biomechanical Effects of Conservative Realignment Bracing: A Case Study", *Knee Surgery and Rehabilitation in 2013: How is Engineering Driving Improved Treatment?* Institution of Mechanical Engineers, London, United Kingdom, 11-12 November.
139. Hinterwimmer, S., Graichen, H., Vogl, T.J. & Abolmaali, N. 2008, "An MRI-based technique for assessment of lower extremity deformities—reproducibility, accuracy, and clinical application", *European Radiology*, vol. 18, no. 7, pp. 1497-1505.
140. Hirokawa, S. & Tsuruno, R. 2000, "Three-dimensional deformation and stress distribution in an analytical/computational model of the anterior cruciate ligament", *Journal of Biomechanics*, vol. 33, no. 9, pp. 1069-1077.
141. Holzapfel, G.A. & Gasser, T.C. 2001, "A viscoelastic model for fiber-reinforced composites at finite strains: Continuum basis, computational aspects and applications", *Computer Methods in Applied Mechanics and Engineering*, vol. 190, no. 34, pp. 4379-4403.
142. Hopkins, A.R., New, A.M., Rodriguez-y-Baena, F. & Taylor, M. 2010, "Finite element analysis of unicompartmental knee arthroplasty", *Medical Engineering & Physics*, vol. 32, no. 1, pp. 14-21.
143. Hrennikoff, A. 1941, "Solution of problems of elasticity by the framework method", *Journal of Applied Mechanics*, vol. 8, no. 4, pp. 169-175.
144. Hsu, R., Himeno, S., Coventry, M.B. & Chao, E. 1990, "Normal axial alignment of the lower extremity and load-bearing distribution at the knee.", *Clinical Orthopaedics and Related Research*, vol. 225, pp. 215-227.
145. Hui, C., Salmon, L.J., Kok, A., Williams, H.A., Hockers, N., van der Tempel, Willem M, Chana, R. & Pinczewski, L.A. 2011, "Long-term survival of high tibial osteotomy for medial compartment osteoarthritis of the knee", *The American Journal of Sports Medicine*, vol. 39, no. 1, pp. 64-70.
146. Imhauser, C., Mauro, C., Choi, D., Rosenberg, E., Mathew, S., Nguyen, J., Ma, Y. & Wickiewicz, T. 2013, "Abnormal tibiofemoral contact stress and its association with altered kinematics after center-center anterior cruciate ligament reconstruction: an in vitro study", *The American Journal of Sports Medicine*, vol. 41, no. 4, pp. 815-825.
147. Inman, V.T. 1947, "Functional aspects of the abductor muscles of the hip", *The Journal of Bone & Joint Surgery*, vol. 29, no. 3, pp. 607-619.

148. Innocenti, B., Bilgen, ÖF., Labey, L., van Lenthe, G.H., Sloten, J.V. & Catani, F. 2014, "Load sharing and ligament strains in balanced, overstuffed and understuffed UKA. A validated finite element analysis", *The Journal of Arthroplasty*, vol. 29, no. 7, pp. 1491-1498.
149. Insall, J.N., Joseph, D.M. & Msika, C. 1984, "High tibial osteotomy for varus gonarthrosis. A long-term follow-up study", *The Journal of Bone and Joint Surgery. American Volume*, vol. 66, no. 7, pp. 1040-1048.
150. Jackson, J., Waugh, W. & Green, J. 1969, "High tibial osteotomy for osteoarthritis of the knee", *The Journal of Bone and Joint Surgery. British Volume*, vol. 51, no. 1, pp. 88-94.
151. Jakob, R.P. & Murphy, S.B. 1992, "Tibial osteotomy for varus gonarthrosis: indication, planning, and operative technique", *Instructional Course Lectures*, vol. 41, pp. 87-93.
152. Jo, C.H., Lee, Y.G., Shin, W.H., Kim, H., Chai, J.W., Jeong, E.C., Kim, J.E., Shim, H., Shin, J.S., Shin, I.S., Ra, J.C., Oh, S. & Yoon, K.S. 2014, "Intra-articular injection of mesenchymal stem cells for the treatment of osteoarthritis of the knee: a proof-of-concept clinical trial", *Stem Cells*, vol. 32, no. 5, pp. 1254-1266.
153. Johnson, F., Leitzl, S. & Waugh, W. 1980, "The distribution of load across the knee. A comparison of static and dynamic measurements", *Journal of Bone and Joint Surgery. British Volume*, vol. 62, no. 3, pp. 346-349.
154. Jones, A.C. & Wilcox, R.K. 2008, "Finite element analysis of the spine: towards a framework of verification, validation and sensitivity analysis", *Medical Engineering & Physics*, vol. 30, no. 10, pp. 1287-1304.
155. Kaufman, K.R., Hughes, C., Morrey, B.F., Morrey, M. & An, K.N. 2001, "Gait characteristics of patients with knee osteoarthritis", *Journal of Biomechanics*, vol. 34, no. 7, pp. 907-915.
156. Kazemi, M., Li, L., Savard, P. & Buschmann, M. 2011, "Creep behavior of the intact and meniscectomy knee joints", *Journal of the Mechanical Behavior of Biomedical Materials*, vol. 4, no. 7, pp. 1351-1358.
157. Kellgren, J. & Lawrence, J. 1957, "Radiological assessment of osteo-arthritis", *Annals of the Rheumatic Diseases*, vol. 16, no. 4, pp. 494-502.
158. Kelly, S., Chapman, R.J., Woodhams, S., Sagar, D.R., Turner, J., Burston, J.J., Bullock, C., Paton, K., Huang, J., Wong, A., McWilliams, D.F., Okine, B.N., Barrett, D.A., Hathway, G.J., Walsh, D.A. & Chapman, V. 2013, "Increased function of pronociceptive TRPV1 at the level of the joint in a rat model of osteoarthritis pain", *Annals of the Rheumatic Diseases*, vol. 0, pp. 1-7.

159. Kendoff, D., Lo, D., Goleski, P., Warkentine, B., O'Loughlin, P.F. & Pearle, A.D. 2008, "Open wedge tibial osteotomies influence on axial rotation and tibial slope", *Knee Surgery, Sports Traumatology, Arthroscopy*, vol. 16, no. 10, pp. 904-910.
160. Kettelkamp, D.B. & Chao, E. 1972, "A method for quantitative analysis of medial and lateral compression forces at the knee during standing", *Clinical Orthopaedics and Related Research*, vol. 83, pp. 202-213.
161. Kettelkamp, D.B., Wenger, D.R., Chao, E.Y. & Thompson, C. 1976, "Results of proximal tibial osteotomy. The effects of tibiofemoral angle, stance-phase flexion-extension, and medial-plateau force", *The Journal of Bone and Joint Surgery.American Volume*, vol. 58, no. 7, pp. 952-960.
162. Keyak, J.H., Meagher, J.M., Skinner, H.B. & Mote, C.D. 1990, "Automated three-dimensional finite element modelling of bone: a new method", *Journal of Biomedical Engineering*, vol. 12, no. 5, pp. 389-397.
163. Keyak, J.H. & Skinner, H.B. 1992, "Three-dimensional finite element modelling of bone: effects of element size", *Journal of Biomedical Engineering*, vol. 14, no. 6, pp. 483-489.
164. Khalilollah, N., Fouladi, A. & Chinigarzadeh, M. 2013, "Double tibial osteotomy for bow leg patients: A case series", *Journal of Research in Medical Sciences*, vol. 18, no. 12, pp. 1092-1096.
165. Kiapour, A., Kiapour, A.M., Kaul, V., Quatman, C.E., Wordeman, S.C., Hewett, T.E., Demetropoulos, C.K. & Goel, V.K. 2014, "Finite element model of the knee for investigation of injury mechanisms: development and validation", *Journal of Biomechanical Engineering*, vol. 136, no. 1, pp. no pagination.
166. Kiapour, A.M., Kaul, V., Kiapour, A., Quatman, C.E., Wordeman, S.C., Hewett, T.E., Demetropoulos, C.K. & Goel, V.K. 2013, "The Effect of Ligament Modeling Technique on Knee Joint Kinematics: A Finite Element Study", *Applied Mathematics*, vol. 4, pp. 91-97.
167. Kirane, Y., Zifchock, R. & Hillstrom, H. 2010, , *Offloading strategies for knee osteoarthritis* [Homepage of Lower Extrimity Review], [Online]. Available: <http://www.lowerextremityreview.com/article/offloading-strategies-for-knee-osteoarthritis> [2011, 01/21].
168. Knudson, D., Noffal, G., Bauer, J., McGinnis, P., Bird, M., Chow, J., Bahamonde, R., Blackwell, J., Strohmeyer, S. & Abendroth-Smith, J. 2003, "Development and evaluation of a biomechanics concept inventory", *Sports Biomechanics*, vol. 2, no. 2, pp. 267-277.



169. Komistek, R.D., Stiehl, J.B., Dennis, D.A., Paxson, R.D. & Soutas-Little, R.W. 1997, "Mathematical model of the lower extremity joint reaction forces using Kane's method of dynamics", *Journal of Biomechanics*, vol. 31, no. 2, pp. 185-189.
170. Koshino, T., Murase, T. & Saito, T. 2003, "Medial opening-wedge high tibial osteotomy with use of porous hydroxyapatite to treat medial compartment osteoarthritis of the knee", *The Journal of Bone and Joint Surgery.American Volume*, vol. 85, no. 1, pp. 78-85.
171. Koshino, T., Morii, T., Wada, J., Saito, H., Ozawa, N. & Noyori, K. 1989, "High tibial osteotomy with fixation by a blade plate for medial compartment osteoarthritis of the knee.", *The Orthopedic Clinics of North America*, vol. 20, no. 2, pp. 227-243.
172. Kozanek, M., Hosseini, A., Liu, F., Van de Velde, Samuel K, Gill, T.J., Rubash, H.E. & Li, G. 2009, "Tibiofemoral kinematics and condylar motion during the stance phase of gait", *Journal of Biomechanics*, vol. 42, no. 12, pp. 1877-1884.
173. Krettek, C., Miclau, T., Schandelmaier, P. & Tscherne, H. 1998, "Intraoperative control of axes, rotation and length in femoral and tibial fractures technical note", *Injury*, vol. 29, pp. 29-39.
174. Kubicek, M. & Florian, Z. 2009, "Stress Strain Analysis of the Knee Joint", *Engineering Mechanics*, vol. 16, no. 5, pp. 315-322.
175. Kumar, D., Manal, K. & Rudolph, K. 2013, "Knee joint loading during gait in healthy controls and individuals with knee osteoarthritis", *Osteoarthritis and Cartilage*, vol. 21, no. 2, pp. 298-305.
176. Kurosawa, H., Walker, P., Abe, S., Garg, A. & Hunter, T. 1985, "Geometry and motion of the knee for implant and orthotic design", *Journal of Biomechanics*, vol. 18, no. 7, pp. 487-499.
177. Kutzner, I., Heinlein, B., Graichen, F., Bender, A., Rohlmann, A., Halder, A., Beier, A. & Bergmann, G. 2010, "Loading of the knee joint during activities of daily living measured in vivo in five subjects.", *Journal of Biomechanics*, vol. 43, no. 11, pp. 2164.
178. Kwan, M.K. & Woo, S. 1989, "A structural model to describe the nonlinear stress-strain behavior for parallel-fibered collagenous tissues", *Journal of Biomechanical Engineering*, vol. 111, no. 4, pp. 361-363.
179. Lanovaz, J.L. & Ellis, R.E. 2005, "Experimental validation of a 3D dynamic finite-element model of a total knee replacement", *International Conference on Medical Image Computing and Computer-Assisted Intervention*, vol. 8, no. Pt 1, pp. 917-924.

180. Lawrence, R.C., Helmick, C.G., Arnett, F.C., Deyo, R.A., Felson, D.T., Giannini, E.H., Heyse, S.P., Hirsch, R., Hochberg, M.C. & Hunder, G.G. 1998, "Estimates of the prevalence of arthritis and selected musculoskeletal disorders in the United States", *Arthritis & Rheumatism*, vol. 41, no. 5, pp. 778-799.
181. Le Pen, C., Reygrobelle, C. & Gerentes, I. 2005, "Financial cost of osteoarthritis in France. The "COART" France study", *Joint, Bone, Spine : Revue du Rhumatisme*, vol. 72, no. 6, pp. 567-570.
182. Lee, D.C. & Byun, S.J. 2012, "High Tibial Osteotomy", *Knee Surgery & Related Research*, vol. 24, no. 2, pp. 61-69.
183. Lasso-Arroyo, R., Jiménez, J.C.S., Castro, R.R. & Lopez, F.B. 2004, "Biomechanical Behavior of the Knee Joint Using ANSYS", *2004 International ANSYS Conference Proceedings*, ANSYS, Pittsburgh, May 24-26.
184. Li, G. & Lopez, O. 1999, "Reliability of a 3D finite element model constructed using magnetic resonance images of a knee for joint contact stress analysis", *23rd Annual Meeting of the American Society of Biomechanics*. Pittsburgh, October 21-23.
185. Li, G., Gil, J., Kanamori, A. & Woo, S. 1999, "A validated three-dimensional computational model of a human knee joint", *Journal of Biomechanical Engineering*, vol. 121, no. 6, pp. 657-662.
186. Li, G., Papannagari, R., Defrate, L.E., Doo Yoo, J., Eun Park, S. & J Gill, T. 2007, "The effects of ACL deficiency on mediolateral translation and varus-valgus rotation", *Acta Orthopaedica*, vol. 78, no. 3, pp. 355-360.
187. Li, J., Evans, S. & Holt, C. 2012, "Effects of Coronary Ligaments on Finite Element Soft Tissue Predictions of Meniscal Biomechanics", *Proceedings of the European Society of Biomechanics Conference*, European Society of Biomechanics, Lisbon, Portugal, July 1-4.
188. Limbert, G. & Taylor, M. 2001, "An explicit three-dimensional finite element model of an incompressible transversely isotropic hyperelastic material: application to the study of the human anterior cruciate ligament.", *First MIT Conference on Computational Fluid and Solid Mechanics*, Cambridge, Massachusetts, pp. 319.
189. Lind, M., Webster, K., Feller, J., McClelland, J. & Wittwer, J. 2012, "Walking Function before and after Opening Wedge High Tibial Osteotomy: A Biomechanical Analysis", *Journal of Bone & Joint Surgery, British Volume*, vol. 94, pp. 91-98.
190. Lind, M., McClelland, J., Wittwer, J.E., Whitehead, T.S., Feller, J.A. & Webster, K.E. 2013, "Gait analysis of walking before and after medial opening wedge high tibial osteotomy", *Knee Surgery, Sports Traumatology, Arthroscopy*, vol. 21, no. 1, pp. 74-81.

191. Liodakis, E., Kenawey, M., Doxastaki, I., Krettek, C., Haasper, C. & Hankemeier, S. 2011, "Upright MRI measurement of mechanical axis and frontal plane alignment as a new technique: a comparative study with weight bearing full length radiographs", *Skeletal Radiology*, vol. 40, no. 7, pp. 885-889.
192. Liu, F., Yue, B., Gadikota, H.R., Kozanek, M., Liu, W., Gill, T.J., Rubash, H.E. & Li, G. 2010, "Morphology of the medial collateral ligament of the knee", *Journal of Orthopaedic Surgery and Research*, vol. 5, no. 1, pp. 69-79.
193. Lo, G., Hunter, D., Nevitt, M., Lynch, J. & McAlindon, T. 2009, "Strong association of MRI meniscal derangement and bone marrow lesions in knee osteoarthritis: data from the osteoarthritis initiative", *Osteoarthritis and Cartilage*, vol. 17, no. 6, pp. 743-747.
194. Lobenhoffer, P. & Agneskirchner, J.D. 2003, "Improvements in surgical technique of valgus high tibial osteotomy", *Knee Surgery, Sports Traumatology, Arthroscopy*, vol. 11, no. 3, pp. 132-138.
195. Losch, A., Eckstein, F., Haubner, M. & Englmeier, K.H. 1997, "A non-invasive technique for 3-dimensional assessment of articular cartilage thickness based on MRI Part 1: Development of a computational method", *Magnetic Resonance Imaging*, vol. 15, no. 7, pp. 795-804.
196. Lundberg, H.J., Knowlton, C. & Wimmer, M. 2013, "Fine Tuning Total Knee Replacement Contact Force Prediction Algorithms using Blinded Model Validation", *Journal of Biomechanical Engineering*, vol. 1, pp. 546-552.
197. Lützner, J., Gross, A., Günther, K. & Kirschner, S. 2010, "Precision of navigated and conventional open-wedge high tibial osteotomy in a cadaver study", *European Journal of Medical Research*, vol. 15, no. 3, pp. 117-120.
198. Maetzel, A., Li, L., Pencharz, J., Tomlinson, G. & Bombardier, C. 2004, "The economic burden associated with osteoarthritis, rheumatoid arthritis, and hypertension: a comparative study", *Annals of the Rheumatic Diseases*, vol. 63, no. 4, pp. 395-401.
199. Majima, T., Yasuda, K., Katsuragi, R. & Kaneda, K. 2000, "Progression of joint arthrosis 10 to 15 years after high tibial osteotomy", *Clinical Orthopaedics and Related Research*, vol. 381, no. 381, pp. 177-184.
200. Maquet, P., Van de Berg, A. & Simonet, J. 1975, "Femorotibial weight-bearing areas", *The Journal of Bone and Joint Surgery. American Volume*, vol. 57, pp. 766-772.
201. Marzo, J.M. & Gurske-DePerio, J. 2009, "Effects of medial meniscus posterior horn avulsion and repair on tibiofemoral contact area and peak contact pressure with clinical implications", *The American Journal of Sports Medicine*, vol. 37, no. 1, pp. 124-129.

202. Masouros, S.D., Bull, A.M.J. & Amis, A.A. 2010, "Biomechanics of the knee joint", *Orthopaedics and Trauma*, vol. 24, no. 2, pp. 84-91.
203. Masouros, S., McDermott, I., Amis, A. & Bull, A. 2008, "Biomechanics of the meniscus-meniscal ligament construct of the knee", *Knee Surgery, Sports Traumatology, Arthroscopy*, vol. 16, no. 12, pp. 1121-1132.
204. Mathers, C.D. & Loncar, D. 2005, October 2005-last update, *Updated projections of global mortality and burden of disease, 2002–2030: data sources, methods and results* [Homepage of World Health Organization], [Online]. Available: <http://www.who.int/healthinfo/statistics/bodprojectionspaper.pdf> [2014, 05/25].
205. Matsumoto, H., Suda, Y., Otani, T., Niki, Y., Seedhom, B.B. & Fujikawa, K. 2001, "Roles of the anterior cruciate ligament and the medial collateral ligament in preventing valgus instability", *Journal of Orthopaedic Science*, vol. 6, no. 1, pp. 28-32.
206. Mattei, L., Campioni, E., Accardi, M.A. & Dini, D. 2014, "Finite element analysis of the meniscectomised tibio-femoral joint: implementation of advanced articular cartilage models", *Computer Methods in Biomechanics and Biomedical Engineering*, vol. 17, no. 14, pp. 1553-1571.
207. Matthews, L.S., Goldstein, S.A., Malvitz, T.A., Katz, B.P. & Kaufer, H. 1988, "Proximal tibial osteotomy: factors that influence the duration of satisfactory function", *Clinical Orthopaedics and Related Research*, vol. 229, pp. 193-200.
208. McKellop, H.A., Sigtholm, G., Redfern, F.C., Doyle, B., Sarmiento, A. & Luck, J.V. 1991, "The effect of simulated fracture-angulations of the tibia on cartilage pressures in the knee joint", *The Journal of Bone and Joint Surgery*, vol. 73, no. 9, pp. 1382-1391.
209. Meakin, J.R., Shrive, N.G., Frank, C.B. & Hart, D.A. 2003, "Finite element analysis of the meniscus: the influence of geometry and material properties on its behaviour", *The Knee*, vol. 10, no. 1, pp. 33-41.
210. Meding, J.B., Keating, E.M., Ritter, M.A. & Faris, P.M. 2000, "Total knee arthroplasty after high tibial osteotomy: a comparison study in patients who had bilateral total knee replacement", *The Journal of Bone and Joint Surgery. American Volume*, vol. 82, no. 9, pp. 1252-1259.
211. Meding, J.B., Wing, J.T. & Ritter, M.A. 2011, "Does high tibial osteotomy affect the success or survival of a total knee replacement?", *Clinical Orthopaedics and Related Research*, vol. 469, no. 7, pp. 1991-1994.
212. Messier, S.P. 2008, "Obesity and osteoarthritis: disease genesis and nonpharmacologic weight management", *Rheumatic Disease Clinics of North America*, vol. 34, no. 3, pp. 713-729.

213. Miller, E.J., Riemer, R.F., Haut Donahue, T.L. & Kaufman, K.R. 2009, "Experimental validation of a tibiofemoral model for analyzing joint force distribution", *Journal of Biomechanics*, vol. 42, no. 9, pp. 1355-1359.
214. Miniaci, A., Ballmer, F., Ballmer, P. & Jakob, R. 1989, "Proximal tibial osteotomy. A new fixation device", *Clinical Orthopaedics and Related Research*, vol. 246, pp. 250-259.
215. Minns, R.J. & Steven, F.S. 1977, "The collagen fibril organization in human articular cartilage.", *Journal of Anatomy*, vol. 123, no. Pt 2, pp. 437-457.
216. Mommersteeg, T., Huiskes, R., Blankevoort, L., Kooloos, J., Kauer, J. & Maathuis, P. 1996, "A global verification study of a quasi-static knee model with multi-bundle ligaments", *Journal of Biomechanics*, vol. 29, no. 12, pp. 1659-1664.
217. Mononen, M., Mikkola, M., Julkunen, P., Ojala, R., Nieminen, M., Jurvelin, J. & Korhonen, R. 2012, "Effect of superficial collagen patterns and fibrillation of femoral articular cartilage on knee joint mechanics—A 3D finite element analysis", *Journal of Biomechanics*, vol. 45, no. 3, pp. 579-587.
218. Mononen, M.E., Jurvelin, J.S. & Korhonen, R.K. 2013, "Implementation of a gait cycle loading into healthy and meniscectomised knee joint models with fibril-reinforced articular cartilage", *Computer Methods in Biomechanics and Biomedical Engineering*, , no. ahead-of-print, pp. 1-12.
219. Mootanah, R., Hillstrom, H.J., Gross, K.D., Niu, J., Nevitt, M.C., Lewis, C.E., Torner, J., Hietpas, J. & Felson, D.T. 2013, "Association of Radiographic Knee Osteoarthritis and Pain with Gait Asymmetry: The Multicenter Osteoarthritis Study", *Proceedings of the 59<sup>th</sup> Annual Orthopaedic Research Society Meeting*. Orthopaedic Research Society, San Antonio, Texas, January 26-29.
220. Mootanah, R., Imhauser, C., Koff, M.F., Potter, H.G. & Hillstrom, H. 2011, "MRI Sequence Influences Geometrical Interpretation of Osseous Tissues", *Proceedings of the 57<sup>th</sup> Orthopaedic Research Society Annual Meeting*. Orthopaedic Research Society, Long Beach, California, January 13-16.
221. Mootanah, R., Imhauser, C., Risse, F., Carpanen, D., Walker, R.W., Koff, M.F., Lenhoff, M., Rozbruch, S.R., Fragomen, A.T., Kirane, Y., Dewan, Z., Cheah, K., Dowell, J.K. & Hillstrom, H.J. 2014, "Development and Validation of a Computational Model of the Knee Joint for the Evaluation of Surgical Treatments for Osteoarthritis", *Computer Methods in Biomechanics and Biomedical Engineering*, vol. (ahead of print), pp. 1-12.
222. Mootanah, R., Dowell, J.K., Cheah, K., Ingle, P. & Shelton, J. 2007, "Configuration of anchorage holes affects fixation of the acetabular component in cemented total hip replacement—a finite element study", *Computer Methods in Biomechanics and Biomedical Engineering*, vol. 10, no. 6, pp. 439-445.

223. Mootanah, R., Hillstrom, H., Imhauser, C., Walker, R., New, A., Mangeot, S., Blanc, E., Dare, C., Burton, A. & Mouton, C. 2009, "Stress distribution in the knee joint following a high tibial osteotomy", *Proceedings of the International Society of Technology in Arthroplasty Meeting*. International Society of Technology in Arthroplasty, Big Island, USA, October 22-24.
224. Moreland, J.R., Bassett, L. & Hanker, G. 1987, "Radiographic analysis of the axial alignment of the lower extremity", *The Journal of Bone and Joint Surgery. American Volume*, vol. 69, no. 5, pp. 745-749.
225. Morimoto, Y., Ferretti, M., Ekdahl, M., Smolinski, P. & Fu, F.H. 2009, "Tibiofemoral joint contact area and pressure after single-and double-bundle anterior cruciate ligament reconstruction", *Arthroscopy: The Journal of Arthroscopic & Related Surgery*, vol. 25, no. 1, pp. 62-69.
226. Morrison, J.B. 1970, "The mechanics of the knee joint in relation to normal walking", *Journal of Biomechanics*, vol. 3, no. 1, pp. 51-61.
227. Most, E., Axe, J., Rubash, H. & Li, G. 2004, "Sensitivity of the knee joint kinematics calculation to selection of flexion axes", *Journal of Biomechanics*, vol. 37, no. 11, pp. 1743-1748.
228. Müller, M. & Strecker, W. 2008, "Arthroscopy prior to osteotomy around the knee?", *Archives of Orthopaedic and Trauma Surgery*, vol. 128, no. 11, pp. 1217-1221.
229. Mündermann, A., Dyrby, C.O. & Andriacchi, T.P. 2005, "Secondary gait changes in patients with medial compartment knee osteoarthritis: increased load at the ankle, knee, and hip during walking", *Arthritis & Rheumatism*, vol. 52, no. 9, pp. 2835-2844.
230. Murphy, L., Schwartz, T.A., Helmick, C.G., Renner, J.B., Tudor, G., Koch, G., Dragomir, A., Kalsbeek, W.D., Luta, G. & Jordan, J.M. 2008, "Lifetime risk of symptomatic knee osteoarthritis", *Arthritis Care & Research*, vol. 59, no. 9, pp. 1207-1213.
231. Nagel, A., Insall, J.N. & Scuderi, G.R. 1996, "Proximal Tibial Osteotomy. A Subjective Outcome Study", *The Journal of Bone & Joint Surgery*, vol. 78, no. 9, pp. 1353-1358.
232. National Institute for Health and Clinical Excellence 2005, [Homepage of World Health Organisation], [Online]. Available: [http://www.nice.org.uk/nicemedia/pdf/osteoarthritis\\_draft\\_scope.pdf](http://www.nice.org.uk/nicemedia/pdf/osteoarthritis_draft_scope.pdf) [2010, November/2].
233. Naudie, D., Bourne, R.B., Rorabeck, C.H. & Bourne, T.J. 1999, "Survivorship of the high tibial valgus osteotomy A 10-to 22-year followup study", *Clinical Orthopaedics and Related Research*, vol. 367, pp. 18-27.

234. Netravali, N.A., Koo, S., Giori, N.J. & Andriacchi, T.P. 2011, "The effect of kinematic and kinetic changes on meniscal strains during gait.", *Journal of Biomechanical Engineering*, vol. 133, no. 1, pp. no pagination.
235. Neu, C., Reddi, A., Komvopoulos, K., Schmid, T. & Di Cesare, P. 2010, "Increased friction coefficient and superficial zone protein expression in patients with advanced osteoarthritis", *Arthritis & Rheumatism*, vol. 62, no. 9, pp. 2680-2687.
236. Nicolella, D.P., Eliason, T.D., Francis, W.L. & Bichon, B.J. 2012, "Dynamic Finite Element Modelling of Knee Mechanics", *Proceedings of the Orthopedic Research Society Annual Meeting*. Orthopedic Research Society, San Francisco, February 4-7.
237. Niemeyer, P., Schmal, H., Hauschild, O., von Heyden, J., Südkamp, N.P. & Köstler, W. 2010, "Open-wedge osteotomy using an internal plate fixator in patients with medial-compartment gonarthrosis and varus malalignment: 3-year results with regard to preoperative arthroscopic and radiographic findings", *Arthroscopy: The Journal of Arthroscopic & Related Surgery*, vol. 26, no. 12, pp. 1607-1616.
238. Nordin, M. & Frankel, V.H. 2001, *Basic biomechanics of the musculoskeletal system*. 3rd edn, Wolters Kluwer Health, Philadelphia.
239. Odenbring, S., Egund, N., Knutson, K., Lindstrand, A. & Larsen, S.T. 1990, "Revision after osteotomy for gonarthrosis: a 10-19-year follow-up of 314 cases", *Acta Orthopaedica*, vol. 61, no. 2, pp. 128-130.
240. Ogden, S., Mukherjee, D.P., Keating, M.E., Ogden, A.L., Albright, J.A. & McCall, R.E. 2009, "Changes in load distribution in the knee after opening-wedge or closing-wedge high tibial osteotomy", *The Journal of Arthroplasty*, vol. 24, no. 1, pp. 101-109.
241. Pandy, M.G., Sasaki, K. & Kim, S. 1997, "A three-dimensional musculoskeletal model of the human knee joint. Part 1: theoretical construction", *Computer Methods in Biomechanics and Biomedical Engineering*, vol. 1, no. 2, pp. 87-108.
242. Papachristou, G. 2004, "Photoelastic study of the internal and contact stresses on the knee joint before and after osteotomy", *Archives of orthopaedic and trauma surgery*, vol. 124, no. 5, pp. 288-297.
243. Papaioannou, G., Nianios, G., Mitroyiannis, C., Tashman, S. & Yang, K.H. 2008, "Patient Specific Knee Joint Finite Element Model Validation with High Accuracy Kinematics from Biplane Dynamic Radiography", *International Conference on Computational & Experimental Engineering and Sciences*, vol. 8, no. 1, pp. 7-12.

244. Park, S., Hung, C.T. & Ateshian, G.A. 2004, "Mechanical response of bovine articular cartilage under dynamic unconfined compression loading at physiological stress levels", *Osteoarthritis and Cartilage, Osteoarthritis Research Society*, vol. 12, no. 1, pp. 65-73.
245. Pauchard, Y., McErlain, D., Milner, J., Ivanov, T., Giffin, J.S., Birmingham, T. & Holdsworth, D.W. 2013, "Patient-Specific Virtual High-Tibial Osteotomy", *Proceedings of the 11th International Symposium on Computer Methods in Biomechanics and Biomedical Engineering*. Computer Methods in Biomechanics and Biomedical Engineering, Utah, April 3-7.
246. Peña, E., Calvo, B., Martinez, M. & Doblare, M. 2006, "A three-dimensional finite element analysis of the combined behavior of ligaments and menisci in the healthy human knee joint", *Journal of Biomechanics*, vol. 39, no. 9, pp. 1686-1701.
247. Peña, E., Calvo, B., Martínez, M. & Doblaré, M. 2008, "Computer simulation of damage on distal femoral articular cartilage after meniscectomies", *Computers in Biology and Medicine*, vol. 38, no. 1, pp. 69-81.
248. Perie, D. & Hobatho, M.C. 1998, "In vivo determination of contact areas and pressure of the femorotibial joint using non-linear finite element analysis", *Clinical Biomechanics*, vol. 13, no. 6, pp. 394-402.
249. Perillo-Marcone, A. & Taylor, M. 2007, "Effect of varus/valgus malalignment on bone strains in the proximal tibia after TKR: an explicit finite element study.", *Journal of Biomechanical Engineering*, vol. 129, no. 1, pp. 1-11.
250. Perry, J. & Davids, J.R. 1992, "Gait analysis: normal and pathological function", *Journal of Pediatric Orthopaedics*, vol. 12, no. 6, pp. 815-826.
251. Pinczewski, L., Hui, C., Salmon, L., Kok, A., Williams, H., Hockers, N., van der Tempel, W. & Chana, R. 2012, "Long Term Survival of High Tibial Osteotomy for Medial Osteoarthritis of the Knee: 8-19 year follow-up in a Series of 455 Patients", *Journal of Bone & Joint Surgery, British Volume*, vol. 94, pp. 11-17.
252. Portney, L.G. & Watkins, M.P. 2008, *Foundations Of Clinical Research: Applications To Practice*, 3rd edn, Prentice Hall, Englewood Cliffs, NJ.
253. Potter, H.G., Jain, S.K., Ma, Y., Black, B.R., Fung, S. & Lyman, S. 2012, "Cartilage Injury After Acute, Isolated Anterior Cruciate Ligament Tear: Immediate and Longitudinal Effect With Clinical/MRI Follow-up", *The American Journal of Sports Medicine*, vol. 40, no. 2, pp. 276-285.
254. Pressel, T., Schofer, M.D., Meiforth, J., Lengsfeld, M. & Schmitt, J. 2010, "A new algorithm for finite element simulation of wedge osteotomies in voxel models with application to the tibia", *Journal: Orthopedic Research and Reviews*, vol. 2, pp. 11-16.



255. Prodromos, C.C., Andriacchi, T.P. & Galante, J.O. 1985, "A relationship between gait and clinical changes following high tibial osteotomy", *The Journal of Bone and Joint Surgery*, vol. 67, no. 8, pp. 1188-1194.
256. Qi, W., Hosseini, A., Tsai, T., Rubash, H.E. & Li, G. 2013, "In Vivo Elongation of the Anterior and Posterior Cruciate Ligaments in High Flexion of the Knee", *Proceedings of the Orthopaedic Research Society Annual Meeting*. Orthopaedic Research Society, San Antino; Texas, Janaury 26-29.
257. Qing-Yu, Z., Chang-Hai, Z., Xiao-Feng, L.I., Hai-Yuan, D., Ai-Lian, Z. & Ling, L.I.N. 2006, "Associated risk factors of knee osteoarthritis: a population survey in Taiyuan, China", *Chinese Medical Journal*, vol. 119, no. 18, pp. 1522-1527.
258. Quapp, K. & Weiss, J. 1998, "Material characterization of human medial collateral ligament.", *Journal of Biomechanical Engineering*, vol. 120, no. 6, pp. 757-763.
259. Radin, E., Burr, D., Caterson, B., Fyhrie, D., Brown, T. & Boyd, R. 1991, "Mechanical determinants of osteoarthritis", *Seminars in Arthritis and Rheumatism*, vol. 21, no. 3, pp. 12-21.
260. Raja Izaham, R.M.A., Abdul Kadir, M.R., Abdul Rashid, A.H., Hossain, M.G. & Kamarul, T. 2012, "Finite element analysis of Puddu and Tomofix plate fixation for open wedge high tibial osteotomy", *Injury*, vol. 43, no. 6, pp. 898-902.
261. Ranawat, C.S., Padgett, D.E. & Ohashi, Y. 1989, "Total knee arthroplasty for patients younger than 55 years", *Clinical Orthopaedics and Related Research*, vol. 248, pp. 27-33.
262. Ranawat, C.S. & Sculco, T.P. 1985, "History of the development of total knee prosthesis at the Hospital for Special Surgery" in *Total-Condylar Knee Arthroplasty* Springer Verlag, New York, pp. 3-6.
263. Reginster, J.Y., Badurski, J., Bellamy, N., Bensen, W., Chapurlat, R., Chevalier, X., Christiansen, C., Genant, H., Navarro, F., Nasonov, E., Sambrook, P.N., Spector, T.D. & Cooper, C. 2013, "Efficacy and safety of strontium ranelate in the treatment of knee osteoarthritis: results of a double-blind, randomised placebo-controlled trial", *Annals of the Rheumatic Diseases*, vol. 72, no. 2, pp. 179-186.
264. Reinbolt, J.A., Haftka, R.T., Chmielewski, T.L. & Fregly, B.J. 2008, "A computational framework to predict post-treatment outcome for gait-related disorders", *Medical Engineering & Physics*, vol. 30, no. 4, pp. 434-443.
265. Reising, K., Strohm, P.C., Hauschild, O., Schmal, H., Khattab, M., Südkamp, N.P. & Niemeyer, P. 2013, "Computer-assisted navigation for the intraoperative assessment of lower limb alignment in high tibial osteotomy can avoid outliers compared with the conventional technique", *Knee Surgery, Sports Traumatology, Arthroscopy*, vol. 21, no. 1, pp. 181-188.

266. Repo, R. & Finlay, J. 1977, "Survival of articular cartilage after controlled impact", *The Journal of Bone and Joint Surgery. American Volume*, vol. 59, no. 8, pp. 1068-1076.
267. Reynard, L.N., Bui, C., Syddall, C.M. & Loughlin, J. 2014, "CpG methylation regulates allelic expression of GDF5 by modulating binding of SP1 and SP3 repressor proteins to the osteoarthritis susceptibility SNP rs143383", *Human Genetics*, vol. 133, no. 8, pp. 1059-1073.
268. Ribeiro, C.H., Severino, N.R. & De Barros Fucs, P.M.M. 2014, "Opening wedge high tibial osteotomy: navigation system compared to the conventional technique in a controlled clinical study", *International Orthopaedics*, vol. 38, no. 8, pp. 1627-1631.
269. Riegger-Krug, C., Gerhart, T.N., Powers, W.R. & Hayes, W.C. 1998, "Tibiofemoral contact pressures in degenerative joint disease", *Clinical Orthopaedics and Related Research*, vol. 348, pp. 233-245.
270. Rigby, B.J., Hirai, N., Spikes, J.D. & Eyring, H. 1959, "The mechanical properties of rat tail tendon", *The Journal of General Physiology*, vol. 43, no. 2, pp. 265-283.
271. Rinonapoli, E., Mancini, G.B., Corvaglia, A. & Musiello, S. 1998, "Tibial osteotomy for varus gonarthrosis: a 10-to 21-year followup study", *Clinical Orthopaedics and Related Research*, vol. 353, pp. 185-193.
272. Robinson, J.R., Bull, A.M., Thomas, R.R. & Amis, A.A. 2006, "The role of the medial collateral ligament and posteromedial capsule in controlling knee laxity", *The American Journal of Sports Medicine*, vol. 34, no. 11, pp. 1815-1823.
273. Saito, T., Kumagai, K., Akamatsu, Y., Kobayashi, H. & Kusayama, Y. 2014, "Five- to ten-year outcome following medial opening-wedge high tibial osteotomy with rigid plate fixation in combination with an artificial bone substitute", *The Bone and Joint Journal*, vol. 96-B, no. 3, pp. 339-344.
274. Salzmann, G.M., Ahrens, P., Naal, F.D., El-Azab, H., Spang, J.T., Imhoff, A.B. & Lorenz, S. 2009, "Sporting Activity After High Tibial Osteotomy for the Treatment of Medial Compartment Knee Osteoarthritis", *The American Journal of Sports Medicine*, vol. 29, no. 2, pp. 312-318.
275. Sambatakakis, A., Attfield, S. & Newton, G. 1993, "Quantification of soft-tissue imbalance in condylar knee arthroplasty", *Journal of Biomedical Engineering*, vol. 15, no. 4, pp. 339-343.
276. Savarese, E., Bisicchia, S., Romeo, R. & Amendola, A. 2011, "Role of high tibial osteotomy in chronic injuries of posterior cruciate ligament and posterolateral corner", *Journal of Orthopaedics and Traumatology*, vol. 12, no. 1, pp. 1-17.

277. Saveh, A.H., Katouzian, H.R. & Chizari, M. 2011, "Measurement of an intact knee kinematics using gait and fluoroscopic analysis", *Knee Surgery, Sports Traumatology, Arthroscopy*, vol. 19, no. 2, pp. 267-272.
278. Schallberger, A., Jacobi, M., Wahl, P., Maestretti, G. & Jakob, R.P. 2011, "High tibial valgus osteotomy in unicompartmental medial osteoarthritis of the knee: a retrospective follow-up study over 13–21 years", *Knee Surgery, Sports Traumatology, Arthroscopy*, vol. 19, no. 1, pp. 122-127.
279. Schipplein, O. & Andriacchi, T. 1991, "Interaction between active and passive knee stabilizers during level walking", *Journal of Orthopaedic Research*, vol. 9, no. 1, pp. 113-119.
280. Scholes, S., Bull, A., Unsworth, A. & Amis, A. 2004, "Biomechanics of articulations and derangments in disease" in *Oxford Textbook of Rheumatology*, 3rd edn, Oxford University Press, Ny, USA, pp. 379-387.
281. Schröter, S., Ihle, C., Mueller, J., Lobenhoffer, P., Stöckle, U. & van Heerwaarden, R. 2013, "Digital planning of high tibial osteotomy. Interrater reliability by using two different software", *Knee Surgery, Sports Traumatology, Arthroscopy*, vol. 21, no. 1, pp. 189-196.
282. Shah, J., Mirza, N. & Patel, V. 2014, "A Comparative study for Safety and Efficacy of Oxaceprol and Diacerein in Osteoarthritis of Knee Joints", *PharmaTutor*, vol. 2, no. 6, pp. 108-114.
283. Shao, Q., MacLeod, T.D., Manal, K. & Buchanan, T.S. 2011, "Estimation of ligament loading and anterior tibial translation in healthy and ACL-deficient knees during gait and the influence of increasing tibial slope using EMG-driven approach", *Annals of Biomedical Engineering*, vol. 39, no. 1, pp. 110-121.
284. Sharma, L., Kapoor, D. & Issa, S. 2006, "Epidemiology of osteoarthritis: an update", *Current Opinion in Rheumatology*, vol. 18, no. 2, pp. 147-156.
285. Sharma, L., Song, J., Dunlop, D., Felson, D., Lewis, C.E., Segal, N., Torner, J., Cooke, T.D.V., Hietpas, J. & Lynch, J. 2010, "Varus and valgus alignment and incident and progressive knee osteoarthritis", *Annals of the Rheumatic Diseases*, vol. 69, no. 11, pp. 1940-1945.
286. Sharma, L., Song, J., Felson, D.T., Cahue, S., Shamiyeh, E. & Dunlop, D.D. 2001, "The role of knee alignment in disease progression and functional decline in knee osteoarthritis", *The Journal of the American Medical Association*, vol. 286, no. 2, pp. 188-195.
287. Shaw, J.A., Dungy, D.S. & Arsht, S.S. 2004, "Recurrent varus angulation after high tibial osteotomy: an anatomic analysis", *Clinical Orthopaedics and Related Research*, vol. 420, pp. 205-212.

288. Shelburne, K.B., Pandey, M.G. & Torry, M.R. 2004, "Comparison of shear forces and ligament loading in the healthy and ACL-deficient knee during gait", *Journal of Biomechanics*, vol. 37, no. 3, pp. 313-319.
289. Shim, J.S., Lee, S.H., Jung, H.J. & Lee, H.I. 2013, "High tibial open wedge osteotomy below the tibial tubercle: clinical and radiographic results", *Knee Surgery, Sports Traumatology, Arthroscopy*, vol. 21, no. 1, pp. 57-63.
290. Shirazi, R. & Shirazi-Adl, A. 2008, "Deep vertical collagen fibrils play a significant role in mechanics of articular cartilage", *Journal of Orthopaedic Research*, vol. 26, no. 5, pp. 608-615.
291. Shirazi, R. & Shirazi-Adl, A. 2005, "Analysis of articular cartilage as a composite using nonlinear membrane elements for collagen fibrils", *Medical Engineering & Physics*, vol. 27, no. 10, pp. 827-835.
292. Shirazi, R. & Shirazi-Adl, A. 2009, "Computational biomechanics of articular cartilage of human knee joint: effect of osteochondral defects", *Journal of Biomechanics*, vol. 42, no. 15, pp. 2458-2465.
293. Skaggs, D.L., Warden, W.H. & Mow, V.C. 1994, "Radial tie fibers influence the tensile properties of the bovine medial meniscus", *Journal of Orthopaedic Research*, vol. 12, no. 2, pp. 176-185.
294. Spahn, G., Hofmann, G.O., von Engelhardt, L.V., Li, M., Neubauer, H. & Klinger, H.M. 2013, "The impact of a high tibial valgus osteotomy and unicondylar medial arthroplasty on the treatment for knee osteoarthritis: a meta-analysis", *Knee Surgery, Sports Traumatology, Arthroscopy*, vol. 21, no. 1, pp. 96-112.
295. Sprenger, T.R. & Doerzbacher, J.F. 2003, "Tibial osteotomy for the treatment of varus gonarthrosis. Survival and failure analysis to twenty-two years", *The Journal of Bone & Joint Surgery*, vol. 85, no. 3, pp. 469-474.
296. Staeheli, J.W., Cass, J.R. & Morrey, B.F. 1987, "Condylar total knee arthroplasty after failed proximal tibial osteotomy", *The Journal of Bone and Joint Surgery. American Volume*, vol. 69, no. 1, pp. 28-31.
297. Standring, S. 2008, *Gray's Anatomy*, 40th edn, Elsevier Limited, Spain.
298. Stein, V., Li, L., Lo, G., Guermazi, A., Zhang, Y., Kent Kwok, C., Eaton, C.B. & Hunter, D.J. 2011, "Pattern of joint damage in persons with knee osteoarthritis and concomitant ACL tears", *Rheumatology International*, vol. 32, no. 5, pp. 1197-1208.
299. Stief, F., Böhm, H., Dussa, C.U., Multerer, C., Schwirtz, A., Imhoff, A.B. & Döderlein, L. 2014, "Effect of lower limb malalignment in the frontal plane on transverse plane mechanics during gait in young individuals with varus knee alignment", *The Knee*, vol. 21, no. 3, pp. 688-693.

300. Strickland, M., Dressler, M., Render, T., Browne, M. & Taylor, M. 2011, "Targeted computational probabilistic corroboration of experimental knee wear simulator: The importance of accounting for variability", *Medical Engineering & Physics*, vol. 33, no. 3, pp. 295-301.
301. Stukenborg-Colsman, C., Wirth, C.J., Lazovic, D. & Wefer, A. 2001, "High tibial osteotomy versus unicompartmental joint replacement in unicompartmental knee joint osteoarthritis: 7-10-year follow-up prospective randomised study", *The Knee*, vol. 8, no. 3, pp. 187-194.
302. Tadepalli, S.C., Erdemir, A. & Cavanagh, P.R. 2011, "Comparison of hexahedral and tetrahedral elements in finite element analysis of the foot and footwear", *Journal of Biomechanics*, vol. 44, no. 12, pp. 2337-2343.
303. Tanamas, S., Hanna, F.S., Cicuttini, F.M., Wluka, A.E., Berry, P. & Urquhart, D.M. 2009, "Does knee malalignment increase the risk of development and progression of knee osteoarthritis? A systematic review", *Arthritis Care & Research*, vol. 61, no. 4, pp. 459-467.
304. Tang, W.C. & Henderson, I.J. 2005, "High tibial osteotomy: long term survival analysis and patients' perspective", *The Knee*, vol. 12, no. 6, pp. 410-413.
305. Tetsworth, K. & Paley, D. 1994, "Malalignment and degenerative arthropathy", *The Orthopedic Clinics of North America*, vol. 25, no. 3, pp. 367-377.
306. Thambyah, A. 2007, "Contact stresses in both compartments of the tibiofemoral joint are similar even when larger forces are applied to the medial compartment", *The Knee*, vol. 14, no. 4, pp. 336-338.
307. Tissakht, M. & Ahmed, A.M. 1995, "Tensile stress-strain characteristics of the human meniscal material", *Journal of Biomechanics*, vol. 28, no. 4, pp. 411-422.
308. Trieb, K., Grohs, J., Hanslik-Schnabel, B., Stulnig, T., Panotopoulos, J. & Wanivenhaus, A. 2006, "Age predicts outcome of high-tibial osteotomy", *Knee Surgery, Sports Traumatology, Arthroscopy*, vol. 14, no. 2, pp. 149-152.
309. Tuncer, M., Cobb, J.P., Hansen, U.N. & Amis, A.A. 2013, "Validation of multiple subject-specific finite element models of unicompartmental knee replacement", *Medical Engineering & Physics*, vol. 35, no. 10, pp. 1457-1464.
310. Vadher, S.P., Nayeb-Hashemi, H., Canavan, P.K. & Warner, G.M. 2006, "Finite element modeling following partial meniscectomy: effect of various size of resection", *28th Annual International Conference of the IEEE Engineering in Medicine and Biology Society*. IEEE, New York, August 31 to September 3, pp. 2098.
311. van Raaij, T., Bakker, W., Reijman, M. & Verhaar, J. 2007, "The effect of high tibial osteotomy on the results of total knee arthroplasty: a matched case control study", *BMC Musculoskeletal Disorders*, vol. 8, no. 1, pp. 74-81.

312. van Raaij, T.M., Reijman, M., Brouwer, R.W., Jakma, T.S. & Verhaar, J.A. 2008, "Survival of closing-wedge high tibial osteotomy: good outcome in men with low-grade osteoarthritis after 10-16 years", *Acta Orthopaedica*, vol. 79, no. 2, pp. 230-234.
313. Vaziri, A., Nayeb-Hashemi, H., Singh, A. & Tafti, B.A. 2008, "Influence of meniscectomy and meniscus replacement on the stress distribution in human knee joint", *Annals of Biomedical Engineering*, vol. 36, no. 8, pp. 1335-1344.
314. Vázquez, A.A., Lauge-Pedersen, H., Lidgren, L. & Taylor, M. 2003, "Finite element analysis of the initial stability of ankle arthrodesis with internal fixation: flat cut versus intact joint contours", *Clinical Biomechanics*, vol. 18, no. 3, pp. 244-253.
315. Veronda, D. & Westmann, R. 1970, "Mechanical characterization of skin-finite deformations", *Journal of Biomechanics*, vol. 3, no. 1, pp. 111-124.
316. Viceconti, M., Bellingeri, L., Cristofolini, L. & Toni, A. 1998, "A comparative study on different methods of automatic mesh generation of human femurs", *Medical Engineering and Physics*, vol. 20, no. 1, pp. 1-10.
317. Virolainen, P. & Aro, H.T. 2004, "High tibial osteotomy for the treatment of osteoarthritis of the knee: a review of the literature and a meta-analysis of follow-up studies", *Archives of Orthopaedic and Trauma Surgery*, vol. 124, no. 4, pp. 258-261.
318. Vos, T., Flaxman, A.D., Naghavi, M., Lozano, R., Michaud, C., Ezzati, M., Shibuya, K., Salomon, J.A., Abdalla, S. & Aboyans, V. 2013, "Years lived with disability (YLDs) for 1160 sequelae of 289 diseases and injuries 1990–2010: a systematic analysis for the Global Burden of Disease Study 2010", *The Lancet*, vol. 380, no. 9859, pp. 2163-2196.
319. Vrana, J. & Michalec, J. 2005, "The material model of human articular cartilage", *2nd International Conference on Computational Bioengineering*. Lisbon, September 14-16.
320. Walker, P.S. & Hajek, J.V. 1972, "The load-bearing area in the knee joint", *Journal of Biomechanics*, vol. 5, no. 6, pp. 581-584.
321. Walker, P.S. 1973, *Knee-Joint Prothesis*, Google Patents, US Patent.
322. Walker, P.S., Blunn, G.W., Broome, D.R., Perry, J., Watkins, A., Sathasivam, S., Dewar, M.E. & Paul, J.P. 1997, "A knee simulating machine for performance evaluation of total knee replacements", *Journal of Biomechanics*, vol. 30, no. 1, pp. 83-89.
323. Walker, P., Heller, Y., Yildirim, G. & Immerman, I. 2011, "Reference axes for comparing the motion of knee replacements with the anatomic knee", *The Knee*, vol. 18, no. 5, pp. 312-316.

324. Walker, R.W. & Ingle, P. 2009, "Finite element modelling the natural human joint", *International Journal of Computer Aided Engineering and Technology*, vol. 1, no. 3, pp. no pagination.
325. Wang, J.W., Kuo, K., Andriacchi, T. & Galante, J. 1990, "The influence of walking mechanics and time on the results of proximal tibial osteotomy.", *The Journal of Bone and Joint Surgery. American Volume*, vol. 72, no. 6, pp. 905-909.
326. Weiss, J.A. & Gardiner, J.C. 2001, "Computational modeling of ligament mechanics", *Critical Reviews in Biomedical Engineering*, vol. 29, no. 3, pp. 303-374.
327. Weiss, J.A., Gardiner, J.C., Ellis, B.J., Lujan, T.J. & Phatak, N.S. 2005, "Three-dimensional finite element modeling of ligaments: technical aspects", *Medical Engineering & Physics*, vol. 27, no. 10, pp. 845-861.
328. Weiss, J.A., Maker, B.N. & Govindjee, S. 1996, "Finite element implementation of incompressible, transversely isotropic hyperelasticity", *Computer Methods in Applied Mechanics and Engineering*, vol. 135, no. 1, pp. 107-128.
329. Westrich, G.H., Peters, L.E., Haas, S.B., Buly, R.L. & Windsor, R.E. 1998, "Patella height after high tibial osteotomy with internal fixation and early motion", *Clinical Orthopaedics and Related Research*, vol. 354, pp. 169-174.
330. Whipple, R., Wirth, C. & Mow, V. 1984, "Mechanical properties of the meniscus" in *Advances in Bioengineering*, American Society of Mechanical Engineers, New York, pp. 32-33.
331. Wildi, L.M., Martel-Pelletier, J., Abram, F., Moser, T., Raynauld, J. & Pelletier, J. 2013, "Assessment of Cartilage Changes Over Time in Knee Osteoarthritis Disease-Modifying Osteoarthritis Drug Trials Using Semiquantitative and Quantitative Methods: Pros and Cons", *Arthritis Care & Research*, vol. 65, no. 5, pp. 686-694.
332. Wilson, W., Van Rietbergen, B., Van Donkelaar, C.C. & Huiskes, R. 2003, "Pathways of load-induced cartilage damage causing cartilage degeneration in the knee after meniscectomy", *Journal of Biomechanics*, vol. 36, no. 6, pp. 845-852.
333. Wilson, W., van Burken, C., van Donkelaar, C., Buma, P., van Rietbergen, B. & Huiskes, R. 2006, "Causes of mechanically induced collagen damage in articular cartilage", *Journal of Orthopaedic Research*, vol. 24, no. 2, pp. 220-228.
334. Wilson, W., Van Donkelaar, C., Van Rietbergen, R. & Huiskes, R. 2005, "The role of computational models in the search for the mechanical behavior and damage mechanisms of articular cartilage", *Medical Engineering & Physics*, vol. 27, no. 10, pp. 810-826.

335. Wismans, J., Veldpaus, F., Janssen, J., Huson, A. & Struben, P. 1980, "A three-dimensional mathematical model of the knee-joint", *Journal of Biomechanics*, vol. 13, no. 8, pp. 677-685.
336. Woo, S.L., Debski, R.E., Withrow, J.D. & Janaushek, M.A. 1999, "Biomechanics of knee ligaments", *The American Journal of Sports Medicine*, vol. 27, no. 4, pp. 533-543.
337. Woo, S.L., Abramowitch, S.D., Kilger, R. & Liang, R. 2006, "Biomechanics of knee ligaments: injury, healing, and repair", *Journal of Biomechanics*, vol. 39, no. 1, pp. 1-20.
338. Wright, J.M., Crockett, H.C., Slawski, D.P., Madsen, M.W. & Windsor, R.E. 2005, "High tibial osteotomy", *Journal of the American Academy of Orthopaedic Surgeons*, vol. 13, no. 4, pp. 279-289.
339. Wright, J.G., Treble, N. & Feinstein, A.R. 1991, "Measurement of lower limb alignment using long radiographs", *Journal of Bone & Joint Surgery, British Volume*, vol. 73, no. 5, pp. 721-723.
340. Yagi, T. & Sasaki, T. 1986, "Tibial torsion in patients with medial-type osteoarthritic knee", *Clinical Orthopaedics and Related Research*, vol. 213, pp. 177-182.
341. Yang, N., Nayeb-Hashemi, H. & Canavan, P.K. 2009, "The combined effect of frontal plane tibiofemoral knee angle and meniscectomy on the cartilage contact stresses and strains", *Annals of Biomedical Engineering*, vol. 37, no. 11, pp. 2360-2372.
342. Yang, N.H., Nayeb-Hashemi, H., Canavan, P.K. & Vaziri, A. 2010, "Effect of frontal plane tibiofemoral angle on the stress and strain at the knee cartilage during the stance phase of gait", *Journal of Orthopaedic Research*, vol. 28, no. 12, pp. 1539-1547.
343. Yang, N.H., Nayeb-Hashemi, H. & Canavan, P.H. 2007, "The effects of tibiofemoral angle and body weight on the stress field in the knee joint", *ASME International Mechanical Engineering Congress and Exposition*. ASME, Seattle, November 11-15, pp. 11.
344. Yao, J., Salo, A.D., Lee, J. & Lerner, A.L. 2008, "Sensitivity of tibio-menisco-femoral joint contact behavior to variations in knee kinematics", *Journal of Biomechanics*, vol. 41, no. 2, pp. 390-398.
345. Yao, J., Snibbe, J., Maloney, M. & Lerner, A.L. 2006, "Stresses and strains in the medial meniscus of an ACL deficient knee under anterior loading: a finite element analysis with image-based experimental validation.", *Journal of Biomechanical Engineering*, vol. 128, no. 1, pp. 135-141.



346. Yim, J., Song, E., Seo, H., Kim, M. & Seon, J. 2013, "Comparison of high tibial osteotomy and unicompartmental knee arthroplasty at a minimum follow-up of 3 years", *The Journal of Arthroplasty*, vol. 28, no. 2, pp. 243-247.
347. Yosibash, Z., Tal, D. & Trabelsi, N. 2010, "Predicting the yield of the proximal femur using high-order finite-element analysis with inhomogeneous orthotropic material properties", *Philosophical Transactions of the Royal Society A: Mathematical, Physical and Engineering Sciences*, vol. 368, no. 1920, pp. 2707-2723.
348. Yosibash, Z., Trabelsi, N. & Milgrom, C. 2007, "Reliable simulations of the human proximal femur by high-order finite element analysis validated by experimental observations", *Journal of Biomechanics*, vol. 40, no. 16, pp. 3688-3699.
349. Zhang, H., Totterman, S., Perucchio, R. & Lerner, A.L. 1999, "Magnetic resonance image based 3D poroelastic finite element model of tibio-menisco-femoral contact", *Proceedings of the 23rd Annual Meeting of the American Society of Biomechanics*. Pittsburgh, October 21-23.
350. Zhang, Y., Xu, L., Nevitt, M.C., Aliabadi, P., Yu, W., Qin, M., Lui, L.Y. & Felson, D.T. 2001, "Comparison of the prevalence of knee osteoarthritis between the elderly Chinese population in Beijing and whites in the United States: the Beijing Osteoarthritis Study", *Arthritis & Rheumatism*, vol. 44, no. 9, pp. 2065-2071.
351. Zhao, D., Banks, S.A., Mitchell, K.H., D'Lima, D.D., Colwell Jr, C.W. & Fregly, B.J. 2007, "Correlation between the knee adduction torque and medial contact force for a variety of gait patterns", *Journal of Orthopaedic Research*, vol. 25, no. 6, pp. 789-797.
352. Zhim, F., Laflamme, G.Y., Viens, H., Saidane, K. & Yahia, L.H. 2005, "Biomechanical stability of high tibial opening wedge osteotomy: internal fixation versus external fixation", *Clinical Biomechanics*, vol. 20, no. 8, pp. 871-876.
353. Zhong, Y., Wang, Y., Wang, H., Rong, K. & Xie, L. 2011, "Stress changes of lateral collateral ligament at different knee flexion with or without displaced movements: a 3-dimensional finite element analysis", *Chinese Journal of Traumatology (English Edition)*, vol. 14, no. 2, pp. 79-83.
354. Zielinska, B. & Donahue, T. 2006, "3D finite element model of meniscectomy: changes in joint contact behavior.", *Journal of Biomechanical Engineering*, vol. 128, no. 1, pp. 115-123.

# Appendices

## Appendix A

### A-1 Donor Summary Report

Science Care  
19301 E 23rd Ave  
Aurora, CO 80011  
Phone: 800-590-8132 Fax: 602-288-0059

Science Care

### Donor Summary Report

Donor ID: C100052

Pre-Procurement Release By: Joshua Meairs  
Final Donor Packet Approved By: Jennen Lamb

Age	50	Specimen ID Range
Height	65 in.	From 59239
Weight	150 lbs.	To 59245
Sex	Male	
Race	Caucasian	
Primary Cause of Death	Passed in Sleep	
Secondary Cause of Death	MI	

### Serology Results

	Initial Results	Confirmatory Results
HBsAg	Non-Reactive	
Anti-HCV	Non-Reactive	
Anti-HIV-1/HIV-2	Non-Reactive	
Other		
Other		
Other		
Other		

Medical Director Comments

Thursday, February 18, 2010

Page 1 of 2

Figure A-1: Donor Summary Report Page 1

Science Care  
19301 E 23rd Ave

Aurora, CO 80011  
Phone: 800-590-8132 Fax: 602-288-0059

Science Care

### Donor Summary Report

Donor ID: C100052

Pre-Procurement Release By: Joshua Meairs  
Final Donor Packet Approved By: Jennen Lamb

#### Medical Social Summary

Bone/Joint None Specified

Cancer None Specified

Medications Any medications? Dosage? Frequency?  
Stress Vitamins, Advil, Baby Aspirin

Organ Any history of any lung disease? Asthma, allergies?  
Respiratory cold in last month

Other Ever any allergies?  
Hay fever

Social Any alcohol or tobacco use?  
Tobacco 30 yrs, under 1ppd; ETOH social to none  
Ever incarcerated or institutionalized?  
6 months in 2000 white collar; no tattoos

Surgeries Any past surgical procedures or major illnesses?  
Rod in leg due to fx 30 yrs ago (unk site)  
Any bone or joint surgery including: knee, elbow?  
Rod in leg due to fx 30 yrs ago (unk site); cracked rib 5 yrs ago

Donor Visual Inspection:

Thursday, February 18, 2010

Page 2 of 2

Figure A-2: Donor Summary Report Page 2

A-2

Ethics approval from HSS to use cadaver

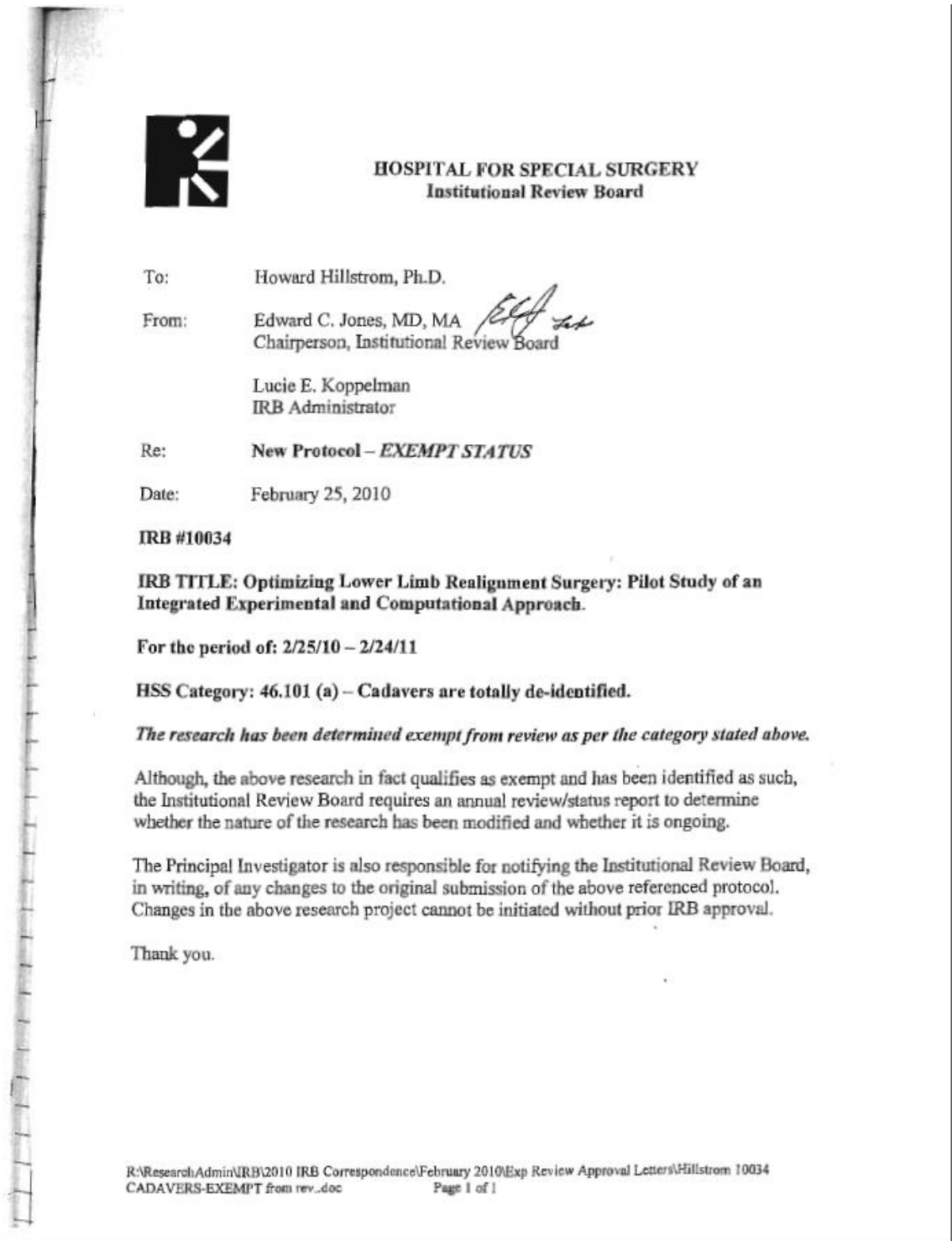


Figure A-3: Ethical approval to carry out cadaveric test

## Appendix B

### B-1 Sensitivity analyses for model with and without hourglass control

**Table B-1: Contact force in the model with and without hourglass control with corresponding errors**

	Contact Force (N)							
	No Hourglass		With Hourglass		%error		square error	
Step Interval	Lateral	Media l	Latera l	Media l	Latera l	Medial	Latera l	Media l
0	21.82	19.78	21.88	19.87	0.30	0.48	0.00	0.01
0.1	34.01	25.55	34.08	25.65	0.20	0.39	0.00	0.01
0.2	53.23	35.15	53.34	35.25	0.22	0.30	0.01	0.01
0.3	84.6	49.70	84.79	49.78	0.22	0.15	0.04	0.01
0.4	134.17	71.09	134.36	71.17	0.14	0.12	0.04	0.01
0.5	210.29	102.75	210.48	102.79	0.09	0.04	0.04	0.00
0.6	325.97	149.97	326.04	150.01	0.02	0.02	0.01	0.00
0.7	369.65	167.74	369.70	167.73	0.01	0.00	0.00	0.00
0.8	435.39	194.42	435.40	194.37	0.00	-0.02	0.00	0.00
0.9	534.37	234.56	534.29	234.43	-0.01	-0.05	0.01	0.02
1	607.34	264.18	607.09	264.14	-0.04	-0.02	0.06	0.00
						MSE	0.02	0.01
						RMS E	0.13	0.08
						%FSE	0.02	0.03

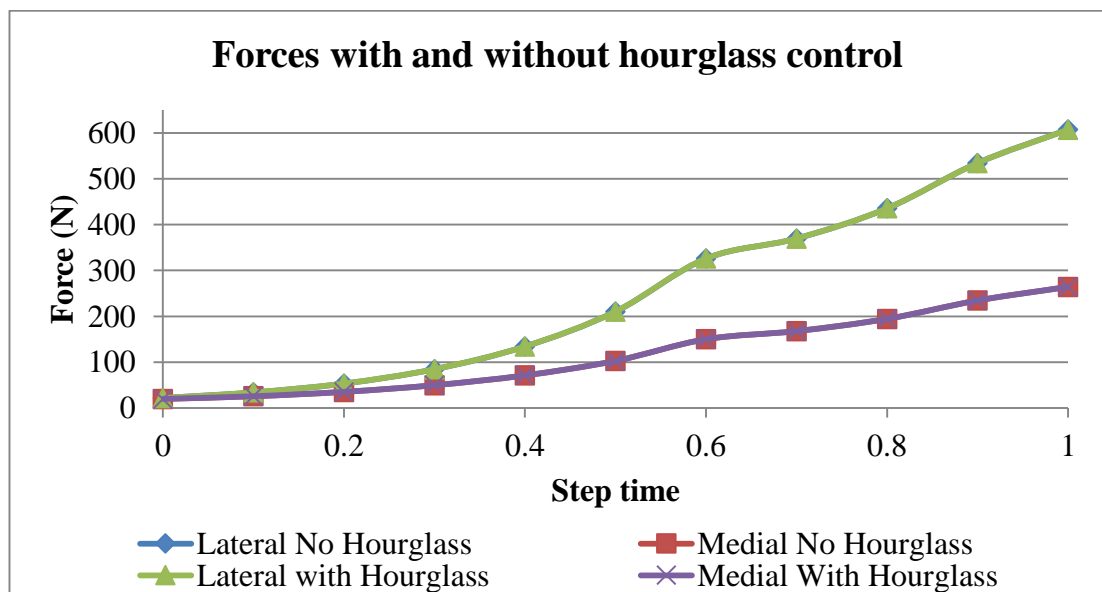


Figure B-1: Contact force in the model with and without hourglass control

Table B-2: Contact pressure in the model with and without hourglass control with corresponding errors

Step Interval	Pressure (MPa)				%error		square error	
	No Hourglass		with Hourglass					
	Lateral	Medial	Lateral	Medial	Lateral	Medial	Lateral	Medial
0	0.00	0.00	0.00	0.00	0.00	0.00	0.00	0.00
0	0.00	0.00	0.00	0.00	0.00	0.00	0.00	0.00
0.1	0.00	0.49	0.32	0.53	-100.00	-7.55	0.10	0.00
0.2	0.42	0.52	0.47	0.55	11.90	5.77	0.00	0.00
0.3	0.72	0.69	0.77	0.77	6.94	11.59	0.00	0.01
0.4	1.09	0.73	1.16	0.79	6.42	8.22	0.00	0.00
0.5	1.37	1.01	1.49	0.91	8.76	-9.90	0.01	0.01
0.6	2.28	1.24	2.25	1.17	-1.32	-5.65	0.00	0.00
0.7	2.62	1.92	2.59	1.88	-1.15	-2.08	0.00	0.00
0.8	3.13	2.19	3.11	2.15	-0.64	-1.83	0.00	0.00
0.9	3.93	2.37	3.91	2.38	-0.51	0.42	0.00	0.00
1	4.50	2.63	4.49	2.63	-0.22	0.00	0.00	0.00
MSE							0.01	0.00
RMSE							0.10	0.05
%FSE							2.31	1.92

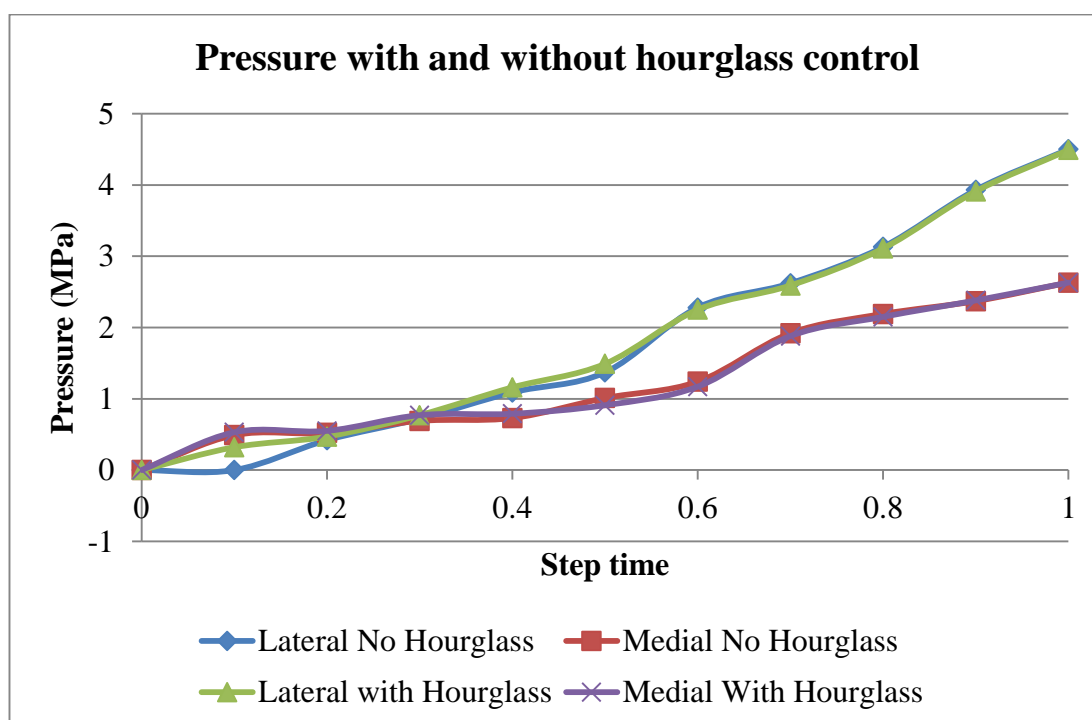
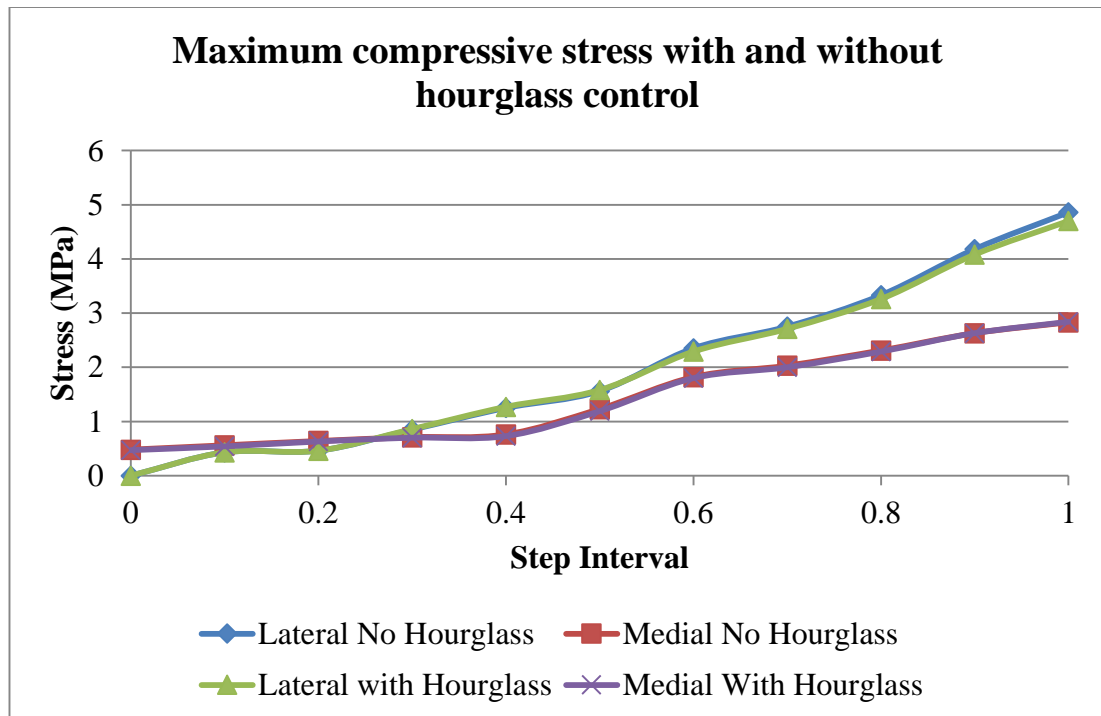


Figure B-2: Contact pressure in the model with and without hourglass control

**Table B-3: Maximum compressive stress in the model with and without hourglass control with corresponding errors**

	Maximum Compressive Stress (MPa)							
	No Hourglass		with Hourglass		%error		square error	
Step Interval	Lateral	Medial	Lateral	Medial	Lateral	Medial	Lateral	Medial
0	0.00	0.48	0.00	0.47	-100.00	-2.08	0.00	0.00
0.1	0.43	0.56	0.43	0.54	0.00	-3.57	0.00	0.00
0.2	0.46	0.64	0.46	0.63	0.00	-1.56	0.00	0.00
0.3	0.85	0.71	0.86	0.70	1.18	-1.41	0.00	0.00
0.4	1.25	0.76	1.27	0.73	1.60	-3.95	0.00	0.00
0.5	1.56	1.23	1.58	1.19	1.28	-3.25	0.00	0.00
0.6	2.35	1.82	2.29	1.80	-2.55	-1.10	0.00	0.00
0.7	2.75	2.03	2.71	2.00	-1.45	-1.48	0.00	0.00
0.8	3.33	2.31	3.26	2.29	-2.10	-0.87	0.00	0.00
0.9	4.18	2.63	4.08	2.63	-2.39	0.00	0.01	0.00
1	4.86	2.83	4.70	2.84	-3.29	0.35	0.03	0.00
						MSE	0.00	0.00
						RMSE	0.06	0.02
						%FSE	1.28	0.72



**Figure B-3: Maximum compressive stress in the model with and without hourglass control**

**Table B-4: Maximum shear stress in the model with and without hourglass control with corresponding errors**

		Maximum shear stress (MPa)							
		No Hourglass		with Hourglass		%error		square error	
Step Interval	Lateral	Medial	Lateral	Medial	Lateral	Medial	Lateral	Medial	
0.0	0.00	0.00	0.00	0.00	0.00	0.00	0.00	0.00	
0.1	0.00	0.33	0.00	0.32	0.00	-3.03	0.00	0.00	
0.2	0.33	0.36	0.31	0.35	-6.06	-2.78	0.00	0.00	
0.3	0.49	0.43	0.49	0.45	0.00	4.65	0.00	0.00	
0.4	0.78	0.48	0.74	0.48	-5.13	0.00	0.00	0.00	
0.5	1.04	0.74	1.03	0.73	-0.96	-1.35	0.00	0.00	
0.6	1.49	1.13	1.41	1.07	-5.37	-5.31	0.01	0.00	
0.7	1.77	1.28	1.70	1.18	-3.95	-7.81	0.00	0.01	
0.8	2.11	1.38	2.01	1.34	-4.74	-2.90	0.01	0.00	
0.9	2.68	1.56	2.56	1.54	-4.48	-1.28	0.01	0.00	
1.0	3.31	1.66	2.93	1.61	-11.48	-3.01	0.14	0.00	
							MSE	0.02	0.00
							RMSE	0.12	0.04
							%FSE	3.72	2.38

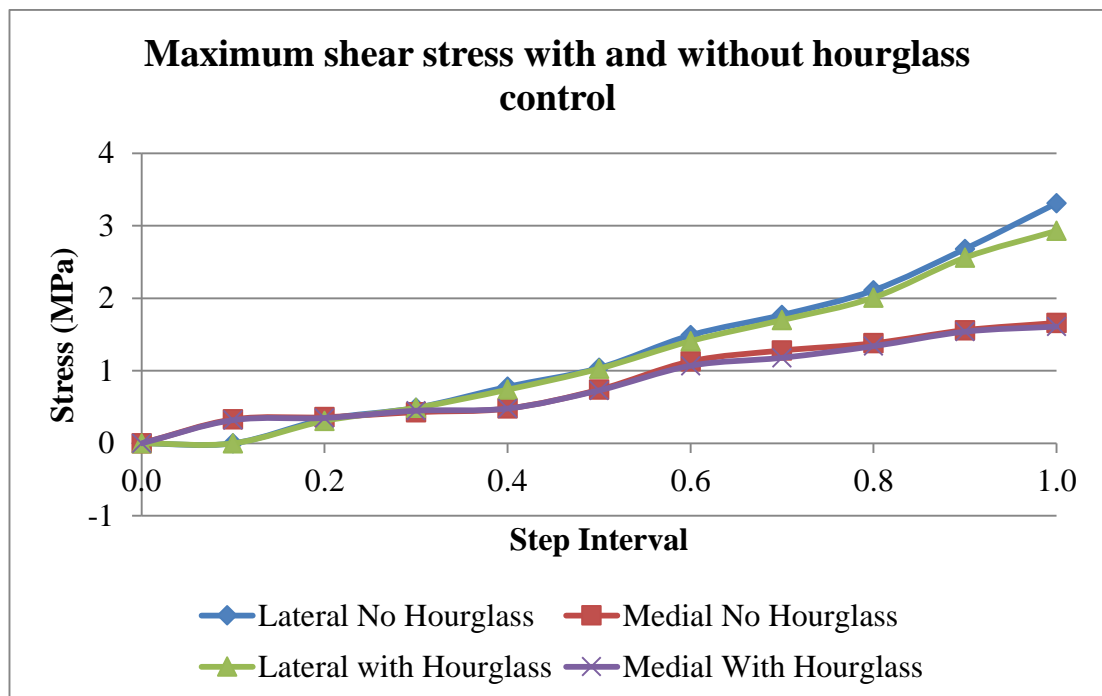


**Figure B-4: Maximum shear stress in the model with and without hourglass control**



## B-2 Sensitivity analysis for model with a pure cortical tibia and a tibia with cortical and cancellous bone

**Table B-5: Contact force in the model with a pure cortical tibia and a tibia with cortical and cancellous bone**

Step Interval	Contact Force (N)							
	Cortical and Cancellous		Pure Cortical		%error		Square error	
	Lateral	Medial	Lateral	Medial	Lateral	Medial	Lateral	Medial
0	11.14	15.47	11.14	15.47	0.00	0.00	0.00	0.00
0.1	23.44	64.05	23.40	64.09	-0.17	0.06	0.00	0.00
0.2	51.72	151.14	51.40	151.44	-0.63	0.20	0.11	0.09
0.3	75.39	212.33	74.70	212.99	-0.92	0.31	0.48	0.43
0.4	100.68	272.65	99.50	273.78	-1.17	0.41	1.39	1.27
0.5	127.55	332.07	125.76	333.78	-1.40	0.52	3.19	2.93
0.6	156.15	390.33	153.64	392.74	-1.61	0.62	6.34	5.81
0.7	186.49	447.39	183.13	450.60	-1.80	0.72	11.28	10.30
0.8	218.57	503.19	214.26	507.30	-1.97	0.82	18.52	16.88
0.9	252.23	557.79	246.84	562.89	-2.13	0.91	29.00	26.01
1	277.39	596.27	271.15	602.15	-2.25	0.99	38.84	34.61
<b>MSE</b>							<b>9.92</b>	<b>8.94</b>
<b>RMSE</b>							<b>3.15</b>	<b>2.99</b>
<b>%FSE</b>							<b>1.14</b>	<b>0.50</b>

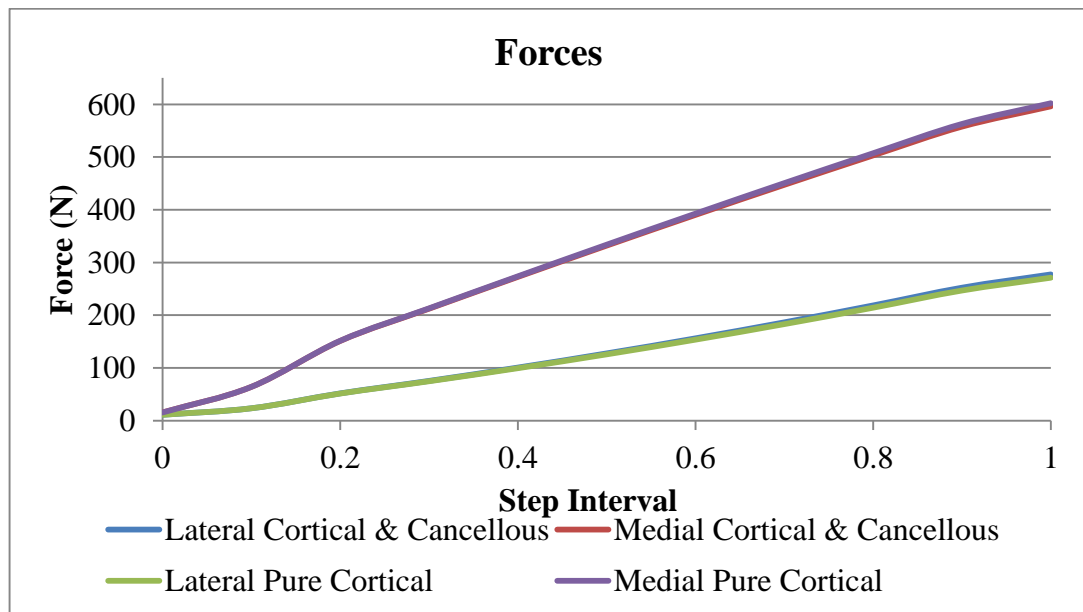


**Figure B-5: Contact force in the model with a pure cortical tibia and a tibia with cortical and cancellous bone**

**Table B-6: Contact pressure in the model with a pure cortical tibia and a tibia with cortical and cancellous bone**

Step Interval	Contact Pressure (MPa)							
	Cortical and Cancellous		Pure Cortical		%error		Square error	
	Lateral	Medial	Lateral	Medial	Lateral	Medial	Lateral	Medial
0	0.29	0.32	0.31	0.32	6.90	0.00	0.00	0.00
0.1	0.34	1.11	0.34	1.12	0.00	0.90	0.00	0.00
0.2	0.69	1.85	0.69	1.85	0.00	0.00	0.00	0.00
0.3	1.04	2.47	1.05	2.49	0.96	0.81	0.00	0.00
0.4	1.27	2.71	1.28	2.72	0.79	0.37	0.00	0.00
0.5	1.39	2.94	1.41	3.01	1.44	2.38	0.00	0.00
0.6	1.55	3.36	1.54	3.40	-0.65	1.19	0.00	0.00
0.7	1.72	3.67	1.69	3.68	-1.74	0.27	0.00	0.00
0.8	1.93	3.76	1.89	3.76	-2.07	0.00	0.00	0.00
0.9	2.23	3.97	2.16	3.83	-3.14	-3.53	0.00	0.02
1	2.48	4.22	2.44	4.16	-1.61	-1.42	0.00	0.00
						<b>MSE</b>	<b>0.00</b>	<b>0.00</b>
						<b>RMSE</b>	<b>0.03</b>	<b>0.05</b>
						<b>%FSE</b>	<b>1.22</b>	<b>1.25</b>

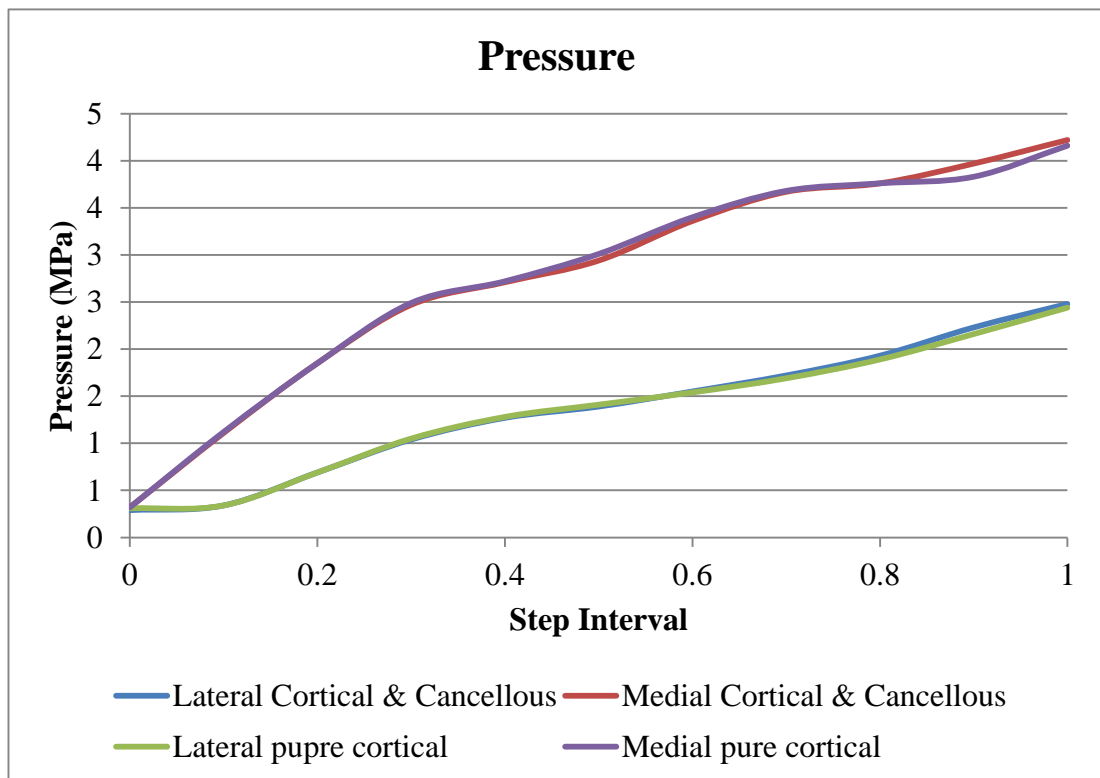


**Figure B-6: Contact pressure in the model with a pure cortical tibia and a tibia with cortical and cancellous bone**

**Table B-7: Maximum compressive stress in the model with a pure cortical tibia and a tibia with cortical and cancellous bone**

Step Interval	Maximum Compressive Stress (MPa)							
	Cortical and Cancellous		Pure Cortical		%error		Square error	
	Lateral	Medial	Lateral	Medial	Lateral	Medial	Lateral	Medial
0	0.38	0.37	0.37	0.36	-2.63	-2.70	0.00	0.00
0.1	0.38	0.65	0.38	0.65	0.00	0.00	0.00	0.00
0.2	0.80	1.79	0.79	1.79	-1.25	0.00	0.00	0.00
0.3	1.09	2.37	1.12	2.37	2.75	0.00	0.00	0.00
0.4	1.33	2.77	1.35	2.77	1.50	0.00	0.00	0.00
0.5	1.57	2.98	1.56	3.05	-0.64	2.35	0.00	0.00
0.6	1.72	3.29	1.70	3.25	-1.16	-1.22	0.00	0.00
0.7	1.95	3.55	1.92	3.57	-1.54	0.56	0.00	0.00
0.8	2.15	3.65	2.12	3.70	-1.40	1.37	0.00	0.00
0.9	2.55	3.94	2.52	3.91	-1.18	-0.76	0.00	0.00
1	2.63	4.03	2.70	4.04	2.66	0.25	0.00	0.00
						<b>MSE</b>	<b>0.00</b>	<b>0.00</b>
						<b>RMSE</b>	<b>0.03</b>	<b>0.03</b>
						<b>%FSE</b>	<b>1.09</b>	<b>0.76</b>

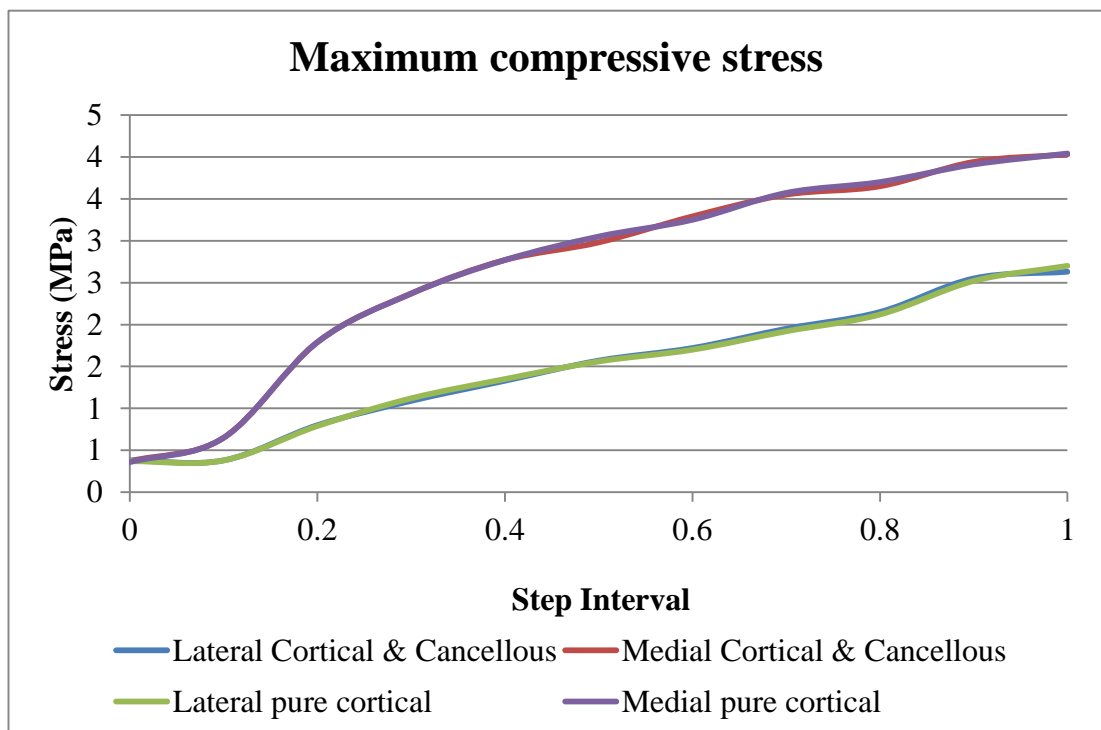


**Figure B-7: Maximum compressive stress in the model with a pure cortical tibia and a tibia with cortical and cancellous bone**

**Table B-8: Maximum shear stress in the model with a pure cortical tibia and a tibia with cortical and cancellous bone**

Step Interval	Maximum shear Stress (MPa)							
	Cortical and Cancellous		Pure Cortical		%error		Square error	
	Lateral	Medial	Lateral	Medial	Lateral	Medial	Lateral	Medial
0	0.22	0.23	0.22	0.23	0.00	0.00	0.00	0.00
0.1	0.25	0.40	0.23	0.40	-8.00	0.00	0.00	0.00
0.2	0.46	1.06	0.46	1.05	0.00	-0.94	0.00	0.00
0.3	0.67	1.38	0.68	1.35	1.49	-2.17	0.00	0.00
0.4	0.83	1.61	0.83	1.57	0.00	-2.48	0.00	0.00
0.5	0.96	1.66	0.97	1.68	1.04	1.20	0.00	0.00
0.6	1.07	1.79	1.08	1.81	0.93	1.12	0.00	0.00
0.7	1.16	1.86	1.17	1.81	0.86	-2.69	0.00	0.00
0.8	1.35	1.94	1.36	1.92	0.74	-1.03	0.00	0.00
0.9	1.54	2.05	1.54	2.04	0.00	-0.49	0.00	0.00
1	1.70	2.10	1.73	2.10	1.76	0.00	0.00	0.00
						<b>MSE</b>	<b>0.00</b>	<b>0.00</b>
						<b>RMSE</b>	<b>0.01</b>	<b>0.02</b>
						<b>%FSE</b>	<b>0.74</b>	<b>1.15</b>

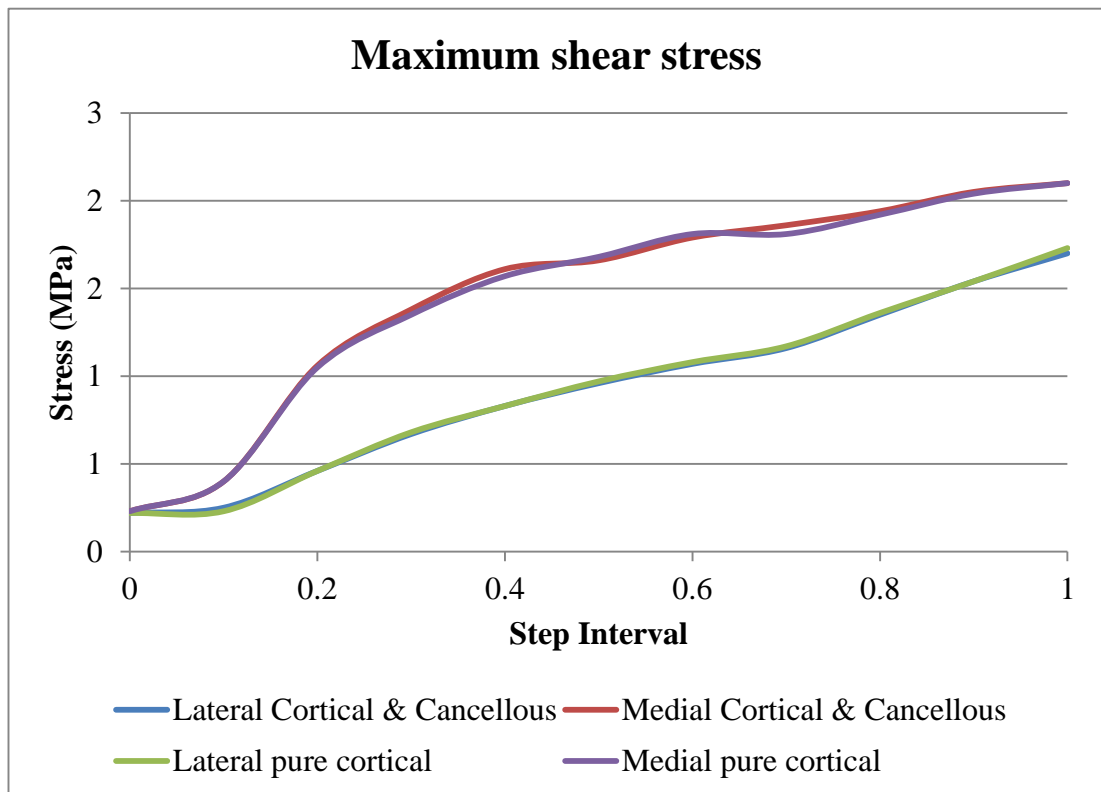


**Figure B-8: Maximum shear stress in the model with a pure cortical tibia and a tibia with cortical and cancellous bone**

### B-3 Sensitivity analysis for model with a short and long tibia

Table B-9: Contact force in the model with a short and long tibia

Step Interval	Force (N)					
	Long		Short		Long rigid extension	
	Lateral	Medial	Lateral	Medial	Lateral	Medial
0	1.71	1.97	1.71	1.97	1.71	1.97
0.1	12.12	67.23	11.91	67.45	11.93	67.42
0.2	23.78	134.36	22.93	135.24	22.97	135.20
0.3	38.22	201.59	36.07	203.71	36.14	203.63
0.4	55.27	268.31	51.34	272.13	51.45	272.01
0.5	73.88	334.35	67.69	340.35	67.85	340.18
0.6	93.96	399.60	85.03	408.24	85.23	408.03
0.7	115.75	463.83	103.53	475.59	103.78	475.33
0.8	139.31	527.15	123.39	542.46	123.69	542.14
0.9	164.57	589.65	144.24	609.04	144.60	608.66
1	191.65	651.15	166.47	675.06	166.89	674.62
Total Force	842.79		841.53		841.51	
		<b>MSE</b>	144.44	131.87	0.05	0.05
		<b>RMSE</b>	12.02	11.48	0.22	0.23
		<b>RMSE <math>F_{total}</math></b>	1.27		0.02	
		<b>%FSD</b>	6.27	1.70	0.13	0.03

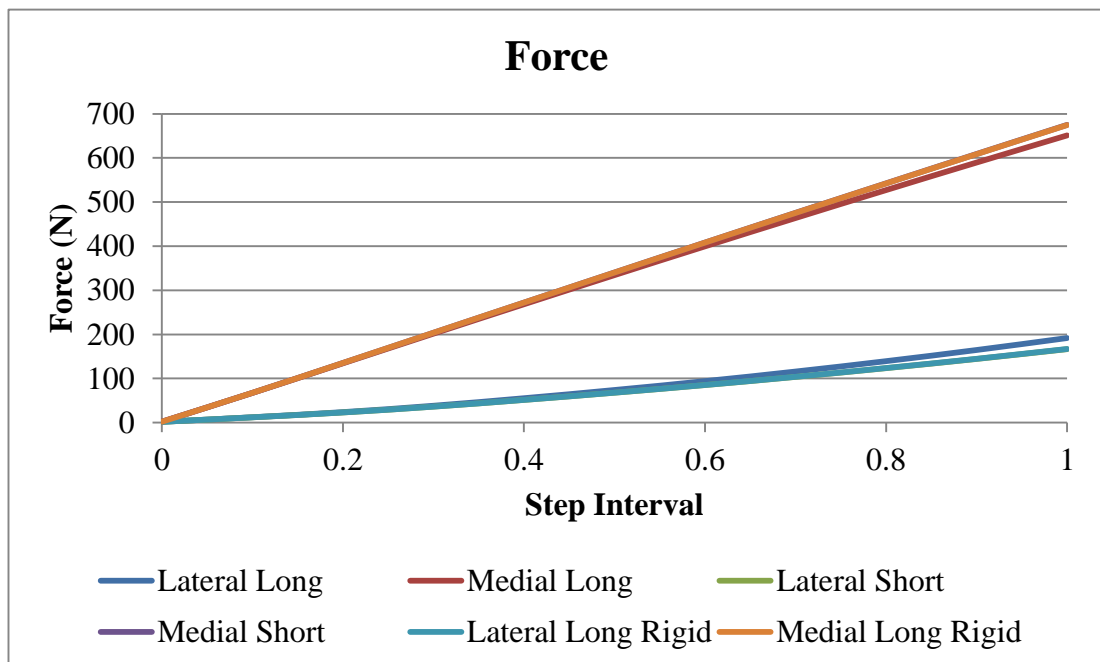
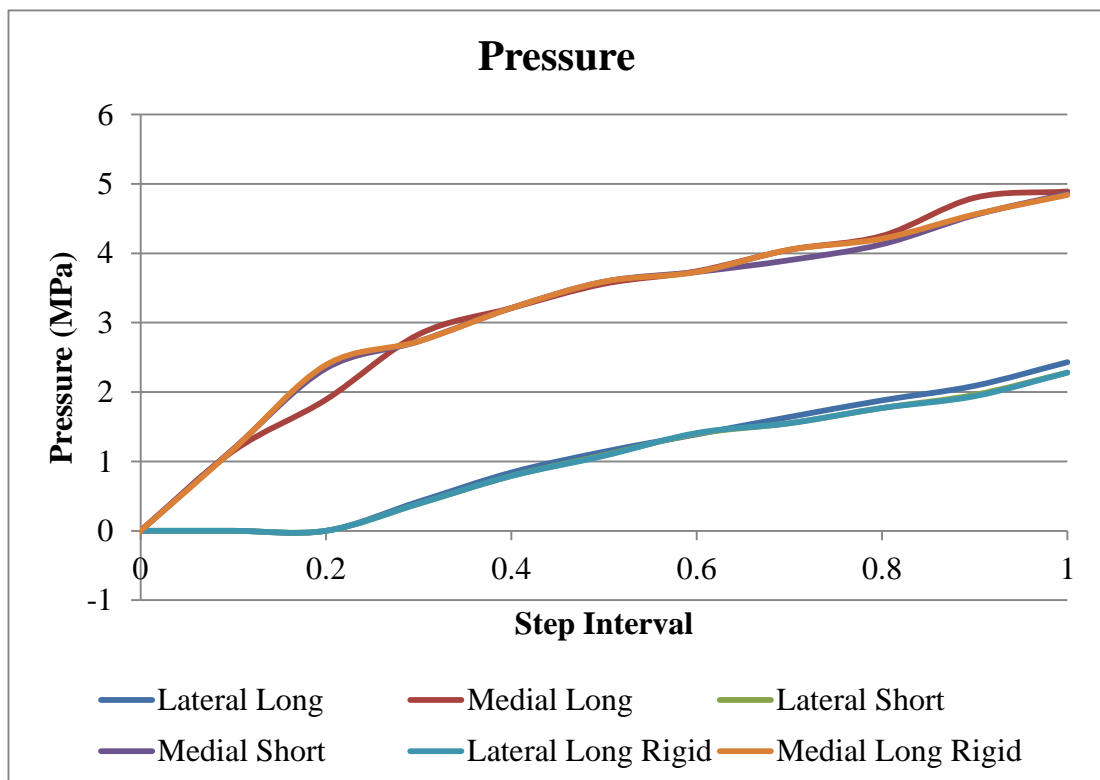


Figure B-9: Contact force in the model with a short and long tibia

**Table B-10: Contact pressure in the model with a short and long tibia**

Step Interval	Contact Pressure (MPa)					
	Long		Short		Long with rigid extension	
	Lateral	Medial	Lateral	Medial	Lateral	Medial
0	0.00	0.00	0.00	0.00	0.00	0.00
0.1	0.00	1.15	0.00	1.18	0.00	1.17
0.2	0.00	1.89	0.00	2.34	0.00	2.39
0.3	0.42	2.83	0.39	2.73	0.39	2.73
0.4	0.84	3.21	0.79	3.21	0.79	3.21
0.5	1.14	3.56	1.09	3.59	1.08	3.59
0.6	1.39	3.74	1.40	3.73	1.41	3.73
0.7	1.64	4.05	1.55	3.90	1.55	4.05
0.8	1.88	4.25	1.77	4.13	1.77	4.21
0.9	2.09	4.80	1.96	4.55	1.94	4.56
1	2.43	4.89	2.28	4.86	2.28	4.84
		<b>MSE</b>	<b>0.01</b>	<b>0.03</b>	<b>0.00</b>	<b>0.00</b>
		<b>RMSE</b>	<b>0.08</b>	<b>0.17</b>	<b>0.01</b>	<b>0.05</b>
		<b>%FSE</b>	<b>3.18</b>	<b>3.46</b>	<b>0.32</b>	<b>1.11</b>



**Figure B-10: Contact pressure in the model with a short and long tibia**

**Table B-11: Maximum compressive stress in the model with a short and long tibia**

Step Interval	Maximum Compressive Stress (MPa)					
	Long		Short		Long with rigid extension	
	Lateral	Medial	Lateral	Medial	Lateral	Medial
0	0.00	0.00	0.00	0.00	0.00	0.00
0.1	0.25	1.17	0.25	1.17	0.25	1.17
0.2	0.30	2.14	0.28	2.14	0.30	2.16
0.3	0.49	2.78	0.46	2.78	0.46	2.78
0.4	0.92	3.23	0.91	3.06	0.89	3.06
0.5	1.29	3.38	1.23	3.37	1.23	3.36
0.6	1.50	3.65	1.41	3.71	1.41	3.71
0.7	1.83	3.98	1.74	3.99	1.74	3.99
0.8	1.99	4.11	1.89	4.14	1.88	4.14
0.9	2.33	4.25	2.19	4.26	2.19	4.29
1	2.66	4.60	2.57	4.59	2.57	4.56
MSE			0.01	0.00	0.00	0.00
RMSE			0.07	0.06	0.01	0.01
%FSE			2.75	1.21	0.35	0.32

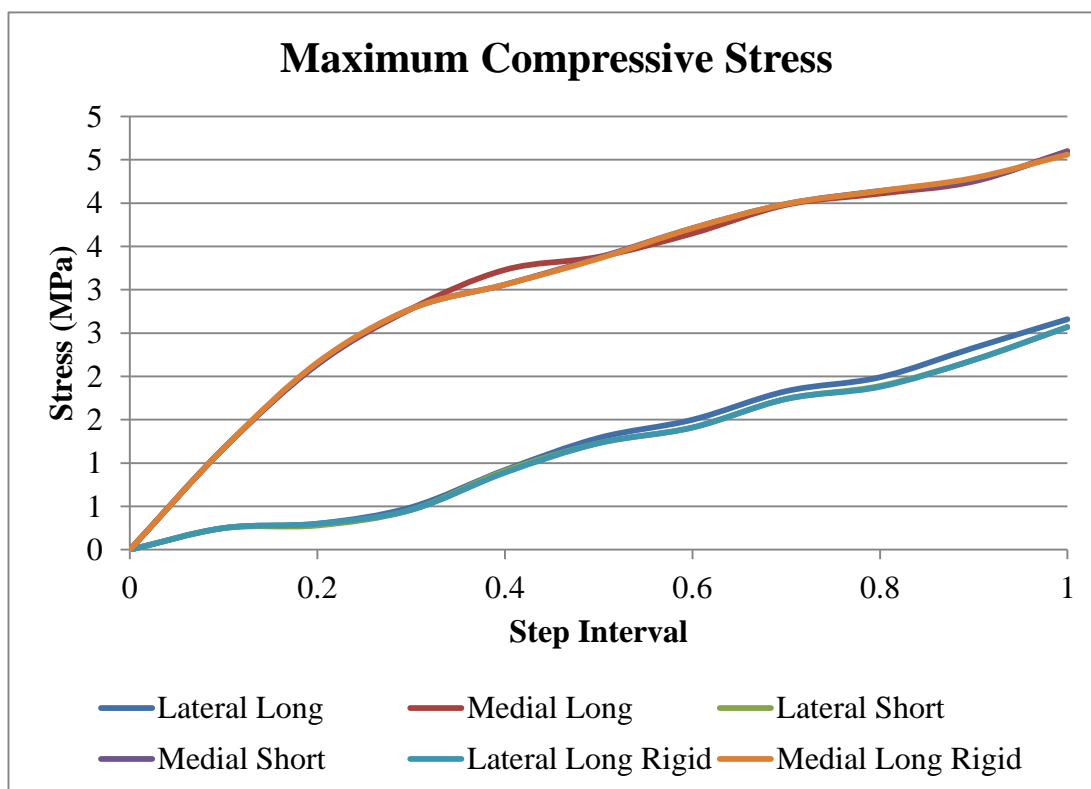


**Figure B-11: Maximum compressive stress in the model with a short and long tibia**

**Table B-12: Maximum shear stress in the model with a short and long tibia**

Step Interval	Maximum shear Stress (MPa)					
	Long		Short		Long with rigid extension	
	Lateral	Medial	Lateral	Medial	Lateral	Medial
0	0.00	0.00	0.00	0.00	0.00	0.00
0.1	0.00	0.66	0.00	0.66	0.00	0.66
0.2	0.25	1.21	0.24	1.21	0.24	1.21
0.3	0.30	1.58	0.28	1.58	0.30	1.58
0.4	0.53	1.69	0.50	1.69	0.54	1.67
0.5	0.70	1.79	0.67	1.79	0.71	1.80
0.6	0.87	1.89	0.89	1.89	0.87	1.89
0.7	1.02	1.97	0.98	1.91	1.03	1.93
0.8	1.25	2.08	1.23	2.08	1.21	2.00
0.9	1.48	2.12	1.48	2.13	1.51	2.12
1	1.71	2.19	1.73	2.20	1.74	2.14
		<b>MSE</b>	<b>0.00</b>	<b>0.00</b>	<b>0.00</b>	<b>0.00</b>
		<b>RMSE</b>	<b>0.02</b>	<b>0.02</b>	<b>0.03</b>	<b>0.03</b>
		<b>%FSE</b>	<b>1.24</b>	<b>0.84</b>	<b>1.54</b>	<b>1.44</b>

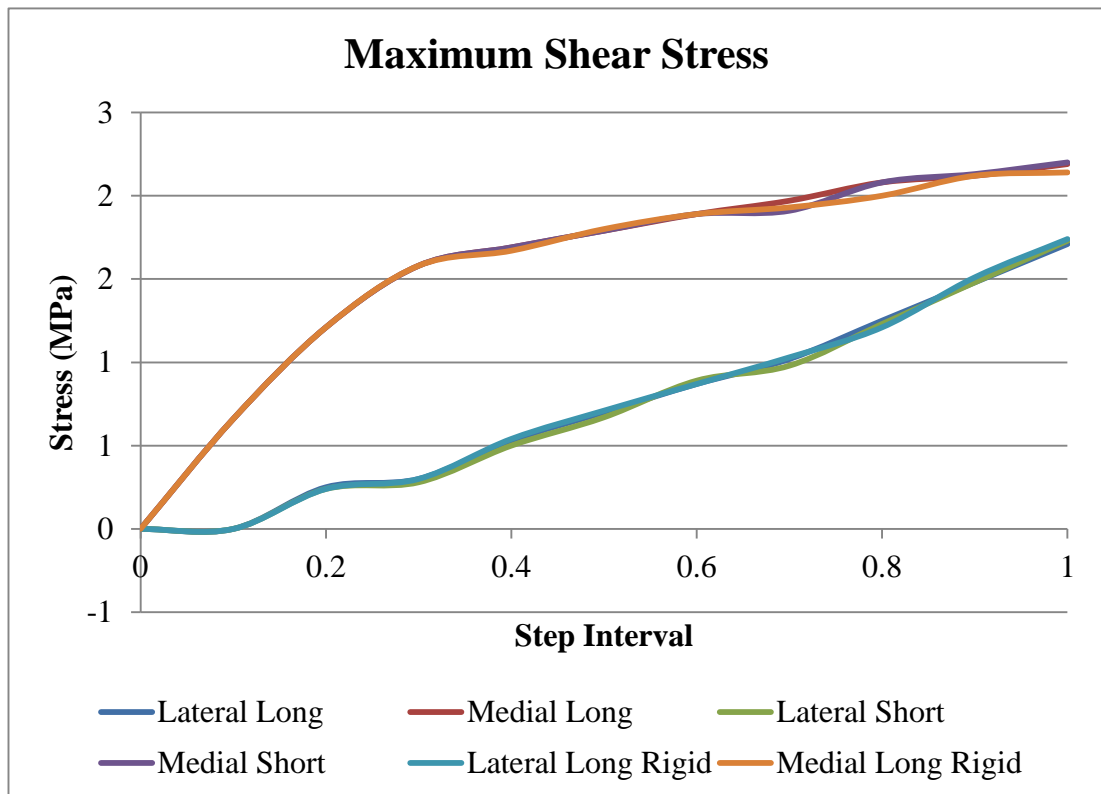


**Figure B-12: Maximum shear stress in the model with a short and long tibia**



## Appendix C

### C-1 Transformation matrices

#### Transformation Matrix Femur to Abaqus

<b>ORG<sub>Fem</sub></b>	72.25785	<b>Point 7</b>	64.69253
	-53.343933	<b>at 0°</b>	-149.51435
	4.1216		9.24365

<b>Point 8</b>	70.1809	<b>Point 9</b>	74.3348
	-52.64711		-54.040756
	-38.7267		46.9699

		<b>unit vector</b>			<b>unit vector</b>
<b>X<sub>femtemp</sub></b>	-7.565	-0.0783	<b>Z = X<sub>femtemp</sub> × Y</b>	0.9933	0.995484
	-96.170	-0.9955		-0.0807	-0.080956
	5.1220	0.0530		-0.0494	-0.049569

		<b>unit vector</b>			<b>unit vector</b>
<b>Y<sub>fem</sub></b>	-4.1539	-0.0484089	<b>X<sub>fem</sub> = Y × Z</b>	-0.0816	-0.08165
	1.393646	0.0162413		-0.9965	-0.99658
	-85.6966	-0.998695		-0.0122	-0.01224

<b>Matrix <math>T_{Fem}^{Aba}</math></b>	-0.081650149	-0.048408938	0.99548472	72.25785
	-0.996585776	0.016241345	-0.080950666	-53.3439
	-0.012249275	-0.998695546	-0.049569768	4.1216
	0	0	0	1

<b>Inverse <math>T_{Aba}^{Fem}</math></b>	-0.081650149	-0.996585776	-0.012249275	-47.211454
	-0.048408938	0.016241345	-0.998695546	8.4805265
	0.99548472	-0.080950666	-0.049569768	-76.045505
	0	0	0	1

### Transformation Matrix Tibia to Abaqus

**Point 7**  
**at 20°**  
 95.5411  
 -146.372  
 8.14257

**Point 10**  
 82.4639  
 -97.2687  
 -33.9168

**Point 11**  
 80.546  
 -101.74  
 42.9596

**ORG<sub>Tib</sub>**  
 81.50495  
 -99.50435  
 4.5214

**unit vector**  
**X<sub>tib</sub>**  
 14.03615  
 -46.86765  
 3.62117  
 0.286112  
 -0.955348  
 0.073813

**unit vector**  
**y<sub>tibtemp</sub>**  
 1.9179  
 4.4713  
 -76.876  
 0.024898  
 0.05804  
 -0.9983

**unit vector**  
**Z<sub>tib</sub>**  
 0.949156654  
 0.287379007  
 0.040394  
 0.956299769  
 0.289541749  
 0.040697995

**unit vector**  
**y<sub>tib</sub>=Z<sub>tib</sub> × X<sub>tib</sub>**  
 0.06025  
 -0.058943  
 -0.996441  
 0.06025  
 -0.0589  
 -0.9964

**T<sub>tib</sub><sup>aba</sup><sub>temp</sub>**  
 0.286112447  
 -0.955348726  
 0.073813817  
 0  
 0.06025296  
 -0.058943933  
 -0.996441264  
 0  
 0.956299769  
 0.289541749  
 0.040697995  
 0  
 81.50495  
 -99.50435  
 4.5214  
 1

$T_{aba}^{tib\text{temp}}$	0.286112447	-0.955348726	0.073813817	-118.7146765
	0.06025296	-0.058943933	-0.996441264	-6.270782689
	0.956299769	0.289541749	0.040697995	-49.31651323
	0	0	0	1

$$\text{ORG}_{\text{Tib fixed}} = \text{ORG}_{\text{fem}} \times T_{aba}^{tib\text{temp}} \quad \text{Translation}_{\text{TibtoFem}} = \text{ORG}_{\text{Tib fixed}} \times T_{tib}^{aba\text{temp}}$$

-46.77451674	66.90239703
-2.879664466	-54.02289829
4.50609723	5.402772091
1	1

$T_{tib}^{aba}$	0.286112447	0.06025296	0.956299769	66.90239703
	-0.955348726	-0.058943933	0.289541749	-54.02289829
	0.073813817	-0.996441264	0.040697995	5.402772091
	0	0	0	1

### Transformation Matrix Tibia to Femur for Abaqus (in this case 20°)

$$T_{tib}^{fem} = T_{aba}^{fem} \times T_{tib}^{aba}$$

0.927821661	0.066028706	-0.367133728	1.098227256
-0.103084079	0.991267342	-0.082235816	-1.031276377
0.358497751	0.114145813	0.92652582	-5.339816314
0	0	0	1

### Transformation Matrix Tibia to Femur for Cadaver (in this case 20°)

$$T_{tib}^{fem} = T_{glo}^{fem} \times T_{tib}^{glo}$$

0.9294	-0.016568	-0.36871	3.3016
0.00072944	0.99907	-0.043055	0.60851
0.36908	0.039746	0.92855	-4.8215
0	0	0	1

$$Inverse = T_{fem}^{tib}$$

0.929394949	0.000729467	0.36907934	-1.28941823
-0.016568012	0.999074886	0.03974625	-0.36160958
-0.368706667	-0.043054722	0.92854498	5.720500795
0	0	0	1

### Identity Check

$$T_{tib}^{fem} (abaqus) \times T_{fem}^{tib} (cadaver)$$

0.999999999	0	0	0
0	1	0	0
0	0	0.999999999	0
0	0	0	1

## Appendix D

### D-1 Matlab file

#### Batch file

```
function batch_GSParams
clear all
clc

%% Import tekscan data
% [file_list path]=uigetfile(...
%     {'*In*_0d*.*','Transform Files (*.csv)'};...
%     '*..*', 'All Files (*.*)'}, ...
%     'Pick a transform file',...
%     'MultiSelect','on');

[file_list path]=uigetfile(...
    {'*. *.*'}, ...
    'Pick a transform file',...
    'MultiSelect','on');

file_list
if iscell(file_list)
    for x=1:length(file_list)
        disp(['Running: ' path file_list{x}])
        [data]=GSParams(file_list{x},path)
        outputdata(x,:)= data
    end
else
    disp(['Running: ' path file_list])
    [data]=GSParams(file_list,path)
    outputdata= data
end

%outputdata_all=[file_list' outputdata]
xlswrite('GS_Params.xls',outputdata,1,'A1')
end
```

### Input for batch file

```
function [data]=GSParams(file_list,path)

%% Import data
% [xfrmfilename]=uigetfile(...
%     {'*tWRTf_Xforms*.csv','Excel Files (*.csv)'; ...
%     '*.*', 'All Files (*.*)'}, ...
%     'Pick a transform file', ...
%     'MultiSelect', 'off');

%% Identify specimen number from file name imported through the
variable: file_list
file_list

[xfrmdata]=csvread(file_list);

%% Extract transforms from 2D vector into a 3D vector. Each z
component of the 3D vector contains a transform matrix
num_rows=size(xfrmdata,1)
numxfirms=(num_rows)/5
for index=1:numxfirms
    xfrm3D(1:4,1:4,index)=xfrmdata(((index-1)*5+1):((index-
1)*5+4),1:4);
end
%% Calculate e2 and position vector, H
Fx=[ones(numxfirms,1)    zeros(numxfirms,1)    zeros(numxfirms,1)]';
% X-axis of Femur=Fx
Fy=[zeros(numxfirms,1)    ones(numxfirms,1)    zeros(numxfirms,1)]';
% Y-axis of Femur=Fy
Fz=[zeros(numxfirms,1)    zeros(numxfirms,1)    ones(numxfirms,1)]';
% Z-axis of Femur=Fz

%% Also calculate GS params from direction cosines in rotation
matrix H describes position of tibia origin wrt femur origin
for index2=1:numxfirms
```

```

Tft_x(1:3,index2)= xfrm3D(1:3,1,index2);
% X-axis of tibia wrt femur reference
Tft_y(1:3,index2)= xfrm3D(1:3,2,index2);
% Y-axis of tibia wrt femur reference
Tft_z(1:3,index2)= xfrm3D(1:3,3,index2);
% Z-axis of tibia wrt femur reference

checknormTft_x(1,index2)= norm(Tft_x(1:3,index2),2);
checknormTft_y(1,index2)= norm(Tft_y(1:3,index2),2);
checknormTft_z(1,index2)= norm(Tft_z(1:3,index2),2);

e2(1:3,index2)=(cross(Tft_x(1:3,index2),Fy(1:3,index2)));
e2norm(1,index2)=norm(e2(1:3,index2),2);
e2unit(1:3,index2)=e2(1:3,index2)/e2norm(1,index2);

alpha_dirxncos(1,index2)=
atan(xfrm3D(3,1,index2)/xfrm3D(1,1,index2))*180/pi;
q2_dirxncos(1,index2)= -
(xfrm3D(3,4,index2)*cos(alpha_dirxncos(1,index2)*pi/180) -
xfrm3D(1,4,index2)*sin(alpha_dirxncos(1,index2)*pi/180)); %AP
coponent SI components of vector from fe to tib origin

H(1:3,index2)=xfrm3D(1:3,4,index2);
Hnorm(1,index2)=norm(H(1:3,index2),2);
Hnorm

beta_dirxncos(1,index2)=-
(acos(xfrm3D(2,1,index2))*180/pi-90); %row2 coll of the
rotation matrix is the Ycomponent of the x-axis of the tibia,
that is the dot product of the x-tibia and Y femur

gamma_dirxncos(1,index2)=atan(xfrm3D(2,3,index2)/xfrm3D(2,2,in
dex2))*180/pi;

```

```

        q1_dirxncos(1,index2)=-H(2,index2);
end

%% Calculate GS parameters
alpha=asin(dot(e2unit,Fx))*180/pi;
alpha_offset0=alpha-(alpha(1)*ones(1,size(numxfirms)))

q2=dot(e2unit,H)
q2_offset0=-(q2-(q2(1)*ones(1,size(numxfirms))))

q3=dot(Tft_x,H);
q3_offset0=q3-(q3(1)*ones(1,size(numxfirms)))

%plot(q2,'r*-')

beta=90-acos(dot(Fy,Tft_x))*180/pi;
beta_offset0=-(beta-(beta(1)*ones(1,size(numxfirms))))

gamma=asin(dot(e2unit,Tft_y))*180/pi;
gamma_offset0=gamma-(gamma(1)*ones(1,size(numxfirms)))

q1=dot(Fy,H);
q1_offset0=-(q1-(q1(1)*ones(1,size(numxfirms))))
q1_dirxncos_offset0=q1_dirxncos-
(q1_dirxncos(1)*ones(1,size(numxfirms)))

data=[q3; q1; q2; gamma; alpha;beta]';

```



## Appendix E

### E-1 Numerical results of contact force

Table E-1: Contact forces in varus and valgus aligned models

	Angle (°)	Corresponding MAD	Force Medial	Force Lateral	% Force Medial	% Force Lateral
<b>valgus</b>	-14	-50.4	0	1571	0	100
	-11.5	-41.4	0	1372.7	0	100
	-9	-32.4	1.7	1144.8	0.2	99.8
	-6.5	-23.4	8.9	954.3	0.9	99.1
	-4	-14.4	195.1	694.8	21.9	78.1
	-1.5	-5.4	380.2	493.3	43.5	56.5
<b>Cadaver</b>	1	3.6	607.7	264.3	69.7	30.3
<b>varus</b>	3.5	12.6	880.6	83.9	91.3	8.7
	6	21.6	1166.9	2.8	99.8	0.2
	8.5	30.6	1359.2	0	100	0
	11	39.6	1665	0	100	0
	16	57.6	2205	0	100	0

### E-2 Numerical results of contact pressure

Table E-2: Contact pressure in varus and valgus aligned models

			Peak Contact pressure (MPa)			
			Tibial Cartilage		Femoral Cartilage	
	Angle (°)	Corresponding MAD	Medial	Lateral	Medial	Lateral
<b>valgus</b>	-14	-50.4	0	8.05	0	7.95
	-11.5	-41.4	0	6.65	0	6.53
	-9	-32.4	0	5.62	0	5.57
	-6.5	-23.4	0	5.07	0	5
	-4	-14.4	1.78	4.06	1.98	4.02
	-1.5	-5.4	2.08	3.15	2.31	3.11
<b>Cadaver</b>	1	3.6	4.28	2.42	4.56	2.41
<b>varus</b>	3.5	12.6	5.41	1.53	5.58	1.48
	6	21.6	6.68	0	6.69	0
	8.5	30.6	7.85	0	8.02	0
	11	39.6	9.24	0	9.41	0
	16	57.6	11.74	0	11.86	0

### E-3 Numerical results of maximum compressive stress

Table E-3: Maximum compressive stress in varus and valgus aligned models

			Maximum Compressive Stress (MPa)			
			Tibial Cartilage		Femoral Cartilage	
	Angle (°)	Corresponding MAD	Medial	Lateral	Medial	Lateral
<b>valgus</b>	-14	-50.4	0	8.5	0	7.99
	-11.5	-41.4	0	6.95	0	6.61
	-9	-32.4	0	5.88	0	5.63
	-6.5	-23.4	0	5.24	0	5.1
	-4	-14.4	1.77	4.19	1.9	4.1
	-1.5	-5.4	2.78	3.25	2.65	3.18
<b>Cadaver</b>	1	3.6	4.02	2.72	4.07	2.54
<b>varus</b>	3.5	12.6	5.5	1.67	5.69	1.59
	6	21.6	6.78	0.87	6.97	0.56
	8.5	30.6	7.92	0	8.17	0
	11	39.6	9.34	0	9.49	0
	16	57.6	11.91	0	12.02	0

### E-4 Numerical results of maximum shear stress

Table E-4: Peak maximum shear stress in varus and valgus aligned models

			Peak Maximum Shear Stress (MPa)			
			Tibial Cartilage		Femoral Cartilage	
	Angle (°)	Corresponding MAD	Medial	Lateral	Medial	Lateral
<b>valgus</b>	-14	-50.4	0	5.01	0	3.45
	-11.5	-41.4	0	3.95	0	2.66
	-9	-32.4	0	3.55	0	2.24
	-6.5	-23.4	0	3.09	0	2.07
	-4	-14.4	1.06	2.68	0.91	1.76
	-1.5	-5.4	1.62	2.14	1.35	1.41
<b>Cadaver</b>	1	3.6	2.04	1.71	1.67	1.32
<b>varus</b>	3.5	12.6	3.09	1.05	2.21	0.86
	6	21.6	3.78	0.73	2.63	0
	8.5	30.6	4.37	0	2.88	0
	11	39.6	5.05	0	3.18	0
	16	57.6	6.34	0	5.38	0

## E-5 Numerical results of contact area

Table E-5: Contact area for varus and valgus aligned models

			Contact Area (mm <sup>2</sup> )	
	Angle (°)	Corresponding MAD	Medial	Lateral
valgus	-14	-50.4	0	196.94
	-11.5	-41.4	0	195.08
	-9	-32.4	0	193.54
	-6.5	-23.4	0	188.66
	-4	-14.4	58.22	174.88
	-1.5	-5.4	177.49	158.57
Cadaver	1	3.6	170.45	115
varus	3.5	12.6	206.94	53.32
	6	21.6	235.77	0
	8.5	30.6	242.67	0
	11	39.6	295.56	0
	16	57.6	352.96	0

## Appendix F

### F-1 List of publications

#### Refereed papers in peer-reviewed journals (Available online, in press)

1. Mootanah, R., Imhauser, C., **Reisse, F.**, Carpanen, D., Walker, R.W., Koff, M.F., Rozbruch, S.R., Fragomen, A.T., Kirane, Y., Cheah, K., Dowell, J.K. & Hillstrom, H.J. Invited for Publication, following MIA2012 award, in press, "Development and Verification of a Computational Model of the Knee Joint for the Evaluation of Surgical Treatments for Osteoarthritis", Computer Methods in Biomechanics and Biomedical Engineering. Impact Factor: 1.573.

#### Refereed Abstracts in peer-reviewed journals

1. Mootanah, R., Imhauser, C., **Reisse, F.**, Carpanen, D., Walker, R.W., Cheah, K., Dowell, J.K., Lenhoff, M., Koff, M. & Hillstrom, H.J. 2012, "Knee joint contact mechanics in a malaligned limb: an integrated finite element and *in vitro* study", Journal of Biomechanics, vol. 45, Supplement 1, no. 0, pp. S388.

#### Refereed abstracts in peer-reviewed conference proceedings

1. **Reisse, F.**; Hillstrom, H.J.; Walker, R.W.; Carpanen, D.; Lenhoff, M.W.; Imhauser, C.W.; Koff, M.F.; Dowell, J.W.; Rozbruch, S.R.; Fragomen, A.T.; Mootanah, R., 2014. "The Effect of Knee Malalignment on Tibial Cartilage Volume Exposed to Maximum Compressive Stress", 12th international Symposium on Computer Methods in Biomechanics and Biomedical Engineering, Amsterdam, 13<sup>th</sup>-15<sup>th</sup> October.
2. **Reisse, F.**; Hillstrom, H.J.; Walker, R.W.; Carpanen, D.; Lenhoff, M.W.; Imhauser, C.W.; Koff, M.F.; Rozbruch, S.R.; Fragomen, A.T.; Mootanah, R., 2014. "Predicting Knee Joint Contact Pressure and Shear Stress for Different Alignments", 24<sup>th</sup> Annual Scientific Meeting of the Limb Lengthening and Reconstruction Society, Montreal, 25<sup>th</sup>-26<sup>th</sup> July.
3. **Reisse, F.**; Hillstrom, H.J.; Walker, R.W.; Carpanen, D.; Lenhoff, M.W.; Imhauser, C.W.; Koff, M.F.; Rozbruch, S.R.; Dowell, J.K.; Mootanah, R., 2014. "Predicting Knee Joint Contact Pressure for Different Malalignment Deformities", 7<sup>th</sup> World Congress of Biomechanics, Boston, 6-11 July.
4. Mootanah, R.; Imhauser, C.; **Reisse, F.**; Carpanen, D.; Walker, R.W.; Koff, M.F.; Lenhoff, M.W.; Rozbruch, R.; Fragomen, A.; Kirane, Y.; Dewan, Z.; Cheah, K.; Dowell, J.K.; Hillstrom, H.J., 2013. "Development and Evaluation of a Computational Model of the Malaligned Knee Joint", Knee surgery and rehabilitation in 2013: How is engineering driving improved treatment?, IMechE, London, 11-12 November.

5. **Risse, F.**, Walker, R.W., Carpanen, D., Lenhoff, M., Imhauser, C.W., Rozbruch, S.R., Koff, M.F., Dowell, J.K., Hillstrom, H.J. & Mootanah, R., 2013. "The effect of malalignment on knee joint contact stresses and forces during heel strike and toe off", 11<sup>th</sup> International Symposium on Biomechanics and Biomedical Engineering, Salt Lake City, 3-7 April.
6. **Risse, F.**, Walker, R.W., Carpanen, D., Imhauser, C.W., Rozbruch, S.R., Koff, M.F., Hillstrom, H.J. & Mootanah, R., "Effect of malalignment on knee joint contact stress: a preliminary finite element study", Pre-ORS, St Antonio, 25<sup>th</sup> of January 2013.
7. Mootanah, R., Imhauser, C., **Risse, F.**, Carpanen, D., Walker, R.W., Cheah, K., Dowell, J., Lenhoff, M., Koff, M.F. & Hillstrom, H.J. 2012, "Knee joint contact mechanics in a malaligned limb: an integrated finite element and *in vitro* study", 18th Congress of European Society of Biomechanics, Lisbon, 1-4 July.
8. **Risse, F.**, Walker, R.W., Carpanen, D., Dowell, J., Dewan, Z., Imhauser, C., Hillstrom, H.J. & Mootanah, R. 2012, "The Effect of High Tibial Osteotomy on Stress in the Tibio-Femoral Joint: A Computer Simulation Study", ", 10<sup>th</sup> International Symposium on Biomechanics and Biomedical Engineering, Berlin, 11-14 April.
9. Mootanah, R., **Risse, F.**, Carpanen, D., Walker, R. & Hillstrom, H.J. 2012, "The effects of the material properties of bones and soft tissues on knee joint contact stress", 10th International Symposium on Biomechanics and Biomedical Engineering, eds. J. Middleton, C. Jacobs, C. Holt & S. Evans, Cardiff, Meditech, Berlin, 10-14 April.
10. **Risse, F.**, Walker, R.W., Dowell, J., Imhauser, C., Hillstrom, H.J. & Mootanah, R. 2011, "Predicting Improved Surgical Reconstruction Techniques for Treating Knee Osteoarthritis, Using Computer Simulation Techniques", International Society of Biomechanics, Brussels, 3-7 July.
11. **Risse, F.**, Carpanen, D., Deri, Y., Cheah, K., Dowell, J., Hillstrom, H.J. & Mootanah, R. 2011b, "Conservative Surgical Treatments for Osteoarthritis: An Integrated Computational and *in Vitro* Study", Advances and New Developments in Osteoarthritis / Degenerative Diseases - Benchtop to BedsideMediTech, Cardiff, 1 June.

## **F-2**                      **List of Awards**

1. June 2014: Best podium presentation at the Eighth Annual Research Student Conference, Anglia Ruskin University. Risse, F.; Hillstrom, H.J.; Walker, R.W.; Carpanen, D.; Lenhoff, M.W.; Imhauser, C.W.; Koff, M.F.; Rozbruch, S.R.; Dowell, J.K.; Mootanah, R. in Predicting Knee Joint Contact Pressure for different Malalignment Deformities", June, Chelmsford, UK
2. June 2014: Highly commended abstract at the Eighth Annual Research Student Conference, Anglia Ruskin University. Risse, F.; Hillstrom, H.J.;

- Walker, R.W.; Carpanen, D.; Lenhoff, M.W.; Imhauser, C.W.; Koff, M.F.; Rozbruch, S.R.; Dowell, J.K.; Mootanah, R. in Predicting Knee Joint Contact Pressure for different Malalignment Deformities”, June, Chelmsford, UK
3. May 2014: Best poster presentation at the Faculty of Science and Technology 4<sup>th</sup> Annual Research and Scholarship Conference, Anglia Ruskin University. Reisse, F.; Hillstrom, H.J.; Walker, R.W.; Carpanen, D.; Lenhoff, M.W.; Imhauser, C.W.; Koff, M.F.; Rozbruch, S.R.; Dowell, J.K.; Mootanah, R. in “Predicting Knee Joint Contact Pressure for Different Knee Alignments”, May, Cambridge, UK.
  4. June 2013: Commended Abstract at the Research Student Conference, Anglia Ruskin University. Reisse, F. in “The Effect of Knee Malalignment on Joint Contact Pressures during Walking”, June, Cambridge, UK.
  5. June 2012: 3<sup>rd</sup> best poster award at the Faculty of Science & Technology conference, Anglia Ruskin University. Mootanah, R., Reisse, F., Carpanen, C., Walker, R.W., Hillstrom, H.J. in: Effects of Material Properties of Bones and Soft Tissues on Knee Joint Contact Stresses, June, Chelmsford, UK.
  6. April 2012: Mimics Innovation Award 2012, Mootanah, R., Imhauser, C., Reisse, F., Carpanen, D., Walker, R.W., Koff, M., Lenhoff, M., Dewan, Z., Rozbruch, R., Fragomen, A., Kirane, Y., Cheah, K., Dowell, J.K. and Hillstrom, H.J., Development and Verification of a Computational Model of the Knee Joint for the Evaluation of Surgical Treatments for Osteoarthritis”, Materialise World Conference 2012, 18-20 April, Leuven, Belgium.
  7. April 2012: Delsys Travel Grant presented at the Computer Methods in Biomechanics and Biomedical Engineering conference, 11-14 April, Berlin, Germany.
  8. June 2011: Best podium presentation at the Joint Meditech - ARU Medical Engineering Conference. Reisse F, Carpanen D, Deri Y, Cheah K, Dowell J, Hillstrom HJ, Mootanah R. In: Conservative surgical treatments for osteoarthritis: An integrated computational and *in vitro* study. Advances and new developments in osteoarthritis / degenerative diseases - benchtop to bedside; 1 June; Chelmsford, UK. Cardiff: MediTech; 2011.
  9. June 2011: Highly Commended poster presentation at the Research Student Conference, Anglia Ruskin University. Reisse, F, Walker, RW, Dowell, J, Hillstrom, HJ in "High Tibial Osteotomy: Predicting Improved Surgical Reconstruction Techniques using Finite Element Method", 16 June, Chelmsford UK.